University of Groningen

The Role of Neutral Hydrogen in the Evolution of Nearby Radio Galaxies

Struve, Rolf Christian

IMPORTANT NOTE: You are advised to consult the publisher's version (publisher's PDF) if you wish to cite from it. Please check the document version below.

Document Version
Publisher's PDF, also known as Version of record

Publication date:
2010

Link to publication in University of Groningen/UMCG research database

Citation for published version (APA):
Struve, R. C. (2010). *The Role of Neutral Hydrogen in the Evolution of Nearby Radio Galaxies*. s.n.

Copyright
Other than for strictly personal use, it is not permitted to download or to forward/distribute the text or part of it without the consent of the author(s) and/or copyright holder(s), unless the work is under an open content license (like Creative Commons).

The publication may also be distributed here under the terms of Article 25fa of the Dutch Copyright Act, indicated by the "Taverne" license. More information can be found on the University of Groningen website: https://www.rug.nl/library/open-access/self-archiving-pure/taverne-amendment.

Take-down policy
If you believe that this document breaches copyright please contact us providing details, and we will remove access to the work immediately and investigate your claim.

Downloaded from the University of Groningen/UMCG research database (Pure): http://www.rug.nl/research/portal. For technical reasons the number of authors shown on this cover page is limited to 10 maximum.

Download date: 05-05-2023

rijksuniversiteit
groningen

The Role of Neutral Hydrogen in the Evolution of Nearby Radio Galaxies

Proefschrift

ter verkrijging van het doctoraat in de
Wiskunde en Natuurwetenschappen
aan de Rijksuniversiteit Groningen
op gezag van de
Rector Magnificus, dr. F. Zwarts,
in het openbaar te verdedigen op
vrijdag 12 november 2010
om 14:45 uur

door

Rolf Christian Struve

geboren op 3 november 1981
te Kiel, Duitsland

Promotor:	Prof. dr. J. M. van der Hulst
Copromotores:	Dr. R. Morganti Dr. T. A. Oosterloo
Beoordelingscommissie:	Prof. dr. P. D. Barthel Prof. dr. J. H. van Gorkom Dr. J. E. Conway

ISBN: 978-90-367-4562-8 Printed version
ISBN: 978-90-367-4563-5 Electronic version

Imagination is more
important than knowledge.

(Albert Einstein)

Cover: The image shows Centaurus A as observed with the Australia Telescope Compact Array at radio wavelengths. The cold gas (neutral hydrogen, orange colors) is located in a disk which is roughly perpendicular to the innermost radio lobes (in blue). These lobes get fueled with relativistic plasma by the active black hole in the centre. The background displays the light emission at optical wavelengths (image kindly provided by Robert Gendler). The image on the backside shows the Westerbork Synthesis Radio Telescope observing the univese. Phote taken by me in 2006.

Printed by: F&N Boekservice, Amsterdam, the Netherlands

Contents

1 Introduction

Approximately 60 years ago, in the late 1940's, several radar devices – previously used by the military – were transformed into research instruments that offered the possibility to observe and study cosmic objects at previously unexplored frequencies. The new instruments introduced a new field in astronomy, which enabled scientists to observe the universe with "radio eyes". First targets were the sun and strong radio emitters located in the Galaxy. However, extragalactic radio emitters were soon detected as well. Among the first three identified extragalactic objects were Virgo A, Centaurus A and Cygnus A (see, e.g., Bolton & Stanley, 1948a,b; Bolton, 1948); these radio emitters are now known to be hosted by galaxies (called "radio galaxies")[1]. Yet back in the 1940's, the nature of these sources was still completely unknown; Walter Baade referred to Centaurus A as a "freak" while Harlow Shapley saw it as a "pathological specimen" because of its peculiar nature. Today, we have a better idea about the nature and origin of such strong radio emitters, but many questions still remain.

This thesis investigates the role of neutral hydrogen in the evolution of radio galaxies – as cold gas is believed to play an important role – and investigates the mechanisms responsible for the strong emission of radiation detected at radio wavelengths. Following, we give a short summary about supermassive black holes which generate radio emission (Sect. 1.1) and describe the hosts of radio sources (Sect. 1.2). Section 1.3 draws an outline of this thesis and gives an overview of the open questions related to radio galaxies and their evolution.

1.1 From Black Holes to Active Galactic Nuclei

Black holes:
A black hole is a mass condensation which forms a singularity in space; no material – not even light – can escape from this singularity if it gets closer to the black hole than the radius of the event horizon. Material and light at larger radii are deflected so that black holes can be indirectly "seen" through observations of the surrounding material.

Observational work suggests that supermassive black holes (SMBHs, with masses in the range $10^6 < M_{\rm BH} < 10^{9.5}\ M_\odot$; Kormendy & Gebhardt, 2001) exist in the centres of all galaxies with bulges (see e.g. Kormendy & Richstone, 1995; Ferrarese &

[1] The study of new radio data of the later-mentioned two objects will be an integral part of this thesis.

Merritt, 2000).

A number of tight scaling relations between the mass of the SMBH and the host galaxy have been found (for instance with stellar bulge mass, stellar velocity dispersion, concentration index; see, e.g., Magorrian et al., 1998; Ferrarese & Merritt, 2000; Gebhardt et al., 2000; Marconi & Hunt, 2003; Häring & Rix, 2004; Graham & Driver, 2007; Hopkins et al., 2007; Gültekin et al., 2009), suggesting a common evolutionary process between SMBHs and host galaxies (see also Cattaneo et al., 2009). The growth of a SMBH occurs generally in two ways, either by coalescence with another SMBH during a merger event, or via the accretion of gas and dust onto the black hole. The SMBH growth is known to be dominated by radiatively efficient accretion during "active" phases (see below) (Soltan, 1982; Marconi et al., 2004; Shankar et al., 2004; Merloni & Heinz, 2008), when gas reaches the direct vicinity of the black hole (< 1 pc; see, e.g., Rees, 1984; Magorrian et al., 1998).

Active Galactic Nuclei:
Supermassive black holes which actively accrete gas and dust are called "Active Galactic Nuclei" (AGN). For a long time, galaxies hosting such active nuclei were treated as exotic objects in the universe with no significant impact on the evolution of the hosts. However, recent cosmological simulations show that mechanical *feedback* strongly regulates the growth of galaxies (e.g. Di Matteo et al., 2005; Springel et al., 2005; Hopkins et al., 2005; Croton et al., 2006). AGN heat the surrounding gas and drives it out of the nuclear environment. Such outflows of neutral, warm or hot gases have been observed in several active galaxies (e.g. Heckman et al., 1981; Holt et al., 2003; Morganti et al., 2005b; Emonts et al., 2005). This suggests that black hole growth has a self-regulating component and therefore, at least in part, explains the observed scaling relationships (see above). Moreover, the existence of these scaling relationships suggest that most, if not all, galaxies go through such active phases during a Hubble time. Hence, understanding these active phases is of uttermost importance, if we want to comprehend how galaxies evolve.

How do supermassive black holes accrete gas and dust? Due to the conservation of angular momentum, the infalling material will form a flattened structure around the black hole, a so-called accretion disk. The expected size of such an accretion disk is very small (typically $\sim 10^{-3}$ pc; see, e.g., Peterson, 1997), the material in the disk rotates at high speeds while large amounts of radiation are emitted, mainly in the optical, ultra-violet and X-ray band (e.g. Rees, 1984; Magorrian et al., 1998; Peterson, 1997). In about 15 – 20% of the AGN (Kellermann et al., 1989) parts of the material falling towards the black hole can escape from the disk to form jet structures perpendicular to the accretion disk on either side. The jets, which can grow into Mpc structures (i.e. much larger than the hosts galaxies which are typically tens of kpc), consist of a plasma of relativistic electrons (the plasma emits radiation at radio wavelengths) which follow the magnetic field helix created by the differential rotation of the black hole and the accretion disk (Meier et al., 2001). The plasma is observable at radio wavelengths. Black holes with strong radio emission are called "radio-loud" AGN, whereas black holes with weak or no radio emission are refered to as being "radio-quiet". There is no distinct border-line between radio-loud and radio-quiet AGN. However, in practice, a radio power of $P_{1.4\mathrm{GHz}} \approx 10^{22} - 10^{23}$ W Hz^{-1} sets

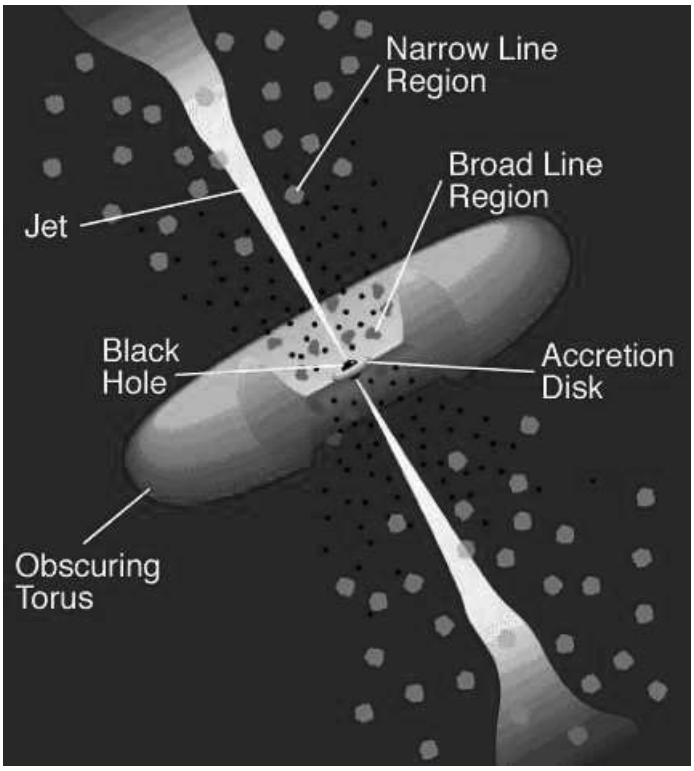

Figure 1.1: *Artist impression of an AGN (Credit: Urry & Padovani, 1995).*

the boundary between radio-loud and radio-quiet. For AGN with lower values, the contribution from stellar emission starts to become a dominant factor for the galaxy's total radio luminosity (see, e.g., Sadler et al., 1989; Wrobel & Heeschen, 1991).

Where does the material, which is feeding the black hole, come from? According to the standard model of AGN (e.g. Antonucci, 1993; Urry & Padovani, 1995), the black hole and the accretion disk are surrounded by a torus (Fig. 1.1) which consists of dust and gas and has a size of approximately 1 – 10 pc. Recent observations directly imaged such dusty torus structures (Jaffe et al., 2004; Tristram et al., 2009; van der Wolk et al., 2010). Further evidence for the existence of tori comes from modelling infrared spectral energy distributions from AGN heated dust (Nenkova et al., 2008b; Privon, 2009). On slightly larger scales (tens of pc), circumnuclear disks of atomic and molecular gas have been detected in a few sources (e.g. Schinnerer et al., 2000; van Langevelde et al., 2000; Peck & Taylor, 2001; Lo, 2005; Hicks et al., 2009). Such circumnuclear disks could provide the gas masses which are needed to trigger the AGN. The exact circumnuclear structures and accretion mechanisms though, remain ambiguous, see Sect. 1.3.1.

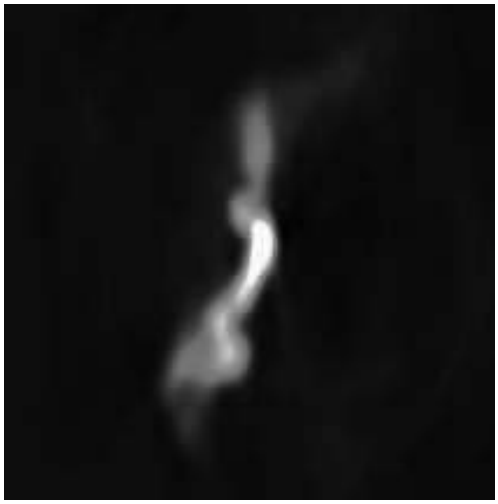

Figure 1.2: *FR-I radio source B2 0104+32. This is one of the sources which we study in Chapter 2.*

1.2 Radio Galaxies

A complete "zoo" of different radio sources exists in addition to the distinction between radio-loud and radio-quiet AGN. This section explains what type of radio sources are hosted by radio galaxies; it reviews several possible triggering mechanisms of the central engine and briefly summarizes previous neutral hydrogen studies of radio galaxies.

1.2.1 Different classes of radio sources

AGN have been found in nearly all galaxy types, showing a great variety of phenomena (e.g. X-ray emission, optical emission lines, radio emission). Some are related to intrinsic differences while others are due to orientation effects. In order to better understand these phenomena, efforts have been made to classify different types of AGN.

Only a fraction of the AGN are radio-loud (Sect. 1.1). Radio-loud sources are predominantly hosted by early-type (i.e. elliptical and lenticular) galaxies, called "radio galaxies". The appearance of the radio morphology depends mainly on the total radio power. Fanaroff & Riley (1974) classified radio galaxies into two groups, the weaker radio sources (Fanaroff-Riley type I, FR-I) have subsonic jets that end in edge-darkened radio lobes (Fig. 1.2). Stronger radio sources (Fanaroff-Riley type II, FR-II) have supersonic jets ending in edge-brightened lobes with a hot-spot (Fig. 1.3). The radio morphology seems to be a function of radio power, with the dividing line at approximately $P_{1.4\mathrm{GHz}} \approx 10^{25}\,\mathrm{W\,Hz^{-1}}$, but the exact value also depends to an extent on the host galaxy's luminosity (e.g. Owen & White, 1991; Ledlow et al., 2002). For

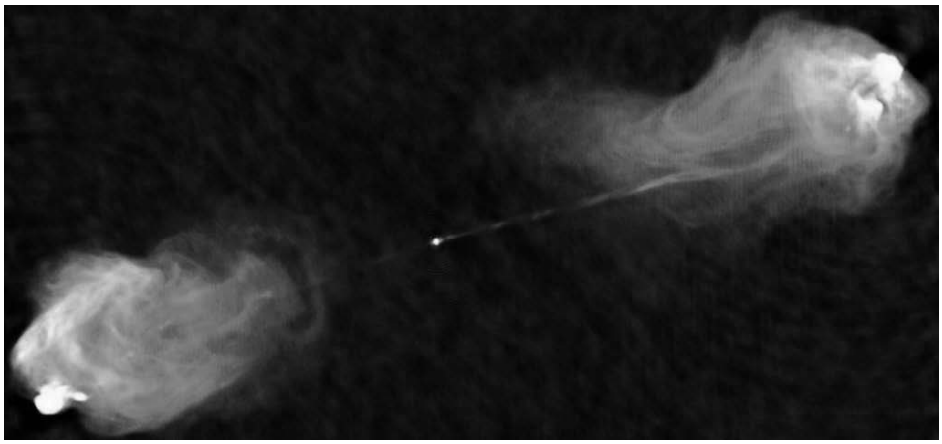

Figure 1.3: *FR-II radio source Cygnus A (Credit: C. Carilli). The core region of this source is studied in Chapter 5.*

both types, the viewing angle (between jet axis and the observer) is large, i.e. the jets propagate (roughly) in the plane of the sky. Radio sources where the jet is directed roughly at the observer are called BL Lacs (FR-I type) and quasars (FR-II type).

Some radio sources are compact (typically $\leq$ 10 kpc), which are believed to be young sources that will grow into the large, classical FR-I or FR-II type sources (for a summary, see O'Dea, 1998). Some of the compact sources, however, might never become a large, extended radio source. The ISM surrounding the black hole could confine or frustrate sources such that they do not manage to grow into classical FR-I or FR-II structures (e.g. van Breugel et al., 1988; O'Dea et al., 1991; Taylor et al., 1998; Giroletti et al., 2005).

Radio activity can also be recurrent, i.e. some galaxies experience more than one phase of radio activity (for a recent review, see Saikia & Jamrozy, 2009). Centaurus A (which will be studied in detail in Chapter 3 and 4) is a prominent example with double-double lobes (see for instance Fig. 1 in Morganti et al., 1999), suggesting that this source has gone through more than one phase of activity.

This thesis only deals with nearby low-power radio galaxies, with the exception of the powerful FR-II source Cygnus A (Chapter 5).

1.2.2 Triggering mechanisms

Several mechanisms have been proposed for supplying and transporting the gas down to the nuclear region where it can trigger an active phase. For this, a variety of processes seem to exist. Below is a brief overview of the most relevant mechanisms.

Major mergers, satellite accretions and galaxy interactions:
A possible way to channel gas to the central region – which is required to trigger a radio-loud phase (Sect. 1.1) – is the disturbance of the galaxy potential. For instance,

mergers and satellite accretions result in tidal interactions, which may enhance cloud - cloud collisions which remove angular momentum from the gas. This low angular momentum gas can then get stired towards the nuclear region where it eventually fuels the black hole (see, e.g., Lin et al., 1988). The orbits of the progenitor galaxies do have an impact on the amount of gas which gets channeled to the circumnuclear region. Direct encounters, for instance, are more efficient in channeling gas to the circumnuclear regions when compared to retrograde encounters. This is because direct encounters, which develop more pronounced asymmetries than retrograde ones, are needed to channel the gas towards the nucleus (Di Matteo et al., 2007).

Numerous studies have searched for signatures of disturbances in radio galaxies. Evidence for merging and/or interaction activity is found in a large fraction of radio galaxies (signs of disturbance have mainly been detected in the optical and infrared band; see, e.g., Heckman et al., 1986; Lin et al., 1988; Smith & Heckman, 1989; Wu et al., 1998; Colina & de Juan, 1995; Canalizo & Stockton, 2001; Canalizo et al., 2007; Bennert et al., 2008; Kuo et al., 2008; Tasse et al., 2008). Observed signs of interactions include tails, fans, bridges, shells and dust lanes. The use of different telescopes (including ground- and space-based facilities) with different observing bands, different resolutions and varying magnitude limits does not allow to give a firm fraction of disturbed host galaxies. However, it seems that the fast majority (> 85%) of radio galaxies do show signs of disturbance provided that sensitive observations are available (e.g. Heckman et al., 1986; Roche & Eales, 2000; Ramos Almeida et al., 2010). It has been a long-known fact that the fraction of FR-Is showing morphological disturbances (in the optical band) is significantly lower than for the more powerful FR-IIs (e.g. Heckman et al., 1986; Baum et al., 1992). Nevertheless, it is important to note that a significant fraction of FR-Is (50% in the sample of Ramos Almeida et al., 2010) *do* show signs of disturbance. This includes the two low-power sources which this thesis studies in detail (Centaurus A and NGC 1167; Chapter 3 and 6 respectively) are clearly perturbed systems. Merging/interaction activity could, therefore, play an important role for low-power radio galaxies.

Recent simulations of hierarchical galaxy evolution include black hole growth and feedback (see Sect. 1.1) in merger processes (e.g. Springel et al., 2005; Hopkins et al., 2008b; Somerville et al., 2008). In some (gas-rich) merger events, the AGN activity is accompanied by a starburst (see, e.g., Di Matteo et al., 2005). Young stars, which are signs of recent or ongoing starbursts, have indeed been detected in about 1/3 of the radio galaxies (e.g. Tadhunter et al., 1996; Emonts et al., 2006; González Delgado et al., 2006; Davies et al., 2007; Wild et al., 2010), suggesting that gas-rich mergers may cause nuclear activity (at least in some cases). A time-delay of up to several 10^8 yr between the starburst and the onset of the AGN has been observed in several sources (Tadhunter et al., 2005; Emonts et al., 2006; Labiano et al., 2008). This time-delay varies from object to object (see, e.g., Wild et al., 2010); the connection between merger, starburst and AGN is therefore far from clear, though several possible reasons have been discussed to explain such a delay. For instance, time-delays might be related to the low accretion rate of some black holes (see, e.g., Baganoff et al., 2003) or could be related to the time necessary to remove enough angular momentum of the gas so that it can be transported to the sub-pc region of the central black hole. Another possibility is that the AGN is obscured during the initial stage

of the starburst (Springel et al., 2005).

While interactions of gas-rich objects may cause nuclear activity, the presence of large amounts of cold gas is not a sufficient condition to trigger the AGN. Several recent observations have detected large amounts of H I and CO (which is a tracer of molecular hydrogen) in early-type galaxies (e.g. Morganti et al., 2006; Oosterloo et al., 2007b; Combes et al., 2007; Ocaña Flaquer et al., 2008), but the majority of the sources do not harbour an AGN.

The amount of gas required to switch-on a quiescent black hole is relatively small. According to van Gorkom et al. (1989), gas masses as little as $10^3 < M_{\rm gas} < 10^5\ M_\odot$ could be sufficient to trigger an AGN over its maximum lifetime, which is believed to be $\sim 10^8$ yr (Leahy et al., 1989; Parma et al., 2002). Gas-rich galaxy mergers are, therefore, not a necessary condition to trigger AGN activity. The accretion of small companion galaxies can easily provide the required gas masses. Another possibility is that close galaxy encounters (which will not lead to a merger) disturb the galaxy potential such that the gas inside the host galaxy is stired towards the nucleus. Finally, it is important to note that "dry" mergers (i.e. merging of gas-poor elliptical galaxies) is yet another possibility of triggering AGN activity. Even in dry mergers, small amounts of gas are likely to be present that could be channeled to the nuclear region. Morphological signatures of dry mergers are weak in the optical band (and undetectable at radio wavelengths) and visible only for about 1.5×10^8 yr (Bell et al., 2006), i.e. hardly longer than the lifetime of an AGN.

Cold accretion:
The possible significance of continuous accretion of cold gas from the intergalactic medium (IGM) necessary for the formation of galaxies has already been pointed out by Binney (1977). Since only small amounts of gas are required to trigger black holes, this may be also a relevant mechanism which can cause a phase of nuclear activity. Several recent simulations suggest that galaxies can indeed slowly accrete cold gas from the IGM along filaments without being shock heated (e.g. Kereš et al., 2005; Kereš & Hernquist, 2009; Kaufmann et al., 2006; Macciò et al., 2006; Dekel & Birnboim, 2008; Peek et al., 2008; Kawata & Mulchaey, 2008; Brooks et al., 2009). There is growing observational evidence that galaxies accrete cold gas from the IGM (for a review, see Sancisi et al., 2008). However, how it works in detail and whether it can cause a radio-loud phase of AGN activity remains unclear.

Hot accretion:
Most early-type galaxies are (expected to be) embedded in a hot (X-ray) halo (for an overview, see, e.g., Mo et al., 2010). Hot gas from the halo can be directly accreted to the vicinity of the black hole, where it feeds the central engine. Allen et al. (2006) has found a correlation between the accretion rate and the jet power, implying that spherical hot gas accretion is the main accretion mechanism which powers the active nuclei in the given sample. Evidence for the steady accretion of hot gas to the vicinity of the black hole has also been found in a few other cases (e.g. Best et al., 2006; Balmaverde et al., 2008). These results are supported by simulations which show that galaxies can efficiently accrete hot gas, whereas cold gas often fragments and gets ionised before it gets close enough to the black hole (Croton et al., 2006). Especially

in massive halos ($M_{\rm halo} > 3 \times 10^{11}\ M_{\odot}$) hot accretion is predicted to be more efficient (Croton et al., 2006). Hot accretion is therefore a plausible mechanism for the fuelling of radio galaxies. This process might work in particular in low-power (FR-I type) radio galaxies (Hardcastle et al., 2007).

Bars and central spirals:
Shlosman et al. (1989) proposed a mechanism in which the accretion onto a supermassive black hole is driven by a stellar bar on the kpc scale, resulting in a gaseous disk with radius few 100 pc. This disk can become unstable, allowing material to flow inwards, where the gas can fuel a black hole or trigger a nuclear starburst. Studies of nearby spiral galaxies suggest that stellar bars can indeed form a gaseous disk (though on somewhat smaller scales [tens of pc]), which lead to a burst of nuclear star formation (e.g. Schinnerer et al., 2007). Observations also suggest that nuclear spiral structures can channel gas to the nucleus (Prieto et al., 2005). In this case, a stellar bar at a larger scale is observed. Most studies on this topic have focused on nearby, late-type objects (i.e. radio-quiet objects), where the nuclear regions can be sufficiently resolved with current-day telescopes. To our knowledge, no observations of radio-loud galaxies exist which show similar structures. However, this could be an observational bias since radio galaxies are usually located at higher redshifts, making the detection of such features difficult. In the only radio galaxy where current instruments do give sufficient linear resolution, Centaurus A, we find no evidence for bars or central spirals (Chapter 3).

1.2.3 Previous H I work

Given the possible importance of cold gas for the triggering of radio sources, several studies have been performed to investigate the neutral hydrogen properties of radio galaxies. H I can be detected in emission and against the radio continuum also in absorption. While the study of the H I emission often allows the investigation of the gas properties on scales of tens of kpc (for instance to search for signs of interactions/disturbances), H I absorption observations usually probe the circumnuclear environment, allowing the study of the gas properties close to the black hole. In the following, the emission/absorption studies are in part briefly summarized.

In the past few decades, H I in absorption has been detected in several radio galaxies, including in Centaurus A (Roberts, 1970). The first systematic search for H I absorption in radio galaxies was performed by van Gorkom et al. (1989). These authors detected absorption in four out of altogether 29 observed sources. For many years, H I detected in absorption against the nucleus of a radio galaxy was seen only at velocities redshifted with respect to the systemic velocity of the host galaxy (e.g. van Gorkom et al., 1989) (including in Centaurus A; van der Hulst et al., 1983). This predominance of redshifted absorption has been interpreted as evidence for cold gas falling into the nucleus. However, the picture has proven to be more complex. In the meantime, H I absorption has been detected in several samples of radio galaxies with detection rates up to 40% (e.g. Morganti et al., 2000; Vermeulen et al., 2003; Pihlström et al., 2003; Morganti et al., 2005b; Gupta et al., 2006). Blueshifted absorption has been observed against the nucleus at least as often as redshifted absorption.

Hence, the detection of nuclear redshifted absorption provides insufficient evidence for the claim that cold gas is fuelling the AGN.

The strength of an absorption signal depends not only on the absorbing gas structure but also on the strength of the underlying continuum. It is therefore possible to detect absorption against strong continuum sources with sensitivities that would not suffice to observe the same structure in emission. In fact, most radio galaxies with an associated H I absorption are located at redshifts that do not suffice to detect H I in emission. As a consequence, very few radio galaxies have yet been successfully imaged in H I emission (usually in single-object studies). Among the detected sources are NGC 4278 (Raimond et al., 1981; Morganti et al., 2006), NGC 1052 (van Gorkom et al., 1986), Centaurus A (van Gorkom et al., 1990; Schiminovich et al., 1994), PKS 1718-649 (Veron-Cetty et al., 1995), B2 0648+27 (Morganti et al., 2003) and IC 5063 (Oosterloo et al., 2007b).

A systematic investigation of the H I (emission) properties of radio galaxies has been performed by Emonts (2006). His sample consists of 23 sources (selected from the B2 catalogue; Colla et al., 1970); H I in emission is detected in seven of them, including the previously detected sources NGC 4278 and B2 0648+27 (for details, see Emonts et al., 2007, 2010)[2]. The morphology of the H I structures varies from unresolved blobs to giant, 190 kpc disks. Most of these sources show an H I kinematics that is dominated by rotation. However, signs of disturbance are observed in all objects. Hence, interactions/merging activity could play a role in the triggering of radio sources.

1.3 This thesis

1.3.1 Open questions and goals of this study

Despite the progress made in understanding radio galaxies since their discovery approximately 60 years ago, several questions remain. These include:

- *which are the mechanisms that cause nuclear activity?*
  Do mergers and accretion events trigger AGN activity or is the accretion of hot or cold gas from the halo/IGM significant? Many mergers/interactions are observed which do not lead to an active phase, whereas activity is also observed in non-interacting systems; the connection between interaction and AGN activity therefore needs to be explored more thoroughly. This will also make it possible to address the question of why some galaxies are radio-loud while others are not and whether all radio sources of a certain type (e.g. low-power radio galaxies) are fuelled by the same mechanism.

- *what fuels the AGN?*
  Direct observational evidence for the infall of gas on the black hole is still missing. It is therefore crucial to explore the circumnuclear environment. Does

[2]Data taken for this thesis contributed to these results, a short summary of the H I properties of the B2 sample is given in Chapter 2.

direct gas infall onto the AGN exist or do the accretion disks get the fuel from circumnuclear disk structures?

- *what timescales are involved in the triggering of radio sources?*
  A phase of radio activity ($\leq 10^8$ yr) is only a short episode in the lifetime of an early-type galaxy. It is, however, not well understood what determines the duty cycle of an AGN. A time-delay between the starburst and the onset of the AGN has been observed (Sect. 1.2.2), but the delay varies from object to object. The triggering of a black hole can occur immediately before, during or after a merger/interaction event (C. Tadhunter in prep.). Another question is what causes a source to re-start. Recurrent AGN activity is observed in several sources, but why the source becomes active again is not known.

- *how does the ISM influence the AGN?*
  What impact does the ISM have on the radio source? Many radio structures grow well beyond the size of the host galaxy (up to the Mpc scale), whereas other sources are compact ($\leq$ 10 kpc). Are these sources young or does the ISM confine them in such a way that they can not grow into large, extended structures (see Sect. 1.2.1)? Several compact sources seem to interact with their environment (see Chapter 7 for an example), but does that imply that they will never grow into large sources?

Our approach for the thesis:
This thesis studies the evolution of nearby low-power radio sources and their hosts. The main topics addressed in this thesis are related to the four questions outlined above:

1. What is the relation between mergers/interactions and the triggering of AGN activity and why are some galaxies active while others are not?
2. Can we find evidence that cold gas fuels the AGN?
3. What determines the life cycle of an AGN?
4. How do the host galaxies form/evolve and what is the effect of the ISM on the AGN?

Since cold gas may play an important part in the triggering of radio sources, it is essential to study the role of neutral hydrogen in the evolution of radio galaxies. H I structures can be observed on very different linear scales. Radio telescopes allow to image the H I morphology and kinematics from a scale ranging from a few hundred kpc down to tens of pc, i.e. across four orders of magnitude – from the environment of the host galaxies down to the circumnuclear region, where the gas is directly influenced by the black hole.

A study of the environment allows the search for signs of interaction and to investigate whether the neighbourhood of radio-loud galaxies differs from their radio-quiet counterparts, which could give indications as to why some galaxies experience an active phase while others do not. The study of extended H I structures (on the

tens of kpc scale) allows to trace the evolution of a galaxy. At large radii from the centre, dynamical timescales become large (up to ~1 Gyr), such that signs of interaction/merging activity can be identified, as well as small gas clumps which get accreted from the IGM. At the same time, it can be investigated whether non-circular motions drive gas towards the ~100 pc nuclear region. Observations of the nuclear absorption probe the core structures surrounding the black hole, which allows to address the fuelling question.

We restrict our study to nearby low-power radio galaxies (with the exception of Cygnus A, Chapter 5), because these objects can be studied in great detail. More powerful radio galaxies are usually found at higher redshifts where the linear resolution is poor and H I can only be detected in absorption. Note that a deep understanding of the mechanisms at work in nearby objects is also invaluable for understanding (radio) galaxy evolution at higher redshifts, where interactions and merging events are more frequent and radio activity is a common phenomenon.

1.3.2 Outline of the thesis

Chapter 2 investigates the H I environment of a sample of radio-loud galaxies previously studied by Bjorn Emonts. Follow-up H I observations for part of the sample are presented. In the sample we do not find a statistically significant difference in the number of companions located in the environment ($r < 300$ kpc) when compared to a radio-quiet comparison sample. Several companions of radio galaxies show signs of disturbance which can be indicative of an interaction with the host galaxy. However, companions of radio-quiet sources show similar signs, suggesting that this is not a distinguishing characteristic between the two samples.

Chapter 3 presents an H I study of the closest radio-loud galaxy, Centaurus A. Our Australian Telescope Compact Array (ATCA) data show the H I morphology and kinematics in great detail. Tilted-ring modelling of the warped disk shows no evidence for non-circular motions for $r < 6$ kpc. Our model parameters also describe the dust morphology as seen by Spitzer and are consistent with the values found for a central stellar ring. At $r > 6$ kpc, asymmetries and arm structures are observed, suggesting that a minor merging event has taken place $1.6 - 3.2 \times 10^8$ yr ago. The merger is too old to directly trigger the AGN, but may have interrupted the previous AGN phase.

Chapter 4 investigates the broad nuclear absorption detected in the ATCA Centaurus A observations already described in Chapter 3. For the first time, blueshifted absorption, with respect to systemic, is detected against the core. Moreover, the data show that the redshifted absorption is broader than previously known. Our tilted-ring model (Chapter 3) shows that a large fraction of the absorption must originate from gas close to the central engine. Different arguments, and in particular a comparison with the molecular gas, suggest that the absorbing H I is located in a circumnuclear disk with $r < 120$ pc. No evidence is found for gas infall into the AGN.

Chapter 5 gives the H I analysis of the only powerful radio galaxy studied in this thesis, Cygnus A. Very Long Baseline Array (VLBA) observations show broad ($FWHM = 231$ km s^{-1}) absorption with high opacity against the counter-jet, low

opacity against the core and no absorption on the jet side. We argue that the absorption is most likely explained by a circumnuclear absorbing H I disk with $r = 80$ pc. The disk has a minimum gas density of $n > 10^4$ cm^{-3}. The torus in Cygnus A does not contain enough mass to trigger the AGN over the typical lifetime of an AGN ($> 10^7$ yr), yet the material in the outer H I absorbing disk can provide a reservoir to fuel the AGN. Also in Cygnus A we do not find evidence for direct gas infall onto the AGN.

Chapter 6 explores the origin of the H I in the massive early-type galaxy NGC 1167, which also hosts a low-power radio source. The kinematics of the 160 kpc size disk is dominated by rotation, but several signs of interaction and merging activity are present. This suggests that the H I is mainly brought-in by fairly massive satellite galaxies. The accretion of small gas clumps is not an important disk-building mechanism. The rotation curve shows a prominent bump at $r \approx 1.3 \times R_{25}$ which is due to large-scale streaming motions in the disk, possibly induced by a minor merger. A possible connection between large-scale streaming motions and H I density distribution in NGC 1167 and other galaxies is discussed.

Chapter 7 shows VLA data of the nuclear absorption that is present in NGC 1167 (Chapter 6). The absorption against the radio source B2 0258+35 is red- and blueshifted, with respect to systemic, suggesting that a circumnuclear disk (with $r < 170$ pc) exists. However, an additional outflow component must be present. The continuum image of the line data presented in Chapter 6 reveals the presence of a faint 240 kpc relic structure. This discovery is exciting because it shows that H I-rich radio galaxies can also host extended radio sources, a result missed in previous studies. It also shows that the presence of a large amount of cold gas is not a sufficient condition to confine a radio source – as previously suggested.

Chapter 8 provides a short summary of the results obtained from this thesis and gives a brief discussion of the main conclusions. Open questions and an outlook for future research lines finally close the chapter.

2 Large-scale H I structures in and around nearby radio galaxies

— based on —
C. Struve, R. Morganti, B. H. C. Emonts, T. A. Oosterloo. In preparation for publication in *M*NRAS
and
B. H. C. Emonts, R. Morganti, C. Struve, T. A. Oosterloo, G. van Moorsel, C. N. Tadhunter, J. M. van der Hulst, E. Brogt, N. Mirabel. 2010. *M*NRAS 406, 987

Abstract

An important open question regarding the evolution of radio galaxies is the role of cold gas. Galaxy mergers, satellite accretions and interactions are suspected to be among the mechanisms that can cause nuclear activity. This chapter investigates the H I environment in a sample of nearby low-power radio galaxies. The study aims at identifying companions and signs of interaction. The results are then compared to a sample of radio-quiet galaxies.

At a high significance level, we find no difference in the nearby environment ($r < 150$ kpc) between the radio-loud and the radio-quiet sample in terms of the average number of companions detected in H I; we neither find a difference for the fraction of targets that have at least one companion within the same volume. Moreover, at radii $150 < r < 300$ kpc there appears no statistically significant difference between the radio-loud and the radio-quiet samples in terms of the average number of companions or the fraction of targets having at least one companion. The average amount of H I gas detected in the environment (within $r < 300$ kpc) is similar in both samples and the companions show a similar radial distribution. Signs of disturbance are found in companions in both samples, hence, are not a distinguishing characteristic. The typical interaction timescale between the target and its companions can be up to $\sim 1 \times 10^9$ yr. Our results show that there is no significant difference in the environment

of radio-loud and radio-quiet galaxies. Hence, no evidence is found that show the vital importance of H I-rich interactions for the triggering of radio sources.

2.1 Introduction

Different mechanisms have been proposed to explain nuclear activity and, undoubtedly, a variety of them do occur in different classes of AGN. A brief summary of the proposed mechanisms has been given in Chapter 1. Among the proposed processes are galaxy mergers, collisions, satellite accretions and interactions, which can provide the gas masses that eventually provide the fuel to trigger the nuclear activity (e.g. Heckman et al., 1986; Wu et al., 1998; Canalizo & Stockton, 2001; Kuo et al., 2008). Besides a direct supply of gas, all these interaction processes can also perturb the host galaxy's potential such that gas inside the host is stired, looses angular momentum (due to cloud-cloud collisions) and gets channeled to the nuclear region where it can trigger the AGN. Gas accretion rates as low as $10^{-5} - 10^{-3}\ M_\odot\ \mathrm{yr}^{-1}$ (that is $M_{\mathrm{gas}}^{\mathrm{total}} < 10^5\ M_\odot$) may be sufficient to power an AGN (van Gorkom et al., 1989).

This is only a fraction of the gas content of many early-type galaxies. Deep observations show that many objects do have more than few $\times 10^6\ M_\odot$ of cold gas (e.g. Morganti et al., 2006). Thus, a direct exchange of gas between galaxies is not necessarily needed to switch on a quiescent black hole, whereas an interaction may be required to stir gas to the nuclear region.

One apparent possibility to investigate the importance of interactions is to search for indicative signs in the optical band, as done by several authors (see Sect. 2.2 for details). However, investigating the environment in this way yields several practical drawbacks. The FOV of optical telescopes is usually small, requiring large amounts of observing time to image the environment for every target. In addition, redshifts are required for every potential companion to ensure that they are also physically close to the target and not merely appearing so in projection.

Observations of neutral hydrogen have partly overcome these problems. The FOV of suitable radio interferometers is often large enough to image the environment with a single pointing; redshifts are simultaneously obtained. The greatest advantage of H I observations, however, is that it enables the identification of interactions between galaxies that have been missed in optical studies (e.g. Yun et al., 1994; Wilcots et al., 2001; Greene et al., 2004). This is because the H I structures often extend the optical host by a factor of a few (e.g. Broeils & van Woerden, 1994) and signs of disturbance are often still visible in the morphology and/or kinematics up to ~1 Gyr after the interaction has taken place (see Chapter 6 for an example). As a result, H I observations of nearby radio galaxies provide a powerful tool to investigate the properties of cold gas in and around radio galaxies and to study the importance of interactions triggering radio activity. A gas-rich environment, an enhanced number of companions (compared to radio-quiet galaxies) and signs of recent disturbance (timescale: few $\times 10^8$yr) in companion galaxies would suggest that interactions and the presence of cold gas play a vital role in triggering AGNs in low density environments.

In order to study the H I properties of classical low-power radio galaxies in a statistical manner, Emonts (2006) selected a suitable sample of nearby objects based on the B2 catalogue composed by Colla et al. (1970). We use this sample to investigate the H I environment of these specific radio galaxies. The aim is to determine whether radio galaxies tend to reside in environments with a high number of gas-rich companions and to search for indications of disturbances that might point towards recent interactions. As part of this thesis, we have performed follow-up observations for part of the B2 sample to get a more uniform sensitivity between different radio galaxy data sets. The initial observations (Emonts, 2006; Emonts et al., 2007) utilized different telescopes with varying bandwidths and sensitivity limits, hindering an analysis of the environment. The new data allow a more thorough study of the H I environment, even though it still has several drawbacks (see Sect. 2.3.4). The follow-up data were also used for the analysis of the radio galaxy properties themselves; the results are presented in Emonts et al. (2010) and summarized in this chapter.

The outline of this chapter is as follows: In Sect. 2.2 we give a brief summary of previous studies on the environment of radio galaxies. In Sect. 2.3 we introduce the radio galaxy sample and a radio-quiet comparison sample from the literature. A summary of the H I properties of the host galaxies is given in Sect. 2.4. Results of the H I environment study are presented in Sect. 2.5 followed by points of discussion, given in Sect. 2.6. We conclude with a short summary (Sect. 2.7). Throughout this chapter we assume $H_0 = 71\ \mathrm{km\,s^{-1}}\ \mathrm{Mpc^{-1}}$ (unless otherwise indicated).

2.2 Previous environment studies

The environment of low-power (FR-I type) as well as of more powerful (FR-II type) radio galaxies has been investigated in the optical band for more than 30 years. Seldner & Peebles (1978) found that radio galaxies (FR-I and FR-II) tend to reside among strongly clustered galaxies. However, there seems to be a difference at low redshifts between FR-I and FR-II sources in the sense that FR-II galaxies – on average – are located in less dense regions compared to FR-I galaxies (Longair & Seldner, 1979); this tendency has been confirmed by several other studies (e.g. Yates et al., 1989; Hill & Lilly, 1991; Zirbel, 1997). However, Prestage & Peacock (1988) noted that there is a large scatter in the environment of FR-I and FR-II galaxies, implying that other factors must be relevant as well. Moreover, at high redshifts, the situation might be different. The most powerful radio galaxies in the distant universe are located in overdense regions, are frequently surrounded by protoclusters and seem to be the progenitors of the brightest cluster galaxies in the local Universe (Miley & De Breuck, 2008). These findings stand in contrast to the results, which support the supposition that the local FR-IIs do not prefer to reside in dense clusters (see above). The effect of environment on the radio source structure is, therefore, far from clear.

In general signs of interactions depend on the environment. This complicates a systematic study of radio sources as they are found in a variety of environments. Nevertheless, several investigations have been performed, searching for disturbances (see Sect 2.1) in radio-loud galaxies. In a recent study, Ramos Almeida et al. (2010)

observed 46 powerful radio galaxies from the southern 2Jy sample (Tadhunter et al., 1993) and found that 85% of the objects show distorted morphologies: these findings hint at recent or still ongoing interactions. Most of these sources are FR-IIs; for the FR-Is in the sample the fraction is significantly lower (50%). However, Ramos Almeida et al. (2010) note that they might have missed signs of disturbance due to their relatively high limiting surface brightness. They conclude that (at least for some FR-Is) interactions and accretion/merging events could be important for triggering the current phase of nuclear activity.

A number of studies in the optical band have also investigated the environment of lower luminosity AGN (mainly Seyfert and LINERs), which are predominantly hosted by late-type galaxies. Overall, there does not seem to be a strong environment trend for Seyfert 1 and Seyfert 2 galaxies. However, Seyfert 2 galaxies may show a small excess of nearby companions with respect to Seyfert 1 and control samples (see, e.g., Monaco et al., 1994; Dultzin-Hacyan et al., 1999; Coziol et al., 2000; Koulouridis et al., 2006, and refs. therein). A difference between Seyfert 1 and Seyfert 2 galaxies would be surprising, given that the unification scheme of AGN (e.g. Antonucci, 1993; Urry & Padovani, 1995) predicts only orientational differences between these two classes (Chapter 1).

Relatively little work has focused on studying the H I environment of radio-loud galaxies; most studies to date have looked at Seyfert and LINER type of galaxies. Wilcots et al. (2001) and Greene et al. (2004) have found a number of cases in which the Seyfert galaxies show (in H I) signs of morphological or kinematic disturbance and/or nearby companions that sometimes have even been missed in the optical band. However, these authors conclude that the interaction features are not a distinguishing characteristic of AGN hosts.

Haan et al. (2008) studied in H I 16 nearby spiral galaxies hosting Seyferts and LINERs; they detected a number of companions in H I, but found no correlation between the presence of companions and the AGN type (Seyfert or LINER). Kuo et al. (2008) studied 23 Seyfert galaxies and found that in up to 94% of the cases the observed H I disturbances can be traced to tidal interactions with companion galaxies also detected in H I. This percentage is much higher than for their radio-quiet comparison sample (15%; Tang et al., 2008), suggesting that interactions play an important role for triggering black holes. Ho et al. (2008a,b) performed H I Arecibo observations of 113 (predominantly low-luminosity, Seyfert type) AGNs and concluded that the host galaxies of AGNs are at least as gas-rich as inactive galaxies and that among early-type galaxies the gas content is markedly enhanced. About 44% of the sources have H I profiles that are asymmetric or single peaked (or both) which is interpreted by Ho et al. as evidence for a recent or ongoing interaction with the environment. This fraction is higher than for non-active galaxies, however, this result is only marginal and requires confirmation.

One drawback of these previous studies is that they have focused on the search for direct signs of ongoing merging, accretion or interaction activity. The asymmetry (or skewness) of an integrated H I profile, for example, was used to infer a relation between interaction and nuclear activity (see e.g. Wilcots et al., 2001; Greene et al., 2004; Haan et al., 2008; Ho et al., 2008b). However, many ongoing interactions between galaxies have been observed without a (direct) onset of nuclear activity. The

relationship between mergers/interactions and nuclear activity is, therefore, far from clear. One possibility suggests that a significant time-delay between the occurrence of mergers/interactions and the turn-on of the black hole exists, which has been observed in some cases (e.g. Tadhunter et al., 2005; Emonts et al., 2006; Labiano et al., 2008), but this needs to be explored in more depth.

A second drawback of previous H I studies is that the analysis this far have been based only on H I detected host galaxies, so that no conclusions can be drawn for non-detected sources. In our study of low-power radio galaxies, we investigate the H I environment independent from the gas content of the radio galaxy itself, in order to get obtain a more complete picture (Sect. 2.5).

2.3 The sample

This section presents the radio-loud and the radio-quiet samples, defines the environment, gives a brief overview of companions detected in the optical band, and summarizes the follow-up observations on part of the radio-loud sample.

2.3.1 Sample properties

The sample of radio-loud galaxies was selected by Bjorn Emonts and further details can be found in Emonts (2006) and Emonts et al. (2010). In summary, the sample contains 21 (optically identified; Grueff & Vigotti, 1972) nearby low-power radio galaxies selected from the flux and distance limited ($F_{408\mathrm{MHz}} > 0.2$ Jy, $z \leq 0.041$) B2 catalogue published by Colla et al. (1970). This sample (hereafter called "B2 sample") is complete, with the exception that sources in *dense* clusters as well as BL-Lac objects have been omitted. Two additional sources (B2 1557+26 and NGC 3894) have been added to the sample to allow for a better comparison of sub-samples (see Emonts, 2006), but have been omitted in the overall statistical analysis. Of the total sample of 23 radio galaxies, eight have a compact radio source, while fifteen have an extended FR-I morphology (with 'compact' defined as not extending beyond the optical boundary of the host galaxy, typically ≤ 10 kpc).

All sources in the sample have a radio power of 22.0 W Hz^{-1} $\leq \log(P_{1.4\mathrm{GHz}}) \leq$ 24.8 W Hz^{-1}, while their host galaxies are classified a priori as early-type galaxies (except for the late-type galaxy B2 0722+30; Emonts et al., 2009). The basic properties of all 23 sample radio sources are given in Tab. 2.1. Please note that the sample does not include powerful FR-II sources, as they have higher power and are usually found at higher redshifts. In this chapter we use the B2 name for both the radio source and the host galaxy.

The number of suitable radio-quiet early-type galaxy samples that can be used for a comparison with the B2 targets is low. This is due to the fact that early-type galaxies used to be perceived to be gas poor. Hence, only very few observations have been performed in the past. Only in recent years has this changed; be now, neutral hydrogen has been detected in a significant fraction of early-type galaxies (e.g. Morganti et al., 2006; Oosterloo et al., 2007b). The best available sample for our purposes is a set of 20 local early-type galaxies (Morganti et al., 2006; Oosterloo et al.,

2010). These 20 sources are part of the SAURON representative survey selected to study stellar and gas properties in local early-type galaxies. The selection criteria for these 20 targets (hereafter called "SAURON sample") conditioned that they do not include galaxies located in dense clusters (see also Sect. 2.3.3). This sample is used in this comparison.

Both samples feature one common source, B2 1217+29 (NGC 4278), which has a radio power similar to the the lowest power B2 sources, but which is more than one order of magnitude stronger than the second strongest SAURON source. Since the aim is to compare radio-loud galaxies with radio-quiet targets, B2 1217+29 has been excluded from the SAURON sample and kept as part of the B2 sample.

2.3.2 Definition of environment

The typical duration of a radio-loud phase is $\leq 1{\times}10^8$ yr (see Chapter 1), so that AGN activity is only a relatively short-lived phenomenon during the evolution of the host galaxy. A possible connection between environment and AGN activity must therefore be of relatively local nature, since the interaction timescales would otherwise be too large. It therefore seems sufficient to investigate the surrounding neighbourhood on the few hundred kpc-scale around (radio) galaxies (where the interaction timescales are $< 1 \times 10^9$ yr), if the aim is to investigate the role of companions in the evolution of (early-type) galaxies and AGN activity.

Literature provides no common definition of what the environment of a galaxy is. Most studies to date define environment based on the boundary conditions of their observations. Almost all definitions are based on two parameters, the projected linear distance and the velocity offset between the target and the candidate companion. In studies at optical wavelengths, the FOV is often small so that e.g. Dultzin-Hacyan et al. (1999) and Koulouridis et al. (2006) defined all companions detected within 100 kpc from the target as environment. In H I observations of nearby Seyferts Wilcots et al. (2001) and Greene et al. (2004) defined the (local) environment to be within r = 160 kpc and r = 200 kpc, respectively. For the relative velocity offset between target and companion, $\Delta v \approx 600$ km s^{-1} is an often used value (e.g. Wilcots et al., 2001; Greene et al., 2004; Koulouridis et al., 2006). This velocity is motivated by the fact that it is about twice the mean pairwise galaxy velocity (when cluster galaxies are excluded) (Marzke et al., 1995).

The redshift of a target essentially determines how much of the environment can be observed in H I, using a single pointing, given the fact that the FOV of the telescope (determined by the primary beam) changes only slowly with redshift. Almost all B2 sources detected exhibit companions at projected distances of several hundred kpc from the target. However, for distances larger than 300 kpc, the interaction timescales become very large ($> 1 \times 10^9$ yr). We therefore define the maximum projected distance of a companion belonging to the environment of the target to be $r \leq 300$ kpc and require in addition $\Delta v \leq 600$ km s^{-1}, which is the value used in previous environment studies (see above).

The galaxies in the B2 sample have a range of redshifts ($0.016 < z < 0.041$), while the observing time also varies from target to target. This results in different sensitivity limits and different H I masses that can be detected. As a result, it is necessary

Table 2.1: *Radio galaxy properties.*

Source B2 name	Environment study?	other name	z	D (Mpc)	Opt. Mor.	log$P_{1.4\mathrm{GHz}}$ (W/Hz)	(ref.)	LS (kpc)	(ref.)	Type source
0034+25	x		0.0318	134	E	23.4	(3)	200	(5,9)	FR-I
0055+30	x	NGC 315	0.0165	70	E	24.2	(6)	1200	(10,14)	FR-I
0104+32	x	3C31	0.0169	71	S0	24.0	(7)	484	(9)	FR-I
0206+35	x		0.0377	159	E	24.8	(2)	69.9	(2,9)	FR-I
0222+36	x		0.0334	141	E	23.7	(4)	4.8	(5)	C
0258+35	x	NGC 1167	0.0165	70	S0	24.0	(4)	1.4	(11)	C
0326+39	x		0.0243	103	E†	24.2	(7)	202	(9)	FR-I
0331+39	x		0.0206	87	E	23.9	(2)	29.1	(2,9)	FR-I
0648+27	x		0.0412	174	S0	23.7	(4)	1.3	(13)	C
0722+30	x		0.0189	80	S	23.0	(4)	13.6	(2,9)	FR-I
0924+30	-		0.0253	107	E†	23.8	(7)	435	(9)	FR-I
1040+31	x		0.036	152	DB†	24.3	(2)	40.3	(2,9)	FR-I
1108+27	-	NGC 3563	0.0331	140	S0	23.3	(2)	1085	(9)	FR-I
1122+39	-	NGC 3665	0.0069	29	S0	22.0	(5)	10.7	(2,9)	C
1217+29	x	NGC 4278	0.0022	16.1[1]	E	22.2	(6)	0.009	(12)	C
1321+31	-	NGC 5127	0.0162	68	E pec	23.9	(7)	246	(9)	FR-I
1322+36	-	NGC 5141	0.0174	73	S0	23.7	(2)	19.1	(2,9)	FR-I
1447+27	x		0.0306	129	S0	23.6	(6)	<2.3	(3)	C
1658+30	x	4C 30.31	0.0344	145	E	24.2	(3)	114	(5,9)	FR-I
2116+26	x	NGC 7052	0.0156	66	E	22.7	(2)	291	(9)	FR-I
2229+39	x	3C 449	0.0171	72	E†	24.4	(8)	473	(9)	FR-I
1557+26	-		0.0442	187	E	23.1	(2)	∼2	(2)	C
-	-	NGC 3894	0.0108	46	E	23.0	(6)	1.6	(14)	C

Notes – The distance D (col. 5) to the radio galaxy and the linear size of the radio source (LS – col. 9) have been determined from the redshift (z – col. 4) and $H_0 = 71$ km s^{-1} Mpc^{-1} (unless otherwise indicated). Redshifts and optical morphology are based on results from the NASA/IPAC Extragalactic Database (NED), unless otherwise indicated. †Information taken from Burbidge & Crowne (1979). *Refs: 1.* Tonry et al. (2001), *2.* Parma et al. (1986), *3.* de Ruiter et al. (1986), *4.* Fanti et al. (1986), *5.* Fanti et al. (1987), *6.* White & Becker (1992), *7.* Ekers et al. (1981), *8.* Laing & Peacock (1980), *9.* Emonts et al. (2010), *10.* Morganti et al. (2009), *11.* Giroletti et al. (2005), *12.* Wilkinson et al. (1998), *13.* Morganti et al. (2003), *14.*. Taylor et al. (1998), Bridle et al. (1979).

to introduce a mass cut-off for the statistical study that is as low as possible yet high enough to ensure that no companions are missed due to insufficient S/N in some of the data sets. We choose a mass cut-off of $M_{\rm HI} = 2 \times 10^8\ M_\odot$, which allows to investigate the H I environment in 16 B2 sources (marked in Tab. 2.1). This mass cut-off is high enough to be able to detect a companion with this mass in the defined environment (see also Sect. 2.3.5) in all 16 B2 data sets. That is, for all targets we are sensitive enough to detect a companion at $r = 300$ kpc with $M_{\rm HI} = 2 \times 10^8\ M_\odot$. The varying mass sensitivity across the primary beam is therefore taken care of. It is not possible to use a lower mass cut-off value because it would reduce the number of targets in which the environment can be investigated. It is therefore important to keep in mind that the study includes only fairly H I-rich companions. All 19 SAURON targets are very nearby objects and have a sensitiviy limit well below the mass cut-off at $r \leq 300$ kpc.

In the appendix we list all companions of the B2 and the SAURON targets that are part of our environment definition (Tab. 2.8 and 2.9); total intensity maps of the environment of the B2 sources are also shown in the chapter's appendix.

2.3.3 Companions detected in the optical band

The majority of the 16 B2 sources are field galaxies. There is no homogeneous data set with redshift information about potential companions detected in the optical band. A literature search using NED shows that four B2 sources used for the environment study (B2 0055+30, B2 0104+32, B2 0206+35 and B2 2229+39) are not field galaxies but Zwicky cluster members, thus residing in an environment with an increased galaxy density. We note, however, that none of the galaxies lives in a *dense* (Abell type) cluster; such sources have been excluded from the sample (Emonts, 2006). The literature search showed that another six B2 sources have at least one or two companions, while the remaining six B2 targets do not have any known companions. This suggests that the radio galaxies live in a variety of environments – from isolated field galaxies to loose cluster environments.

The SAURON galaxies have also been selected as field galaxies and are therefore not located in a cluster environment. Nevertheless, more than 58% of the targets show at least one companion and are therefore not isolated galaxies. Based on this comparison, it seems that the environment of B2 and SAURON galaxies is similar, with the exception that four B2 sources reside in denser regions, compared to the SAURON and the remaining B2 sources.

2.3.4 Limitations of the sample

In the ideal case, one would like to have a large sample with uniform mass sensitivity across the different data sets at $r = 300$ kpc and a bandwidth covering more than $\Delta v = 1200\ \mathrm{km\,s^{-1}}$. Unfortunately, this is not the case for our B2 sample, which is nevertheless the best available sample to study the H I environment. The radio galaxies (originally selected by Emonts, 2006, to study the H I content of the host galaxies) span a range in redshift making it impossible to detect all targets to the same mass sensitivity. Our follow-up observations (see Sect. 2.3.5) aimed at getting

a more uniform mass sensitivity across the sample, but a spread in mass sensitivity remains such that we have to impose the mass cut-off value (Sect. 2.3.2) to allow for a fair comparison.

There are further limitiations: both, the B2 sample (16 targets) and the SAURON sample (19 targets) are based on small numbers so that the presence (or absence) of one or two companions can already have an impact on the analysis. We therefore note that all results from our analysis have to be taken with care. Where possible, errorbars indicate what the effect of one additional object (or one less) would be.

The data sets of one B2 source and two SAURON sources show a number of velocity channels that cannot be used for the environment study because of either strong RFI or galactic foreground emission/absorption. However, it is probable that these missing velocity channels do not alter our analysis/results since the missing volume is relatively small compared to the overall sample size. A more severe limitation is that the data cubes of some sources are smaller than the desirable 300 kpc. The maximum cube size created to investigate the environment is 70′, which is approximately twice the primary beam size. Making even larger cubes is not feasible since the sensitivity at $r > 35'$ is too low to reliably detect companions in most cases. As a consequence, for part of the target galaxies (which have very low redshifts) not the entire environment can be imaged. This is in particular the case for some of the SAURON galaxies, where cubes with a radius of 300 kpc can only be made for ten objects. Eleven cubes are at least 250 kpc, 14 cubes 200 kpc in size (in radius). All 19 cubes have a radius of at least 150 kpc. In the B2 sample, the B2 0722+30 cube (167 kpc in radius) is smaller than the desirable 300 kpc. In all cases with insufficient cube sizes, the environment has been considered only in radial bins extending to the size of the corresponding cube (i.e. B2 0722+30 out to 150 kpc). In Tab. 2.6 and 2.7 of the appendix we summarize the cube sizes, the available velocity ranges and the detection limits for individual data cubes. We note once more that in all cubes we are sensitive to H I masses of at least the cut-off value.

Before investigating the environment and starting a comparison between radio-loud and radio-quiet galaxies attention has to be drawn to intrinsic differences between both samples. Figure 2.1 shows the optical morphological class. In the B2 sample, the fraction of ellipticals is considerably larger when compared to the SAURON sample, but the S0 fraction is therefore 30% lower. The two B2 sources classified as S and DB are not expected to change the overall conclusions.

One difference between both samples is that on average the SAURON galaxies have a higher absolute *B*-band magnitude and are therefore potentially less massive (see Fig. 2.2). This could be an important difference, since the fraction of radio-loud galaxies is a strong function of stellar mass, in the sense that the probability for a radio-loud phase is higher for more massive galaxies (Best et al., 2005). Moreover, the radio luminosity also increases with increasing stellar mass. That is, the most powerful radio sources are found in the most massive host galaxies. Based on this result, it would be preferable to compare radio-loud and radio-quiet galaxies that have similar stellar mass. However, the available samples are of too small size to create sub-samples that match in magnitude/stellar mass, which would still allow a statistical comparison. Note, however, that B2 1217+29 (NGC 4278) has an absolute optical magnitude comparable to the highest absolute magnitudes of the SAURON

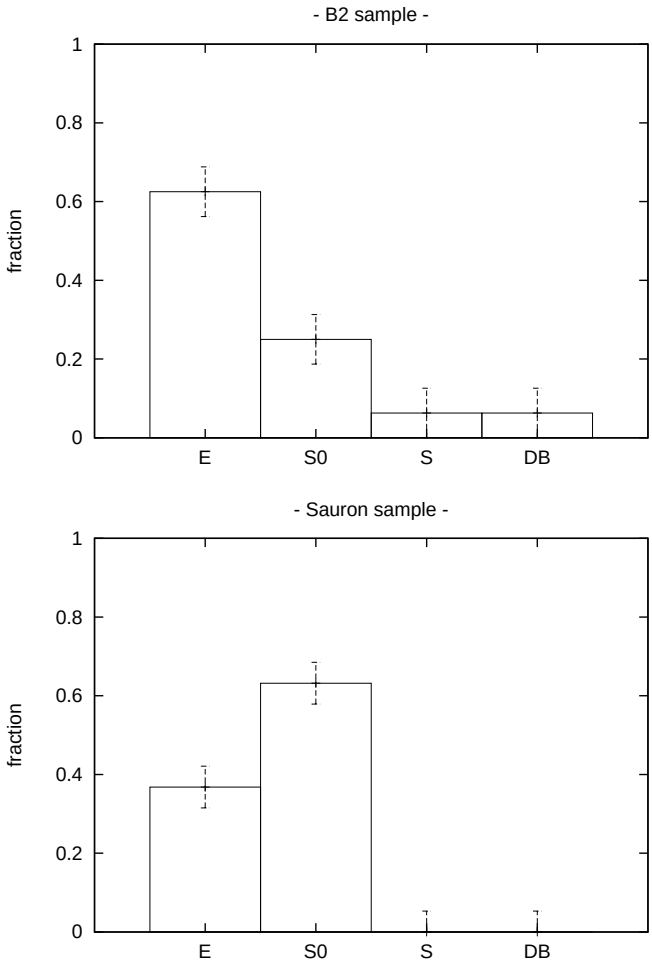

Figure 2.1: *Histogram of the optical morphological type (information taken from NED and Burbidge & Crowne (1979)). Left panel: B2 sample, right panel: SAURON sample. The error-bar shows by how much the fraction would change if one galaxy would be added/subtracted.*

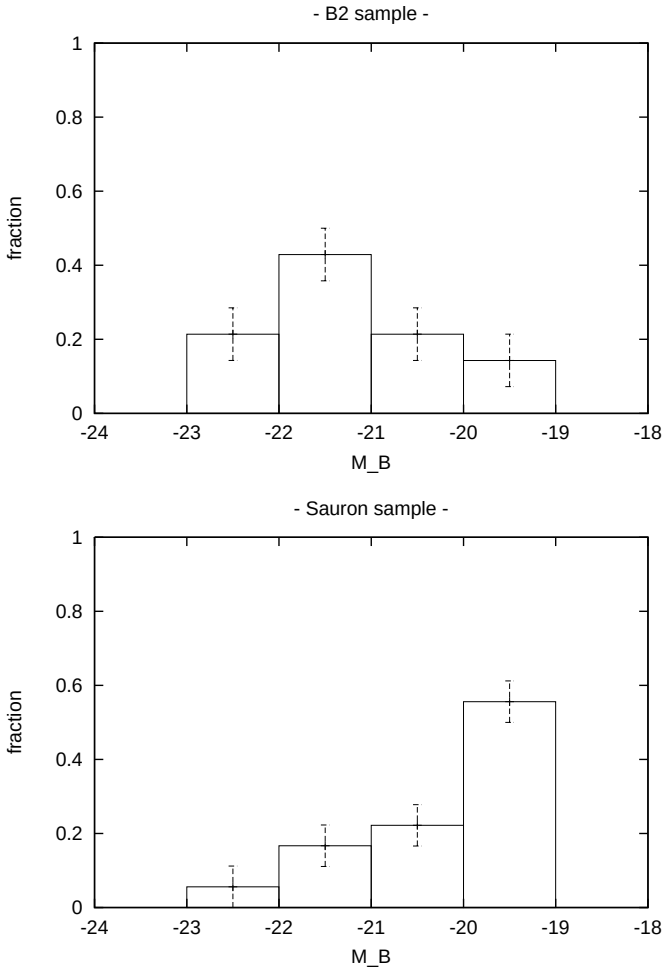

Figure 2.2: *Histogram of the absolute B-band magnitude. Left panel: B2 sample, right panel: SAURON sample. The errorbar shows by how much the fraction would change if one galaxy would be added/subtracted.*

targets. Hence, all the SAURON galaxies are expected to be able, in principle, to experience a radio-loud phase of similar radio power (i.e. $P_{1.4\mathrm{GHz}} > 10^{22}$ W Hz^{-1}).

Terminology: In the remainder of this chapter we refer to the B2 and SAURON galaxies as the *"targets"* and to the (additionally) detected H I sources as *"companions"* that are located in the *"environment"*. Our terminology does not necessarily imply that a "companion" is less massive than the "target", even though this will often be the case.

2.3.5 Observations and follow-up

Radio-loud (B2) sample

The initial observations aimed at detecting H I in radio galaxies and yield seven detections in emission in 22 observed sources (see Emonts, 2006; Emonts et al., 2007, 2010). Because of different telescopes (WSRT and VLA) and different amounts of observing time in various observing runs, follow-up observations of the initial data sets (Emonts, 2006) have been performed with the WSRT between August 2007 and November 2008. The aim has been to detect H I in radio galaxies and their environments and to significantly lower the upper H I mass limits in case of non-detections. Re-observing eight previously non-detected radio galaxies (B2 0034+25, B2 0104+32, B2 0206+35, B2 0222+36, B2 0326+39, B2 0331+39, B2 2116+26 and B2 2229+39), a more uniform sensitivity throughout the sample was attained. B2 1658+30 was also observed as it had been omitted in the original analysis of Emonts (2006), due to the poor quality of the previous VLA data. In addition, new, deep WSRT observations of B2 0258+35 (NGC 1167, see Chapter 6) have been undertaken; all ten new observations were performed using 20 MHz bandwidth with 1024 channels and two IFs; details of the follow-up observations are given in Tab. 2.2.

The data reduction has been performed using the MIRIAD data reduction software (Sault et al., 1995). After flagging, a standard bandpass and phase calibration has been performed on the data. Further, a self-calibration of the continuum has been performed and the solutions then applied to the uv-data. The continuum model has been subtracted from the line data by making a second order (third order for B2 0258+35) fit to the line-free channels of each visibility record. After subtracting the fit from the spectrum, the signal was cleaned using the CLARK algorithm, after applying a Fourier transformation to the uv-data.

Although continuum images are not shown here, they are very similar to the ones presented in Emonts (2006); the radio source structures and fluxes agree with (better suited, broader band) continuum observations in the literature (Parma et al., 1986; de Ruiter et al., 1986; Fanti et al., 1986, 1987). Uniform weighting has been used to study H I in absorption against the radio continuum, while robust weighting (Briggs, 1995) provides the best sensitivity to trace H I in emission. Table 2.3 gives an overview of the properties of the ten new data sets.

The new observations significantly lower the upper H I mass limits for the non-detected radio galaxies. However, with the exception of the previously detected source B2 0258+35, none of the follow-up targets showed H I in emission directly

Table 2.2: *WSRT follow-up observations.*

B2 Source	Obs. date(s) (dd/mm/yy)	t_{obs} (hrs)
0034+25	09+11/08/07	24
0104+32	23+29/08/07	24
0206+35	22/08/07; 11/09/07	31[b]
0222+36	12+13/09/07	24
0258+35[a]	22/10/06;12/07/08; 19/08/08;26+29/09/08; 01+02+07+10/10/08; 07+12+17/11/08	107
0326+39	17+18/09/07	24
0331+39	19+20/09/07	30[b]
1658+30	03+04/08/07	24
2116+26	01+07/08/07	24
2229+39	08+10/08/07	24

Notes – a) Data presented and analyzed in detail in Chapter 6. b) Observing time includes data from previous observing runs.

associated with the source. The results of the new observations (including the upper limits) are summarized in Tab. 2.4, details can be found in Emonts et al. (2010).

Radio-quiet (SAURON) sample

For the SAURON sources, data cubes presented in Morganti et al. (2006) and Oosterloo et al. (2010) have been used. All sources have been observed with the WSRT and 20 MHz bandwidth, allowing to investigate the environment in the desired way. For some data sets, we have taken the calibrated data and made larger data cubes, in order to be able to study the environment out to 300 kpc (or as far as feasible). Companions have been identified and catalogued for all 19 cubes; detail can be taken from the description provided below.

Companions

In principle, the requirement for a target or a companion to be considered as a legitimate detection is that the signal is above 3σ in three consecutive channels. In addition, all cubes have been visually inspected to avoid any false detections. In practise, most B2 data cubes have a detection limit below $1 \times 10^8\ M_\odot$, so that we are confident that no false detections above $2 \times 10^8\ M_\odot$ have been mistakenly included, which would have an influence on our statistics. Neither we expect to have missed any companions, whose absence would alter our analysis. All SAURON sources are

Table 2.3: *Properties of the new* H I *data.*

Source	Δv	Uniform – absorption			Robust/Natural – emission			
B2 name	(km/s)	(1)	(2)	(3)	(1)	(2)	(3)	(4)
0034+25	16.5	0.43	26.2×11.8	(-1.0)	0.22	44.6×25.6	(-2.7)	+2
0104+32	16.5	0.41	22.2×14.3	(17.2)	0.20	40.0×26.7	(3.4)	+2
0206+35	16.5	0.34	21.4×11.9	(9.2)	0.16	42.2×24.7	(8.6)	+2
0222+36	16.5	0.43	16.7×15.6	(39.2)	0.22	35.0×30.4	(23.4)	+2
0258+35	16.5	-	-	-	0.13	28.9×16.8	(1.5)	+0.4
0326+39	16.5	0.39	19.2×13.4	(2.4)	0.19	38.1×26.8	(-1.2)	+2
0331+39	16.5	0.37	17.5×14.7	(-11.1)	0.18	38.7×24.9	(1.3)	+2
1658+30	16.5	0.39	23.8×12.6	(1.9)	0.20	41.8×24.6	(1.3)	+2
2116+26	16.5	0.38	25.2×12.6	(-3.4)	0.19	45.3×24.6	(-1.7)	+2
2229+39	16.5	0.38	18.7×13.2	(1.5)	0.19	35.6×25.9	(-2.4)	+2

Notes – Δv = channel separation; (1) = noise level (mJy beam^{-1}); (2) = beam-size (arcsec^2); (3) = position angle (°); (4) robustness parameter.

close-by objects that have a detection limit well below the chosen mass cut-off.

Total H I images have been obtained by smoothing the data to lower resolution and by using the smoothed cube to create a mask (blanking all signal below $+3\sigma_{\rm rms}$ in the smoothed cube) that is then applied to the original cube. Figure 2.A shows the total intensity images of all 16 B2 sample sources and their companions. Tables 2.8 and 2.9 list all companions of the B2 and SAURON targets. All H I masses and contour levels given are corrected for the primary beam attenuation. Note that only the companions that are included in our environment definition have been listed. In the data cubes, additional galaxies are detected outside the required volume and/or with H I masses below $2 \times 10^8\ M_\odot$. That is to say that there is certainly more H I in the environment (of B2 and SAURON targets) than can be considered in our analysis (see also Sect. 2.6).

2.4 Summary of the H I properties of the radio-loud sample

Before investigating the H I environment of the radio galaxies, a brief summary of the H I properties of the radio galaxies is provided. The results of this study provide – for the first time – a systematic insight into the properties of cold gas in nearby, low-power radio galaxies. A full analysis is given in Emonts et al. (2010); initial results have been presented by Emonts (2006) and Emonts et al. (2007). The follow-up observations of ten out of 23 targets represent an integral part of the study and has led to a more uniform sensitivity throughout the sample, significantly lowering the upper H I mass limits (typically by a factor of three or more).

Table 2.4: H I *emission and absorption results of new* H I *data.*

Source B2 name	H I emission	H I mass ($\times 10^8 M_\odot$)	H I absorption	τ (%)	$N_{\rm HI}$ ($T_{\rm spin}$ = 100K) $\times 10^{20}$ cm^{-2}
0034+25	-	<1.6	-	<8.7	<16
0104+32	-	<0.41	-	<0.3	<0.6
0206+35	-	<1.6	-	<0.3	<0.5
0222+36	-	<1.8	(+)	1.0	1.0
0258+35	+	180	+	0.23	1.2
0326+39	-	<0.82	-	<1.5	<2.8
0331+39	-	<0.55	-	<0.2	<0.3
1658+30	-	< 1.7	-	<1.3	<2.3
2116+26	-	<0.34	-	<1.3	<2.4
2229+39	-	<0.40	-	<0.7	<1.2

Notes – '+' = detection, '(+)' = tentative detection, '-' = non-detection.

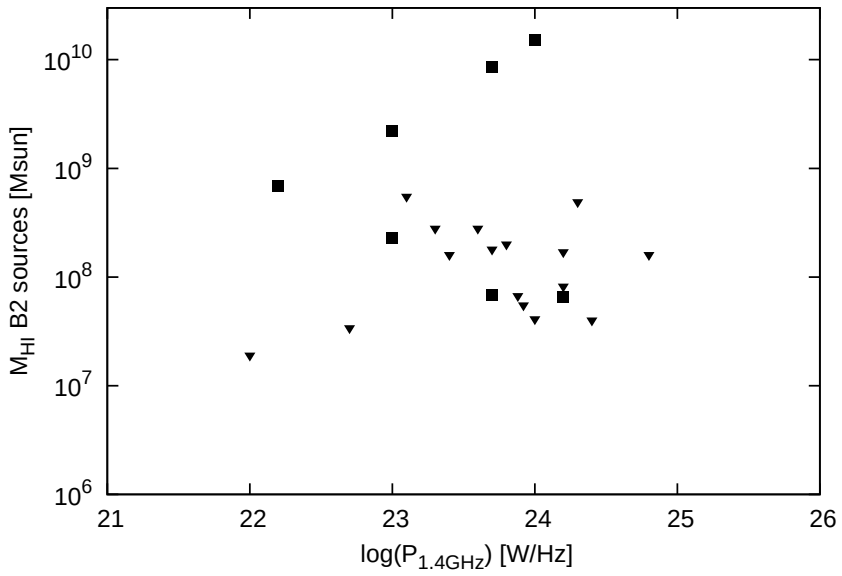

Figure 2.3: H I *mass of the source vs. radio luminosity for the complete B2 sample (including B2 1557+26 and NGC 3894). Filled squares show the detections, filled triangles the upper* H I *mass limits.*

H I emission

H I emission has been detected in seven of altogether 23 sample galaxies. When taking into account only the complete sample (i.e. without B2 1557+26 and NGC 3894; Sect. 2.3.1), the detection rate is 29%. Figure 2.3 shows the H I emission mass or the upper limit for the entire sample.

For five of the seven detections in emission (B2 0258+35, B2 0648+27, B2 0722+30, B2 1217+29 and NGC 3894) the H I gas is distributed in a regularly rotating disk- or ring-like structure with a mass of a few $\times 10^8 - 10^{10}\ M_\odot$ and a diameter of several tens to hundreds of kpc. For two radio galaxies (B2 0055+30 and B2 1322+36), patchy H I emission is observed, but the total mass associated with it is comparable to the upper limits derived for the non-detections. Since B2 0055+30 and B2 1322+36 are in the lower part of the redshift range of sample sources (Tab. 2.1), it is possible that sensitivity issues limit finding similar patchy, low-mass H I emission in the higher redshift sources in our sample.

One intriguing result from the H I study is that galaxies with large amounts of extended H I ($M_{\rm HI} \gtrsim 10^9 M_\odot$) all have a *compact* radio source, while none of the host galaxies of the more extended FR-I type radio sources show similar amounts of H I (but in Chapter 7 we are presenting the discovery of a relic structure around one of these compact radio sources). This segregation in large-scale H I content between compact sources and extended FR-I sources led Emonts et al. (2007) to suggest that there is a physical link between the properties of the central radio source and the large-scale properties of the ISM (see their paper for details).

H I absorption

H I absorption is unambiguously detected against the radio continuum of six of the sample sources (B2 0055+30, B2 0258+35, B2 0648+27, B2 0722+30, B2 1322+36 and NGC 3894), while another three show tentative evidence for absorption (B2 0222+36, B2 1321+31 and B2 1447+27), which has to be confirmed with additional observations. All sources for which H I has been detected in emission also show unambiguous H I absorption, with the exception of B2 1217+29. For all nine sources that show (tentative) absorption, an H I absorption is seen against the central region of the galaxy. The detection rate of H I absorption in our complete sample is therefore 24 – 38% (depending on whether or not the three tentative detections are included). For the compact sources and extended FR-I sources, the detection rates are 33 – 67% and 20 – 27% respectively (again, depending on whether or not the tentative detections are included). Table 2.4 lists the optical depth and column density of the absorption features for the followed-up sources.

Many of the H I absorption profiles within the sample are resolved in velocity and show both blue- and redshifted components, consistent with what is frequently observed in compact radio sources (Vermeulen et al., 2003; Pihlström et al., 2003; Gupta et al., 2006). In contrast to the H I emission results, there is no clear trend between radio source size and the presence of H I absorption. It is important to note however that the strength of the underlying radio continuum is an important selection effect

that can influence the absorption results: gas with a given column density is more easily detected against a strong continuum source. Moreover, only the gas in front of the radio source can be detected in absorption (gas located behind the source is not observed), such that the geometry of the absorbing gas is an important factor as well.

All galaxies in the sample that are unambiguously detected in absorption, also show H I emission-line structures at the same velocity. In fact, B2 1217+29 is the only galaxy that is detected in emission but not in absorption. The remaining three H I absorption systems show only tentative detections. *This strongly suggests that at least a significant fraction of the* H I *gas in many nearby absorption systems is part of gaseous structures on scales larger than just the (circum-) nuclear region.*

H I characteristics

The H I morphology in our radio sample sources show a trend in the sense that toward the high-mass end, all H I structures are fairly regularly rotating disks/rings, similar to the findings for radio-quiet early-type galaxies (e.g. Oosterloo et al., 2007b, 2010). Only two H I detections at the low-mass end (several $\times 10^7\ M_\odot$) appear much more irregular/clumpy. However, this can be due to an observational bias because regular rotating disks with H I masses of several $\times 10^7\ M_\odot$ would have too low H I column density to be detectable. The regular kinematics of the large-scale H I disks/rings suggest that the gas is either settled or in the process of settling. The sizes of these large-scale H I structures vary significantly from object to object (15 to 190 kpc) and their optical host galaxies show a range of morphologies. Following is a brief summary of the implications regarding the physical processes that may have formed the H I structures. This provides information about the evolutionary history of the host galaxy.

There is no clear evidence for *ongoing* gas-rich major mergers (i.e. mergers between galaxies with roughly equal mass) – in the form of long gaseous tidal tails or bridges of H I gas – among the sample sources. However, Emonts et al. (2006) have shown that B2 0648+27 is the result of a recent major merger that took place roughly 1.5 Gyr ago. Despite the sign that the H I kinematics is dominated by rotation, all four additional sources with $M_{\rm HI} \gtrsim 10^9\ M_\odot$ show hints of recent or ongoing interactions with the environment: B2 0258+35 shows various signs of interaction and accretion activity (for details, see Chapter 6), B2 0722+30 is likely undergoing a gas-rich interaction (Emonts et al., 2009), B2 1217+29 shows two prominent tails suggesting that the system is currently accreting gas (see Morganti et al., 2006), and the H I ring of NGC 3894 is distorted at the location towards a nearby companion galaxy. The patchy H I emission in B2 0055+30 (see Morganti et al., 2009) and B2 1322+36 can also be the result of accretion of small companion galaxies. The accretion of cold gas – likely over long timescales – may be a common feature among field early-type galaxies (see SAURON study by Oosterloo et al., 2010).

A possible alternative for (radio) galaxies to acquire cold gas, besides through mergers and interactions, is the slow accretion of small gas clumps from the IGM (see

Table 2.5: H I *detection rates of the various samples of early-type galaxies.*

	B2	SAURON (field sample)	HIPASS
# galaxies	21*	20	818
detection limit ($M_\odot$)	few $\times 10^8$	few $\times 10^6$	$\sim 10^9$
detection rate (%)	29	70	9†
% with $M_{\rm HI} > 10^9 M_\odot$	10	10	9†
% with $M_{\rm HI} \gtrsim 10^8 M_\odot$	29	35	-

Note – * Complete B2 sample, does not include NGC 3894 and B2 1557+26 (see Sect. 2.3.1).
† From Sadler et al. (in prep.); for early results see Sadler (2001).

Chapter 1). However, in most data sets, the sensitivity necessary to investigate this possibility in detail is missing. In the one case where we do have deep observations (B2 0258+35 [NGC 1167]), there is no evidence supporting the occurrence of this mechanism (Chapter 6).

Comparison with radio-quiet early-type galaxies

We can compare the gas content of the B2 sample with radio-quiet comparison samples. The SAURON sample (Morganti et al., 2006; Oosterloo et al., 2010, see also Sect. 2.3.5) is one of them. A second study by Oosterloo et al. (2007b) involves follow-up imaging of H I in early-type galaxies detected by Sadler (2001) in the single-dish H I Parkes All-Sky Survey (HIPASS; Barnes et al., 2001; Meyer et al., 2004).

Table 2.5 summarises both the H I detection limits and the H I detection rates of the B2, SAURON and HIPASS samples. There is a substantial difference in sensitivity between the three samples, which makes a comparison of the H I detection rates difficult. Nevertheless, looking at the high-mass end, the percentage of sample sources with $M_{\rm HI} \gtrsim 10^9 M_\odot$ is roughly the same for the three samples. Towards the low-mass end, the percentage of radio-quiet galaxies in the SAURON field sample with $M_{\rm HI} \gtrsim 10^8 M_\odot$ is also very similar to that of the B2 sample of radio-loud galaxies.

Thus – as far as can be concluded from the limited comparison between the three systematic studies – there appears to be no major difference in both H I detection rate and H I morphology between the radio-quiet and radio-loud early-type galaxies. Certainly, across the range of masses studied, there is no evidence that the radio-loud sample has a higher content of large-scale H I gas (see Tab. 2.5) or contains more tidally distorted H I structures than the radio-quieter samples.

Conclusions

Our H I work suggests that minor merging and interaction events could play a role in the triggering process in *some* sources, but one must take into consideration that most radio galaxies are not detected in H I. The lack of detectable amounts of H I is in agreement with the growing evidence that many low-power AGN are *not* associated with galaxy mergers or interactions that involve significant amounts of cold gas. Our H I results provide – for the first time systematically – *direct* evidence for this. This suggests that, in particular, extended (FR-I type) radio sources could be fed through a quasi-spherical accretion of hot gas from the galaxy's halo or IGM (Best et al., 2006; Allen et al., 2006; Balmaverde et al., 2008). For compact radio sources, the feeding mechanism remains ambiguous (see Emonts et al., 2007, 2010): the H I detection rate is higher (44% compared to 13%) and hence, the accretion of cold gas may play a more decisive role for the triggering than for the FR-Is.

2.5 The H I environment: Results

The aim of this section is to provide a statistical study of the H I that is located in the environment of classical low-power radio galaxies. In the 16 B2 data cubes used for the environment study (marked in Tab. 2.1), we detect a total of 23 H I companions that fulfil the environment definition ($M_{\rm HI} \geq 2 \times 10^8\ M_\odot$, $D < 300$ kpc from target and $|\Delta v| < 600\ {\rm km\,s^{-1}}$). For the 19 SAURON galaxies, 16 companions that belong to the defined environment have been identified. The H I properties of the B2 and SAURON companions are listed in Tab. 2.8 and 2.9; total intensity maps of the H I environment of B2 sources are shown in the appendix at the end of this chapter.

Figure 2.4 shows the average number of *all* companions within a certain radius from the target. In this plot, as well as in the following ones, we have corrected for the fact that some of the SAURON data cubes (and the cube of B2 0722+30) are smaller than the desirable 300 kpc in the following way: First, the average number of companions for each radial bin has been calculated by dividing the number of detected companions (in that bin) by the number of cubes that have a size larger or equal to the bin. In a second step, the average number of companions found for bins at smaller radii have been added to the average number of the radial bin of interest (i.e. the plotted number in Fig. 2.4 is the cumulative average number of companions).

For $r < 150$ kpc, that is for a radius where all B2 and SAURON cubes are large enough, there is *no* indication of differences between the radio-loud and radio-quiet samples (Fig. 2.4) at the 98% significance level (when applying a Mann-Whitney U-Test). That is, B2 galaxies have – on average – the same number of companions as the SAURON targets (≈0.51); thus, no difference exists between the two samples in the close environment. At larger radii, $150 < r < 300$ kpc, slightly more companions around B2 targets have been detected, although this is statistically not significant. Applying again the Mann-Whitney U-Test (considering only cubes with size $r = 300$ kpc), gives a probability of 69% ($\approx 1\sigma$) for an increase in the average number

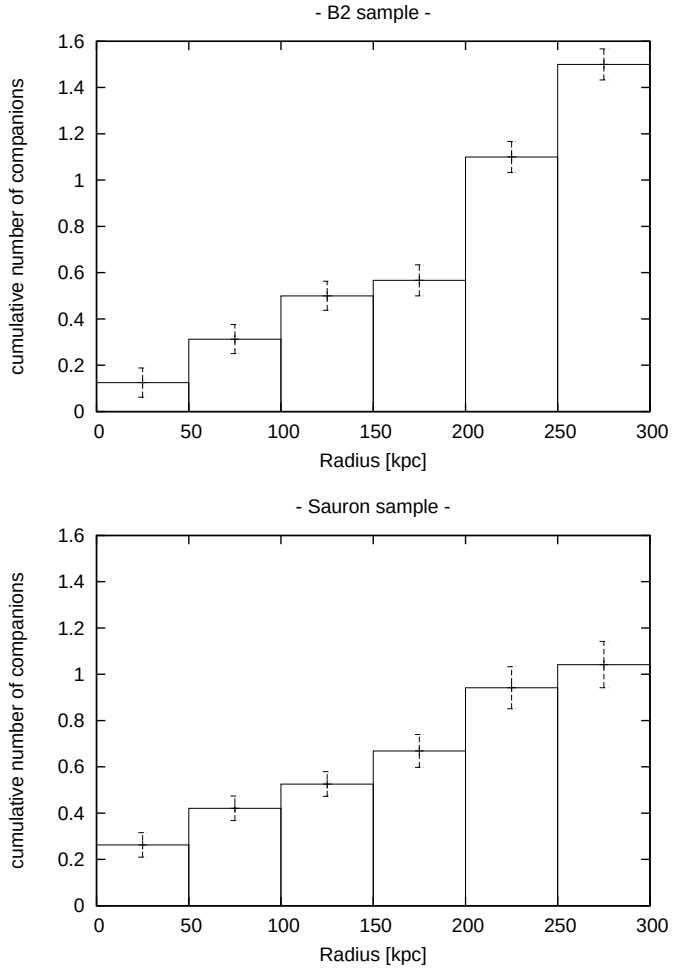

Figure 2.4: *Histogram of the cumulative average number of companions. Top panel: B2 sample. Bottom panel: SAURON sample.*

of B2 companions, in comparison to the SAURON sample. As a result, the data is consistent in that no statistically significant difference is found between the two samples for $r < 300$ kpc in terms of the average number of companions.

Similar results are found when investigating the fraction of targets that have at least one companion within a given radius (Fig. 2.5). Also, at the 98% significance level, no difference is found between the two samples for $r < 150$ kpc. This means that B2 galaxies have as often at least one companion as SAURON targets (≈31%). At larger radii, 78% of the B2 targets have at least one companion, whereas only 37% of the SAURON galaxies show a companion. Taking again only data sets with cubes reaching 300 kpc, the significance level of B2 having more often at least one compan-

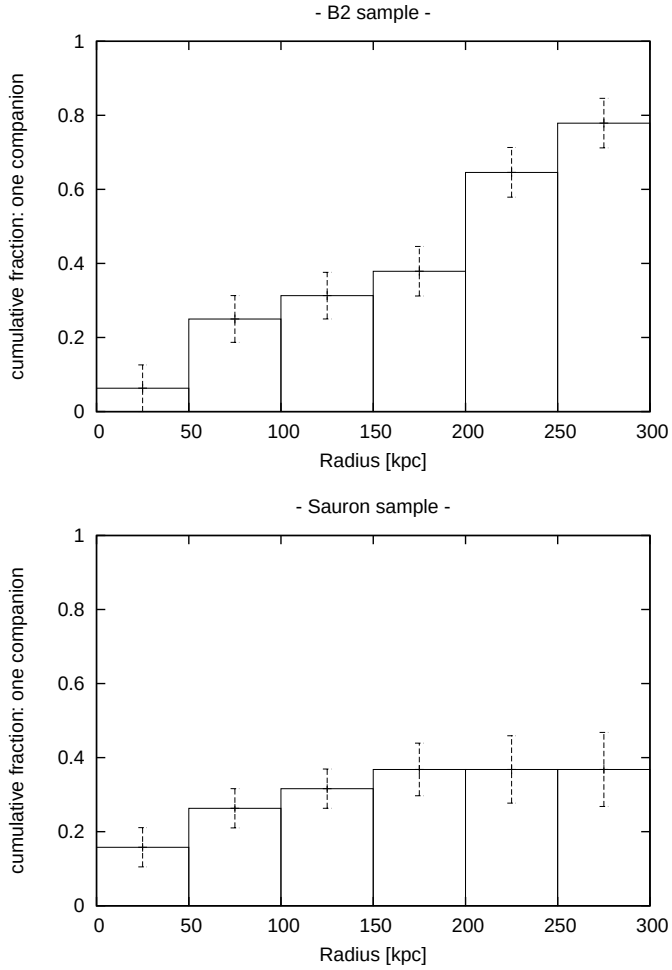

Figure 2.5: *Histogram of the cumulative fraction that the target has at least one companion. Top panel: B2 sample. Bottom panel: SAURON sample.*

ion (compared to SAURON targets) is again only $\approx 1\sigma$ (76%). Hence, our data are consistent with showing no statistically significant difference between the samples.

The main result of this study is that in our defined environment, no significant difference between radio-loud and radio-quiet sources is found in terms of the number of companions present.

A second interesting question, in addition to the number of companions around the targets, is whether the sample sources reside in particular gas-rich or gas-poor environments. Figure 2.6 shows the average H I mass in the environment of the sample sources. At a first glance, the SAURON targets seem to reside in an H I-richer neigh-

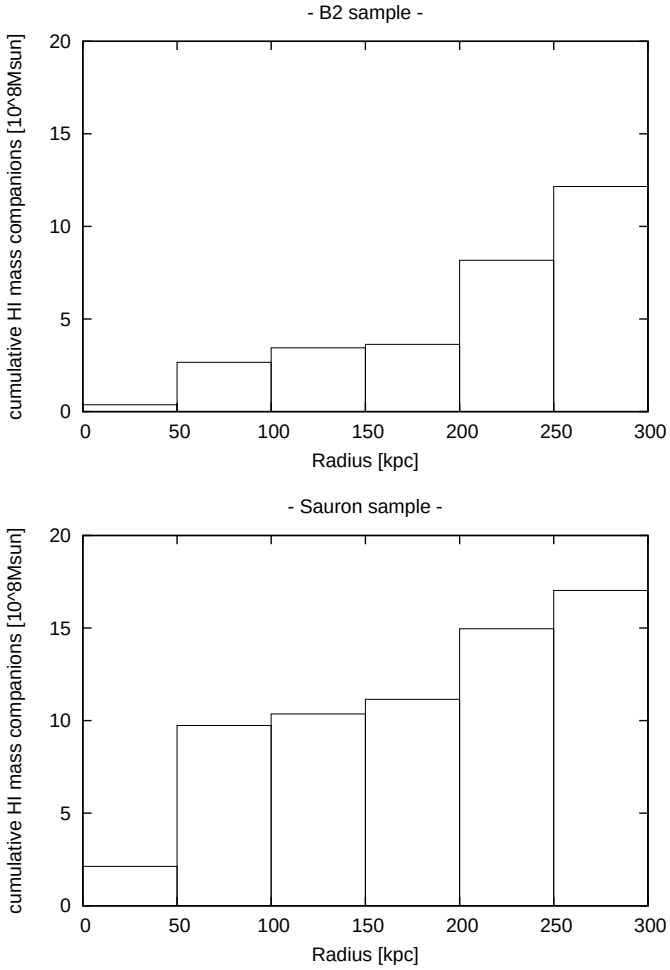

Figure 2.6: *Histogram of the cumulative average* H I *mass in the environment of the targets. Top panel: B2 sample. Bottom panel: SAURON sample.*

bourhood. However, this high average H I mass solely depends on a single companion ($M_{\rm HI} = 1.4 \times 10^{10}\ M_{\odot}$, see Tab. 2.9) of NGC 5982, which contributes > 40% of the average H I mass to the entire sample. Without this companion, the average H I mass in the environment of the SAURON targets would be slightly below the values for the B2 sample. Hence, no significant difference is found for the typical amount of H I located in the environment of the two target groups.

The remainder of this subsection examines whether any more subtle trends between the different samples can be identified:

- Do any differences between the radio-loud and the radio-quiet sample exist in

relation to the distance of the (nearest) companions and either the H I mass of the targets or the companions?

- Does the H I mass of the targets correlate with the number of companions and how does the distribution of the number of companions compare between the different samples?
- Does the H I morphology of the companions show signs of distortion that might hint towards recent interactions?

H I mass vs. distance of the (nearest) companions:

Figure 2.7 shows the H I mass of the target (or the upper limit) plotted against the distance to the nearest companion. The number of detections above the H I mass cut-off value is low for both samples, but it is clear that gas-rich targets (B2 and SAURON) do not necessarily have a nearby companion. While some targets have at least one nearby companion, other targets have no detected H I companions within 300 kpc.

No difference is found between the samples for the typical H I mass of companions (see Fig. 2.8), which is several $\times 10^8$ $M_\odot$. Moreover, most companions with $M_{\rm HI} > 10^9$ $M_\odot$ are found at radii larger than 200 kpc.

H I mass of the target vs. the number of companions:

In Figure 2.9 and 2.10, the H I mass (or the upper limit) of the target is plotted against the number of companions in the environment, for a radius of 150 kpc and 300 kpc respectively. No significant difference is observed between the two samples. No correlation between the H I mass of the B2 target and the number of companions exists, neither within a volume of 150 kpc in radius, nor for the larger volume ($r < 300$ kpc). No clear trend is observed for the SAURON galaxies. However, the most gas-rich targets preferentially have no H I companions. Thus, they are not located in particular gas-rich environments.

H I morphology of the companions:

In total, six (out of the 23) B2 companions show signs of recent or ongoing interaction. Companions of B2 0034+25, B2 0206+35 and B2 0331+39 show gas structures offset from what is expected for regular rotating galaxies (see Fig. 2.11). All three companions are well within the primary beam (7.′6, 6.′1 and 11.′7 respectively) such that the morphology is reliably determined. In the case of the B2 0206+35 companion, a tail structure is visible, pointing towards a second companion that actually lacks a counterpart in the optical. One companion of B2 0258+35 shows a very distorted morphology and kinematics (see Chapter 6) as well as two companions of B2 0722+30, which interact with one another (Emonts et al., 2009).

However, signs of disturbance found in companion galaxies are not a distinguishing characteristics between the B2 and the SAURON samples. Companions

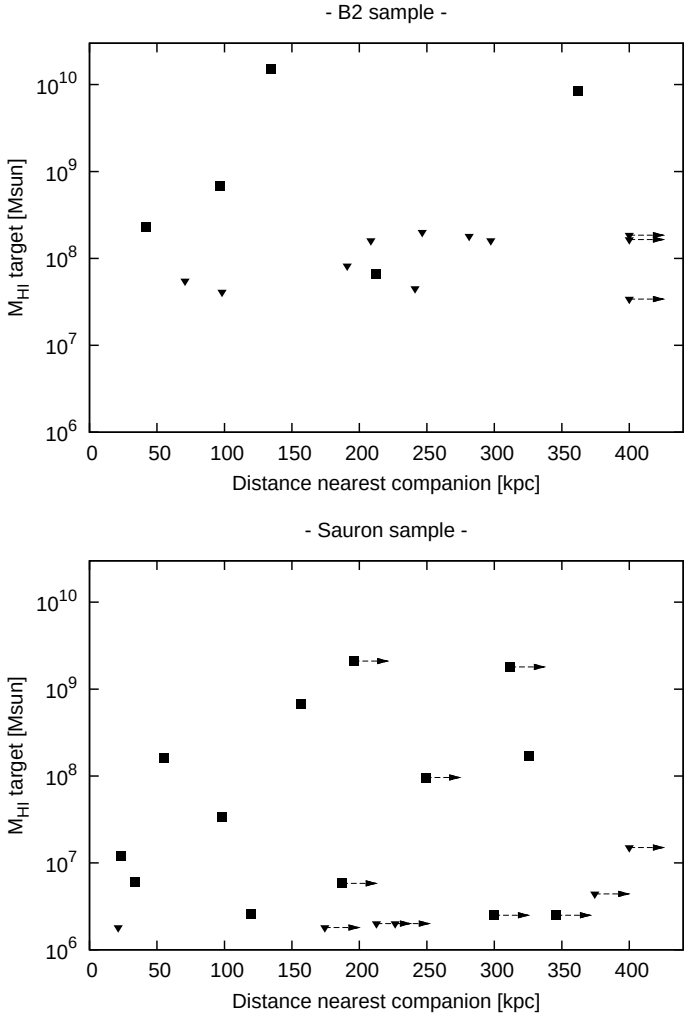

Figure 2.7: HI *mass of the target vs. the distance of the closest companion (in projection). Filled squares show the target detections, filled triangles the upper* HI *mass limits of the targets. Arrows indicate the lower limit. Top panel: B2 sample. Bottom panel: SAURON sample.*

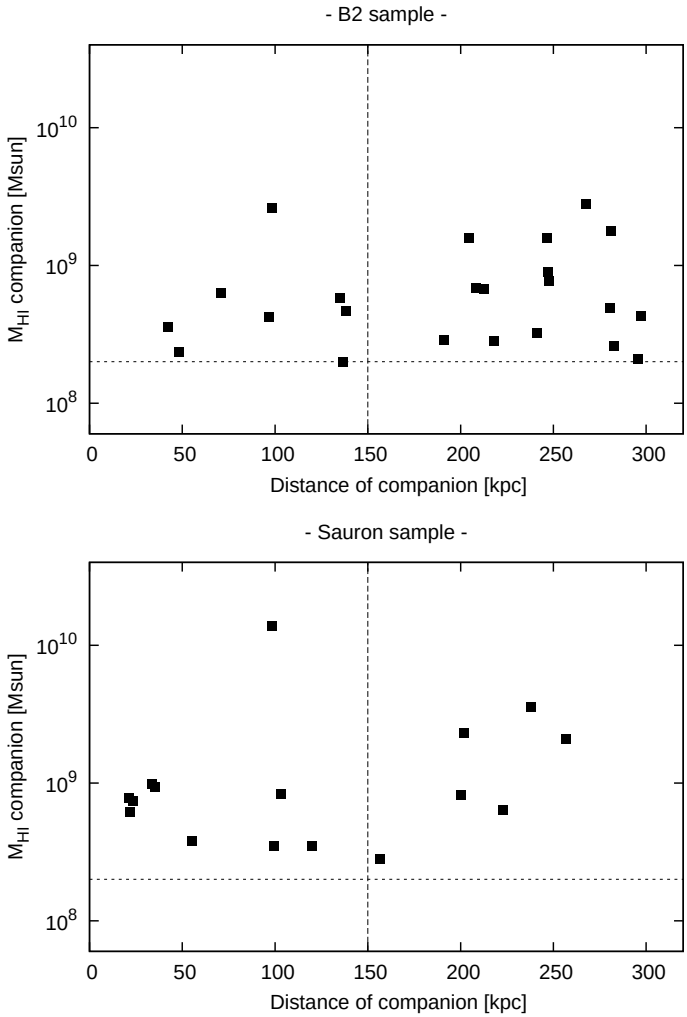

Figure 2.8: H I *mass of the companion vs. the (projected) distance to the target. The vertical line indicates the radius out to which both samples are complete. Top panel: B2 sample. Bottom panel: SAURON sample.*

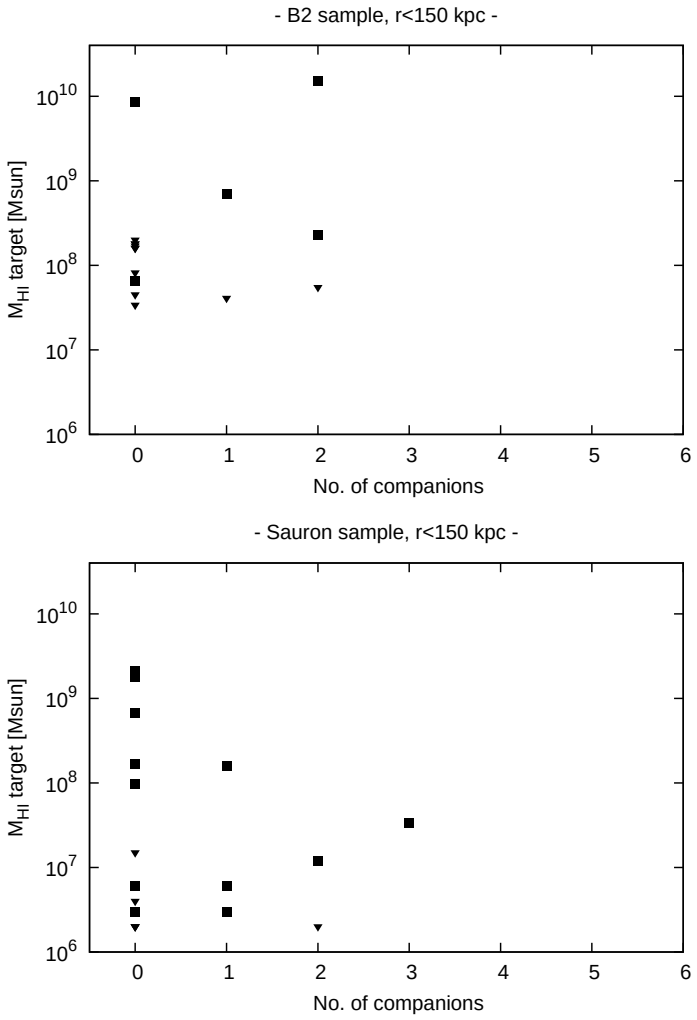

Figure 2.9: HI *mass of target vs. the number of* HI *detections in the environment,* $r_{\rm max}$ = 150 *kpc. Top panel: B2 sample. Bottom panel: SAURON sample.*

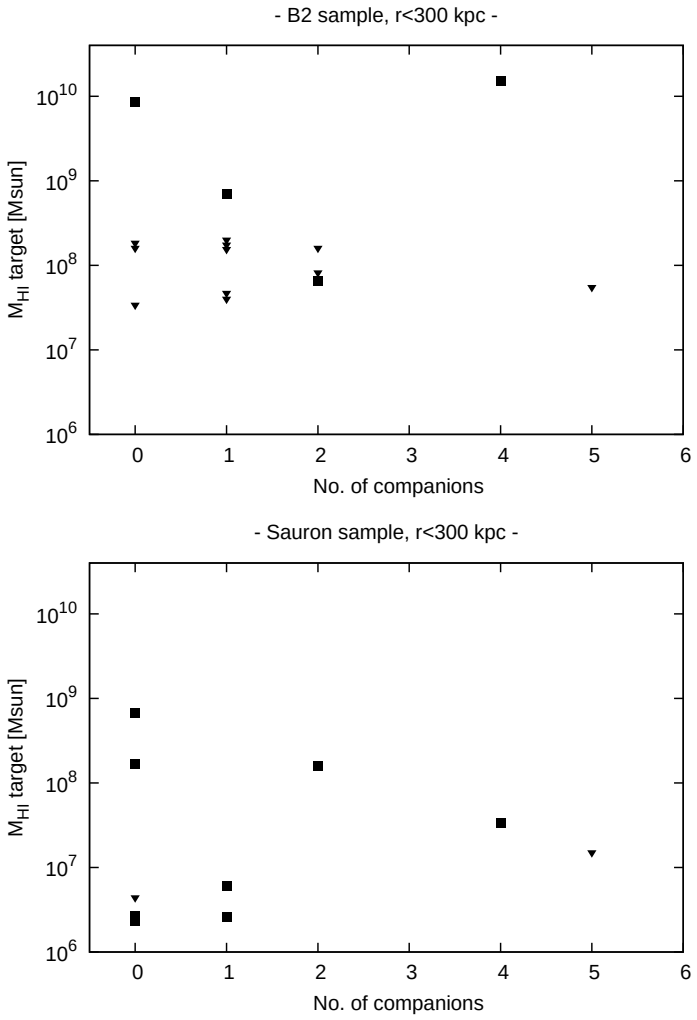

Figure 2.10: H I *mass of target vs. the number of* H I *detections in the environment,* $r_{\max}$ = 300 *kpc. Top panel: B2 sample. Bottom panel: SAURON sample.*

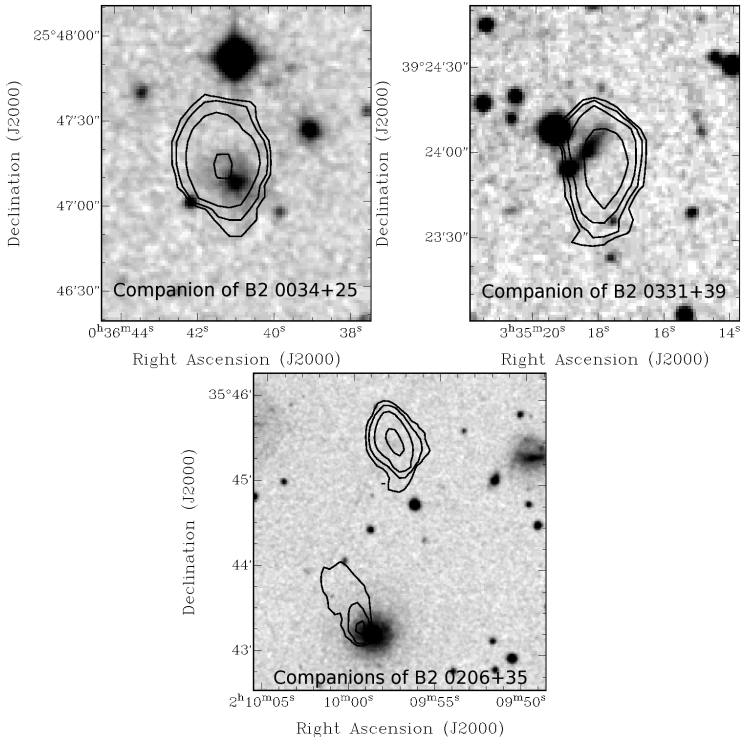

Figure 2.11: *Companions of B2 targets that show an offset in* H I *with respect to the optical counterpart indicating a recent interaction. Contour levels are:* 2×10^{19} *atoms cm*$^{-2}$ *and increasing with a factor of 2.*

with signs of recent or ongoing interactions are also found in the radio-quiet sample. A total of seven out of the 16 SAURON companions recently interacted (or are in the process of interacting). Thus, no significant difference between both samples is found.

2.6 Discussion

Given the limitations of the data (see Sect. 2.3.4), the analysis needs to be evaluated with due consideration. The main result of this analysis is that no statistically significant difference is found in the environment of radio-loud and radio-quiet galaxies. At a high significance level of 98%, the same average number of companions within $r < 150$ kpc has been found for both samples. The fraction of targets having at least one companion is approximately the same in both samples, at a significance level of 98%. At radii $150 < r < 300$ kpc, slightly more companions around B2 targets have been detected, but this is not statistically significant. We find neither a trend/difference for the H I mass of the targets, nor for the companions, with respect

to the distance or the number of companions. Moreover, no significant difference in the average amount of H I, located in the environment of the samples, could be identified. This study is only sensitive to fairly H I-rich companions ($M_{\rm HI} \geq 2 \times 10^8\ M_\odot$) which should not affect the total amount of H I gas located in the environment too greatly, since the amount of H I in the environment depends mainly on the most gas-rich companions. Consequently, even with lower detection limits, the result that both target groups reside in environments with similar amounts of H I is expected to hold.

However, the relatively high H I mass cut-off could be a severe limitation when comparing the number of companions detected in the two samples, since it only includes gas-rich companions. The B2 data sets show at least another 15 companions that are part of the environment (as defined), but have H I masses within the range of $\sim 10^7\ M_\odot < M_{\rm HI} < 2 \times 10^8\ M_\odot$. Given the different sensitivity limits in the different data sets, the number of companions is largely incomplete. It would therefore be desirable to investigate with more sensitive observations as to whether or not this here-presented conclusion – that no statistically significant differences between the samples exists – still holds when taking less gas-rich companions into account.

While it can not be excluded that in single objects interactions stimulate radio activity, no evidence is found that gas-rich interactions in general play a dominant role in causing nuclear activity. The properties of the B2 and SAURON environments (e.g. amount of H I, number of H I companions, distribution of companions etc.) are too similar to infer essential differences between the two samples.

Our results are in line with previous environment studies of AGN hosts. Ramos Almeida et al. (2010) found signs of disturbance in 50% of FR-I sources and concluded that their results are consistent with the idea that many low-power radio galaxies are triggered by the accretion of hot gas and not by interactions that involve large amounts of cold gas. Our results are similar to what has been found for the H I environment of Seyfert type of AGN hosts, in the sense that signs of disturbance are commonly observed but are not a distinguishing characteristic, when compared to radio-quiet sources (e.g. Wilcots et al., 2001; Greene et al., 2004, see also Sect. 2.2). The role of interactions for the triggering of AGN therefore remains ambiguous.

2.7 Summary

In this chapter we have investigated the neutral hydrogen environment of a sample of nearby low-power radio galaxies by comparing the properties of fairly H I-rich companions to a sample of radio-quiet sources. The main conclusions are:

- No statistically significant difference is found that would allow to infer the importance of gas-rich interactions for the triggering of radio galaxies.
- At the high significance level of 98%, no differences between the radio-loud and radio-quiet samples (in terms of the average number of companions within $r < 150$ kpc or the fraction of targets having at least one companion in the same volume) are found. No statistically significant difference between the samples is found for $150 < r < 300$ kpc.

- We neither find a difference for the average amount of H I located in the environment. This means that radio-loud galaxies reside in an environment that contains a similar amount of cold gas as found in the neighbourhood of their radio-quiet counterparts.
- No difference is found between the two samples in terms of the typical H I mass (which is a few $\times 10^8$ $M_\odot$) of the companions or their radial distribution. The most gas-rich companions ($M_{\rm HI} > 10^9$ $M_\odot$) are predominantly located at $r >$ 200 kpc.
- Signs of disturbance are found in companions of radio-loud and radio-quiet targets and are therefore not a distinguishing characteristic.

The data used for this analysis has a number of limitations (Sect. 2.3.4). Most central is the number statistics available. Future studies, which investigate the impact of cold gas on the triggering of AGN should therefore be based on larger sample sizes. Deep observations, which allow the investigation of number and distribution of less gas-rich companions are desirable because the amount of gas needed to trigger an AGN (see Sect 2.1) is much lower than the H I mass cut-off value imposed in this study. Moreover, future samples should be well-matched in (stellar) mass, optical morphology and in environment to ensure an adequate comparison between radio-loud and radio-quiet samples, as these properties may have an influence on the AGN activity and perhaps the triggering mechanism.

Acknowledgements: The Westerbork Synthesis Radio Telescope is operated by ASTRON (Netherlands Institute for Radio Astronomy) with support from the Netherlands Foundation for Scientific Research (NWO). The NASA/IPAC Extragalactic Database (NED) is operated by the Jet Propulsion Laboratory, California Institute of Technology, under contract with the National Aeronautics and Space Administration. The Digitized Sky Survey was produced at the Space Telescope Science Institute under US government grant NAG W-2166.

2.A Appendix: Tables and total intensity maps

Tables 2.6 and 2.7 list the properties of the H I cubes of all B2 and SAURON sources. The properties of the companions for all targets are summarized in Tab. 2.8 and 2.9 and the corresponding total intensity images of the B2 cubes are shown in Fig. 2.A. Contour levels in all images are 2×10^{19} atoms cm^{-2}, increasing by a factor of 2. All galaxies belonging to the environment are labeled with numbers; the remaining H I detections shown in the images do not fulfil the requirements of the environment definition (i.e., H I mass too low, or radius too large, or velocity offset too large). The image showing the environment of B2 0648+27 is taken from Emonts et al. (2006).

Table 2.6: *Properties of the B2 data cubes.*

Name	Radius cube (kpc)	$-\Delta v$ (km s^{-1})	$+\Delta v$ (km s^{-1})	Detection limit ($10^8 M_\odot$)	No. of companions
B2 0034+25	> 300	> 600	> 600	0.9	1
B2 0055+30	> 300	> 600	> 600	0.7	2
B2 0104+32	> 300	> 600	> 600	0.2	1
B2 0206+35	> 300	> 600	> 600	0.9	2
B2 0222+36	> 300	> 600	> 600	1.0	0
B2 0258+35	> 300	> 600	> 600	< 0.1	4
B2 0326+39	> 300	> 600	> 600	0.5	2
B2 0331+39	> 300	> 600	> 600	0.3	5
B2 0648+27	> 300	> 600	> 600	0.9	0
B2 0722+30	167	595	597	0.2	2
B2 1040+31	> 300	> 600	> 600	1.9	1
B2 1217+29	> 300	530	> 600	< 0.1	1
B2 1447+27	> 300	> 600	> 600	1.8	1
B2 1658+30	> 300	> 600	> 600	1.0	0
B2 2116+26	> 300	> 600	> 600	0.2	0
B2 2229+39	> 300	> 600	> 600	0.2	1

Notes – Col. 4 gives the velocity width below systemic of the target; col. 5 the velocity width above systemic of the target. Col. 6 gives the number of companions according to our definition in Sect. 2.3.2.

Table 2.7: *Properties of the SAURON data cubes.*

Name	Radius cube (kpc)	$-\Delta v$ ($\mathrm{km\,s^{-1}}$)	$+\Delta v$ ($\mathrm{km\,s^{-1}}$)	Detection limit ($10^8 M_\odot$)	No. of companions
NGC 0524	> 300	> 600	> 600	< 0.1	1
NGC 0821	> 300	> 600	> 600	< 0.1	0
NGC 1023	201	520	> 600	< 0.1	0
NGC 2549	212	> 600	> 600	< 0.1	0
NGC 2685	155	> 600	> 600	< 0.1	0
NGC 2768	> 300	> 600	> 600	< 0.1	0
NGC 3032	250	> 600	> 600	< 0.1	0
NGC 3377	174	> 600	> 600	< 0.1	0
NGC 3379	165	> 600	> 600	< 0.1	2
NGC 3384	165	> 600	> 600	< 0.1	2
NGC 3414	> 300	> 600	> 600	< 0.1	2
NGC 3489	189	> 600	> 600	< 0.1	0
NGC 3608	> 300	> 600	> 600	< 0.1	0
NGC 4150	> 300	150	> 600	< 0.1	0
NGC 5198	> 300	> 600	> 600	0.2	5
NGC 5308	> 300	> 600	> 600	0.2	0
NGC 5982	> 300	> 600	> 600	0.2	3
NGC 7332	> 300	> 600	> 600	< 0.1	1
NGC 7457	226	> 600	> 600	0.1	0

Notes – Col. 4 gives the velocity width below systemic of the target; col. 5 the velocity width above systemic of the target. Col. 6 gives the number of companions according to our definition in Sect. 2.3.2.

Table 2.8: *Properties of companions of B2 sources.*

Target name	No. comp.	RA	Dec	FWHM	Δv	Dist.	$M_{\rm HI}$	optical counterpart; name
B2 0034+25	-	00 37 05.5	25 41 56.4	-	-	-	< 0.9	-
B2 0034+25	1	00 36 40.9	25 47 09.8	88.1	580	297.4	4.3	yes
B2 0055+30	-	00 57 48.9	30 21 08.8	117	-	-	0.7	-
B2 0055+30	1	00 57 31.5	30 11 08.9	107	101	212.6	6.8	yes; 2MASX J00573150+3011098
B2 0055+30	2	00 56 59.8	30 27 16.3	145	391	247.6	8.9	yes
B2 0104+32	-	01 07 25.0	32 24 45.2	-	-	-	< 0.2	-
B2 0104+32	1	01 07 03.6	32 23 22.0	221.7	16	98.2	26.1	yes; UGC 679
B2 0206+35		02 09 38.6	35 47 50.0	-	-	-	< 0.9	-
B2 0206+35	1	02 09 58.7	35 43 14.8	33.9	-433	282.7	2.6	yes; CGCG 522-122
B2 0206+35	2	02 09 57.3	35 45 27.3	84.8	-450	208.5	6.9	no
B2 0222+36		02 25 27.3	37 10 28.0	-	-	-	< 1.0	-
B2 0258+35	-	03 01 42.4	35 12 20.7	520	-	-	153.2	-
B2 0258+35	1	03 01 48.6	35 05 42.4	213	-48	134.8	5.8	yes; 2MASX J03014864+3505423
B2 0258+35	2	03 00 37.4	35 10 08.7	529	114	267.6	28.1	yes; UGC 2465
B2 0258+35	3	03 02 09.5	35 16 30.8	77	-48	138.0	4.7	no
B2 0258+35	4	03 02 30.7	35 16 58.1	128	194	217.9	2.8	no
B2 0326+39	-	03 29 24.2	39 47 42.0	-	-	-	< 0.5	-
B2 0326+39	1	03 28 37.6	39 50 41.4	260.3	450	280.5	4.9	yes; 2MASX J03283761+3950417
B2 0326+39	2	03 29 32.8	39 53 45.0	103.9	190	191.0	2.9	yes
B2 0331+39	-	03 34 18.4	39 21 24.6	-	-	-	< 0.3	-
B2 0331+39	1	03 33 57.4	39 17 39.1	102.7	408	136.5	2.0	yes
B2 0331+39	2	03 33 29.6	39 18 16.8	85.2	-88	247.7	7.8	yes

Table 2.8 — continued: *Properties of companions of B2 sources.*

Target name	No. comp.	RA	Dec	FWHM	Δv	Dist.	$M_{\rm HI}$	optical counterpart; name
B2 0331+39	3[1]	03 33 36.7	39 20 43.8	289.0	-547	204.8	15.8	yes; 2MASX J03333667+3920437
B2 0331+39	4	03 35 18.4	39 24 00.2	170.8	132	295.8	2.1	yes
B2 0331+39	5	03 34 12.3	39 24 02.1	187.7	32	70.8	6.3	yes
B2 0648+27	-	06 52 02.5	27 27 38.9	481.0	-	-	85.0	-
B2 0722+30	-	07 25 37.4	29 57 14.8	453	-	-	2.3	-
B2 0722+30	1	07 25 44.2	29 57 06.7	150	-20	42.1	3.6	yes; UGC 3841 NED01
B2 0722+30	2	07 25 47.1	29 57 11.2	280	194	48.4	2.4	yes; UGC 3841 NED02
B2 1040+31	-	10 43 18.4	31 31 01.6	-	-	-	< 1.1	-
B2 1040+31	1	10 43 43.2	31 33 44.4	176	-507	246.6	15.9	yes; 2MASX J10434317+3133438
B2 1217+29	-	12 20 06.8	29 16 50.7	503	-	-	6.9	-
B2 1217+29	1	12 19 50.7	29 36 54.8	486	185	96.8	4.2	yes; NGC 4274
B2 1447+27	-	14 49 27.9	27 46 50.3	-	-	-	0.3	-
B2 1447+27	1	14 49 54.3	27 42 05.1	148	-309	281.3	17.9	yes; IC 4512
B2 1658+30	-	17 00 45.2	30 08 12.9	-	-	-	< 1.0	-
B2 2116+26	-	21 18 33.0	26 26 49.3	-	-	-	< 0.2	-
B2 2229+39	-	22 31 20.9	39 21 48.0	-	-	-	< 0.2	-
B2 2229+39	1	22 30 21.1	39 20 11.7	119.0	-583	241.2	3.3	yes

Notes – The number of the companion (col. 2) corresponds to the number in the total intensity image (Fig. 2.A). The FWHM of the companion (col. 5) and the velocity offset from the target, Δv (col. 6) are given in km s^{-1} , the projected distance (col. 7) in kpc and the H I mass in 10^8 $M_\odot$ (primary beam corrected) (col. 8).

[1] interacting with 2MASX J03333857+3920097?

Table 2.9: *Properties of companions of SAURON sources.*

Target name	No. comp.	RA	Dec	FWHM	Δv	Dist.	$M_{\rm HI}$	optical counterpart; name
NGC 0524	-	01 24 47.2	09 32 19.8	-	-	-	< 0.1	-
NGC 0524	1	01 25 17.2	09 15 52.6	412	-23	120.0	3.5	yes; NGC 0532
NGC 0821	-	02 08 21.1	10 59 41.7	-	-	-	< 0.1	-
NGC 1023	-	02 40 24.0	39 03 47.7	581	-	-	21.0	-
NGC 2549	-	08 18 58.4	57 48 11.0	-	-	-	< 0.1	-
NGC 2685	-	08 55 34,7	58 44 03.8	315	-	-	18.0	-
NGC 2768	-	09 11 37.5	60 02 14.0	160	-	-	1.7	-
NGC 3032	-	09 52 08.2	29 14 10.4	165	-	-	1.0	-
NGC 3377	-	10 47 42.4	13 59 08.3	-	-	-	< 0.1	-
NGC 3379	-	10 47 49.6	12 34 53.9	-	-	-	< 0.1	-
NGC 3379	1	10 47 38.2	12 25 16.8	214	65	21.2	7.7	no
NGC 3379	2	10 48 28.2	12 31 53.2	91	362	21.6	6.2	yes; NGC 3389
NGC 3384	-	10 48 16.9	12 37 45.4	99	-	-	0.1	-
NGC 3384	1	10 47 38.2	12 25 16.8	214	213	35.4	9.3	no
NGC 3384	2	10 48 28.2	12 31 53.2	91	510	23.5	7.4	yes; NGC 3389
NGC 3414	-	10 51 16.2	27 58 30.4	420	-	-	1.6	-
NGC 3414	1	10 51 15.8	27 50 52.7	210	-275	55.2	3.8	yes; UGC 5958
NGC 3414	2	10 49 12.3	27 55 32.9	185	-69	200.0	8.3	yes; UGC 5921
NGC 3489	-	11 00 18.6	13 54 04.4	-	-	-	< 0.1	-
NGC 3608	-	11 16 59.0	18 08 55.3	-	-	-	< 0.1	-
NGC 4150	-	12 10 33.7	30 24 05.5	-	-	-	< 0.1	-
NGC 5198	-	13 30 11.4	46 40 14.8	310	-	-	6.8	-
NGC 5198	1	13 29 15.1	46 30 08.0	151	-9	156.4	2.8	yes; CGCC 246-006

Table 2.9 — continued: *Properties of companions of SAURON sources.*

Target name	No. comp.	RA	Dec	FWHM	Δv	Dist.	$M_{\rm HI}$	optical counterpart; name
NGC 5198	2	13 28 33.6	46 29 57.8	202	17	222.6	6.4	yes; MCG +08-25-006
NGC 5198	3	13 28 25.3	46 35 30.9	243	-92	201.8	23.1	yes; NGC 5173
NGC 5198	4	13 28 09.9	46 40 18.6	285	-134	238.1	35.5	yes; NGC 5169
NGC 5198	5	13 28 33.4	46 55 38.5	252	168	257.0	20.7	yes; IC 4263
NGC 5308	-	13 47 00.4	60 58 23.4	-	-	-	< 0.2	-
NGC 5982	-	15 38 39.8	59 21 21.0	42	-	-	0.3	-
NGC 5982	1	15 39 36.9	59 19 57.6	587	-407	98.3	137.2	yes; NGC 5985
NGC 5982	2	15 37 53.7	59 23 27.0	470	-332	103.0	8.3	yes; NGC 5981
NGC 5982	3	15 39 29.8	59 25 20.4	143	-223	99,3	3.5	yes; SDSS J153930+592519
NGC 7332	-	22 37 24.5	23 47 54.0	-	-	-	< 0.1	-
NGC 7332	1	22 37 47.1	23 47 11.8	375	122	33.7	9.8	yes; NGC 7339
NGC 7457	-	23 00 59.9	30 08 41.6	-	-	-	< 0.1	-

Notes – The FWHM of the companion (col. 5) and the velocity offset from the target, Δv (col. 6) are given in km s^{-1} , the projected distance (col. 7) in kpc and the H I mass in 10^8 $M_\odot$ (primary beam corrected) (col. 8).

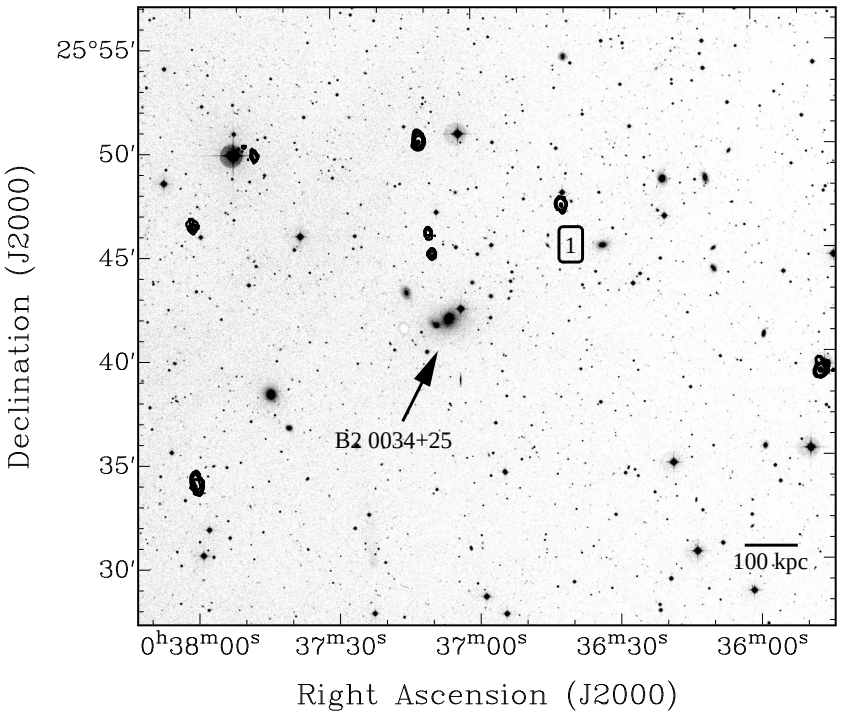
25°55′
50′
45′
40′
35′
30′
Declination (J2000)
B2 0034+25
1
100 kpc
0h38m00s
37m30s
37m00s
36m30s
36m00s
Right Ascension (J2000)

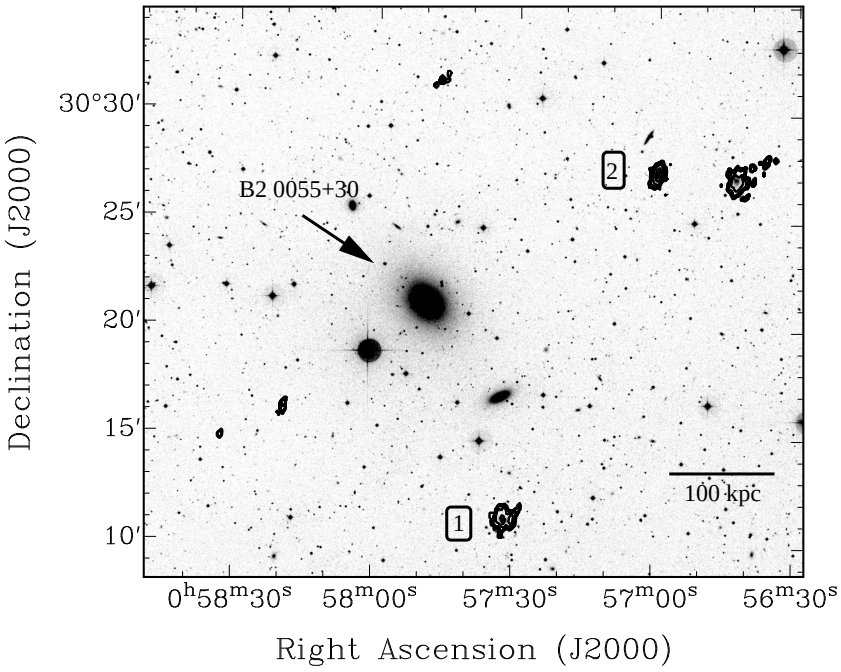
30°30′
25′
20′
15′
10′
Declination (J2000)
B2 0055+30
2
1
100 kpc
0h58m30s
58m00s
57m30s
57m00s
56m30s
Right Ascension (J2000)

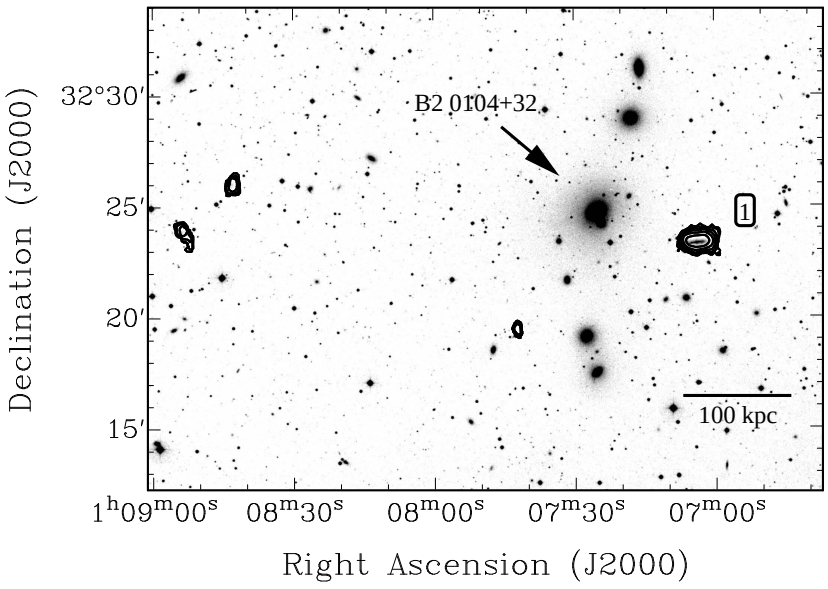
B2 0104+32
1
100 kpc
32°30′
25′
20′
15′
Declination (J2000)
1h09m00s
08m30s
08m00s
07m30s
07m00s
Right Ascension (J2000)

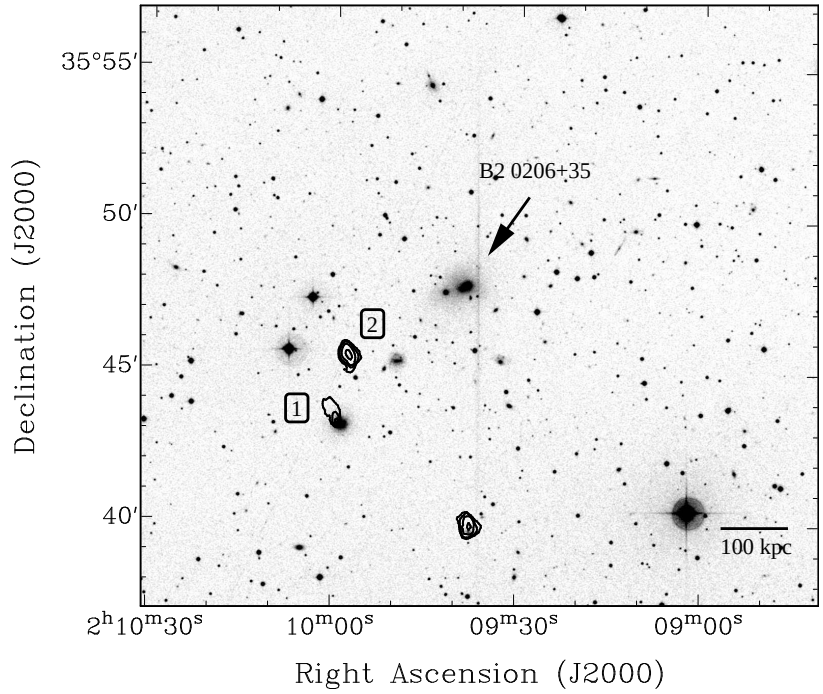
B2 0206+35
2
1
100 kpc
35°55′
50′
45′
40′
Declination (J2000)
2h10m30s
10m00s
09m30s
09m00s
Right Ascension (J2000)

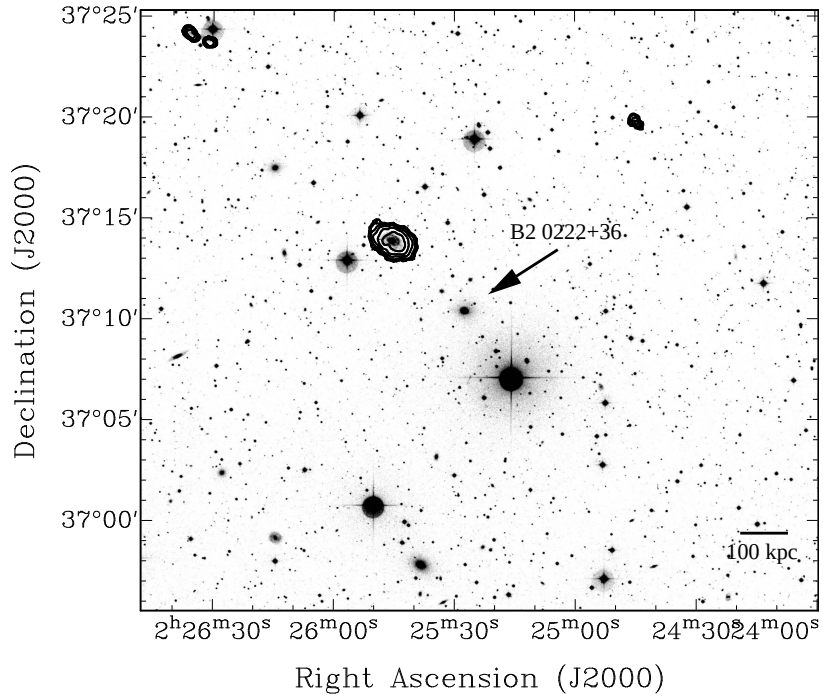
37°25′
37°20′
37°15′
37°10′
37°05′
37°00′
Declination (J2000)
B2 0222+36
100 kpc
2h26m30s
26m00s
25m30s
25m00s
24m30s
24m00s
Right Ascension (J2000)

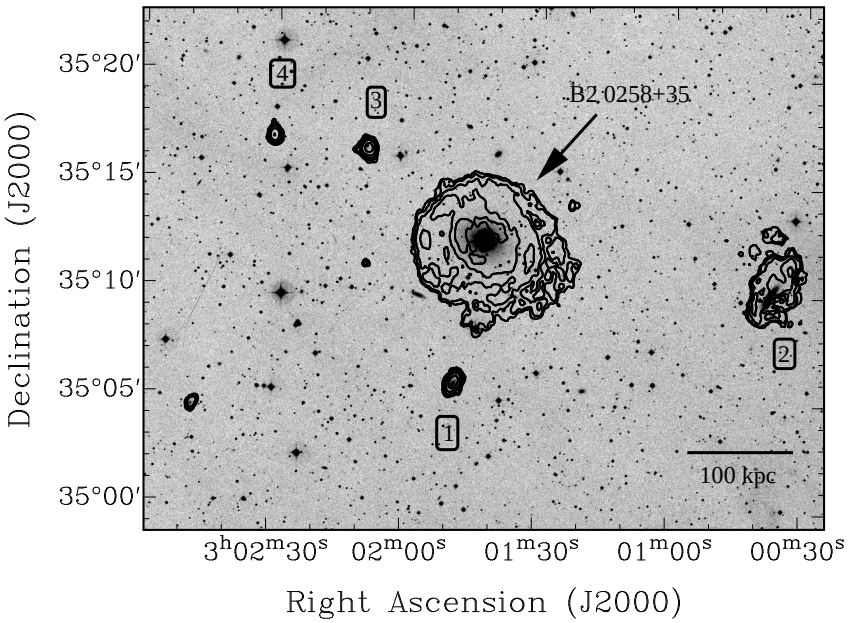
35°20′
35°15′
35°10′
35°05′
35°00′
Declination (J2000)
4
3
B2 0258+35
2
1
100 kpc
3h02m30s
02m00s
01m30s
01m00s
00m30s
Right Ascension (J2000)

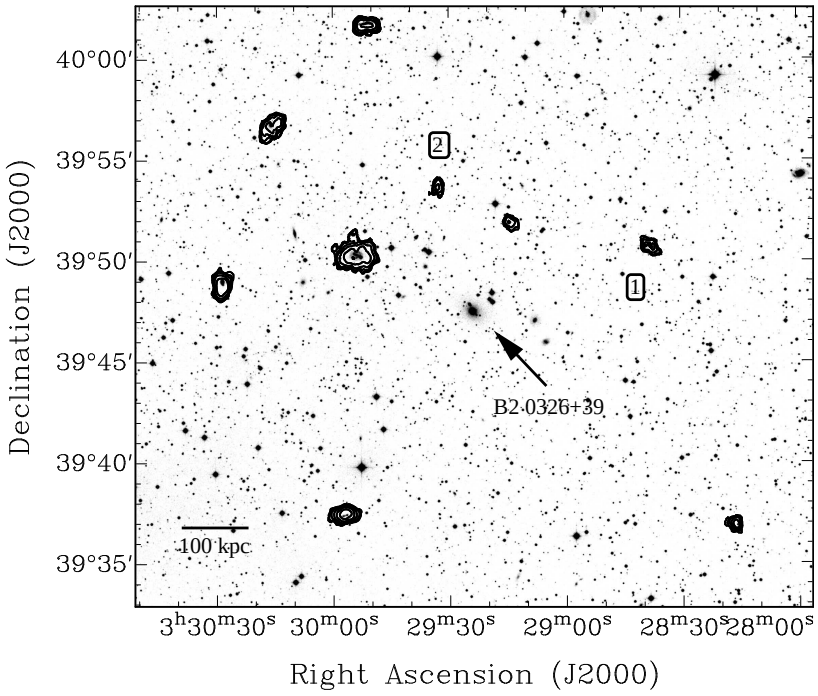
40°00′
39°55′
39°50′
39°45′
39°40′
39°35′
Declination (J2000)
2
1
B2 0326+39
100 kpc
3h30m30s
30m00s
29m30s
29m00s
28m30s
28m00s
Right Ascension (J2000)

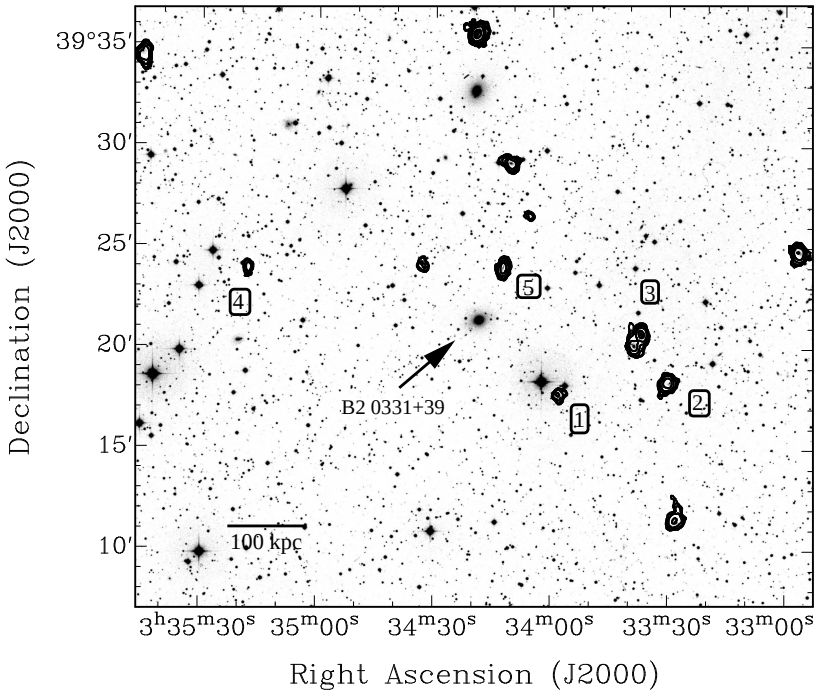
39°35′
30′
25′
20′
15′
10′
Declination (J2000)
4
5
3
2
1
B2 0331+39
100 kpc
3h35m30s
35m00s
34m30s
34m00s
33m30s
33m00s
Right Ascension (J2000)

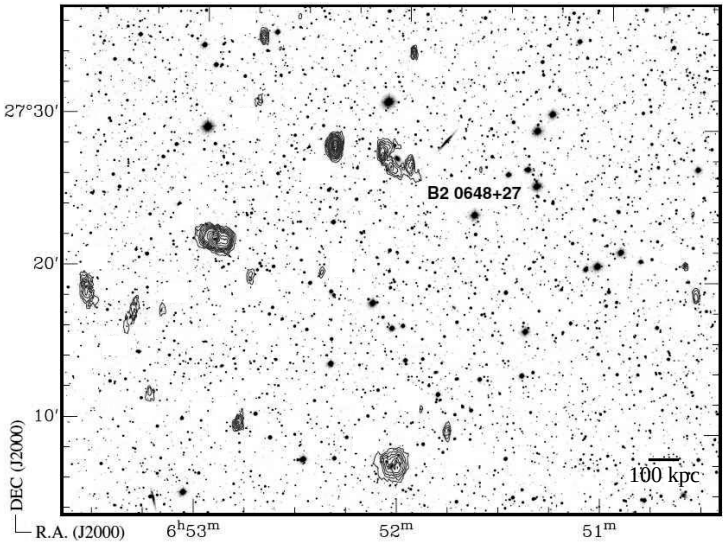
27°30′
20′
10′
DEC (J2000)
R.A. (J2000)
6h53m
52m
51m
B2 0648+27
100 kpc

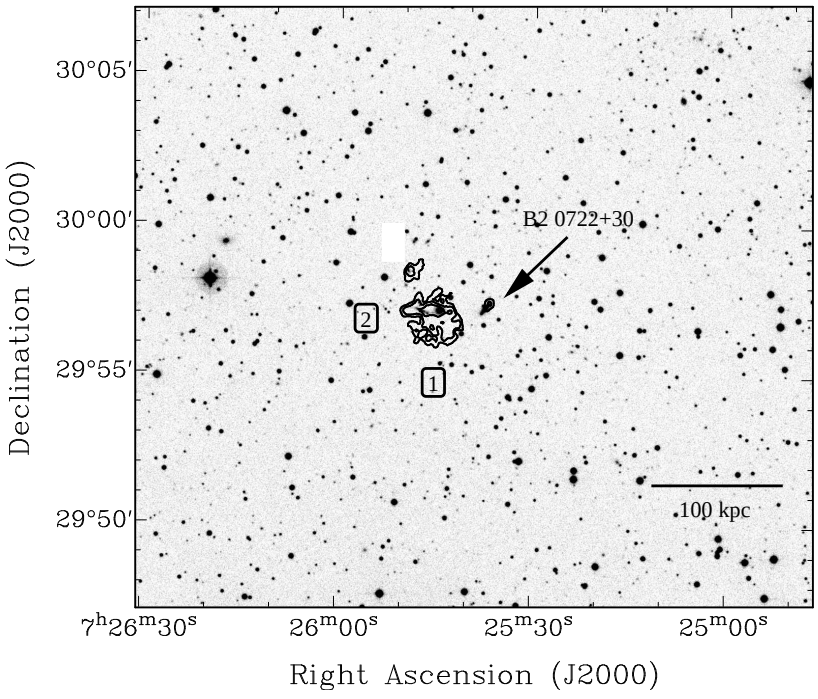
30°05′
30°00′
29°55′
29°50′
Declination (J2000)
7h26m30s
26m00s
25m30s
25m00s
Right Ascension (J2000)
B2 0722+30
2
1
100 kpc

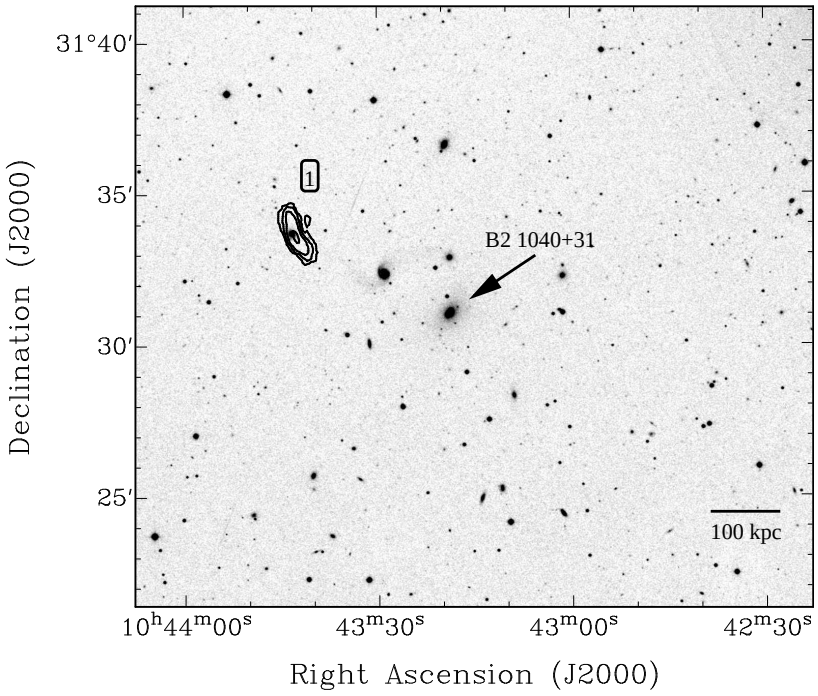
31°40′
35′
30′
25′
Declination (J2000)
1
B2 1040+31
100 kpc
10h44m00s
43m30s
43m00s
42m30s
Right Ascension (J2000)

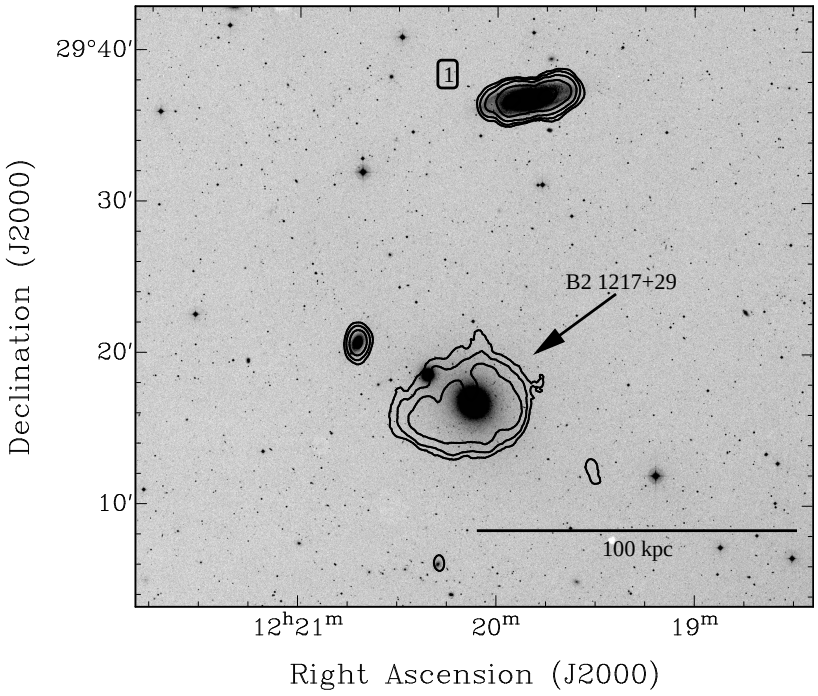
29°40′
30′
20′
10′
Declination (J2000)
1
B2 1217+29
100 kpc
12h21m
20m
19m
Right Ascension (J2000)

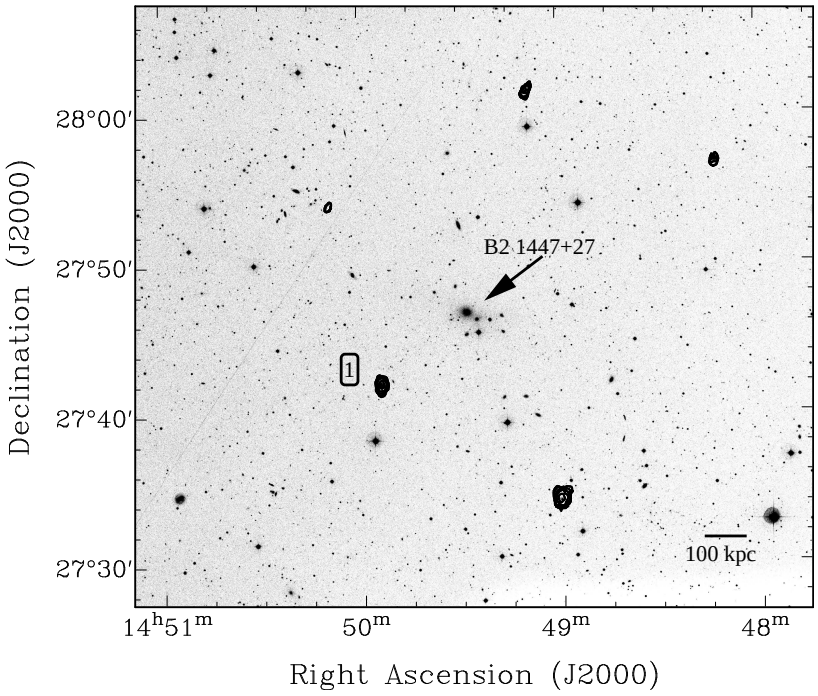
28°00′
27°50′
27°40′
27°30′
Declination (J2000)
B2 1447+27
1
100 kpc
14h51m
50m
49m
48m
Right Ascension (J2000)

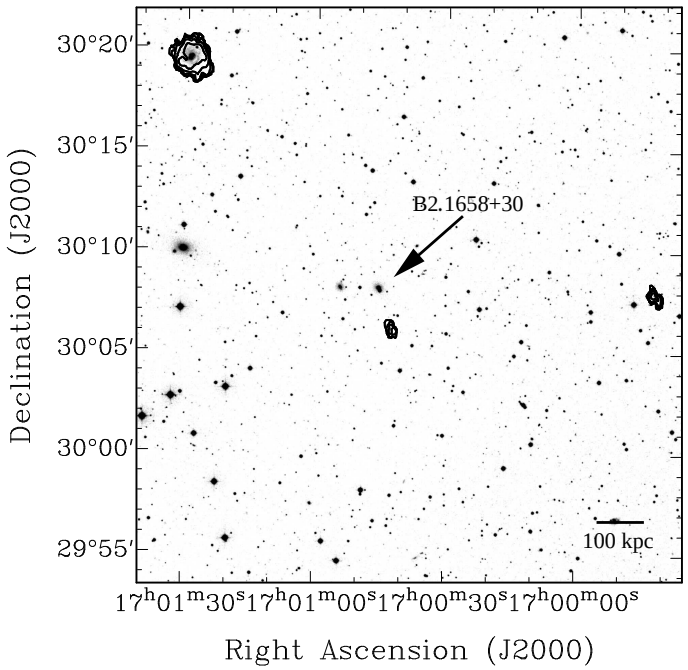
30°20′
30°15′
30°10′
30°05′
30°00′
29°55′
Declination (J2000)
B2.1658+30
100 kpc
17h01m30s
17h01m00s
17h00m30s
17h00m00s
Right Ascension (J2000)

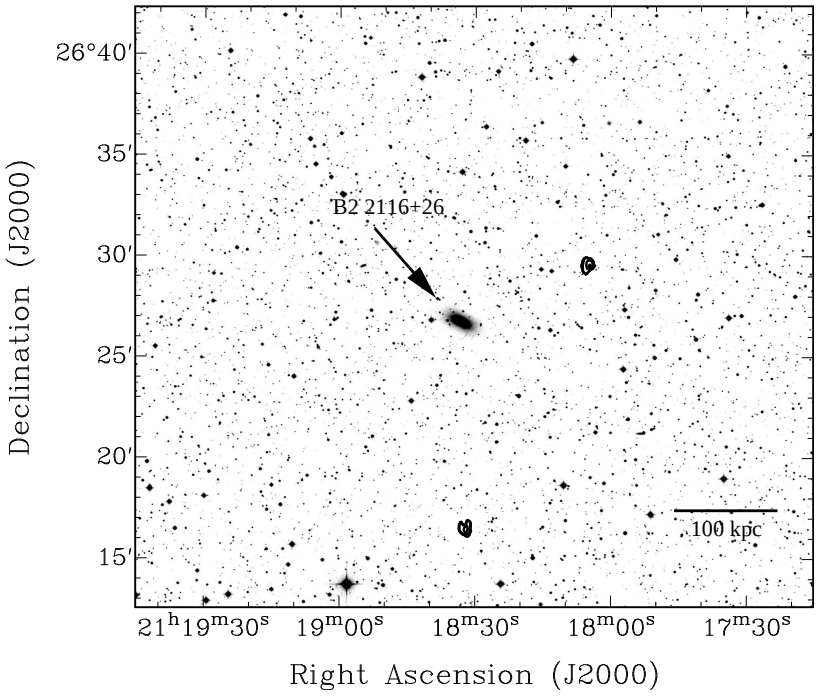
26°40′
35′
30′
25′
20′
15′
Declination (J2000)
B2 2116+26
100 kpc
21h19m30s
19m00s
18m30s
18m00s
17m30s
Right Ascension (J2000)

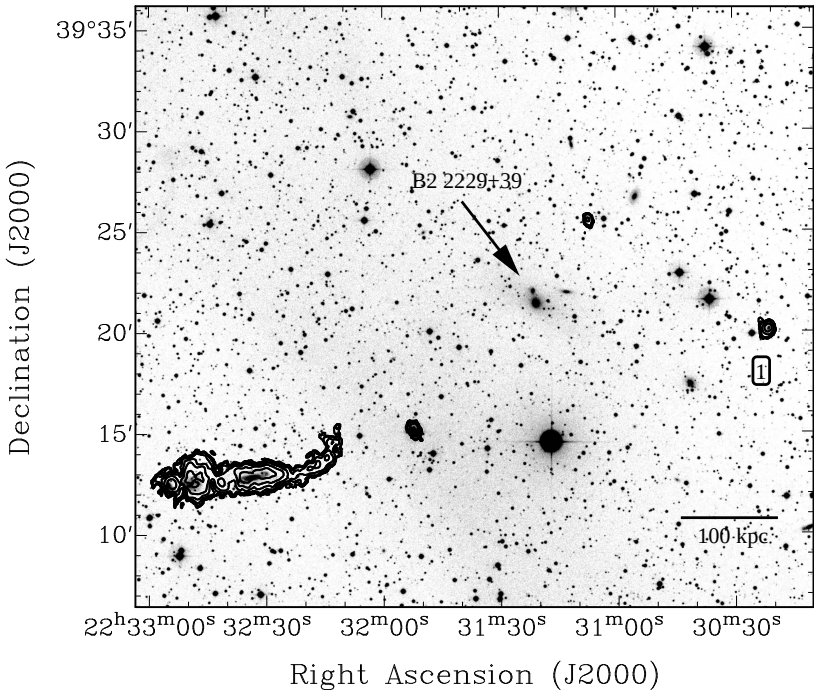
39°35′
30′
25′
20′
15′
10′
Declination (J2000)
B2 2229+39
100 kpc
22h33m00s
32m30s
32m00s
31m30s
31m00s
30m30s
Right Ascension (J2000)

3 Centaurus A: morphology and kinematics of the atomic hydrogen

— based on —
C. Struve, T.A. Oosterloo, R. Morganti & L. Saripalli. 2010. A&A 515, A67
and
C. Struve, R. Morganti, T.A. Oosterloo & B.H.C. Emonts. 2010. PASA in press

Abstract

We present new ATCA 21-cm line observations of the neutral hydrogen in the nearby radio galaxy Centaurus A. We image in detail (with a resolution down to 7″, ~ 100 pc) the distribution of H I along the dust lane. Our data have better velocity resolution and better sensitivity than previous observations. The H I extends for a total of ~ 15 kpc. The data, combined with a titled-ring model of the disk, allow to conclude that the kinematics of the H I is that of a regularly rotating, highly warped structure down to the nuclear scale. The parameters (in particular the inclination) of our model are somewhat different from some of the previously proposed models but consistent with what was recently derived from stellar light in a central ring. The model nicely describes also the morphology of the dust lane as observed with Spitzer. There are no indications that *large-scale* anomalies in the kinematics exist that could be related to supplying material for the AGN. Large-scale radial motions do exist, but these are only present at larger radii ($r > 6$ kpc). This unsettled gas is mainly part of a tail/arm like structure. The relatively regular kinematics of the gas in this structure suggests that it is in the process of settling down into the main disk. The presence of this structure further supports the merger/interaction origin of the H I in Cen A. From the structure and kinematics we estimate a timescale of $1.6-3.2\times10^8$ yr since the merging event. No bar structure is needed to describe the kinematics of the H I. The comparison of the timescale derived from the large-scale H I structure and those of the radio structure together with the relative regularity of the H I down to the sub-kpc regions does not suggest

a one-to-one correspondence between the merger and the phase of radio activity. Interestingly, the radial motions of the outer regions are such that the projected velocities are *redshifted* compared to the regular orbits. This means that the blueshifted absorption detected against the nucleus, and discussed in detail in Chapter 4, cannot be caused by out-moving gas at large radius projected onto the centre; instead we argue that the blueshifted absorption, together with at least a fraction of the redshifted nuclear absorption, is evidence for a regular inner disk (Chapter 4). Finally, we also report the discovery of two unresolved clouds detected at 5.2 and 11 kpc away (in projection) from the H I disk. They are likely an other example of a left-over of the merger that brought the H I gas.

3.1 Introduction

The assembly of early-type galaxies and its connection to the presence of an active nucleus (and in particular a radio-loud nucleus) is still a matter of debate. Gas-rich galaxy mergers and interactions could play an important role in providing the fuel to trigger nuclear activity (including the radio phase). However, recent studies of radio galaxies have shown that the activity in some of these galaxies may be associated instead with the *slow* accretion of (hot) gas. This is thought to be the case in particular, for edge-darkened radio galaxies where advective low efficiency/rate flows could be the dominant mode of accretion (see e.g. Allen et al., 2006; Balmaverde et al., 2008).

One way to address the issue of the relation between interaction/merger and AGN, is by studying the gas in radio galaxies. Nearby sources are prime targets as the morphology and kinematics of the gas — both at large scales and in the nuclear region — can be studied in detail and related to each other. Atomic hydrogen can be a useful tracer for these purposes. In particular, H I gas found at kiloparsec scales, or larger, can be used to trace the evolution of the host galaxies (e.g. major merger vs. small accretions). On the other hand, H I in absorption is one of the diagnostics to probe the central regions of active galactic nuclei and the interaction of the AGN with its immediate environment. H I absorption studies offer the unique possibility of tracing the nature of the accretion or the energetics of the outflow (e.g. Morganti et al., 2005b).

Unfortunately, the number of radio-loud galaxies where the atomic neutral hydrogen can be studied in such details both in emission *and* in absorption is limited. Due to its proximity[1], the nearby radio galaxy Centaurus A (Cen A) is a unique object where to study the different phases of the gas, including H I, in a radio-loud AGN. This can be done on spatial scales ranging from the inner kpc, where the influence of the AGN can still be relevant, up to many kpc where the signature of past merger(s) might be still visible through unsettled gas.

Cen A harbours a well known radio source classified as a Fanaroff-Riley type-I source (FR-I, Fanaroff & Riley, 1974) with a total power $P_{2.7\mathrm{GHz}} = 10^{24.26}$ W Hz^{-1}. The total extent of the radio source reaches more than 8°, making Cen A the largest extragalactic radio source in the sky (Cooper et al., 1965). The radio source shows a

[1] At the assumed distance of Cen A of 3.8 Mpc (Harris et al., 2009), 1 arcmin corresponds to 1.1 kpc.

variety of features on different scales. A radio jet extends from sub-parsec scales (e.g. Jones et al., 1996; Horiuchi et al., 2006) to a projected distance of ~ 6 kpc from the nucleus, ending in an inner radio lobe (Burns et al., 1983; Clarke et al., 1992). Vast regions of fainter emission extend beyond the inner lobes: the middle lobe extends out to 40 kpc, while the outer lobe is even more diffuse extending out to more than 500 kpc (see Fig. 1, in Morganti et al., 1999). The different orientation and morphologies of the various structures could be the result of precession (e.g. Haynes et al., 1983) of the central engine combined with strong interaction with the surrounding medium. Alternatively, the nuclear activity in Cen A has been recurrent, although recent spectral index studies suggest that the large-scale structure is currently undergoing (or has very recently undergone) some particle injection event (Hardcastle et al., 2009a, and refs. therein).

Most of the cold and warm gas in Cen A is concentrated along the strongly warped dust lane (e.g. Nicholson et al., 1992; Quillen et al., 2006). The neutral hydrogen present in this region (both in emission and absorption) has been studied by e.g. van der Hulst et al. (1983); van Gorkom et al. (1990); Sarma et al. (2002). The morphology and kinematics of the outer regions of the H I disk suggest that some of the gas has not yet settled into regular rotating orbits (van Gorkom et al., 1990).

H I has also been found well outside this disk. At a distance between 10 and 15 kpc from the nucleus, Schiminovich et al. (1994) have found a partial ring structure with a smooth N-S velocity gradient and rotating perpendicular to the gas located along the dust lane (but co-rotating with the stellar body). In the north-eastern region of this ring, young stars have been detected that have possibly formed by the interaction between the radio jet and the neutral hydrogen in the ring (Oosterloo & Morganti, 2005).

Cen A was shaped through hierarchical merging over many Gyr as revealed by the spread in ages of globular clusters (see e.g. Woodley et al., 2010). The last major merger event happened about 5 Gyr ago (Peng et al., 2004). The prominent warped dust and gas disk in the central region, and the outer partial ring structure, suggest that Cen A experienced a recent merging event where its large elliptical body merged with a smaller gas-rich galaxy (Baade & Minkowski, 1954; Tubbs, 1980). Quillen et al. (1993) calculated a timescale of about 200 million years since the core of the infalling galaxy merged with the centre of the elliptical galaxy. This is consistent with the timescales derived by the presence of tidal debris and by the shell-like features containing atomic hydrogen (Schiminovich et al., 1994; Peng et al., 2002) and molecular gas (Charmandaris et al., 2000).

H I absorption is detected against the nucleus, the northern jet and the southern lobe (e.g. Roberts, 1970; van der Hulst et al., 1983; van Gorkom et al., 1990; Sarma et al., 2002). The absorption against the jet and southern lobe has been interpreted as gas that is part of the large-scale disk which is roughly perpendicular to the jet axis ($PA = 50^\circ$, Tingay et al., 1998). Since no absorption is found against the northern radio lobe, this lobe is likely pointing towards us whereas the southern radio lobe points away. Van Gorkom et al. (1990) and Burns et al. (1983) concluded that the northern part of the gas disk is (at least partly) behind the radio source and the southern part of the H I disk is in front. For the component of H I absorption against the nucleus, earlier observations have shown the presence of redshifted absorption

against the (unresolved) core (e.g. van der Hulst et al., 1983; van Gorkom et al., 1990; Sarma et al., 2002), but our new observations (see below) show that blueshifted absorption against the core is also present (see also Chapter 4 and Morganti et al., 2008).

Despite the many studies devoted to Cen A, there are a number of open questions that are essential for the understanding of the formation and evolution of Cen A and its AGN. For example, the relation between the age of the radio structures and the timescale of the merger is not completely clear. In particular, it is unclear what triggers the current AGN activity (i.e. the activity producing the inner radio lobe) and whether it is related to the merging event. Thus, it is important to obtain the morphology and kinematics of the gas disk to the largest possible radii and investigate the structure of the disk. This can provide an estimate of the timescale of the merger and allow to investigate the presence and kinematics of unsettled gas (e.g. whether significant radial motions are present and, if so, on which scale). At the same time, it is important to investigate the distribution of H I down to the most inner parts of Cen A to understand whether kinematical signatures of gas connected with the fuelling of the AGN are present.

The large amount of H I present in Cen A and its proximity allow to obtain deeper observations which can be used to investigate the questions above. To achieve this, we have performed new spectral-line observations of Cen A that have higher spatial and velocity resolution and better sensitivity than those of previous studies. These new observations have allowed us to detect blueshifted absorption against the nucleus while also the redshifted absorption extends to higher velocities compared to previously known. These results are presented in Chapter 4. This gas will be interpreted as part of a circumnuclear disk, likely the counterpart of what was already detected in CO and other lines, leaving still open the question of what triggers the current AGN activity. To further investigate this issue, we present in this chapter the study of the kinematical state of the H I disk and the results from 3D modelling.

This chapter is organised in the following way. In Sect. 3.2 we present the new observations while in Sect. 3.3 we describe the results. In Sect. 3.4 we derive and discuss tilted-ring models of the H I disk that are based on the 3D data cube that describe the strongly warped H I disk as well as previously published data. We show that the H I is dominated by rotation, with radial motions giving a significant contribution in the outer parts. Furthermore, we argue that the blue- and redshifted absorption against the nucleus must be mainly caused by gas close to the nucleus. In Sect. 3.5 we discuss the consequences of the observational and modelling results for the formation and evolution process of Cen A, the merger timescales involved and the implications for the AGN activity. A short summary is given in Section 3.6.

3.2 Observations and data reduction

Cen A was observed with the ATCA in April 2005. In Tab. 3.1 some basic information about the observations is summarised. Three different standard configurations (750 m, 1.5 km and 6 km) were used, each for a full 12-h run. This setup gives sufficient *uv*-coverage as well as good spatial resolution. In addition, it avoids baselines shorter than 77 m. This is important because the very strong, very extended contin-

Table 3.1: *Summary of observations.*

Total on-source integration time		3×12 h
Observation dates		12/14/22 April 2005
Bandwidth		16 MHz
Number of channels in the cubes		512
Channel spacing (dV)		6.6 km s^{-1}
Velocity resolution (Δv, after Hanning)		13.2 km s^{-1}
Shortest/longest baseline		77 m/6 km
Bandpass/flux calibrator		PKS 1934–638
Gain/phase calibrator		PKS 1315–46
Data cube	high resolution	low resolution
Weighting scheme	uniform	robust 0
Beam (HPBW)	$8\farcs1 \times 6\farcs8$	$19\farcs6 \times 18\farcs2$
Beam position angle	–12.3°	–48.3°
rms noise (mJy beam^{-1}) in the cubes	1.3	1.2
rms noise (10^{19} atoms cm^{-2})	30.92	4.45
rms noise ($M_\odot$ pc $^{-2}$)	2.48	0.36
Peak flux continuum (Jy beam^{-1})	4.41	4.95
rms noise (mJy beam^{-1}) continuum	32.2	26.7

uum emission of Cen A makes bandpass calibration in practice impossible on short baselines where the flux is well over 100 Jy (see below).

The total bandwidth covered was 16 MHz – corresponding to a velocity range of 3000 km s^{-1} – with 512 frequency channels. This is much broader than used in earlier observations (e.g. van der Hulst et al., 1983; van Gorkom et al., 1990; Sarma et al., 2002). In order to have enough line-free channels for the continuum subtraction, the central velocity of the observing band was about 200 km s^{-1} below that of the systemic velocity of Cen A to account for the Galactic H I emission/absorption. The spectral resolution is 13.2 km s^{-1} after Hanning smoothing. We used PKS 1934–638 as bandpass and flux calibrator. To monitor the system gain and phase changes, PKS 1315–46 was observed as a secondary calibrator for ten minutes every hour, although self calibration was also employed (see below). The data reduction was performed using the MIRIAD package (Sault et al., 1995).

The extremely strong radio continuum requires careful bandpass calibration in order to obtain flat spectral baselines. Following a technique applied successfully by Oosterloo & Morganti (2005) on earlier observations of Cen A, we smoothed the bandpass calibration obtained from PKS 1934–638 with a box-car filter 15 channels wide. Since the instrumental features in the bandpass are fairly broad in frequency, this procedure is allowed and it minimises the contribution of extra-noise from the bandpass calibration that otherwise would have occurred since the bandpass calibrator is fainter than the very extended emission of Cen A. Through this smoothing, the effective flux level of PKS 1934–638 increases to about 60 Jy which is higher than the detected flux on almost all baselines. The smoothed bandpass correction was

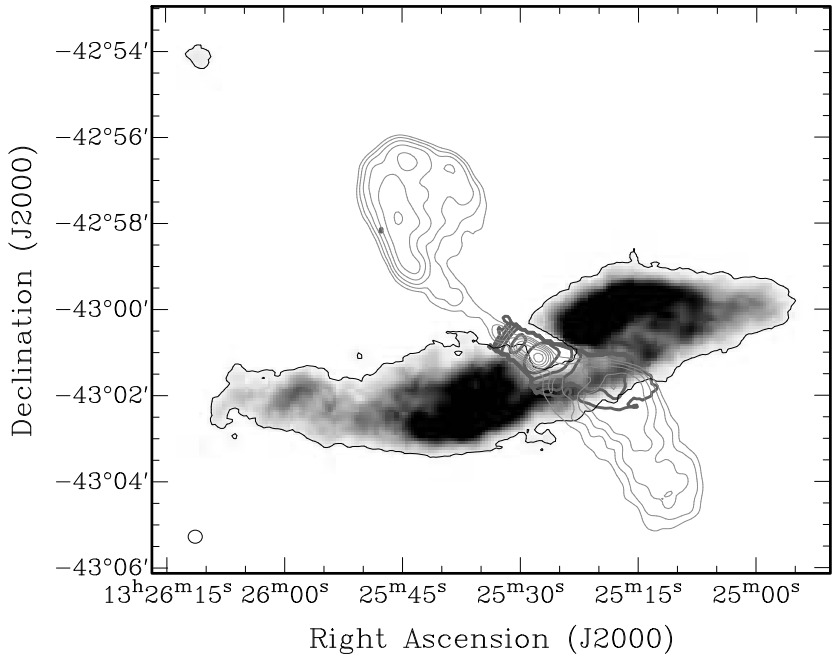

Figure 3.1: H I *emission in greyscale overlaid with the low resolution radio continuum (thin, grey contour levels: 0.5 Jy beam*$^{-1}$ *increasing with a factor of 1.5) and absorption contour levels on top (thick contours). Absorption contour levels:* 0.33×10^{19} *cm*$^{-2}$ *increasing with a factor 3. Emission contour level:* 1.5×10^{20} *cm*$^{-2}$*. The beam is plotted in the bottom left corner.*

applied to the unsmoothed data of Cen A. This procedure ensures that the velocity resolution is preserved without increasing too much the noise of the data. The strongest H I absorption is just over 2 Jy and the dynamic range in the spectral line cubes is better than 1:1000.

The continuum was subtracted using UVLIN by making a second-order fit to the line-free channels of each visibility record and subtract this fit from the spectrum. The line cube, as well as the obtained continuum image, was cleaned. Hanning smoothing was applied to the line cube. Frequency independent self-calibration of the phase using the channel with the strongest nuclear absorption improved the image quality, but a few channels with the strongest absorption still show some calibration artifacts. The final cube was derived by combining the datasets of the three observations. The beam size in the resulting uniformly weighted cube is $8\farcs1 \times 6\farcs8$, PA = $-12\fdg3$. The image noise is about 1.3 mJy beam^{-1}. For the kinematic modelling of the disk (see Sect. 3.5), a cube with robust weighting set to 0 was made while also tapering the visibility data with a Gaussian taper. The resulting beam size for this cube is $19\farcs6 \times 18\farcs2$, PA = $-48\fdg3$. This lower resolution cube is a compromise between spatial resolution and sensitivity.

3.3 Results

3.3.1 The structure of the H I emission

As expected from previous observations, H I is detected both in emission and in absorption and most of the gas is concentrated in a relatively edge-on, warped structure that mainly follows the dust lane (see Fig. 3.1 and 3.2). Channel maps of the data cube are shown in Sect. 3.A[2]. On both the eastern and western side, the H I extends beyond the visible dust lane and, in total, has an extent of $\sim$ 15 kpc in diameter. The total mass of the H I disk is $4.9 \times 10^8\ M_\odot$. This is slightly higher than what was derived from VLA observations ($4.2 \times 10^8\ M_\odot$, after correcting for the difference in the assumed distance; van Gorkom et al., 1990). The difference is likely due to better separation of emission and absorption in the central regions (due to our better spatial resolution), and to the higher sensitivity of our observations.

In Sect. 3.4 we present detailed modelling of the geometry and the kinematics of the H I, but we briefly discuss the main points here. The main conclusion is that the kinematics of the H I is regular in the inner regions of the disk. Large-scale radial motions exist, but are only present at larger radii. There are no indications of anomalies in the kinematics of the gas (on the scale down to the inner beam, $\sim$ 100 pc) that could be related to supplying material for the AGN.

Interestingly, the radial motions of the outer regions are such that the projected velocities are *redshifted* compared to the regular orbits (see below and Fig. 3.3). This means that the blueshifted absorption, discussed in detail in Chapter 4 (see also Sect. 3.3.2), cannot be caused by out-moving gas at large radius projected onto the centre. In Chapter 4 we will argure that the blueshifted absorption, together with the already known redshifted nuclear absorption, is evidence for a regular inner disk.

Previous studies have already shown that the kinematics of the gas in the dust lane is dominated by rotation (see also the *pv*-diagram in Fig. 4.2 of Chapter 4). Although there is a fair degree of symmetry in the H I distribution, significant deviations from symmetry are present, not only in morphology, but also in kinematics. As can be seen from Fig. 3.2, the famous optical dust lane has a clear counterpart in H I. Below the dust lane, south-west of the nucleus, a similar amount of H I is present as in the dust lane itself. Previous observations (e.g. Schiminovich et al., 1994) had already shown the presence of this H I, but it is better visible in our data. Most of the H I south-west of the centre can be explained in a simple way. In the optical, the dust lane is only visible where the gas and dust disk is in front of the galaxy, i.e. the north-eastern side. South-west of the nucleus, the disk is behind most of the stellar body and it will be much less visible in absorption. However, the H I of the disk is seen in emission and therefore both the back and the front side of the disk are visible equally well.

The kinematics of the H I also shows that the outer gas disk south of the centre is not perfectly regular. The position-velocity plot given in Fig. 3.3 shows the kinematics of part of the south-western disk. Since the position-velocity plot was taken far from the nucleus, both the emission and absorption should reflect the kinematics of the same outer H I disk. The only difference between absorption and emission

[2]The channel maps were not part of the original publication.

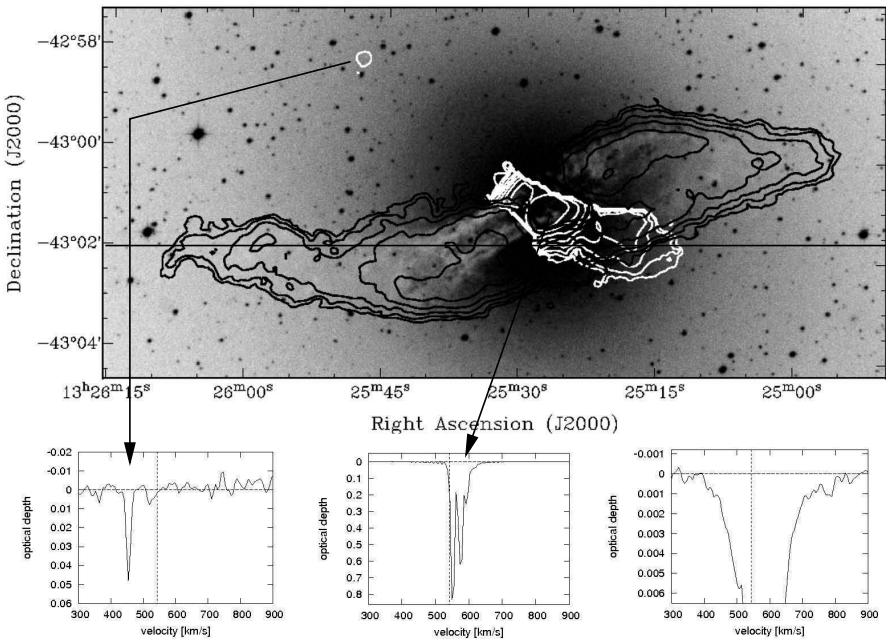

Figure 3.2: *Top panel: Total intensity contours over-plotted on DSS image. Contour levels: 0.2, 0.4, 0.8, 1.6 (absorption only), 3.2, 6.4, 12.8, 25.6 and* 51.2×10^{20} *atoms cm*$^{-2}$ *for the emission (black) and absorption (white).* $T_{\rm spin}$ = 100 *K. The horizontal line indicates the position of the pv-slices in Fig. 3.3 and 3.8. Bottom left panel: spectrum of* H I *absorption cloud. Bottom middle panel: spectrum of the nuclear absorption. Bottom right panel: zoom-in of bottom middle panel.*

should be that the absorption comes from that part of the south-western disk that happens to be in front of the radio continuum lobe, but the kinematics of the absorption should smoothly fit that of the emission. However, the absorption is offset in velocity with respect to the emission, something that is not expected for a regular rotating disk with circular orbits. In addition, the absorption structure has a faint continuation in emission, see the box in Fig. 3.3.

The presence of this gas is interesting for various reasons. The part in emission represents a spatially and kinematically continuous structure that appears to be, at least partly, connected to the large-scale disk. The gas originating the emission and the absorption (inside the box in Fig. 3.3) is likely to be one continuous structure, representing front and back of one continuous structure (called "outer arm"). The observed *broad* profiles suggest that radial motions must be affecting the gas in addition to the rotation. Further intriguing is the fact that we do not detect similar structures on the opposite (northern) side of the dust lane. This already points to an asymmetry at large radius in the distribution of gas that is clearly a complication in the modelling of the data (see Sect. 3.4).

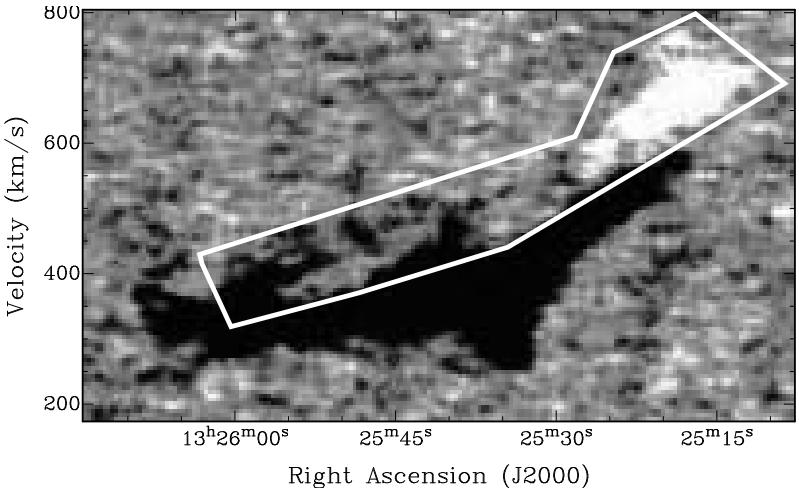

Figure 3.3: *Position-velocity plot obtained along a slit in PA = 90° as illustrated in Fig. 3.2. The data is integrated over 24″ in Declination to better highlight the faint outer* H I *arm structure in emission (black, inside the white box) which connects with the absorption (white) on the western side. Note that the greyscale is inverted (i.e. absorption white, emission black) compared to Fig. 3.4, 3.5 and 3.8 to better highlight the faint emission.*

Table 3.2: *Absorption-line properties.*

Component	V [km/s] (1)	Δv [km/s] (2)	τ (3)	$N_{\rm H\,I}\,/T_{\rm S}$ (4)
Nucleus	550	18	0.83	2.74×10^{19}
Nucleus	574	23	0.62	2.61×10^{19}
Nucleus	592	20	0.26	9.52×10^{18}
Nucleus (shallow)	*	400	*	*
Jet	550	19	0.64	2.23×10^{19}
Jet	544	25	0.64	2.93×10^{19}
Cloud	454	13	0.07	1.72×10^{18}

Notes – (1) Velocity of the peak. (2) FWHM (3) Peak optical depth. (4) H I column density [$\rm cm^{-2}\ K^{-1}$].

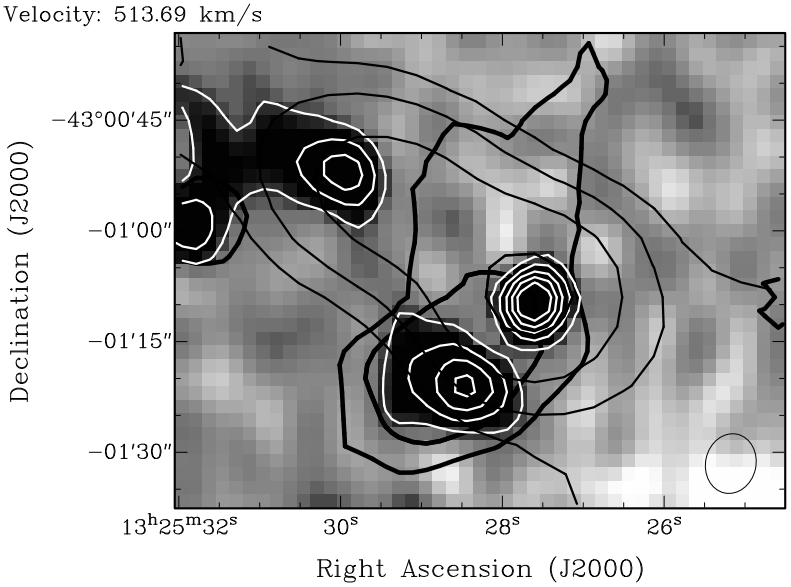

Figure 3.4: *Velocity channel of the high-resolution cube (greyscale). The white contours show the* H I *absorption (-15, -12, -9, -6 and −3σ). The thick black contours give the CO emission Liszt (2001). In thin black contours (0.5, 1.0, 2.0 and 4.0 Jy beam*$^{-1}$*) the low-resolution continuum image is shown. The beam of the* H I *cube is indicated in the lower right corner.*

3.3.2 H I in absorption

The ATCA observations reveal new features also for the H I absorption. Figure 3.1 shows the total intensity of the H I in absorption as well as the low-resolution continuum as obtained from the line-free channels. The radio continuum shows the inner lobes and the inner jet, in agreement with previous observations (e.g. Clarke et al., 1992; Burns et al., 1983). The H I absorption is detected against the southern radio lobe, the northern jet and the unresolved nucleus, see Fig. 3.2 for more details. In addition, we detect absorption up to ∼ 20″ (corresponding to ∼ 3 beams) east of the core, in the direction perpendicular to the jet (Fig. 3.4), indicating the presence of background radio continuum extended in that direction. There is a close correspondence between this absorption and the CO emission as detected by Liszt (2001) (see Fig. 3.4).

Figure 3.5 shows a position-velocity plot along the jet PA. This illustrates how complex the absorption is and, in particular, that there is redshifted absorption everywhere. The outer filament at large radius is redshifted and partly in front of nucleus (see Sect. 3.3.1 and Fig. 3.3). It is therefore difficult to disentangle whether at least part of the redshifted absorption is at all associated to infalling gas. No equivalent, large-scale blueshifted gas seems to be present.

As shown in Fig. 3.2, the absorption against the northern jet and the beginning southern lobe has a typical column density (assuming $T_{\rm spin}$ = 100 K) of the order of

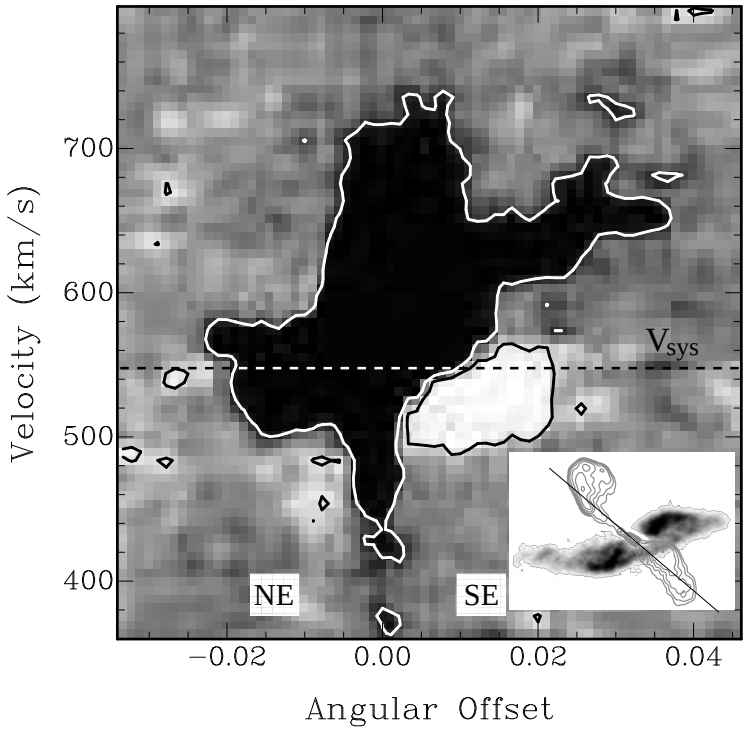

Figure 3.5: *Position-velocity plot obtained along the radio jet, as illustrated in the inset in the lower right corner. Contour levels: -3 (white) and 3σ (black). The systemic velocity is indicated by the dashed line.*

10^{21} cm^{-2} which is of the same order as the column densities of the neighbourhing emission. Because both seem to be connected to the large-scale disk (Sect. 3.4), this suggests that 100 K is a reasonable choice for the spin temperature in this region. However, the south-western parts of the absorption have more than an order of magnitude lower column densities – i.e. $\leq 10^{20}$ atoms cm^{-2} (see Fig. 3.2) – and hence these column densities are below the detection limit (3σ level per channel) of the H I emission.

While the extended H I absorption against the northern jet and the southern lobe is in agreement with previous observations, most exciting is the result that the absorption against the unresolved nucleus is much broader than previously known (Fig. 3.2). In particular, the blueshifted part of the absorption was undetected in previous studies. A complete analysis and discussion of the origin and nature of this absorption against the nucleus is presented in Chapter 4. While the shallow part of the nuclear absorption is new, the deep components close to the systemic velocity are in agreement with van der Hulst et al. (1983). Peak velocities, width of the profiles, optical depths and column densities are summarized in Tab. 3.2.

For the nuclear components of the H I absorption, the value of the spin temper-

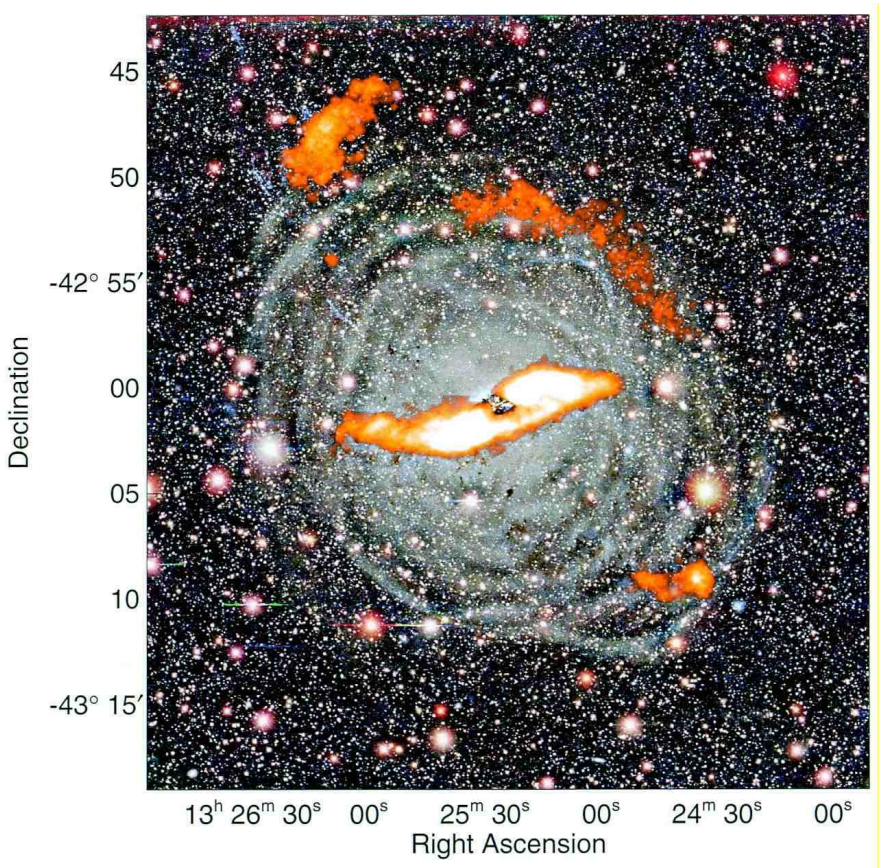

Figure 3.6: H I *emission obtained from the ATCA observations (orange) superimposed to an optical BVR image obtained after unsharp masking and adaptive histogram equalisation by Peng et al. (2002).*

ature is much more uncertain as the gas could be located closer to the AGN (see Sect. 3.4 and 3.5) and therefore $T_{\rm spin}$ = 100 K could underestimate the real value. According to Bahcall & Ekers (1969) and Maloney et al. (1996) the spin temperature can easily reach a few times 10^3 K for gas close to an AGN. Assuming a spin temperature of a few 1000 K, we estimate column densities of $\sim 10^{22} - 10^{23}$ cm^{-2}, similar to what is found in other radio galaxies (e.g. Peck & Taylor, 2001; Momjian et al., 2002, 2003; Morganti et al., 2004). We can compare the H I column density of Cen A with the value derived from X-ray observations. Evans et al. (2004) have estimated a column density for the nucleus (from Chandra and XMM-Newton data) of 10^{23} atoms cm^{-2} that is comparable to our value if we assume $T_{\rm spin} \approx 3000$ K. It is worth noting, that the column density derived for Cen A from the X-ray is relatively high compared to other radio galaxies of similar radio power (see e.g. Balmaverde et al., 2008).

3.3.3 Two newly discovered H I clouds in the environment of Centaurus A

H I at large distances from the dust lane was detected and studied by Schiminovich et al. (1994). These large-scale structures are also detected in our data as illustrated in Fig. 3.6 which shows an overlay of the H I emission on an optical image obtained by Peng et al. (2002). The optical image emphasises the low-contrast features and in particular the complex and extended set of shells and the faint dust extensions. However, our observations include only one pointing on the centre of Cen A and therefore these structures are not imaged as well as in the work of Schiminovich. We therefore consider the study of this large-scale H I structure beyond the scope of this chapter.

However, it is interesting to note that two additional unresolved clouds are detected in our observations, far away from the H I disk (see Fig. 3.1). The first cloud is detected in absorption against the NE radio-lobe (see also Fig. 3.2) at a distance of 4.′7 (about 5.2 kpc) from the nucleus (PA = 50.°5) and has a velocity width (FWHM) of only $\Delta v = 19$ km s^{-1} . The velocity of this cloud (454 km s^{-1}) is below the systemic velocity of Cen A. The optical depth is $\tau = 0.05$ corresponding to a column density of about 10^{20} atoms cm^{-2}, resulting in an upper detection limit of 10^5 $M_\odot$ (assuming a spin temperature of 100 K and a filling factor of unity). The second cloud is located 11 kpc from the nucleus at a position angle of about 48.°5 w.r.t. the nucleus and is detected in emission at $v = 418$ km s^{-1} . The cloud is only visible in the low resolution cube, which indicates a diffuse nature. Also this cloud has a small velocity width ($\Delta v = 24$ km s^{-1}) and an H I mass of about 8×10^5 $M_\odot$. Both clouds are located along the jet axis where also ionised gas has been detected (e.g. Dufour & van den Bergh, 1978; Morganti et al., 1991).

3.4 The H I model

The modelling of the H I has at least two main goals. It allows to investigate the formation and evolution of Cen A (e.g. its merger history) through the study of the morphology and kinematics of the gas over the whole disk. The molecular and ionised gas disks are not as extended as the H I. The second reason is to pin down the location of the gas responsible for the nuclear absorption. Is the absorbing gas located in the vicinity of the nucleus or at large distance projected in front of the core? The answer to this question is important for the understanding of the AGN activity (see Sect. 3.1 and Chapter 4).

A number of modelling studies of the large-scale gas disk of Cen A have been done in the past (see Morganti, 2010, for a review), but previous H I emission-line studies (van Gorkom et al., 1990) did not allow such a detailed investigation as presented here. Bland et al. (1987) and Nicholson et al. (1992) used the velocity field derived from Hα observations to obtain models describing the warped dust-lane structure with a set of tilted-rings. The largest radius fitted corresponds to about 245″ ($\sim$ 4.5 kpc, see also Fig. 3.10). Quillen et al. (1992) obtained from CO observations a first warped disk model that matches the optical appearance of the dust

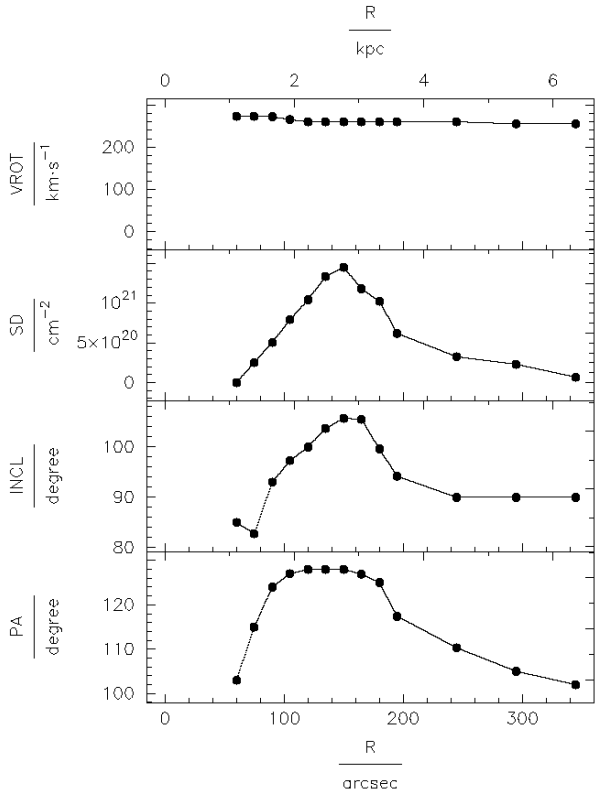

Figure 3.7: *Parameters of the* H I *model described in Sect. 3.4.*

lane and which is also consistent with the H I rotation curve derived by van Gorkom et al. (1990). In the most recent model of Quillen et al. (2006), derived from new mid-infrared observations, the position angle is quite similar – at large radii – to the one of Nicholson et al. (1992) although the inclination is closer to edge-on for $r > 140''$ (see also Fig. 3.10).

Sparke (1996) developed a number of dynamical models to explain the geometry of the disk as that of a near-polar structure precessing around the symmetry axis of an approximately oblate galaxy potential. These models compare well with the orientation of the model by Nicholson et al. (1992). According to all these models, the gas disk is strongly warped and crosses the line-of-sight several times at different radii. With this complex geometry, it is impossible to unambiguously assign velocities to a position on the sky and, therefore, to derive a reliable tilted-ring model (Rogstad & Shostak, 1972) and a rotation curve based on the velocity field only. Thus, a construction of model cubes is needed for a proper comparison with the data.

To achieve this, we have created full 3D model cubes using GASMOD, a phyton code to calculate the tilted-ring models (kindly provided by Paolo Serra). The initial parameters of inclination and position angle for the large-scale disk were taken from

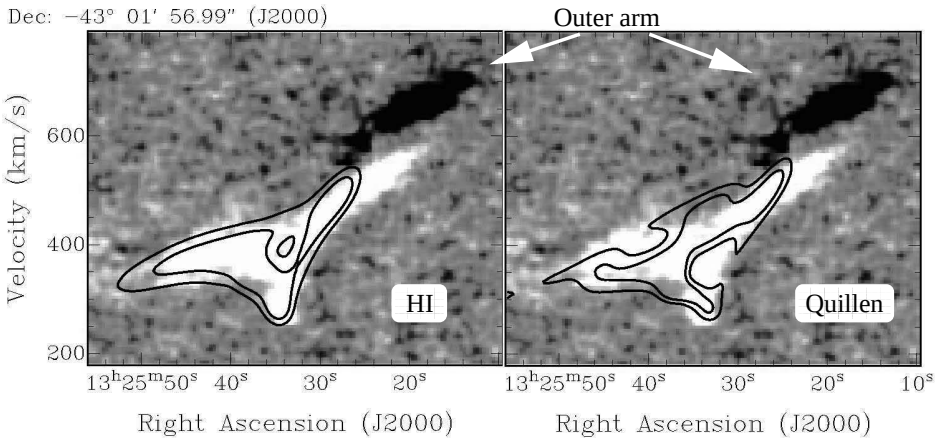

Figure 3.8: *Position-velocity plot along the PA indicated in Fig. 3.2.*

Quillen et al. (2006). Because these parameters do not extend to the entire range of radii covered by the H I, we have extrapolated them to larger radii. A flat rotation curve, that rises steeply inside our first ring has been assumed. The best values for the coordinates of the centre and for the systemic velocity are in agreement with literature values. For the systemic velocity the value of $v_{\rm sys} = 546$ km s^{-1} was used, similar to the value of van Gorkom et al. (1990, $v_{\rm sys} = 542$ km s^{-1}). All parameters (surface brightness, rotation velocity, inclination, position angle) were then independently varied from their initial values for every single ring.

The model cubes were compared with the H I data cube to make sure that the model would describe the kinematics of the observed gas. The changes to the model were made based on a visual inspection of model cube and data. We also produced from the model the distribution of the total intensity of the H I that was then compared with the Spitzer image in order to make sure that the model would also reproduce the overall characteristics of this image. In order to perform this comparison, models were produced with the spatial resolution of the Spitzer data (see below).

The starting parameters clearly did not provide a satisfactory description of the data. The final value of the parameters as function of the radius are shown in Fig. 3.7. The rotation curve is essentially flat and midly decreasing with radius, a phenomenon also observed in other early-type galaxies (see e.g. Noordermeer et al., 2007). Figure 3.8 shows a comparison between a slice of the data and the starting and final model. The slice is close to what is shown in Fig. 3.3 and, therefore, it includes some of the unsettled gas described in Sect. 3.3.1 that we do not expect to see described by the model. However, the region of strong H I emission is clearly better reproduced by our H I model (figure on the left) compared to the model of Quillen et al. (2006). In addition, our H I model also describes the dust morphology (Spitzer image) as shown in Fig. 3.9.

Thus, the model (Fig. 3.7) describes most of the H I morphology and kinematics confirming the regular rotation of the H I structure for $r < 6$ kpc. The orientation

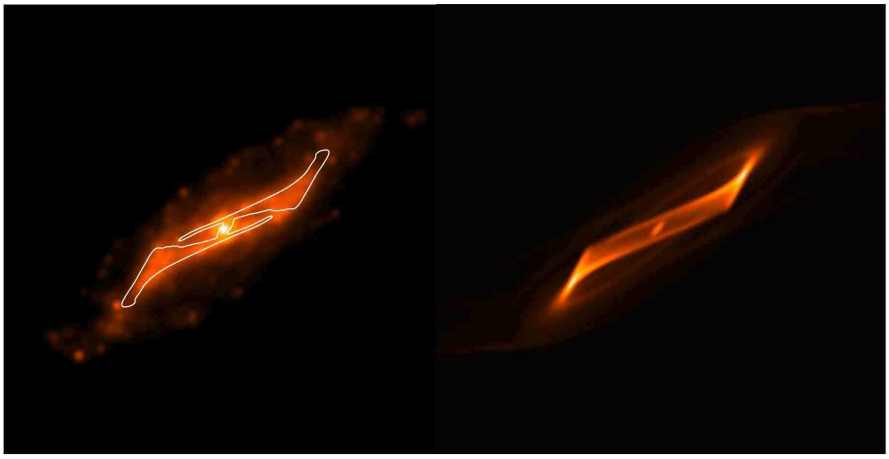

Figure 3.9: *Left panel: Spitzer image (Quillen et al., 2006) over plotted with intensity contours of the high resolution* HI *model. Right panel: Total intensity map of the* HI *model at the resolution of the Spitzer data.*

parameters (position angle and inclination) confirm the heavily warped structure of the disk. In addition, the model shows that in HI a gap in the distribution of the gas is present between 10″ and ∼ 45″ (from 0.2 to 0.8 kpc), confirming what was already found by other studies (e.g. Nicholson et al., 1992; Quillen et al., 1992, 2006; Espada et al., 2009) for the dust, molecular and ionised gas (e.g. Hα and CO).

Our best model uses parameters different from what was found in previous modelling. Figure 3.10 shows a comparison between the parameters of our best model and the parameters from Quillen et al. (2006). The main noticeable difference is in the inclination that appears to stay closer to edge-on for $r > 90''$ in our model. Remarkable is the similarity of our parameters with the independent results from the study of the stellar light emerging from the kiloparsec-scale, ring-like structure detected using the VLT (Kainulainen et al., 2009).

Our model description of the data is solely based on circular rotation and does not require a bar structure (previously claimed to be present by Mirabel et al., 1999), in agreement with the results from the Spitzer images of Keene et al. (2004) and Quillen et al. (2006).

Recently, Espada et al. (2009) have modelled high-resolution CO data obtained with the SMA for the central kpc of Cen A and invoked the presence of a weak bar in these central regions. Interestingly, while their model seems to very poorly describe the jump in velocity observed in the CO velocity field at about 15″ from the centre (see their Fig. 4 compared with their Fig. 11), our model naturally explains this as only due to the geometry of the disk. The presence of a small-scale bar is also ruled out by the near-IR data presented by Neumayer et al. (2007).

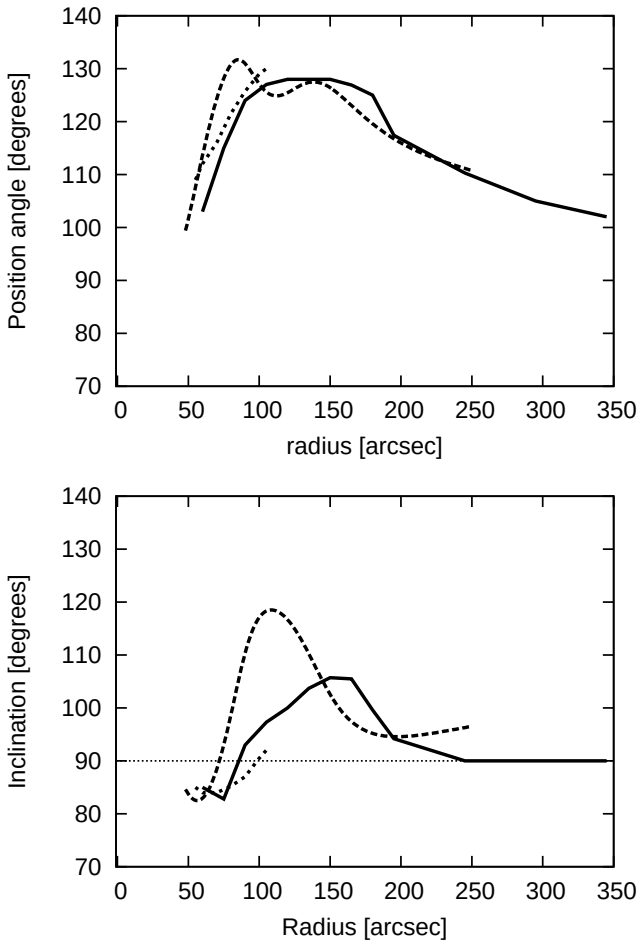

Figure 3.10: *Position angle (top panel), inclination (bottom panel) of our* H I *model (solid line) superimposed to the values from the Quillen et al. (2006) model (long dashed line, similar to those of Nicholson et al. (1992). In addition, also the values from the stellar modelling of Kainulainen et al. (2009) are plotted (dotted line).*

3.5 Discussion

The new data presented here have allowed to image in detail the H I emission and absorption of the warped disk of Cen A and to identify new features in the gas. In this section we discuss the implications of the H I results for the formation and evolution (e.g. merger history) of Cen A and the different phases of AGN activity.

3.5.1 Modelling implications: The large-scale H I distribution

Our data confirm that the structure and kinematics of the H I in Cen A is dominated by rotation, down to the central regions, and most of the H I (but clearly not all) is confined to a fairly regular, warped disk (for $r < 6$ kpc).

In addition to this, we detect outer unsettled gas that appears to be located in an arm-like structure. Therefore, some of the gas in emission and absorption is observed below the dust-lane and it is not reproduced by our modelling. This arm shows a smooth velocity gradient - similar for absorption and emission but with an offset in velocity between the two. Because of the regular velocity characteristics of this structure, it is likely that it will become part of the outer part of the rotating disk in the near future.

This type of structure is expected as a result of a merger or accretion as shown in many numerical simulations (e.g. Hibbard & van Gorkom, 1996; Barnes, 2002). Thus, the H I further support the hypothesis of Cen A being the result of a relatively recent merger of an elliptical galaxy with a smaller gas-rich (SMC-like?) disk galaxy (e.g. Baade & Minkowski, 1954; Quillen et al., 1993, see also Sect. 3.1).

Using the results of our modelling, we can derive a rough estimate of how long ago the merger must have taken place to allow a large fraction of the H I to settle down in the warped disk we observe. We can assume that the gas located at larger radii than we can model (i.e. $r > 350''$) has performed at least one or two revolutions since the merger took place giving a rough estimate resulting in $1.6 - 3.2 \times 10^8$ yr. This time estimate is in agreement, inside the uncertainties, with Quillen et al. (1993, 2×10^8 yr) and Peng et al. (2002, 3×10^8 yr), while it is shorter than what derived by Sparke (1996) – 7.5×10^8 yr – that would correspond to almost five revolutions. Such a long timescale would be sufficient to relax most of the gas in the disk, in contradiction with our H I results.

The merger hypothesis does find further support from the partial ring structure discovered by Schiminovich et al. (1994, see also Sect. 3.1). In that respect the existence of additional, low mass ($< 10^6\ M_\odot$) H I clouds is not surprising. The velocities of the two newly discovered H I clouds (see Sect. 3.3.3) are in rough agreement with the spatial velocity distribution of the "outer ring" structure. Clouds and filaments of ionised gas have been found in this region along the jet direction (e.g. Dufour & van den Bergh, 1978; Morganti et al., 1991). For the origin of these structures, two hypothesis have been put forward. In addition to the merger origin, an alternative scenario was the cooling condensations in a tenuous, thermally unstable hot component of the interstellar medium gas. This scenario was somewhat favoured to explain the filaments of ionised gas, as it would explain the highly turbulent velocity structure observed there (see also Oosterloo & Morganti, 2005). However, such high velocity gradients are not seen in the H I profile of the newly detected clouds, which could mean that the clouds were not hit by the jet. Whether the newly discovered H I clouds are a cooling condensation or are more likely the left over of the interaction/merger discussed above, remains unclear.

As a final remark, we would like to note that also the distribution of the H I confirms what was found by other studies of the molecular gas and dust (Nicholson et al., 1992; Quillen et al., 2006), i.e. the lack of gas in region between 10'' and

45'' (0.2 kpc to 0.8 kpc) while on the smallest scales circumnuclear disks are found (Chapter 4 and ref. therein). The peak in the surface brightness around 150'' from the centre suggests a ring-like structure in the distribution of H I in Cen A (see Fig. 3.7). H I ring-like structures are often detected around early-type galaxies and there are a number of possible scenarios for the formation of such a structure (see e.g. Donovan et al. 2009 for a summary and references). A ring morphology can be the result of the presence of a bar structure but we found no evidence for such a structure in Cen A and indeed many other galaxies with gas rings do not show bars. In some cases, "burning out" of the gas in the central regions of the galaxies has been proposed, but the famous example of IC 2006 (Schweizer et al., 1989) shows that also gas accretion can form these structures.

3.5.2 Merger and different phases of radio activity

The kinematics of the H I in Cen A is dominated by rotation down to the nuclear regions. The discovery that the nuclear absorption is also partly blueshifted, (see also Chapter 4) questions the interpretation that H I against the nucleus represent evidence for the *direct* fuelling of the AGN. Furthermore, our analysis presented here shows that the nuclear blueshifted absorption is not due to gas at large radius seen in projection against the core. The nuclear absorption is likely originating from a nuclear disk that represents the H I counterpart of the structure seen from the molecular gas (see Chapter 4 for a detailed discussion). This nuclear disk is part of the overall warped disk structure. Thus, the nuclear H I gas does not constitute direct evidence of gas infall into the AGN.

However, it is worth mentioning that radial motions (in addition to rotation) on the scale of tens of pc have been detected in the high resolution, near-IR data obtained by Neumayer et al. (2007). Surprisingly, they found that for higher excitation lines [SiVI] and [FeII] the velocity pattern is increasingly dominated by a non-rotating component, elongated along the radio jet. Interestingly, these non-rotational motions were detected *along* the jet with redshifted velocities (compared to the systemic) seen on the main-jet side and blueshifted on the counter-jet side. These motions (stronger in [SiVI]) can be explained as backflow of gas accelerated by the plasma jet. This gas can perhaps be involved in the fuelling of the AGN. Whether a similar situation is also occurring in the H I gas can only be investigated with deep VLBI observations.

In order to investigate in more detail whether a link can be found between the merger/accretion event and the nuclear activity, it is important to compare the timescales of these events. Cen A shows a complex radio structure with lobes on different scales, from a few kpc of the inner lobe (see Fig. 3.1) to tens of kpc for the middle lobe and up to several hundred kpc for the outer lobe (Sect. 3.1). These three radio structures could be either the result of precession (Haynes et al., 1983, see also Sect. 3.1) or the nuclear activity in Cen A has been recurrent. However, the large-scale structure is currently experiencing a particle injection event, as recent spectral-index studies suggest (Hardcastle et al., 2009a, and refs. therein).

The ages of these lobes are not easy to estimate. According to Saxton et al. (2001) the age of the northern *middle* lobe can be estimated to be about 1.4×10^8 yr assuming

this lobe has been created by an old episode of jet activity that has been *interrupted* by the disruption of the jet by the merger. Since then, this structure has been rising buoyantly away from the nucleus. If this is the case, the merger that has brought the H I would actually be the cause of the disruption of the old radio activity. The timescale of the merger derived from the H I could support this idea. The timescale of the inner radio lobe, $\sim 5-10\times10^6$ yr (Croston et al., 2009, and refs. therein), would indicate that it takes quite some time for the system to recover from this disrupting event and for the gas to settle again in a steady accretion flow. A (possible) time-delay between the merger and the onset of the AGN has also been detected in a few other nearby radio galaxies (e.g. Tadhunter et al., 1996; Emonts et al., 2006; Davies et al., 2007; Wild et al., 2010).

It is worth noting that if the scenario proposed by Saxton et al. (2001) is correct, the delay between the disruptive merger and the onset of a new phase of activity could be related to the time required by the X-ray halo to build up again (see Sansom et al., 2000).

On the other hand, recent spectral-index studies have suggested different time-scales for the large-scale radio structure. High frequency studies show a spectral break for the southern lobe that would suggest a life time of 3×10^7 yrs (see Hardcastle et al., 2009a). Furthermore, no spectral break is observed in the northern lobe (both the giant and the middle lobe), suggesting that they have very recently undergone some particle injection event (Alvarez et al., 2000; Hardcastle et al., 2009a, and refs. therein). Thus, if the timescales derived from the spectral index are correct, it would indicate that that the *overall* radio emission starts relatively late compared to the merger.

In both cases, the comparison of the timescale derived from the H I and the radio structure, together with the relatively regularity of the H I down to the sub-kpc regions, do not suggest a one-to-one correspondence between the merger and the phase of radio activity. In particular, if the timescales derived from spectral index are correct, *more than one radio burst can be produced while the merger is settling in*. This would indicate that, while the merger could be responsible for bringing gas in the vicinity of the nucleus, the accretion mechanism that fuels the AGN is likely not related to the merger.

This is in agreement with the idea that in radio galaxies of relatively low radio power (i.e. FR-I type) the fuelling of the black hole proceeds directly from the hot phase of the interstellar medium in a manner analogous to the Bondi accretion. As suggested by a number of authors (see e.g. Allen et al., 2006; Hardcastle et al., 2007) the hot, X-ray emitting phase of the intergalactic medium (IGM) is sufficient to power the jets of several nearby, low-power radio galaxies. In the case of Cen A, a mass accretion rate $\dot{M}_{Bondi} = 6.4\times10^{-4}\ M_\odot\ \mathrm{yr}^{-1}$ and a Bondi efficiency of ~ 0.2 % has been derived from Chandra observations (Evans et al., 2004). However, it would decrease if the new value of the BH mass derived by Neumayer et al. (2007) and Cappellari et al. (2009) is used. These values are consistent with what is found for other FR-I radio galaxies (Balmaverde et al., 2008) while the efficiency appears to be lower than the "canonical" 0.1 for the high efficiency optically thick accretion disks. On the other hand, and to complicate the picture, it is known (from the Fe Kα line and the large column density measured in the X-ray towards the nucleus; Evans et al., 2004)

that Cen A has large quantities of cold gas in a molecular torus at about 1pc from the black hole, more typical of FR-II galaxies.

3.6 Summary

In this paper we have reported ATCA H I synthesis observations which have higher spatial and velocity resolution than previous studies of atomic hydrogen in Cen A. Our study concentrates mainly on the distribution and kinematics of the gas associated with the dust-lane of this galaxy. These data show that the kinematics of the H I in Cen A is dominated by rotation down to the nuclear regions.

The warped morphology and kinematics of the H I can be described with a tilted-ring model with gas on circular orbits. Regular kinematics of the gas is observed for $r < 6$ kpc. We find no need for non-circular motions between 1-6 kpc. There is a lack of H I between 0.1 – 1 kpc, confirming results from observations of CO, ionised gas and dust. The parameters of the model (in particular the inclination) are different from what derived in previous models (Quillen et al., 2006; Nicholson et al., 1992) but nicely consistent with those from the study of the central stellar ring of Kainulainen et al. (2009). Outside 6 kpc radius, asymmetries and arm structures are observed as well as radial motions.

The H I fraction in Cen A ($M_{\rm H\,I}/L_B = 0.01$) is relatively low for an early-type galaxy, indicating that the H I disk might well be the result of accretion of a small (SMC-like?) galaxy. Based on the regular kinematics we suggest that this accretion occured about $1.6 - 3.2 \times 10^8$ yr ago, in agreement with previous estimates. This is too old to *directly* trigger the current phase of AGN activity (the age is a few $\times 10^6$ yr for the inner radio lobes), but might have interrupted the previous episode of AGN activity.

We find extensive H I absorption, against nucleus, jet and lobes. Part of the absorption (in particular with velocities close to $v_{\rm sys}$) is part of the regular rotating disk, while some of the absorption against the southern lobe is part of an outer arm structure. A large fraction of the *nuclear* absorption is not produced by outer gas. This is in particular the case for the newly discovered blueshifted absorption. This absorption is, at least partly, due to a circumnuclear disk at $r < 100$ pc (see Chapter 4 for details). Whether part of the (redshifted) gas is infalling and fuelling the AGN is difficult to establish with our data. The results of Neumayer et al. (2007) – who detected radial motions along the jet axis in near-IR observations – suggest that it could be worth exploring with deep VLBI data whether such a component also exists in H I.

All in all these results suggest that in galaxies with an AGN where a merger/accretion event has clearly occurred in the recent past, the connection between these two events (merger and activity) is far from clear. In the case of Cen A, the AGN may instead be fuelled via a low efficiency/rate accretion, as suggested for other FR I galaxies of similar radio power. The merger may actually have played the opposite role of temporarily disrupting the radio jet and producing the northern middle radio lobe. The delay in creating the much younger inner radio lobe, may be connected to the time that it takes the gas to settle again in a steady accretion flow.

Acknowledgements: We would like to thank Paolo Serra for kindly providing his code to calculate the tilted-ring models, GASMOD. His code can be found under: http://www.astron.nl/~serra/ We thank Alice Quillen for providing her model in digital form and the Spitzer image in fits format. This work is based on observations with the Australia Telescope Compact Array (ATCA), which is operated by the CSIRO Australia Telescope National Facility. This research was supported by the EU Framework 6 Marie Curie Early Stage Training programme under contract number MEST-CT-2005-19669 "ESTRELA".

3.A Appendix: Channel maps

Channel maps of the low resolution cube. The synthesised beam is $18\farcs2 \times 19\farcs6$. The velocity of every channel is shown in the top right corner in $\mathrm{km\,s^{-1}}$. Every second velocity channel is shown. The location of the nucleus is indicated by the cross. Contour levels are: -24, -12, -6, -3 (grey), 3, 6, 12 and 24σ (black).

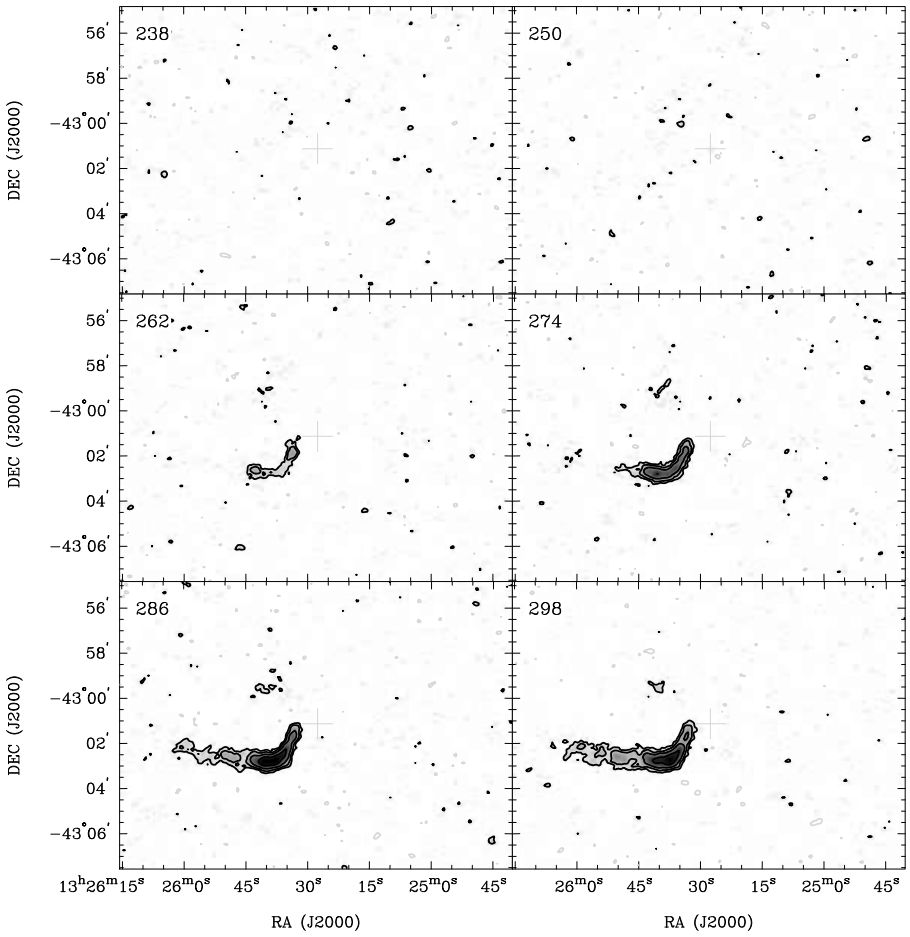

This appendix was not part of the original publication.

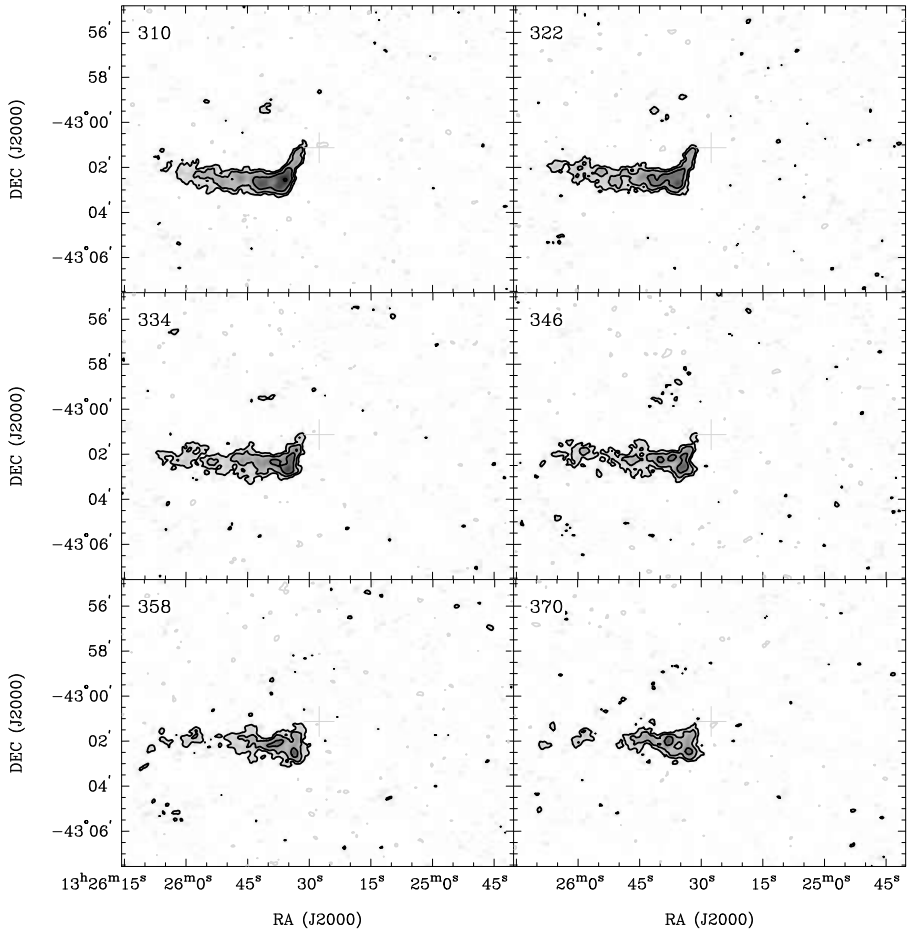
310
322
334
346
358
370
DEC (J2000)
RA (J2000)
56′
58′
−43°00′
02′
04′
−43°06′
13h26m15s
26m0s
45s
30s
15s
25m0s
45s

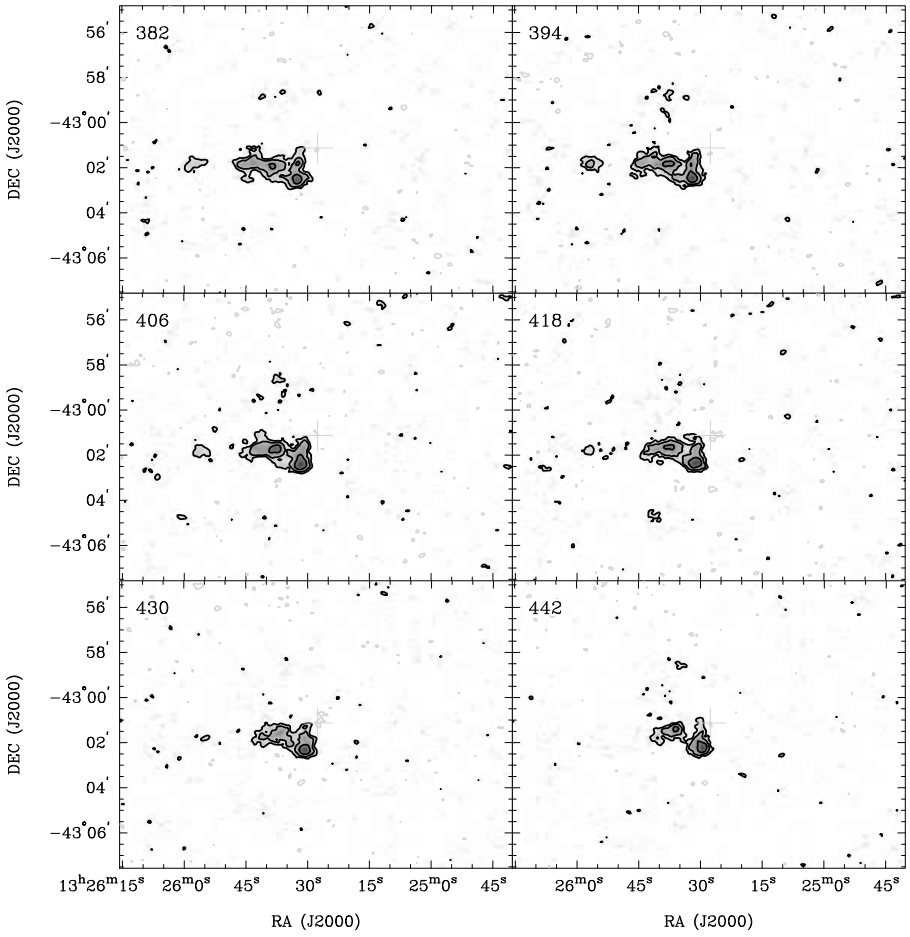
382
394
406
418
430
442
DEC (J2000)
RA (J2000)
56′
58′
−43°00′
02′
04′
−43°06′
13h26m15s
26m0s
45s
30s
15s
25m0s

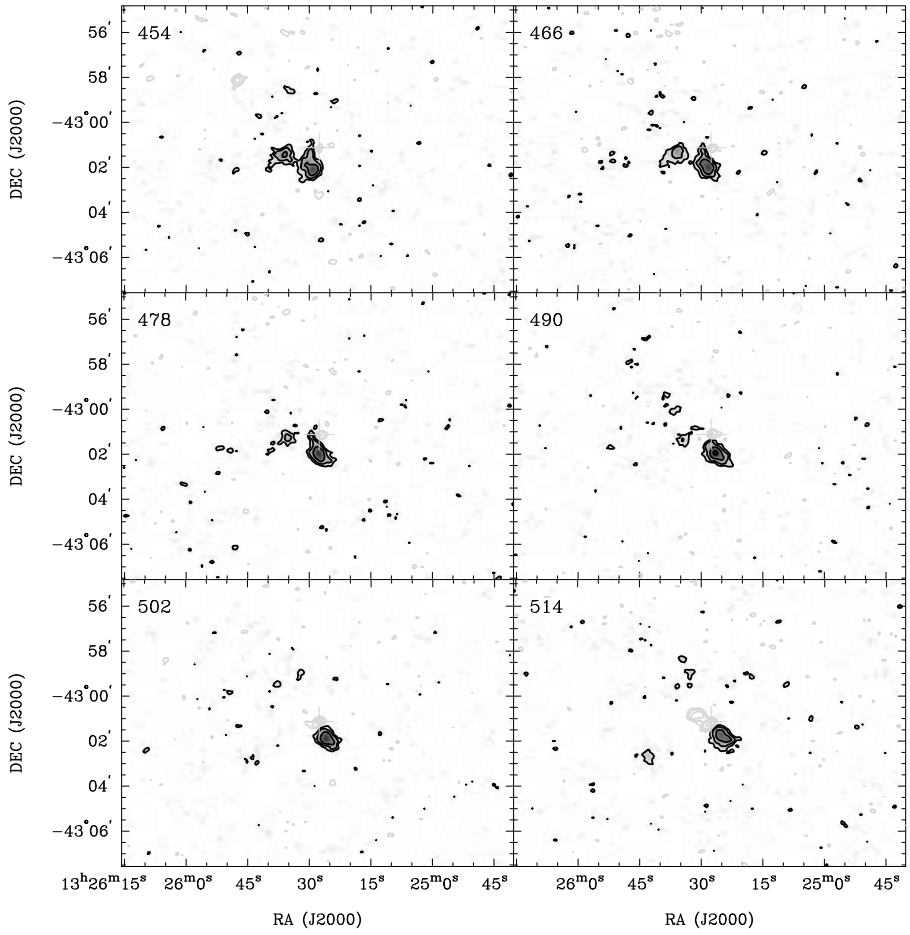
454
466
478
490
502
514
DEC (J2000)
RA (J2000)
56′
58′
−43°00′
02′
04′
−43°06′
13h26m15s
26m0s
45s
30s
15s
25m0s
45s

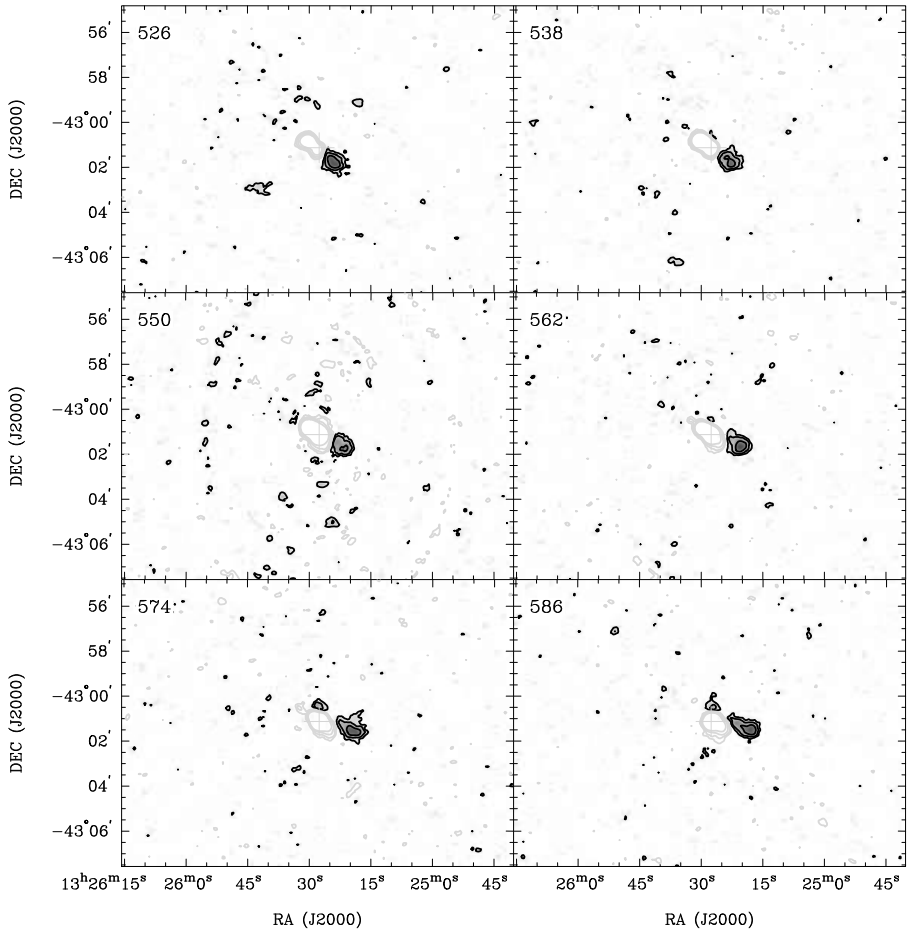
526
538
550
562
574
586
DEC (J2000)
RA (J2000)
56′
58′
−43°00′
02′
04′
−43°06′
13h26m15s
26m0s
45s
30s
15s
25m0s
45s

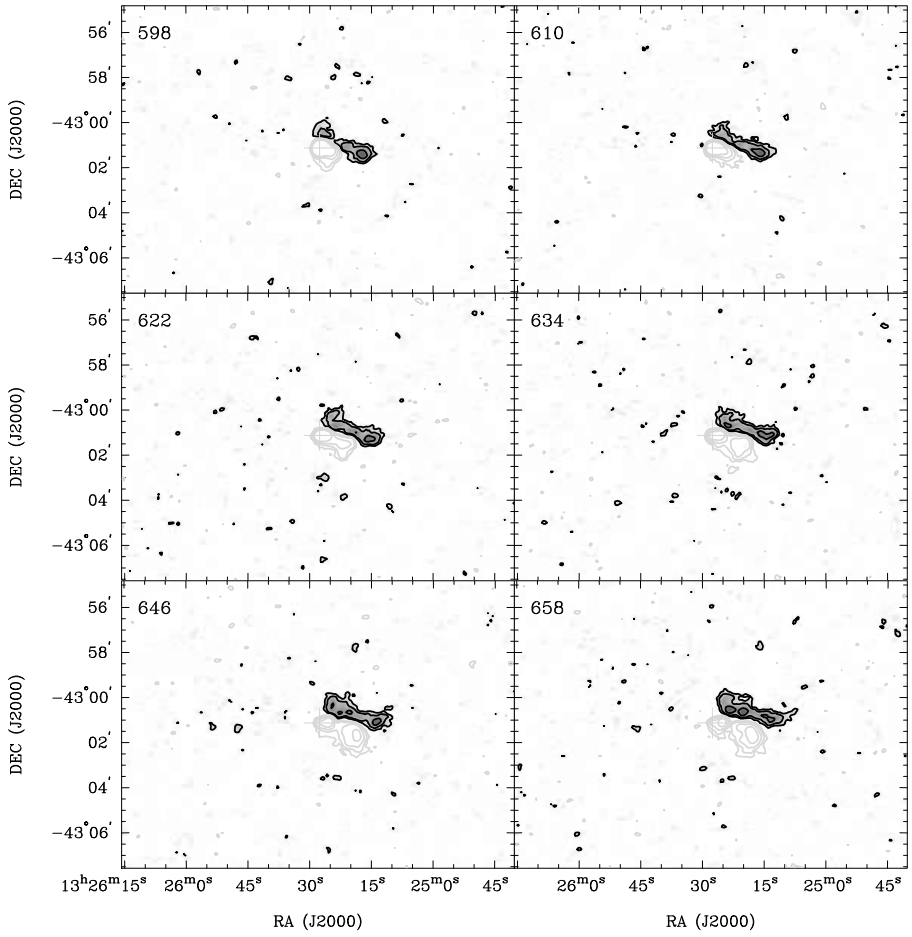
598
610
622
634
646
658
DEC (J2000)
RA (J2000)
56′
58′
−43°00′
02′
04′
−43°06′
13h26m15s
26m0s
45s
30s
15s
25m0s

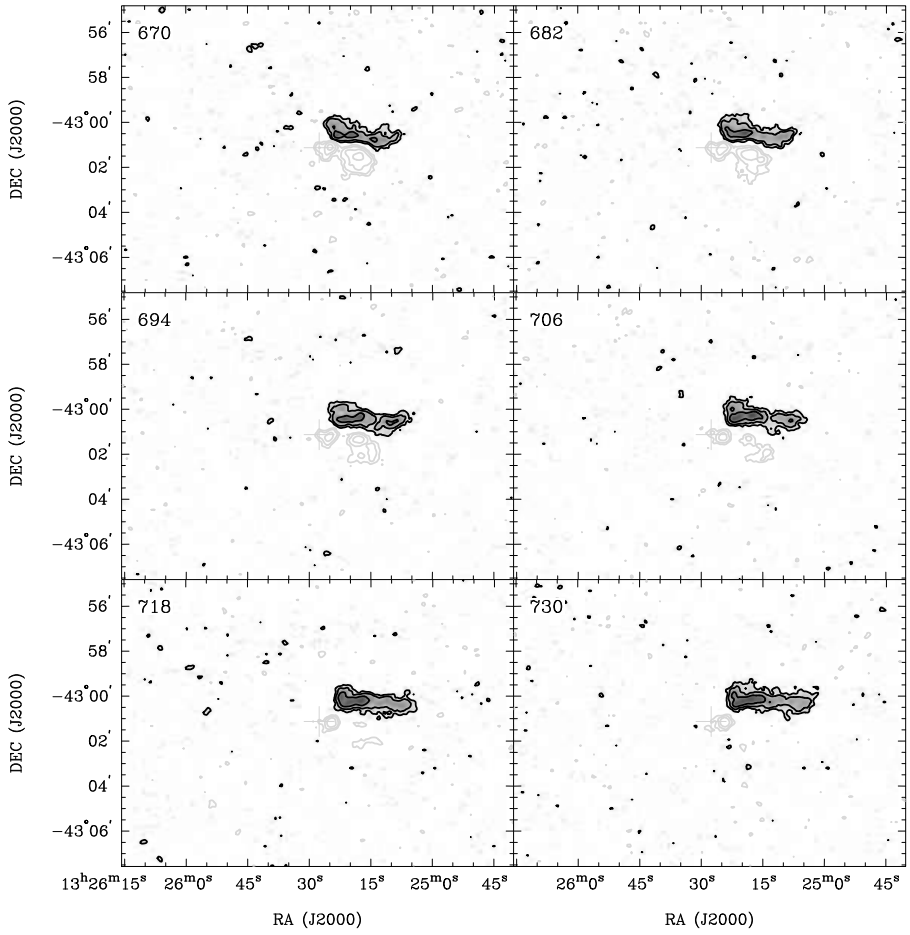
670
682
694
706
718
730
DEC (J2000)
RA (J2000)
56′
58′
−43°00′
02′
04′
−43°06′
13h26m15s
26m0s
45s
30s
15s
25m0s
45s

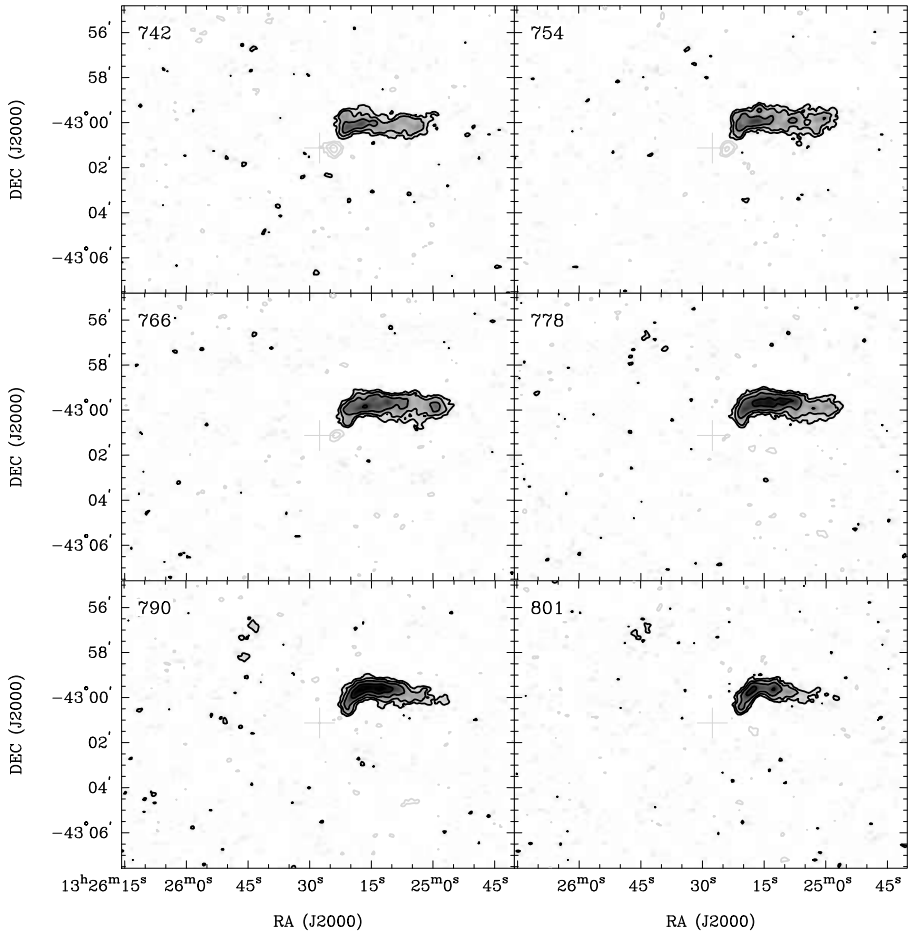
742
754
766
778
790
801
DEC (J2000)
RA (J2000)
56′
58′
−43°00′
02′
04′
−43°06′
13h26m15s
26m0s
45s
30s
15s
25m0s

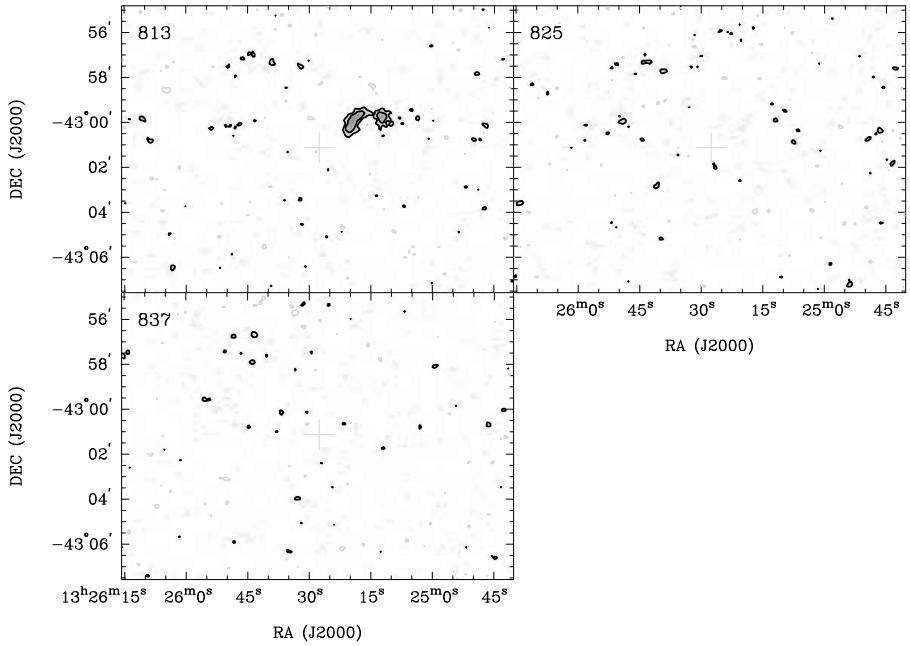
813
825
837
DEC (J2000)
RA (J2000)
56′
58′
−43°00′
02′
04′
−43°06′
13h26m15s
26m0s
45s
30s
15s
25m0s

3.B Appendix: Is Centaurus A special?

In this chapter we have studied the morphology and kinematics of Cen A in detail in order to understand the evolution of this radio-loud source. At the same time, it is important to compare the results to other sources of the same class (i.e. early-type galaxies in general and radio galaxies in particular) to see how Centaurus A fits into the global picture of early-type/radio galaxy evolution.

In this appendix we briefly discuss whether Cen A is special as seen from the neutral hydrogen perspective. That is, do the Cen A properties (such as e.g. HI mass, morphology, kinematics etc.) differ from other early-type galaxies and does Cen A share properties with radio galaxies that have comparable luminosity? Section 3.B.1 compares Cen A with other nearby early-type galaxies and in Sect. 3.B.2 Cen A is compared to a complete sample of nearby radio galaxies (presented in Chapter 2). Conclusions are summarized in Sect. 3.B.3.

3.B.1 Comparison with other early-type galaxies

Although early-type galaxies used to be perceived to be gas poor, different gas phases are in fact detected in many objects, provided deep observations are available. Ionised gas has recently been found in 75% in early-type galaxies (Sarzi et al., 2006) and molecular gas was detected in up to 54% of the observed sources (e.g. Combes et al., 2007; Ocaña Flaquer et al., 2008). The presence of ionised, molecular and atomic gas in Cen A is therfore not surprising (for a summary of the gas properties in Cen A, see Morganti, 2010).

Also in HI more than 50% of non-cluster early-type galaxies are detected with HI masses between 10^6 and 10^{10} $M_\odot$ (Morganti et al., 2006; Oosterloo et al., 2007b). A variety of gas morphologies is present, ranging from very extended (up to 200 kpc) regularly rotating disk/ring structures of low column density (Oosterloo et al., 2007b) to long tidal tails and barely resolved blobs (< 4 kpc diameter) (Morganti et al., 2006). Disks in early-type galaxies can form simultaneously with their host, from major mergers of gas-rich galaxies (see e.g. Hibbard & van Gorkom, 1996; Barnes, 2002). In those mergers, about half the gas is quickly funneled to the centre, partly consumed in a burst of star formation and partly settling in a nuclear central disk (Bournaud et al., 2005). The other half is ejected to large distances but might remain bound to the merger remnant and eventually will fall back settling in a large-scale disk. Compared to other galaxies, the presence of a large-scale rotating HI disk with unsettled gas in the outer parts of the disk (at $r > 6$ kpc), as well as the partial ring structure at larger distances from the nucleus is not unusual.

The observed, essentially flat and only mildly decreasing HI rotation curve (Fig. 3.7) is a commonly observed phenomenon in other early-type (disk) galaxies (see e.g. Noordermeer et al., 2007). In addition, some early-type galaxies (e.g. NGC 3108, ESO 381-47, IC 2006) have ring structures, for instance they have a depression of HI towards the nucleus (Oosterloo et al., 2002; Donovan et al., 2009; Franx et al., 1994). Therefore, neither the rotation curve nor the radial HI surface density distribution of Cen A is unusual when compared with other early-type galaxies.

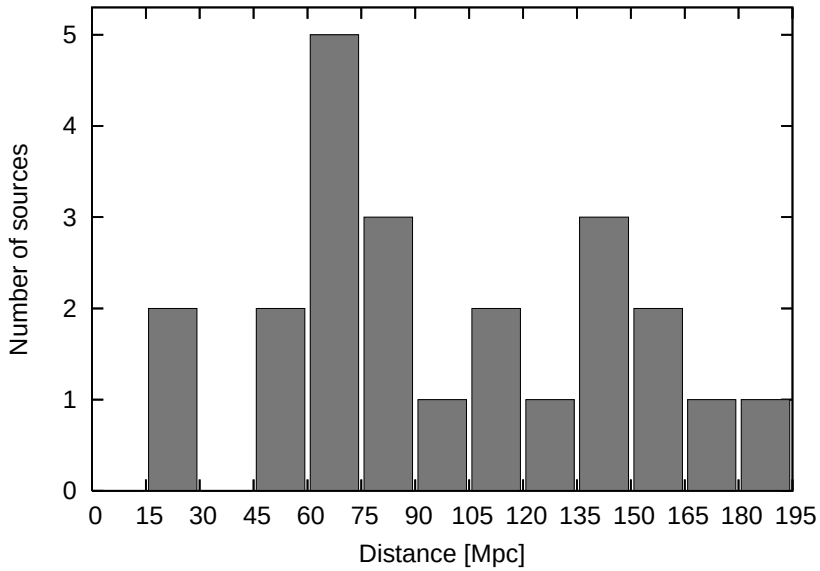

Figure 3.11: *Distances of the radio sources of the complete sample of nearby radio galaxies (Chapter 2, see also Emonts, 2006; Emonts et al., 2010). Cen A (D = 3.8 Mpc) is located a factor > 4 closer than the closest sample source and a factor ~ 26 than the average sample source ($\langle D_{\rm sample} \rangle$ = 101 Mpc).*

One of the well known characteristic of the gas/dust disk in Cen A is the warped structure. While the origin of warps (e.g. mergers, interactions, accretion of gas from the intergalactic medium) is still under debate and may differ from object to object (for a discussion see e.g. Briggs, 1990; García-Ruiz et al., 2002), it is an observational fact that most disk galaxies are at least mildly warped in H I (e.g. García-Ruiz et al., 2002). Most extended H I disks/rings in early-type galaxies are warped, e.g. in IC 4200 or ESO 381-47 (Serra et al., 2006; Donovan et al., 2009). In some cases, the warping amplitude can be large (i.e. approaching 90°) and also start well within the optical disk as is observed in NGC 2685 (Józsa et al., 2009). Considering the merger history of Cen A, it is therefore not unusual that the gas disk in Cen A is warped (Sect. 3.4), neither is the warping amplitude spectacularly high. It is rather its proximity and the orientation on the sky that make Cen A appear as a peculiar warped object.

3.B.2 Comparison with other radio galaxies

In the previous section we have shown that Cen A has an H I morphology and kinematics that is also found in a number of other early-type galaxies and that in this respect Cen A is not special. However, it is still important to compare Cen A with other radio sources as it could be an exceptional radio galaxy.

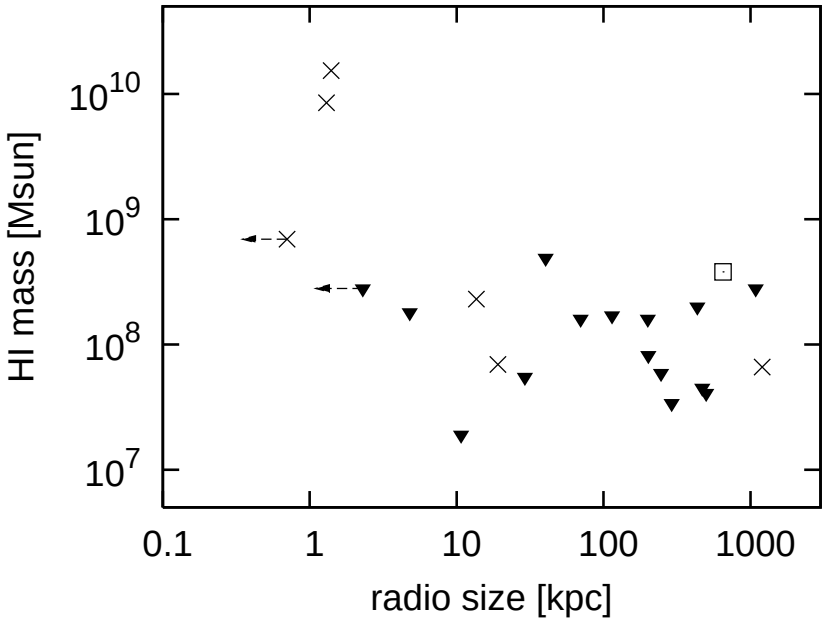

Figure 3.12: *Total* H I *mass detected in emission plotted against the linear size of the radio sources of the complete sample of radio galaxies (Chapter 2; Emonts et al., 2010). The crosses denote the* H I *detections, the filled triangles the upper limits of the non-detections. The open square represents Cen A.*

Radio activity is a short lived (sometimes recurrent) phenomenon (typically believed to be $< 10^8$ yr; based on spectral index studies, e.g. Parma et al., 2002) in the evolution of an early-type galaxy. It is therefore natural that the number density of radio galaxies in the (local) universe is significantly lower than that of early-type galaxies in general. This makes Cen A a unique object only because it can be observed in great detail as it is much closer to us than any other radio source with comparable radio luminosity. Figure 3.11 shows the distances of the complete sample of nearby low-luminosity radio sources presented in Chapter 2 (see also Emonts, 2006; Emonts et al., 2010). The distance advantage of Cen A (and hence the linear resolution) is evident from the figure as even the closest sample source is located more than 4 times as far away as Cen A. For details of the sample and the analysis we refer the reader to Chapter 2, Emonts (2006) and Emonts et al. (2007).

Six out of the 21 sample sources (= 29%) are detected in H I emission. The reason for the slightly lower detection rate (compared to radio-quiet early-type galaxies, > 50%) is that the upper H I mass limits of the non-detections are higher (see Chapter 2). Therefore, the difference is believed to be the result of observational limitations and not to be an intrinsic feature of radio galaxies (Emonts, 2006; Emonts et al., 2010). Similar to the sample of early-type galaxies, a variety of H I structures is found

for the radio galaxies, including (settling) disk structures. However, the striking result from this analysis is that large amounts of H I, rotating in regular disks, are only detected around *compact* sources (typically < 10 kpc, Emonts et al., 2007). Extended radio sources – comparable to Cen A – do only show modest amounts of H I (few times 10^8 $M_\odot$), Fig. 3.12 (see also Emonts et al., 2007). If Cen A would be located at a distance of 70 Mpc the peak of the emission would correspond to about $4\sigma_{\rm rms}$ resulting in a blob like structure, extended over 1-2 beams. In addition, the deep part of the absorption would be detected. However, at larger distances (D > 70 Mpc), the emission of Cen A would not have been detected. Therefore, the results from the statistical sample are not in conflict with Cen A's H I mass.

Cen A, with its 650-kpc continuum structure (see e.g. Feain et al., 2009), is believed to have gone through multiple phases of AGN activity. Recurrent radio activity is also found in a number of other sources (see e.g. Schoenmakers et al., 2000). We note that at least one H I detected compact radio sample source shows a 240 kpc relic structure at the sub-mJy level (B2 0258+35 [NGC 1167], see Chapter 7), showing that also some of these compact sources had previous phases of AGN activity. Therefore, also the radio continuum structure of Cen A does not appear unusual compared to other radio galaxies.

H I in absorption has been detected in a large number of radio galaxies which can be red- and blueshifted (see refs. in Chapter 1 and 2). In some cases, the H I absorption is centred on the systemic velocity of the galaxy and is often interpreted as a circumnuclear disk/torus, (see e.g. Chapter 5; Conway & Blanco, 1995; van Langevelde et al., 2000; Peck & Taylor, 2001) which is actually in agreement with theoretical predictions (e.g. Maloney et al., 1996). The H I ATCA observations of Cen A are in agreement with such a circumnuclear structure (see Chapter 4 and Morganti et al., 2008), which is further supported by the existence of a molecular circumnuclear disk (Liszt, 2001; Neumayer et al., 2007).

3.B.3 Conclusion

Our brief comparison shows that the H I mass, its distribution and the mainly settled kinematics of Cen A is also commonly found in other early-type/radio galaxies. The fact that the current phase of AGN activity is not connected to the recent merger is in line with the results from our sample of radio galaxies (Chapter 2). In addition, the interpretation of the red- and blueshifted nuclear absorption as evidence for a circumnuclear H I disk/torus structure (see Chapter 4 for details) agrees with the results found for other sources. Hence, in the context of galaxy formation and evolution, Centaurus A seems to be – from an H I perspective – a typical galaxy of its class.

4 A circumnuclear disk of atomic hydrogen in Centaurus A

— published as R. Morganti, T.A. Oosterloo, C. Struve & L. Saripalli. 2008. A&A 485, L5 —

Abstract

We investigate the H I absorption in the central regions of Centaurus A using the ATCA data presented in Chapter 3. For the first time, absorption is detected against the radio core at velocities blueshifted with respect to the systemic velocity. Moreover, the data show that the nuclear redshifted absorption component is broader than reported before. With these new results, the kinematics of the H I in the inner regions of Cen A appears very similar to that observed in emission for the molecular circumnuclear disk. This suggests that the central H I absorption is not, as was previously claimed, evidence of gas infall into the AGN, but instead is due to a cold, circumnuclear disk.

4.1 Introduction

In the central regions of galaxies with an active galactic nucleus (AGN), gas can play different, sometimes competing roles. This gas is considered to be essential for fuelling the AGN and for turning a dormant black hole into an active one. On the other hand, the gas can also be expelled from these regions as a result of the release of energy from the active nucleus, so that fuelling and star formation are quenched. Moreover, some of the nuclear gas can be arranged in regular structures. Such circumnuclear disks, under certain geometries, can hide the active nucleus from our direct view and can play an important role in explaining the apparent differences between the various types of AGN. The conditions in these central regions are clearly harsh, nevertheless, they are such that not only very dense or highly-ionised clouds, but also atomic and molecular gas, can survive.

It has been suggested that neutral hydrogen falling onto the central black hole is a possible mechanism for fuelling an AGN. For many years, the available data seemed to indicate that if H I absorption is detected against the core of a radio-load AGN, it is seen at velocities redshifted with respect to the systemic (see, e.g., van Gorkom et al., 1989). Although other factors, such as non-circular motions, can explain redshifted absorption in a single galaxy (see, e.g., García-Burillo et al., 2007), the strong predominance of redshifted absorption has been interpreted as evidence for gas falling into the nucleus. However, it turns out that the relatively narrow observing bands used in the past have led to an incomplete picture (see, e.g., Morganti et al., 2005b). Many cases of blueshifted H I absorption against the radio-core are now known (Vermeulen et al., 2003; Morganti et al., 2005b) and as a result, the evidence for nuclear H I absorption to be more often redshifted than blueshifted, and hence for gas infall fuelling the AGN, has disappeared in recent years. A particularly well-known example of possible H I infall is the detection of redshifted absorption against the nucleus of the closest radio galaxy, Centaurus A[1] (van der Hulst et al., 1983). This case is important because if it were indeed due to gas falling into the AGN, the proximity of Cen A would allow a detailed study of the infall and related processes.

In this chapter, we show that the new observations of Cen A (presented in Chapter 3) suggest a different interpretation of what causes the H I absorption against the core of this galaxy. The broad observing band used has allowed us to detect, for the first time, *blueshifted* H I absorption against the core of Cen A. This obviously complicates the interpretation of the H I absorption as infall. Below, we discuss the various possibilities and we conclude that the H I absorption is caused by a cold, circumnuclear disk and not by infall into the AGN.

4.2 The ATCA Data

The new neutral hydrogen observations of Cen A are presented in detail in Chapter 3. Here, we only summarise the final data cube properties. For the analysis of the nuclear absorption in this chapter, we use the high-resolution cube obtained with uniform weighting. The restoring beam is $8\farcs1 \times 6\farcs8$ with PA $= -12.3°$. The velocity resolution is 13.2 km s^{-1} (after Hanning smoothing) and the rms noise per channel ($\Delta v = 6$ km s^{-1}) is ~ 1.3 mJy beam^{-1}. The continuum image obtained from the line-free channels is shown in Fig. 4.1. More details on the data reduction can be found in Sect. 3.2.

4.3 Broad nuclear H I absorption

As described in detail in Chapter 3, we detect H I in emission and, against the strong continuum, in absorption. In this chapter, we focus on the H I absorption detected against the *very central regions*.

Both deep H I absorption near the systemic velocity and fainter redshifted absorption against the radio core had been detected before by van der Hulst et al. (1983)

[1] At the assumed distance of Cen A of 3.8 Mpc, 1″ corresponds to ~ 18 pc, or equivalently, 1′ to 1.1 kpc.

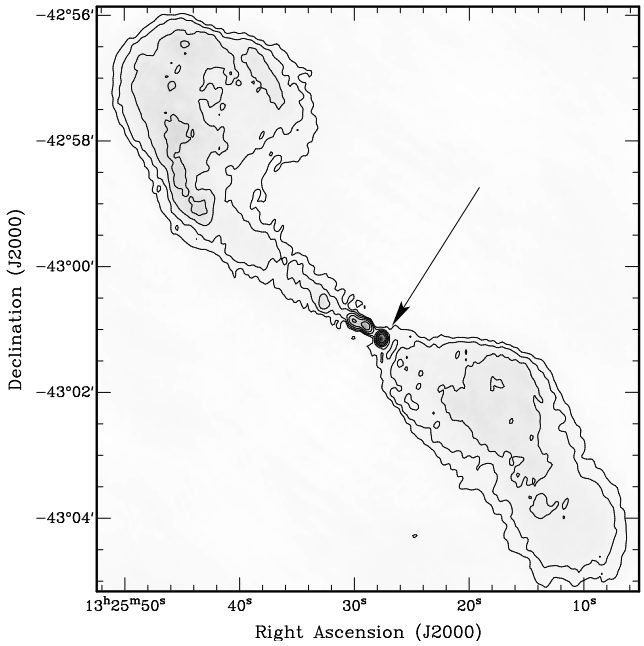

Figure 4.1: *The continuum image of Cen A obtained from the line-free channels. The absorption discussed here is against the central bright source (indicated by the arrow).*

and Sarma et al. (2002). Our data show, of course, the deep absorption component near the systemic velocity. However, the new and interesting result is that in our new data, the fainter absorption against the nucleus *covers a much larger velocity range compared to previous observations*. This larger width of the fainter component is due to both the fact that the redshifted absorption extends to more extreme velocities and to a newly-detected blueshifted component. The absorption spectrum is shown in Fig. 4.2. The total velocity width is about 400 km s^{-1} . The bandwidth used by van der Hulst et al. (1983) was 300 km s^{-1} , while that used by Sarma et al. (2002) was only 150 km s^{-1} . It is therefore clear that, due to the limited bandwidth used, only part of the redshifted H I absorption was detected in those observations and that the blueshifted absorption was not detected at all.

The nuclear H I absorption appears asymmetric with respect to the systemic velocity (542 km s^{-1} ; van Gorkom et al. (1990), covering (heliocentric) velocities from ∼400 km s^{-1} (about −140 km s^{-1} blueshifted compared to systemic) up to ∼800 km s^{-1} (i.e., about +260 km s^{-1} redshifted relative to systemic). The peak absorption has an optical depth of $\tau = 0.83$. The column density of the deeper absorption component is $N_{\rm H\,I} \sim 2.7 \times 10^{19}\, T_{\rm spin}$ cm^{-2}. This column density is in good agreement with what was derived by van der Hulst et al. (1983, see also Sect. 3.3). One should note that the spin temperature $T_{\rm spin}$ for H I absorption, occurring close to an AGN, is a very uncertain parameter. Another uncertainty in $N_{\rm HI}$ is that above we have assumed that

the absorption covers the entire underlying continuum source (see also below).

4.3.1 A circumnuclear H I disk?

One of the central questions is of course what structure is causing the faint, broad nuclear H I absorption. The detection of blueshifted absorption obviously complicates the interpretation that it is due to infall. We can exclude that the broad, fainter absorption is produced by gas located at large (kpc) distance from the nucleus (see also Chapter 3). Figure 4.2 shows that the gas in the large-scale disk is on (almost) circular orbits and that absorption due to the large-scale disk against the radio core is near the systemic velocity. Projected on the centre, the large disk shows some spread in velocity (due to non-circular motions) but this spread is much smaller than required to explain the broad central absorption. If some of the absorption would instead occur against the inner continuum jet, the fact that the jet is more or less aligned with the minor axis of the large-scale gas disk means that we would still expect this absorption to be near the systemic velocity. The deep absorption component near the systemic velocity is most likely due to the large-scale gas disk seen in front of the core and jet, but the fainter, broad absorption cannot be caused by it.

One possibility for explaining the nuclear absorption at velocities away from systemic is to assume that the large-scale gas disk is quite thick. In the models of Eckart et al. (1990), the redshifted nuclear absorption components are explained by high-latitude clouds of the large-scale disk at radii of ∼500 pc. However, such models fail to explain the simultaneous occurrence of bluesifted and redshifted absorption. This means that to reproduce the observed width of the broad, shallow absorption, large radial motions, both inward and outward, would be required to exist in the large-scale disk and such motions are not observed (see also Chapter 3).

An entirely different possibility is that the broad, shallow absorption is caused by a circumnuclear H I disk. If so, one of the prime cases for cold gas falling into an AGN would disappear.

The presence of a cold circumnuclear disk with a size of roughly 100 pc has been suggested by a number of studies (see, e.g., Israel, 1998, and references therein). The central regions of Cen A are highly obscured in the optical, but they have been studied in detail using observations at longer wavelengths. Ionised and molecular gas was observed in the K-band with both long-slit (Marconi et al., 2001) and integral-field spectroscopy (Krajnović et al., 2007; Neumayer et al., 2007). The most recent observations (Neumayer et al., 2007) show that in the central few arcseconds (i.e. tens of pc) very different morphologies are found between the high- and low-ionisation lines. The highly-ionised gas shows a strong kinematical influence of the jet. On the other hand, the molecular gas (H_2) appears to be in a regularly rotating disk, influenced only by gravity. The velocity channel maps (Fig. 8 in Neumayer et al., 2007) show the kinematics of this inner molecular disk, with velocities ranging from ~ -230 km s^{-1} to ~ 230 km s^{-1} compared to systemic. Part of this velocity range is due to the velocity dispersion of the gas, whose origin is not known, and the rest is due to rotation. The H_2 kinematics are best modelled by a tilted-ring model of a warped gas disk that, in the inner part, appears quite face on (34°) and with position angle of the kinematic major axis of $\sim 155°$.

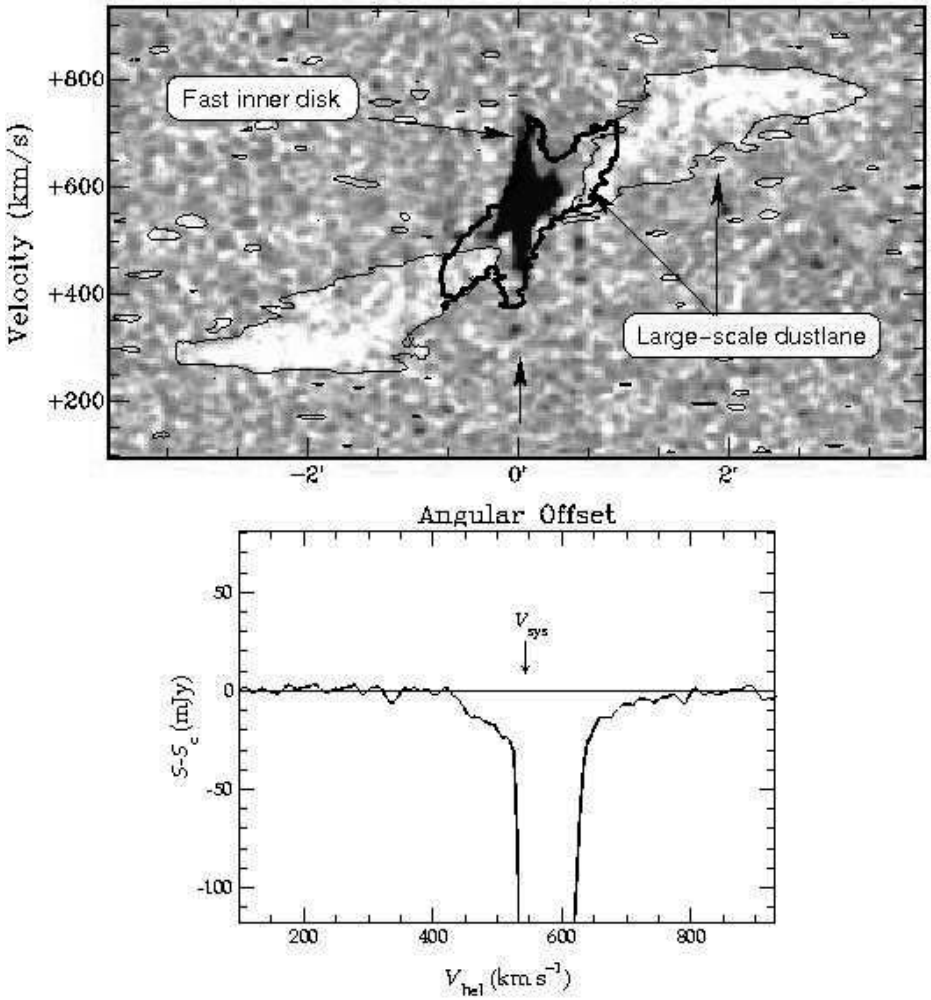

Figure 4.2: *Top panel: Position-velocity plot of the* H I *(grey-scale and thin contours) and superimposed the CO emission Liszt (thick contours; from 2001), taken along position angle 139°. The grey-scale represents the high-resolution* H I *data (beam 8″) while the thin contour is from the same dataset smoothed to 15″. Note that the CO observations do not extend beyond a radius of about 1′. Bottom panel: The absorption profile against the central radio core (indicated by the arrow in the left panel) showing the blue- and redshifted wings of the absorption profile.*

Other evidence for a circumnuclear molecular disk comes from CO observations (Eckart et al., 1990; Israel, 1998; Rydbeck et al., 1993). In particular, CO J=3-2 observations (Liszt, 2001) have been explained by a disk of radius 168 pc seen nearly edge-on (in position angle 138.5° on the sky, therefore perpendicular to the base of the radio jet). In these observations, which have a resolution of 14″, this disk is barely resolved. For both the CO and the H_2 data the kinematic modelling is somewhat uncertain. Nevertheless, the difference in the inclination derived for the inner H_2 disks and the somewhat larger CO structure suggests that it is heavily warped at all spatial scales.

In an attempt to see whether the broad H I absorption could be related to this circumnuclear disk, we have compared the CO J=3-2 data (kindly provided by H. Liszt) and the H I data cubes. Figure 4.2 shows the position-velocity plot obtained along a line (position angle 139°) through the nucleus of Cen A. The grey-scale and the thin contours represent the H I data, while the CO data is given by the thick contours. Note that the field of view of the CO observations was only 2′ × 2′ so the CO information does not extend beyond 1′ radius. The CO data clearly show two kinematical components: a large component with a relatively shallow velocity gradient and a smaller, inner component with a steep velocity gradient. The large CO component corresponds to the large-scale gas disk associated with the dust lane, while the inner component is the circumnuclear disk modelled by Liszt (2001). The comparison with the H I clearly suggests that both the outer (in emission, and part in absorption) and the inner component (in absorption) are seen also in H I. Figure 4.2 illustrates the point made earlier that the kinematics of the large disk is clearly such that it cannot explain the large velocity range seen in the very centre (see also Chapter 3).

For the inner part, Fig. 4.2 shows that the broad, inner H I absorption corresponds very well with the fast rotating, inner CO disk. In particular, the redshifted H I absorption covers the same velocity range as the CO, suggesting that it is not associated with infalling gas. It is also clear that the H I and CO show differences: the extent of the CO, both spatially and in the blueshifted velocities, is larger than of the inner H I. Such differences can be expected given that the characteristics of the inner H I absorption is set by the size of the background continuum emission, *not* by the H I structure itself. With the spatial resolution of our H I data (8″), the inner H I absorption is unresolved while the total extent of the CO disk is about 20″. If the background continuum against which we see the H I absorption is smaller than the circumnuclear CO disk (see below), this would explain the apparent difference in size and velocity range.

4.3.2 The nature of the absorbed continuum

As already eluded to above, for the interpretation of the H I absorption, it is important to understand what the continuum background could be. It turns out that this is not easy to unravel. It is natural to assume that the strongest absorption is against the very inner radio core. However, this is unlikely to be the case. The radio continuum emission on the sub-kpc scale has been studied with high-frequency Very Large Array (about 0.5″ resolution at 8.4 GHz, Hardcastle et al., 2003) as well as VLBI observations at frequencies 2.3 GHz and higher, with very high spatial resolution (a few

milliarcsec resolution at 2.3 GHz; Jones et al., 1996; Tingay et al., 1998). The highest frequency data show that, on parsec and sub-parsec scales, the radio continuum in the central region is dominated by a core-jet structure. However, the VLBI data also show that the core has a strongly-inverted spectrum and that it is actually *not visible at 2.3 GHz*. This suggests that the very innermost part of the radio source (up to $\sim 0.4-0.8$ pc) is seen through a disk or torus of ionised gas which is opaque at lower frequencies due to free-free absorption (Tingay & Murphy, 2001). The above means that the radio core is unlikely to be detected also at 1.4 GHz, and it is *not* the core itself against which the 21-cm absorption is occurring.

Given that, at 1.4 GHz, the radio core is not seen, the radio continuum on the milli-arcsec scale appears concentrated in the jet and counter-jet. Given the circumnuclear disk structure discussed above, with a PA close to perpendicular to the jet axis, the fact that the main jet is coming toward us means that it is likely to be in front of the circumnuclear disk and that it cannot cause the absorption. One possibility would be then that the H I absorption is against the *counter-jet*. However, this can be excluded, given the small opening angle of the jet, as most of the absorption would be seen at velocities close to systemic.

An interesting clue is that extra flux (at least 50 mJy) is clearly present on the short baselines in the 1.4-GHz VLBI experiments (Tingay priv. comm.), indicating the presence of large-scale structures that are not evident in the images. This structure would be still well inside the 1'' (~18 pc) imaged at the highest VLA resolution (for 21 cm). It is difficult to quantify the amount of flux on larger scales from a comparison of VLBI data with lower-resolution data due to the variability of the nuclear regions (Romero et al., 1997; Abraham et al., 2007) because simultaneous observations are needed. It is therefore unclear whether this extra component can cause the absorption.

If, however, this were the case, we would have a situation similar to the one suggested to be the case for Mrk 231 (Carilli et al., 1998). In this source, H I absorption against a diffuse component has been found, allowing Carilli et al. (1998) to identify the H I and the radio continuum disk as the inner part of the molecular disk seen on the larger scale.

If the scenario described above is correct, we can make some remarks about the conditions of the H I material and whether the location of the H I and of the molecular gas are what is expected from the physical models of the circumnuclear disks/tori. In this case, the column density of the H I is going to be much larger than estimated above, because the absorption will likely cover only a small fraction of the sub-arcsec continuum. For example, if the absorption is only against the counterjet-side, and assuming the jet/counterjet ratio from Jones et al. (1996) of 4 - 8, the column density is at least a factor four higher. This factor would be even higher in the case of the absorption against the more diffuse component. In addition, in a circumnuclear structure, $T_{\rm spin}$ is likely to be a few $\times 10^3$ K, as the H I is affected by the central AGN (Maloney et al., 1996). Therefore, the column density could easily be as high as 5×10^{23} cm^{-2}. Interestingly, this is a similar column density as derived from the hard X-ray spectrum of Cen A, which is fitted with an heavily absorbed power-law model with a column density of $\sim 10^{23}$ cm^{-2} (Evans et al., 2004).

Physical models of circumnuclear disks/tori have been investigated by Maloney

et al. (1994, 1996, and refs. therein). They identify an effective ionisation parameter that determines whether, given the distance from the nucleus, the material is atomic or molecular. This effective ionisation parameter is $\xi_{\rm eff} = L_{\rm X} N_{22}^{-0.9} n^{-1} r^{-2}$, where $L_{\rm X}$ is the luminosity of > 2 keV X-rays; n is the gas density; r is the distance to the nucleus; and N_{22} is the total column density in units of 10^{22} cm^{-2}. For $\xi_{\rm eff} > 10^{-3}$, the gas will be largely atomic, otherwise mainly molecular. For Cen A, the X-ray luminosity is $L_{\rm X} = 5 \times 10^{41}$ erg s^{-1} (Evans et al., 2004) and the X-ray column density is 10^{23} cm^{-2}. A rough estimate of the density can be derived from the H I column density if we assume that the region of absorption is comparable to the region with free-free absorption (that covers the innermost $\sim 0.4 - 0.8$ pc). This gives a density of $1 - 2 \times 10^5$ cm^{-3}. These values give a radius of 1-3 pc for $\xi_{\rm eff} = 10^{-3}$. Thus, we may hypothesise that the central region of Cen A hosts a gaseous disk composed of multiple phases where the inner part (but outside the fully ionised region) is mainly atomic and beyond that molecular.

4.4 Conclusions

Using new, broadband, H I observations of Cen A (presented in detail in Chapter 3) we have shown that the nuclear absorption is broader than previously known and that it has a blueshifted component. Using various arguments, but in particular the comparison with the molecular gas data, we have shown that the H I absorption is likely to be caused by a cold, circumnuclear disk and that it does not constitute direct evidence of gas infall into the AGN.

Sensitive VLBI observations are now needed to further explore the characteristics of the nuclear H I as well as the picture proposed in this chapter and, in general, to learn more about the central regions of this fascinating, nearby AGN.

Acknowledgements: We are most grateful to Harvey Liszt for providing us the CO cube that has been crucial in this work. Based on observations with the Australia Telescope Compact Array (ATCA), which is operated by the CSIRO Australia Telescope National Facility. This research was supported by the EU Framework 6 Marie Curie Early Stage Training programme under contract number MEST-CT-2005-19669 ESTRELA.

5 An H I absorbing circumnuclear disk in Cygnus A

— published as C. Struve & J.E. Conway. 2010. A&A 513, A10 —

Abstract

We present Very Long Baseline Array (VLBA) H I absorption observations of the core region of the powerful radio galaxy Cygnus A. These data show both broad (FWHM = 231 ± 21 km s^{-1}) and narrow (FWHM < 30 km s^{-1}) velocity width absorption components. The broad velocity absorption shows high opacity on the counter-jet, low opacity against the core and no absorption on the jet side. We argue that these results are most naturally explained by a circumnuclear H I absorbing disk oriented roughly perpendicular to the jet axis. We estimate that the H I absorbing gas lies at a radius of $\sim$ 80 pc, has a scale height of about 20 pc, density $n > 10^4$ cm^{-3} and total column density in the range $10^{23}-10^{24}$ cm^{-2}. Models in which the H I absorption is primarily from an atomic or a molecular gas phase can both fit our data. Modelling taking into account the effective beam shows that the broad H I absorbing gas component does not cover the radio core in Cygnus A and therefore does not contribute to the gas column that blocks our view of the hidden quasar nucleus. If however Cygnus A were observed from a different direction, disk gas on $\sim$ 100 pc radius scales would contribute significantly to the nuclear column density, implying that in some radio galaxies gas on these scales may contribute to the obscuration of the central engine. We argue that the circumnuclear torus in Cygnus A contains too little mass to power the AGN over $> 10^7$ yr but that material in the outer H I absorbing gas disk can provide a reservoir to fuel the AGN and replenish torus clouds. The second narrow H I absorption component is significantly redshifted (by 186 km s^{-1}) with respect to the systemic velocity and probably traces infalling gas which will ultimately fuel the source. This component could arise either within a tidal tail structure associated with a recent (minor) merger or be associated with an observed infalling giant molecular cloud.

5.1 Introduction

Circumnuclear obscuring tori/disks are an essential component of unified schemes of active galactic nuclei (e.g. Antonucci, 1993; Tadhunter, 2008). Recently there has been much progress in obtaining direct evidence for such structures especially in Seyfert luminosity objects. This evidence includes modelling of the IR SEDs from AGN heated dust in clumpy tori (Nenkova et al., 2008b) and direct IR interferometric imaging of this dust on 1 pc - 10 pc scales (Jaffe et al., 2004; Tristram et al., 2009).

On larger scales adaptive optics IR observations of molecular hydrogen lines (Hicks et al., 2009) have revealed geometrically thick gas at radii 30 pc in Seyferts. Additionally, millimetre interferometry also detects molecular gas in emission on scales r = 70 pc (e.g. Schinnerer et al., 2000) albeit in more flattened disk-like structures. Such outer disk structures may be continuous with inner obscuring tori and provide both the fuel and a conduit for feeding the central engine. The relationship between these circumnuclear disks and obscuring tori is however far from clear.

Radio observations provide another means to study the circumnuclear gas environment. This can for instance be achieved by VLBI observations of maser emission from molecular gas (Lo, 2005), free-free absorption from ionised gas and absorption from atomic gas (H I). Examples of the use of the latter two tracers include observations of NGC 1275 (e.g. Vermeulen et al., 1994), Centaurus A (e.g. Jones et al., 1996; Morganti et al., 2008), Hydra A (e.g. Taylor, 1996), NGC 4261 (van Langevelde et al., 2000; Jones et al., 2001) and 1946 + 708 (Peck & Taylor, 2001). Because of their high spatial resolution such radio observations are especially suitable for studying circumnuclear obscuring matter in powerful narrow line radio galaxies which are expected (see Tadhunter, 2008) to be unified via orientation with radio-loud quasars. There is strong evidence from X-ray observations (Hardcastle et al., 2009b) for the expected obscuration by large column densities in the former objects, however they are usually too distant and faint for optical and IR observations to directly observe the circumnuclear gas.

A prime target for studies of circumnuclear gas in a luminous 'hidden quasar' radio galaxy is the closest Fanaroff-Riley (Fanaroff & Riley, 1974) type II (FR-II) radiogalaxy Cygnus A. A review of the properties of Cygnus A is presented in Carilli & Barthel (1996). Spectropolarmetric observations of this source, which revealed a hidden BLR in scattered light (Ogle et al., 1997), were a major milestone in the general acceptance of the orientation unification scheme for powerful radio galaxies and radio-loud quasars. Further evidence for shadowing from a central torus comes from the bi-cones observed in both optical emission lines (Jackson et al., 1998) and IR continuum (Tadhunter et al., 1999). The sharpness of the edges of these bi-cones suggest that the inner face of any torus occurs at radii < 50 pc from the central engine (Tadhunter, 2008). Tadhunter et al. (2003) have from optical/IR emission line observations measured a rotation curve from gas rotating around the bi-cone/radio-jet axis at $r \approx 300 - 1000$ pc allowing a central black hole mass to be estimated. These observations may trace the outer parts of a circumnuclear gas structure which connects with the inner obscuring torus. The ultimate origin of this material could be related to the merger activity detected in Cygnus A (Canalizo et al., 2003).

The central radio core and inner jets of Cygnus A are relatively bright from mil-

limetre to centimetre wavelengths allowing searches in absorption to constrain circumnuclear gas properties on small (< 100 pc) scales. Molecular absorption observations so far give ambiguous results with only upper limits or marginal detections being reported (see e.g. Barvainis & Antonucci, 1994; Fuente et al., 2000; Salomé & Combes, 2003; Impellizzeri et al., 2006). VLBI observations by Krichbaum et al. (1998) have however found evidence for ionised circumnuclear gas on scales < 20 pc via the detection of free-free absorption toward the counter-jet. Additionally Conway & Blanco (1995) detected broad H I absorption toward the core in VLA observation which were interpreted in terms of a circumnuclear disk/torus model, with the H I absorption either tracing the small atomic fraction of a mainly molecular medium or a purely atomic structure. To better constrain the scale and geometry of this H I absorbing gas we have performed high resolution NRAO Very Long Baseline Array (VLBA[1]) H I absorption observations. A short report on an initial reduction of this data was given by Conway (1999), this present chapter presents a fuller re-analysis of the data. The organisation of this chapter is as follows, in Sect. 5.2 we describe the observations while Sect. 5.3 presents the observational results including modelling of opacity profiles along the source. A discussion of the results is given in Sect. 5.4 and a summary in Sect. 5.5. At the redshift of Cygnus A ($z = 0.056$), for cosmologies with $H_o = 73\ \mathrm{km\,s^{-1}}$, 1 mas corresponds to approximately 1 pc, a scaling which we adopt throughout this paper. All total recession velocities quoted are heliocentric (optical definition).

5.2 Observations

Observations were performed on August 31st 1995 using the ten stations of the VLBA plus the phased VLA. Two IFs (left and right circular polarisation) with a bandwidth of 12.5 MHz and 256 channels were centred at the frequency of the previously observed H I absorption (~ 1340 MHz, Conway & Blanco, 1995). A number of bright compact sources were observed as fringe finders and for bandpass calibration. The data were correlated in Socorro, USA. A standard data reduction using AIPS was performed including fringe fitting, calibration and flagging of the data. Cygnus A lies at a relatively low galactic latitude ($b = 5.^{\circ}7$) and the effects of interstellar scattering are significant at VLBI resolution. For this reason four antennas which participated only in long baselines, namely Brewster, Hancock, Mauna Kea and St. Croix showed no fringes to Cygnus A and so were deleted from the subsequent data analysis. Initial amplitude calibration was accomplished for VLBA antennas using the recorded system temperature values (which took into account the dominant contribution to the noise from the lobes of Cygnus A). For the phased VLA the calibrator T_{ant}/T_{sys} values were used with a correction applied to take into account the system noise contribution from Cygnus A. Offsets in the VLA amplitude calibration scale were then corrected by comparing the correlated Cygnus A flux densities on long baselines to respectively the VLA and Pie Town. Initial continuum images were made via iterative phase self-calibration/deconvolution starting from a point

[1]The VLBA is operated by the National Radio Astronomy Observatory which is a facility of the National Science Foundation operated under co-operative agreement by Associated Universities, Inc.

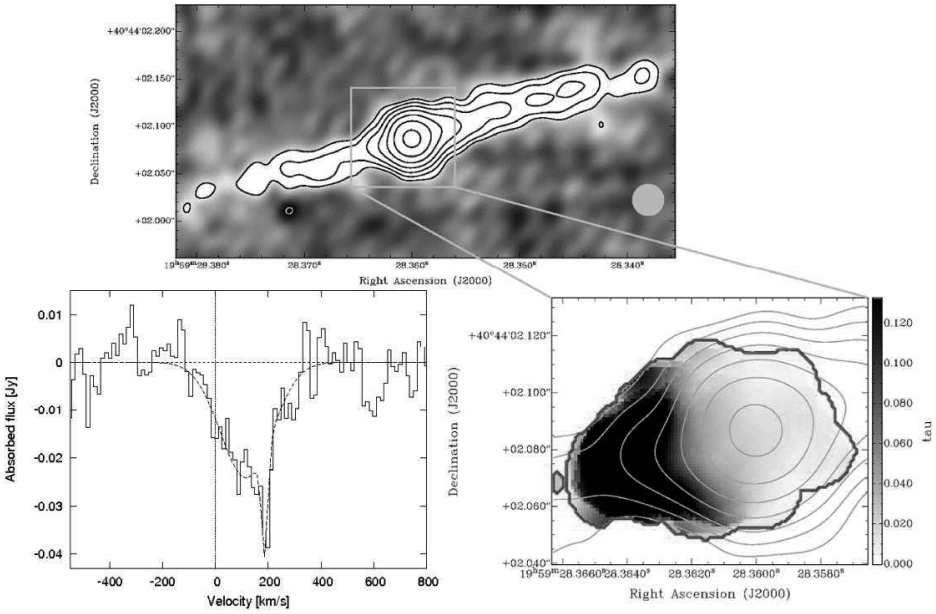

Figure 5.1: *Top panel: Continuum image at 1340 MHz. The lowest contour is at 2 mJy beam*$^{-1}$ *with subsequent contours increasing by factors of 2. The effective beam FWHM (see Sect. 5.2) is indicated in the lower right corner. Bottom left panel: Integrated absorption spectrum from the blanked cube with the velocities shifted to the rest frame of Cygnus A (see Sect. 5.4.1). The dashed line shows the two component Gaussian fit. Bottom right panel: Contours show continuum. Greyscale shows the mean opacity over the rest frame velocity range* -80 *to* $+170$ km s^{-1} *. The thick dark line shows the un-blanked region over which the integrated absorption spectra (shown in the bottom left panel) is calculated.*

source. A couple of cycles of amplitude and phase self-calibration were performed at the very end to obtain a noise limited continuum map.

Extensive experiments were carried out to determine the optimum uv weighting which gave the best combination of sensitivity and resolution for both continuum and spectral line. Final images were made using uniform weighting with robustness factor 0.5; giving rise to an almost circular dirty beam with main lobe width FWHM $\approx$ 25 mas. Since the uv point weights also took into account the sensitivity of each baseline (by weighting by 1/noise variance) the final continuum and spectral line images are dominated by the baselines to the VLA. CLEAN images were restored with a circular FWHM 25 mas Gaussian; however the effective image resolution is less than this because of the effects of foreground interstellar scattering. The observed effective resolution (i.e. the clean beam convolved with the interstellar scattering) is 32.7 mas, as determined by measuring the FWHM of the continuum profile perpendicular to the jet at the core position – implying an interstellar scattering contribution of 21 mas.

The resulting continuum image (see Fig. 5.1) has rms noise of 0.43 mJy beam^{-1}

and shows besides the unresolved core a jet and counter-jet structure (see Sect. 5.3). In principal it is possible that the counter-jet structure could be an artefact of phase self-calibration starting from a point source. To check this possibility we re-mapped the data only allowing flux density on the jet side to be included in the model in the initial cycles, but in all cases emission on the counter-jet side remained. The existence of a counter-jet confirms previous observations (e.g. Krichbaum et al., 1998). In making our final continuum and spectral-line images, we used data self-calibrated against continuum models including both jet and counter-jet emission. Before making our spectral line cube, we removed the continuum contribution using the AIPS task UVLIN and then imaged using the same weighting as used for our continuum image and the same CLEAN restoring beam. In order to increase sensitivity when creating our spectral line cube the uv data were averaged in frequency to give a final channel separation equivalent to 14.0 $\mathrm{km\,s^{-1}}$ in velocity or a velocity resolution of 28.0 $\mathrm{km\,s^{-1}}$ after Hanning smoothing. The noise achieved in the final line cube was $\sigma_{\mathrm{rms}} = 2.36$ mJy beam^{-1} per channel.

5.3 Results

5.3.1 Continuum image

The 1340 MHz continuum image (Fig. 5.1, top panel) is very similar to the 1660 MHz image shown by Krichbaum et al. (1998). We clearly detect the unresolved core, the jet and the weaker counter-jet (SE of the core). The PA of the jet is 105°±2°, in agreement with VLBI observations at higher frequencies (Krichbaum et al., 1998) and the kpc-size jet structure (Carilli et al., 1991). The continuum peak has brightness 0.16 Jy beam^{-1} and the total continuum flux recovered in our observations is 0.50 Jy.

5.3.2 H I absorption

An integrated absorption spectrum over our spectral-line cube is shown in Fig 5.1, bottom left. Broad ($\Delta v = 456$ $\mathrm{km\,s^{-1}}$) H I absorption is detected in the velocity range from 16679 to 17135 $\mathrm{km\,s^{-1}}$ with the peak being located at $v = 17002$ $\mathrm{km\,s^{-1}}$ ($z = 0.05667$). The integrated spectrum is well fitted by two Gaussian components, yielding centroid velocities of 16916 ± 10 $\mathrm{km\,s^{-1}}$ ($z = 0.05639 \pm 0.00003$) and 16986 ± 5 $\mathrm{km\,s^{-1}}$ ($z = 0.05662 \pm 0.00002$), with FWHM= 231 ± 21 and 29 ± 10 $\mathrm{km\,s^{-1}}$ respectively (after correcting the line widths to the rest frame of the host galaxy). The second, narrow component has a FWHM velocity width similar to our velocity resolution and hence we consider this velocity width as an upper limit of the true line width. The presence of two components in the integrated spectrum suggests that the H I absorption consists of two different overlapping structures. Despite small differences in the flux scale (for continuum and absorption spectrum) the VLBA data agree in absorption width, profile shape and radial velocity with the VLA A- and B-array observations of Conway & Blanco (1995). These authors found slightly different Gaussian fits for the absorption spectrum, their data however potentially suf-

fers from bandpass calibration and continuum subtraction problems (since two IFs — only slightly overlapping in velocity — had to be used to achieve sufficient spectral resolution and velocity coverage). Given these issues we conclude that both data sets agree within the noise of both observations so that we have recovered the full absorption seen by the VLA. The difference seen in flux scale between our VLBI and the published VLA observations are likely due to inaccuracies in amplitude calibrations of the VLA. This instrument, unlike VLBI, did not record the antenna system temperatures which are greatly enhanced due to the presence of the bright radio lobes of Cygnus A in the primary beam of each antenna, complicating the amplitude calibration.

Inspection of the data cube shows that the absorption is spatially resolved and is detectable over 95 mas in angle along the radio axis (i.e. ~ 3 effective beam FWHMs). Below the second contour of the continuum image, it is not possible to constrain the H I absorption because the background is too weak. The deepest absorption measured in mJy is toward the counter-jet and unresolved core but the highest opacities occur for the broad velocity component on the counter-jet side (see Fig. 5.1, bottom right). We find no indication of changes in spectral-line absorption profiles in directions perpendicular to the jet axis - which is as expected given the small jet width (Krichbaum et al., 1998) compared to our effective resolution; this means we need to only consider the spectral profile as a function of position along the jet axis as shown in Fig. 5.2. In this figure the top panel shows the rotated continuum image while the middle panel shows the absorbed flux density (greyscale) and absorbed flux/continuum ratio (greyscale; note: saturated over 0.2) versus velocity and position along the jet.

The highest contours in the middle panel of Fig. 5.2 belong to the narrow velocity absorption component at recession velocity 16986 $\mathrm{km\,s^{-1}}$ seen against the core. At the same velocity a slight extension on the jet-side is detectable, consistent with having the same $\tau \approx 0.1$ opacity as seen on the core. Because of the rapid fall-off of continuum intensity further along the jet and counter-jet, further information about the spatial distribution of the narrow velocity component is limited. That is to say that the underlying continuum is not strong enough to detect the narrow velocity absorption component even if the opacity remains $\tau \approx 0.1$.

The broad absorption component in Fig. 5.2, middle panel (seen at velocities around 16900 $\mathrm{km\,s^{-1}}$) is detected from the core position out to 65 mas along the counter-jet. Over this spatial range the broad component has absorbed flux densities (contour levels) which stay almost constant; given the rapid fall off in background continuum this corresponds to a rapid increase in line-to-continuum ratio (greyscale). Over the range of position from -50 mas to -65 mas spectra taken show the absorption to be flat bottomed and the absorbed flux density comparable with the continuum, both implying H I opacities $\tau \gg 1$. The absorption shows an apparent sharp decrease beyond -65 mas, though in a region with very weak continuum (we discuss further the reality of this decrease in Sect. 5.3.3). The broad absorption also apparently has a small but significant opacity ($\tau \approx 0.03$) at the position of the core, however, this may be due only to the limited spatial resolution causing "leakage" of absorption onto the core position. Quantitative estimates of broad line opacity along the source are made in Sect. 5.3.3 where the above two points are addressed.

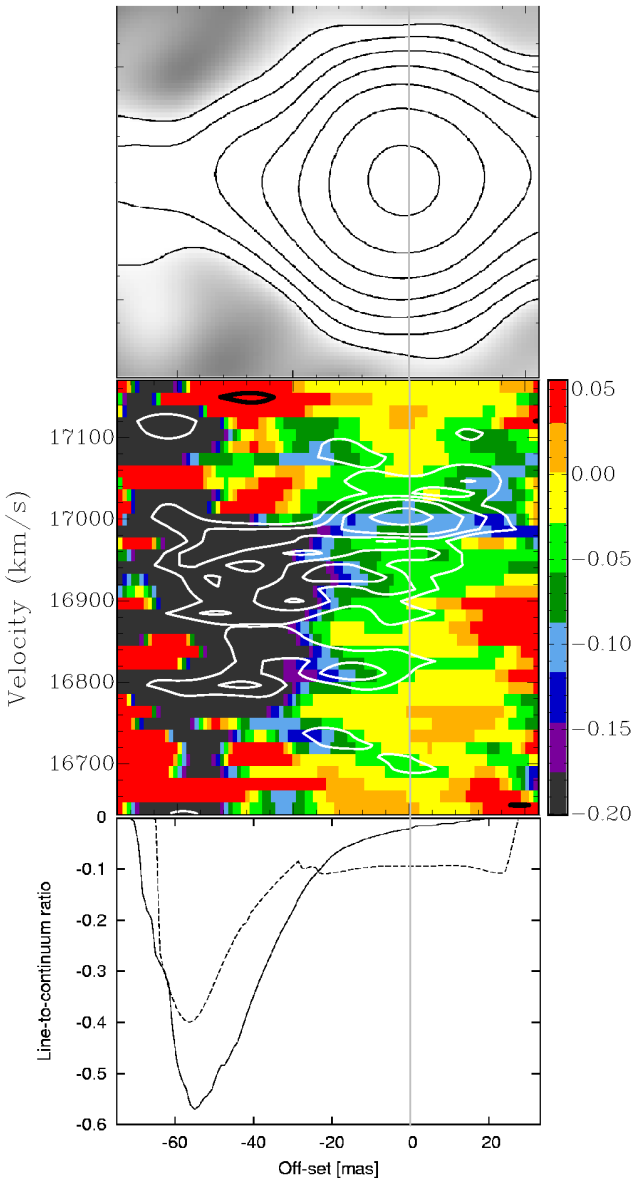

Figure 5.2: *Top panel: Radio continuum image of the core region rotated such that the jet is pointing to the right and the counter-jet to the left. Contour levels are the same as in Fig. 5.1. Middle panel: Position-velocity diagram along the radio axis. Greyscale shows the line-to-continuum ratio. Over-plotted in contours is the absorbed flux density in mJy beam^{-1}. Contour levels are -15, -10, -7.5, -5.0 (white) and 5.0 mJy beam^{-1} (black). Bottom panel: Velocity averaged line-to-continuum ratio along the source for two different velocity ranges. The solid line is for a velocity range dominated by the broad velocity component (*16720 − 16970 km s^{-1} *), the dashed line for a velocity range (*16971 − 17012 km s^{-1} *) centred on the narrow absorption system velocity.*

Reinforcing the above description of the two velocity components, the bottom panel of Fig. 5.2 shows the line-to-continuum ratio averaged over different velocity ranges versus position. The solid line shows the average line-to-continuum ratio for velocity ranges where the broad component dominates, while the dashed line is for a velocity range where the narrow absorption is most dominant. The broad component shows rapidly increasing absorption along the counter-jet reaching a peak velocity averaged line-to-continuum ratio of almost 0.6 at −55 mas (with peak ratios within the velocity profile at this position in fact reaching up to 1 and beyond). The second profile (dashed line) for the velocity range where the narrow velocity component normally dominates has approximately the same mean opacity on the core and jet. On the counter-jet side the average opacity over this velocity range increases; this is however consistent with the narrow absorption component having the same opacity as on the core and jet-side but with the average line-to-continuum ratio becoming dominated by contamination from the high velocity wings of the broad velocity component.

5.3.3 Modelling spatial variations in broad line opacity

The increase in line-to-continuum ratio of the broad absorption seen on the counter-jet side (see Sect. 5.3.2 and Fig. 5.2) implies a rapid increase in opacity. As noted in Sect. 5.3.2, at the position of maximum absorption the spectral profiles are flat-bottomed and saturated implying large opacity. To more accurately convert the line-to-continuum ratios versus velocity to peak opacity, and therefore estimate H I column density variations, we have carried out a detailed modelling of the data. In this modelling we describe both continuum and peak opacity estimates with a set of seven point sources separated by 15 mas along the jet/counter-jet axis (i.e. just under half an effective beam FWHM width). Additionally by taking into account the effective beam width this modelling provides a modest super-resolution of the data, important because interstellar scattering limits our spatial resolution (Sect. 5.2). Specifically, we are interested in the question of whether the weak broad absorption apparently seen at the core position (see Fig. 5.1 bottom right panel) is real or whether it can be explained by the combination of very strong absorption on the counter-jet side combined with limited spatial resolution.

In our modelling we first made estimates for the underlying continuum profile for each model point source (referred to as a "pixel") where there was detectable absorption. Continuum intensities were varied at each of these seven pixels until after convolution with the effective restoring beam the model continuum profile versus position fitted the observations. In a similar way we estimated for each pixel the absorbed line area (mJy km s^{-1}) at velocities in the range 16720 - 16970 km s^{-1} (where the broad absorption component dominates). Pixel values were again adjusted such that after convolution by the effective beam the model fitted the observations. Finally, an estimate was made at each pixel of the peak H I opacity versus velocity by combining the pixel-based continuum and spectral line absorption estimates. In estimating this quantity we assumed the broad-component opacity spectrum was Gaussian with fixed velocity centroid and fixed FWHM.

The resulting fits reproduce (see Fig. 5.3), to first order, both the observed con-

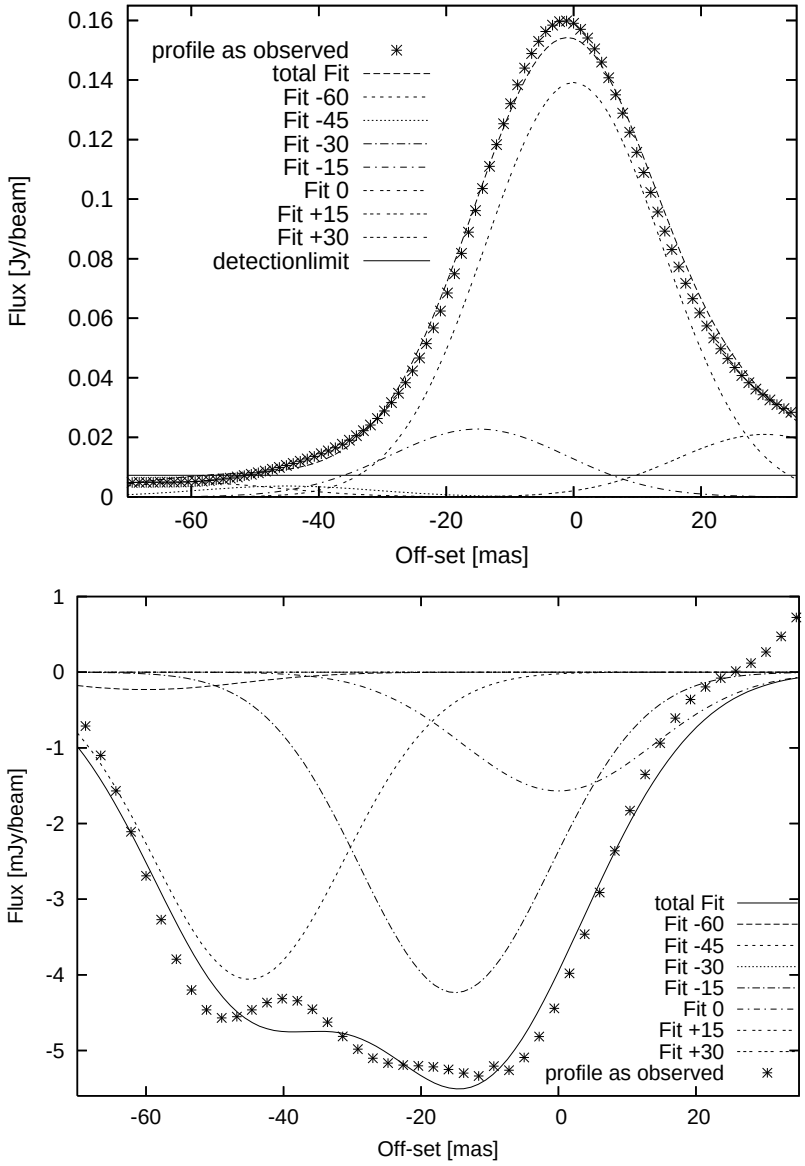

Figure 5.3: *Modelling of continuum and broad absorption along the jet axis (see Sect. 5.3.3). Top panel: Comparison of model fit and data for the observed continuum profile found by adjusting pixel values while assuming an effective Gaussian beam of FWHM of 32.7 mas. Bottom panel: Comparison of model and data for average absorbed line flux over the broad component velocity range from* $16720 - 16970\ \mathrm{km\,s^{-1}}$ *. In both plots negative offsets correspond to counter-jet, positive offsets to jet side.*

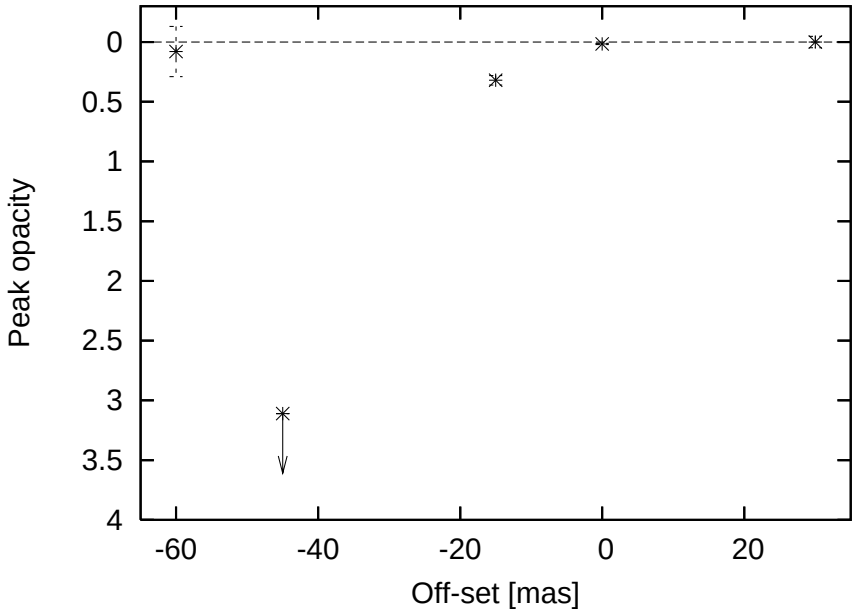

Figure 5.4: *Estimates of broad absorption opacity at line centre versus position along the radio axis after taking into account beam effects (see Sect. 5.3.3). The opacities and errors plotted are taken from Tab. 5.1.*

tinuum and the absorbed flux profiles along the source. Deviations of the fits from the data are likely due to the background continuum being more complicated (see Krichbaum et al., 1998) than our parameterisation of it. Table 5.1 gives our results and the line centre peak opacity as plotted in Fig. 5.4. Note that no opacity estimate is plotted at positions -30 and +15 mas because the fitted continuum intensity at these positions was zero. We estimate the error of the line-to-continuum ratio (Tab. 5.1, column 4) assuming it is dominated by the rms noise in the line data. At position $r = -45$ mas the lower limit on line centre opacity is set by subtracting 2σ from the line-to-continuum ratio.

The peak opacity (column 5) takes into account that part of the absorption spectrum is flat bottomed and the attached error is calculated based on a $1\sigma_{\rm rms}$ uncertainty in our line data. Our results are consistent with no broad HI absorption on the jet-side and any opacity against the core being very low (0.016). Moving outward from the core along the counter-jet, the opacity increases and peaks at 45 mas ($N_{\rm HI} = 1.6 \times 10^{21} {\rm T_{spin}}$) before it sharply decreases to 0.078 at 60 mas from the core. Based on uncertainty estimates of the absorbed flux this drop in opacity is real and not an observational artefact due to insufficient signal-to-noise.

Table 5.1: *Results of modelling of continuum and broad* H I *absorption profiles along the jet axis (see Sect. 5.3.3).*

r (mas)	F_C (mJy)	F_L (mJy)	$F_L F_C^{-1}$	τ_0
-60	4.73	0.23	0.05 ± 0.12	0.080 ± 0.210
-45	3.62	4.06	1.12 ± 0.15	> 3.110
-30	0.02	0.00	0.00	-
-15	22.78	4.24	0.19 ± 0.02	0.320 ± 0.040
0	139.16	1.57	0.01 ± 0.004	0.016 ± 0.006
15	0.00	0.00	-	-
30	20.98	0.00	0.00 ± 0.03	0 ± 0.0478

Notes – Column 1 gives the distance from the core of the fitted pixel, negative offsets correspond to positions along the counter-jet, positive to positions on the jet side. Columns 2 to 4 give respectively the fitted continuum flux density, H I absorbed flux density averaged over fitted frequency range and the line-to-continuum ratio. Column 5 gives the modelled opacity at line centre.

5.4 Discussion

5.4.1 A disk geometry for the broad absorption component

The fact that the broad velocity width absorption is seen at high opacity only against the counter-jet and not against the jet is similar to the situation found for other powerful cores of radio galaxies observed in H I absorption, for instance in the FR-I source NGC 4261 (van Langevelde et al., 2000). The most natural explanation for these observations is that the H I absorption lies in a flattened structure roughly in a plane perpendicular to the radio axis (i.e. a circumnuclear disk). Alternative explanations involving foreground clouds in the ISM of the host galaxy seem unlikely, requiring within elliptical hosts a large covering factor of 10 pc-100 pc sized clouds with uncharacteristically large internal velocity dispersion (of order 300 km s^{-1}).

Converting our observations of the location and distribution of H I absorption along the counter-jet to an exact of radius in the disk depends on the precise orientation of the disk. Over the range of plausible disk orientations however this radius varies over a fairly narrow range as can be seen by examining two limits, first when the disk is close to edge-on and when at its maximum plausible tilt. In the former case the H I profile width in Fig. 5.4 measures the scale height of the disk. Since we know an estimate of the central black hole mass ($M_{\rm BH} = 2.5 \times 10^9\ M_\odot$, Tadhunter et al., 2003) the radius at which the H I absorption occurs can be calculated (following Krolik & Begelman, 1988) via:

$$\frac{\Delta h}{r} \sim \frac{\Delta v}{v_{\rm rot}(r)} \tag{5.1}$$

where Δh is the disk scale height, r the radius from the core, $\Delta v = 98.5$ km s^{-1} the velocity dispersion (estimated from the Gaussian fit in Sect. 5.3.3) and $v_{\rm rot}(r)$ the Keplerian rotation velocity at radius r from the central black hole. Assuming $\Delta h = 25$ pc and solving for r we obtain $r = 88$ pc. In the other limit we consider a maximally inclined disk. Based on VLBI observations of the jet to counter-jet brightness ratio of the parsec scale jet (Krichbaum et al., 1998) the jet axis is oriented at an angle $\theta > 80°$ to the line of sight. Based on measured misalignments of larger scales (Tadhunter et al., 2003) we estimate a maximum misalignment between disk and radio axes of 30° – which gives a maximally inclined disk which is 40° from edge-on. The peak H I opacity is observed to occur at projected distance 45 pc along the counter-jet, which when de-projected corresponds to a radius of 70 pc. Using again eq. 1 this gives a scale height of $\sim$ 18 pc. Based on the above two limits we will assume in the following that the H I peaks at a radius 80 pc from the black hole and has a scale height of about 20 pc. The resulting opening angle of the circumnuclear H I disk is $\sim$ 14° which is similar to what is found in other sources (e.g. in NGC 4261; van Langevelde et al., 2000).

An important question in considering the feasibility of the disk hypothesis is the velocity of the broad absorption relative to the systemic velocity of the galactic nucleus. For a disk which is perfectly normal to the jet axis these velocities will be the same. Our best estimate of the systemic velocity we take to be $z = 0.05600 \pm 0.00008$ (= 16800 ± 24 km s^{-1}), which is the mean of six published optical/IR emission line estimates (see Tab. 1, in Tadhunter et al., 2003). The centroid of the broad component at 16916 km s^{-1} is therefore 116 km s^{-1} beyond the mean systemic velocity. The observed offset however can be accommodated if there were a fairly modest misalignment between the disk axis and the jet. VLBI observations constrain the jet axis to be within 10° of the sky plane. For such an orientation misalignments between projected jet axis and disk axis will be similar to intrinsic misalignments. Given the arguments above that the H I absorption occurs at $\sim$ 80 pc radius and given the estimated central black hole mass of ($M_{\rm BH} = 2.5 \times 10^9\ M_\odot$; Tadhunter et al., 2003) the orbital velocity is $v_{\rm rot}(r = 80\ {\rm pc}) = 367$ km s^{-1} . Given this orbital velocity a misalignment of only 21° is sufficient to explain the difference between the H I centroid and systemic velocities.

5.4.2 Physical properties of the broad absorption component gas

According to Maloney et al. (1996) the physical state of gas around an AGN is controlled by an ionisation parameter determined from the ratio of the hard X-ray photon flux to local gas density. At a given radius r this ionisation parameter equals

$$\xi_{\rm eff} = L_{\rm X} \times n^{-1} \times r^{-2} \times N_{22}^{-0.9} \tag{5.2}$$

where $L_{\rm X}$ is the luminosity in > 2 keV X-rays and n is the gas number density. The final term takes account of the effects of X-ray photoelectric absorption where N_{22} is the the column density in units of 10^{22} cm^{-2} (in Cygnus A, X-ray observations give an estimate of $N_{22} = 20$ along the line of sight to the core; Young et al., 2002).

According to the model of Maloney et al. (1996, see their Fig. 3) for Cygnus A, at $r = 80$ pc, the gas fraction is predominantly atomic (> 90%) for a density range $10^3 < n < 1.6 \times 10^5$ cm^{-3}. The remaining < 10% of the gas is ionised at low densities ($n = 10^3$ cm^{-3}) and becomes molecular at higher densities ($n \approx 10^5$ cm^{-3}). Above densities of 3.3×10^5 cm^{-3} the gas is mostly molecular.

The Maloney et al. (1996) model can be used to predict the disk H I and free-free absorption opacity as a function of gas density; comparison with observations can then constrain the density. In order to predict opacities we need to convert gas volume densities to column densities which requires estimates of the path length through the absorbing gas. Based on our estimate of the disk thickness of 20 pc and the maximum disk inclination angle with respect to the line of sight (Sect. 5.4.1), we estimate the geometric path length through the disk to be at least 31 pc. This is a strict lower limit and we adopt $L_{\rm geom} = 40$ pc as a more likely value. Note that if the gas exists in clouds the effective path length through absorbing gas can be less than $L_{\rm geom}$ but it cannot be larger. Using the above assumptions we find that upper limits on free-free absorption toward the counter-jet do not give any useful gas density constraints. This is because, although the free-electron fraction increases at lower densities this is compensated for by a lower total gas column such that the free-free opacity continuum absorption at 21cm wavelength against the counter-jet is less than 0.1 over all reasonable densities.

For modelling H I absorption the relevant parameters given by Maloney et al. (1996) are the predicted gas temperature and atomic fraction versus effective ionisation parameter $\xi_{\rm eff}$. At the radius of the absorbing H I assuming densities high enough to give a predominately atomic (and not ionised) column, the increase of $T_{\rm spin}$ due to radiative excitation from the radio core is negligible (see e.g. Bahcall & Ekers, 1969). Given this we assume the atomic gas is thermalised and that its spin temperature ($T_{\rm spin}$) equals the gas temperature (T). The predicted H I line width in this cases is proportional to $N_{\rm HI}T^{-1}$ where $N_{\rm HI}$ is the H I column density and T the temperature. Both of the above quantities can be calculated as functions of the local density n. The former quantity equals the product of the total column density $N = n \times L_{\rm geom}$ (for a uniform filled column) multiplied by the H I abundance. This abundance is a function of $\xi_{\rm eff}$ (calculated using Fig. 3 in Maloney et al., 1996) which in turn is a function of n via eq. 2 (where $N_{22} = N/10^{22}$). Likewise T can be derived as a function of n, again using Fig. 3 in (Maloney et al., 1996). Combining the $N_{\rm HI}$ and T dependencies on n, we can predict $N_{\rm HI}T^{-1}$ and hence the expected H I absorption linewidth versus local density and then compare to observations. For densities $n > 10^4$ cm^{-3} the predicted H I absorption is larger than observed, this can however easily be reconciled with observations if the H I absorption is concentrated in clouds (see below). At densities $n < 10^4$ cm^{-3} however, there are no solutions that can provide enough H I absorption to match what we observe, hence we can set a minimum density of 10^4 cm^{-3} for our H I absorbing gas.

For the gas density range 1.0×10^4 cm^{-3} $< n < 3.2 \times 10^4$ cm^{-3} there exist pure atomic phase gas solutions which fit the H I observations. These solutions require the absorption to occur in clouds such that only a fraction $f_{\rm LOS}$ of a typical LOS passes through clouds. At the higher densities within this range the requirements on total gas column density are reduced because gas/spin temperatures decline making

hydrogen atoms more efficient at absorption. At the boundary in density between having predominately atomic or molecular phase clouds (at density 4.6×10^4 cm^{-3}) the spin temperature is $\sim$ 114 K the cloud line of sight filling factor is $f_{\rm LOS} = 0.032$ and $N = 1.82 \times 10^{23}$ cm^{-2}. This is comparable to the X-ray absorption column along the line of sight to the central engine. At higher densities the clouds become predominately molecular but the observed H I absorption can still be fitted by similar total gas column densities. The reason is that although the atomic fraction declines rapidly with increasing density the temperature also declines, this increases the efficiency of absorption per hydrogen atom which almost exactly compensates for the reduced abundance.

In summary, we cannot on the basis of our H I observations alone distinguish between models for the H I absorbing gas phase which are primarily atomic or molecular. We can however set at minimum density ($n > 10^4$ cm^{-3}) and a range for the total gas column density through the H I absorbing disk (10^{23} cm^{-2} $< N <$ 10^{24} cm^{-2}). Estimating total gas masses is complicated for those solutions invoking clouds in that these solutions only fix the line of sight filling factor, converting to volume filling factors requires knowing the cloud size, on which we have no constraint. For the minimum density solution where the gas column is continuous we can make a rough estimate of disk gas mass of $M_{\rm gasdisk} = 1.0 \times 10^8$ $M_\odot$ within the inner 80 pc radius of the disk. For higher density solutions, both total required column densities and cloud filling factors decrease so that total gas mass requirements are significantly less. In all cases the total disk mass is much less than that of the central black hole ($M_{\rm BH} = 2.5 \times 10^9$ $M_\odot$, Tadhunter et al., 2003) which therefore dominates the kinematics in the inner part of the nucleus that we observe.

5.4.3 Constraints on circumnuclear torus properties and relation to the H I disk

It is interesting that the estimated total gas column density through the H I absorbing gas (see Sect. 5.4.2) is comparable to that estimated by X-ray photoelectric absorption toward the core of 2×10^{23} cm^{-2} (see Young et al., 2002). Is it possible that most of this column density and most of the material that hides the quasar nucleus occurs as far out as $r = 80$ pc? An obvious problem with such a scenario is the absence of broad H I absorption along the direct line-of-sight to the radio core (peak opacity is $\tau_0 = 0.016 \pm 0,006$, compared to > 1 on the counter-jet, see Sect. 5.3.3 and Fig. 5.2). A change in gas physical state with scale-height in the disk while keeping almost constant column density seems unlikely. If the high scale-height gas covering the core were still predominately atomic or molecular we find no density solutions that fit the low limit on H I absorption seen. On the other hand if the high scale-height gas were wholly ionised at this column density it would strongly free-free absorb the radio core. Although there are signs of free-free absorption at $r \leq 20$ pc (Krichbaum et al., 1998) along the counter-jet this absorption does not cover the core position itself.

It seems likely instead that most of the X-rays absorbing column in Cygnus A and other hidden quasars occurs on scales $\ll$ 100 pc in a compact circumnuclear *torus*. The inner radius of such a torus is set by the dust sublimation radius, $r_{\rm d}$ =

$0.4 \times (L_{\rm bol} \times 10^{-45}$ erg^{-1} s$)^{0.5}$ pc (Nenkova et al., 2008b) where $L_{\rm bol}$ is the AGN bolometric luminosity. For Cygnus A $L_{\rm bol}$ is estimated to be 1.5×10^{45} erg s^{-1} (Whysong & Antonucci, 2004) giving $r_{\rm d} = 0.5$ pc. It should be noted that the Whysong & Antonucci (2004) mid-IR estimate of the bolometric luminosity is significantly lower (by factors $5 - 20$) than estimates based on the unabsorbed hard X-ray luminosity (see Tadhunter et al., 2003), possibly because of uncorrected torus extinction at mid-IR wavelengths (C. Tadhunter, private communication). However, an increase by a factor of 20 in bolometric luminosity results in the sublimation radius increasing only to $r_{\rm d} = 2.2$ pc, still significantly smaller than the radius of the H I structure. The outer radius ($r_{\rm out}$) is probably not as cleanly defined as in some early depictions of doughnut-like tori (Padovani & Urry, 1992) and may even be continuous with larger circumnuclear disks (see references in Sect. 5.1). Consistent with these more general geometries the term 'torus' can be thought of, if one prefers, as an acronym for 'Thick/ toroidal Obscuration Required by Unified Schemes' (Conway, 1999; Elitzur, 2008) rather than referring to a specific fixed geometry.

Recently Privon (2009) has fitted the observed Spectral Energy Distribution (SED) of the Cygnus A nucleus with a combined synchrotron jet, starburst and torus model. The torus fitting assumed the clumpy model of Nenkova et al. (2008a,b). A wide range of solutions were obtained depending on assumptions about the disk inclination and synchrotron jet spectrum. Most plausible solutions however had cloud number density per unit volume declining as r^{-q} with $q = 1$ and ratios of outer to inner radius, $Y = 30$ (giving $r_{\rm out} = 18$ pc for Cygnus A). Satisfyingly, the predicted total column density matches the X-ray absorption estimate within the errors. Despite the relatively large formal outer radius the concentration of clumps toward the inner edge means that most of the column density is concentrated at small radii. For a radial exponent of $q = 1$ half of the total column density occurs within $\sqrt{Y} \times r_{\rm in}$ corresponding to 2.8 pc, i.e. on a much smaller scale than our observed H I absorption.

The above results beg the question of the relationship between the H I absorbing disk and the circumnuclear torus in Cygnus A. The mass in the torus is very low (6×10^5 $M_\odot$, following Elitzur, 2008) and the lifetime of large scale-height clouds within it is short (due to intercloud collisions, see e.g. Krolik & Lepp, 1989). Hence, both to fuel the quasar-like nucleus at the expected rate of ~ 1 $M_\odot$ yr^{-1} and to replenish the torus clouds a much larger reservoir of material is required, which could reside in the H I absorbing disk. The mass in such a disk (see Sect. 5.4.2) is sufficient to power the source for 10^7 to 10^8 yr and may form part of a 'feeding structure' which funnels gas from kilo-parsec scales into the central black hole. A feeding connection between disk and torus seems likely but the mechanisms of gas transport between the two scales is unclear.

Pertinent to the feeding question is whether the torus and the H I absorbing disk are a continuous structure with one gradually melding into the other, or if they are dynamically distinct and contain gas with very different physical conditions. The former possibility is motivated by the fitted torus outer radius $r_{\rm out} = 18$ pc which is of the same order of magnitude as the radius of the H I absorption ($r = 80$ pc). Furthermore the torus outer radius determined from SED fitting is not well constrained by the data and may extend beyond this limit. However, in such a continuous model for clouds with approximately fixed density the clouds would likely be in an increas-

ingly molecular state over a projected radius from 1 to 70 pc as the excitation parameter decreased. It is hard to see how the rapid gradient in H I absorption seen along the counter-jet could be reproduced in such a case. Furthermore the observation of free-free absorption at intermediate positions ($r < 20$ pc, Krichbaum et al., 1998) is inconsistent with such a continuous model. It seems more likely that the torus – although ultimately fed from gas in the disk – is a distinct structure, perhaps generated in an accretion disk wind as in the model of Elitzur & Shlosman (2006). Clearly, more work is required to understand how the observed components in Cygnus A and other radio galaxies of 100 pc scale H I absorbing disks, inner ionised gas and circumnuclear tori are connected in self-consistent structures which both obscure and feed the central engine.

An additional remark concerning the disk/torus inter-relationship is that although in Cygnus A the H I absorbing disk likely does not contribute to the total absorbing column toward the central engine (as estimated from the X-ray observations), it could have done so if we had observed Cygnus A from a different direction.

Further progress on understanding the circumnuclear gas environment in Cygnus A probably requires the reliable detection of molecular absorption and its imaging with VLBI. Single dish searches at commonly observed molecular transitions such as the ground and higher rotational transitions of CO (Barvainis & Antonucci, 1994; Salomé & Combes, 2003) have so far yielded only upper limits. In contrast, a tentative detection of CO+ in absorption using the IRAM 30m was reported by Fuente et al. (2000) with a centroid velocity and FWHM velocity width (170 $\mathrm{km\,s^{-1}}$) very similar to that of our broad H I absorption. This detection has yet to be confirmed interferometrically (A. Fuente, private communication). Given the results in this paper, despite the similarity in spectral shape, it seems unlikely that these observations are probing the same gas column as seen in H I absorption. The counter-jet which provides the background continuum against which the atomic hydrogen absorption is seen will have negligible flux density at millimetre wavelengths. Instead the line-of-sight probed at 3mm wavelength will probably lie at projected distances < 1 pc from the central engine. While this is comparable to the scales on which the circumnuclear torus has its largest column density (~ 3 pc) we would expect that the velocity dispersion of clouds in such a geometrically thick torus would be comparable to the orbital velocity at this radius (i.e. 1900 $\mathrm{km\,s^{-1}}$), which is much broader than is observed. Similar considerations apply to the tentative VLBA observations of exited OH absorption reported by Impellizzeri et al. (2006) at projected radii < 3 pc which only have observed width ~100 $\mathrm{km\,s^{-1}}$.

5.4.4 The narrow absorption component

While we argue that the broad absorption component is caused by gas rotating around the central black hole (Sect. 5.4.1) the narrow (< 30 $\mathrm{km\,s^{-1}}$, see Sect. 5.3) absorption gas is likely to have a different origin. This narrow velocity component is significantly redshifted (~ 186 $\mathrm{km\,s^{-1}}$) with respect to the optical systemic velocity implying foreground gas moving inward toward the nucleus. This component is detected over the whole continuum region (i.e. jet, core and counterjet) where the

observations are sensitive enough to detect an opacity of ~ 0.1 (see Sect. 5.3.2 and Fig. 5.2). A very similar opacity and centroid velocity is seen at the core position and one effective beam away on the jet side. The apparent increase in opacity at the velocity of the narrow absorption that is seen on the counter-jet side in Fig. 5.2 can be explained entirely by contamination by the broad velocity wings of the broad velocity absorption. While we do not have many independent samples of the narrow velocity component opacity versus position, those we do have are consistent with a constant narrow component opacity of 0.1 over the whole VLBI radio source. Although the foreground distance from the narrow H I absorption to the VLBI continuum source is not well constrained, we suspect that it must be > 100 pc given its narrow velocity width and the position stability of its velocity centroid; if the gas was closer one would expect tidal forces to widen the velocity width and increase velocity centroid variations.

The structure and origin of the narrow H I absorption is unclear. Physically it could be related to a minor merging event, detected 400 pc South-West of the core (Canalizo et al., 2003). As a result of this interaction the narrow H I component could arise in a tidal tail of gas that is moving towards the nucleus. According to galaxy merger simulations (Bournaud et al., 2005) part of the progenitor's gas that gets expelled in tidal tails during a merging event will eventually fall back on the disk. The narrow component could also be connected to the giant infalling molecular cloud located 1.35 kpc to the North-West of the nucleus (Bellamy & Tadhunter, 2004). However, the projected distances from the core are rather different such that a direct connection is not obvious. Both of the above gas components are relatively large (> 100 pc) and thus would be consistent with having fairly constant H I opacity over the whole VLBI structure.

Further progress with constraining the size and origin of the narrow H I absorption system might be made by making future sensitive (and high spectral resolution) e-MERLIN or EVLA observations to try to trace the narrow H I absorption further along the jet.

5.5 Summary

We have presented VLBA H I absorption data of the core region of Cygnus A. H I absorption is detected over a linear scale of 95 pc, but is seen mainly along the counter-jet and on the nucleus. The integrated spectrum can be well-fitted by two Gaussian profiles suggesting a broad (FWHM= 231 ± 21 km s^{-1}) and a narrow (< 30 km s^{-1}) component. Modelling the data shows that the broad absorption occurs only against the counter-jet and not against the jet. Against the unresolved core the opacity is very low. The broad velocity component can be explained by a circumnuclear disk which has its highest opacity 45 mas away (in projection) from the black hole. The narrow velocity component could be explained as an infalling tidal tail, presumably left from a past minor merging event.

The radius at which the broad H I absorption occurs can be constrained with the help of limits on the orientation of the disk. We find a relatively narrow range of possible parameters, resulting in an estimated radius of ~ 80 pc for the peak opacity,

a disk scale height of about 20 pc and hence an opening angle of 14°. The offset between the centroid of the broad velocity component and the mean systemic velocity can be explained by a tilt of 21° of the disk axis compared to the jet axis.

Based on the derived geometry of the circumnuclear disk we derived physical properties of the H I absorbing gas. We find the minimum gas density to be $n > 10^4$ cm^{-3} with a spin temperature $T_{\rm spin} < 740$ K. With the H I observations alone we cannot distinguish between models for the H I absorbing gas phase which are primarily atomic or molecular. We can however set a range for the total gas column density through the H I absorbing disk of 10^{23} cm$^{-2} < N < 10^{24}$ cm^{-2}. An upper limit on the gas mass within a radius of 80 pc is $M_{\rm gasdisk} = 10^8\,M_\odot$, which is a factor 25 less than the black hole mass estimated by Tadhunter et al. (2003).

The circumnuclear torus in Cygnus A has an estimated fiducial radius $\sim$ 3 pc, which is a much smaller scale than our observed H I absorption. The estimated mass in the torus clouds ($6\times10^5\,M_\odot$) is too low to power (alone) the source for $10^7 - 10^8$ yr. In contrast, the H I disk has enough mass to feed the AGN and replenish the torus clouds.

Higher sensitivity, broader band observations are needed to study the properties of the atomic circumnuclear disk in more detail, to search for a connection with the torus and to investigate whether the torus contains a very broad (2000 km s^{-1} wide) H I absorption component. Higher spectral resolution e-MERLIN or EVLA observations of the narrow absorption component are needed to try to trace absorption further out along the jet to constrain its physical size.

Acknowledgements: This research was supported by the EU Framework 6 Marie Curie Early Stage Training programme under contract number MEST-CT-2005-19669 ESTRELA. JC acknowledges financial support from the Swedish Science Research Council. We thank the referee Clive Tadhunter for his comments that helped to improve the paper. We wish to thank Joan Wrobel of NRAO for extensive help in setting up the phased VLA for VLBI observations at a non-standard observing frequency.

6 Cold gas in massive early-type galaxies: The case of NGC 1167

— based on C. Struve, T. Oosterloo, R. Sancisi, R. Morganti, B.H.C. Emonts. 2010. A&A accepted —

Abstract

We present a study of the morphology and kinematics of the neutral hydrogen in the gas-rich ($M_{\rm HI} = 1.5 \times 10^{10}\ M_\odot$), massive early-type galaxy NGC 1167, which was observed with the Westerbork Synthesis Radio Telescope (WSRT). The H I is located in a 160 kpc disk ($\approx 3 \times D_{25}$) and has low surface density ($\leq 2\ M_\odot\ {\rm pc}^{-2}$). The disk shows regular rotation for $r < 65$ kpc but several signs of recent and ongoing interaction and merging with fairly massive companions are observed. No population of cold gas clouds is observed – in contrast to what is found in some spiral galaxies. This suggests that currently the main mechanism bringing in cold gas to the disk is the accretion of fairly massive satellite galaxies, rather than the accretion of a large number of small gas clumps. NGC 1167 is located in a (gas-) rich environment: we detect eight companions with a total H I mass of $\sim 6 \times 10^9\ M_\odot$ within a projected distance of 350 kpc. Deep optical images show a disrupted satellite at the northern edge of the H I disk. The observed rotation curve shows a prominent bump of about 50 km s^{-1} (in the plane of the disk) at $r \approx 1.3 \times R_{25}$. This feature in the rotation curve occurs at the radius where the H I surface density drops significantly and may be due to large-scale streaming motions in the disk. We suspect that both the streaming motions and the H I density distribution are the result of the interaction/accretion with the disrupted satellite. Like in other galaxies with wiggles and bumps in the rotation curve, H I scaling describes the observed rotation curve best. We suggest that interactions create streaming motions and features in the H I density distribution and that this is the reason for the success of H I scaling in fitting such rotation curves.

6.1 Introduction

Observations show that early-type galaxies (ETGs) continue to form their structures over cosmic times down to the present day. Evidence comes from studies of ionised gas (e.g. Sadler & Gerhard, 1985; Sarzi et al., 2006), fine structure in optical morphology (e.g. Malin & Carter, 1983; Schweizer & Seitzer, 1992) and from stellar-population investigations (e.g. Trager et al., 2000; Tadhunter et al., 2005). Numerous studies of the properties of H I in and around ETGs (see, e.g., Knapp et al., 1985; Roberts & Haynes, 1994; Grossi et al., 2009) are strongly supporting the picture of an on-going assembly of ETGs. About 50% of the field ETGs have detectable amounts of H I, sometimes forming large, regular rotating disk structures (e.g. Morganti et al., 2006; Oosterloo et al., 2007b).

In order to be able to evolve, ETGs need to keep on accreting cold gas. For instance, cold gas is required to explain the stellar kinematical properties observed in ETGs (Emsellem et al., 2007). Serra & Oosterloo (2010) find evidence that up to 5% of the stellar mass in ETGs is contained in young stars that formed during the past ~1 Gyr. Moreover, Serra & Oosterloo (2010) argue that a large fraction of ETGs have accreted about 10% of their baryonic mass as cold gas over the past few Gyr.

In addition, theoretical work suggests that cold gas is an essential ingredient for the evolution of ETGs. While dissipationless (gas-free or "dry") mergers can explain boxy, slowly rotating massive galaxies (e.g. Faber et al., 1997; Kormendy et al., 2009), a comparison of N-body simulations with observations suggests that present-day ETGs can not have assembled more than 50% of their mass via dry merging (Nipoti et al., 2009). Jesseit et al. (2007) and Hopkins et al. (2009) have shown that simulations of dry mergers are not able to reproduce some observed quantities such as counter-rotating cores, velocity dispersion features and structural properties of ETGs, whereas the inclusion of a gas component in the simulations (10% of the baryonic mass) helps to reproduce the main observed features. Moreover, dissipative mergers and satellite accretion events are needed to explain, e.g., the dynamical structure of disk-like ETGs (Naab et al., 2006).

The accretion/merging of fairly massive companion galaxies is one possible process to provide the required gas masses to ETGs, but other mechanisms can be important as well. In particular the slow but long-lasting infall of cold gas from the IGM is predicted as a possible mechanism which can provide large gas masses over cosmic times (e.g. Binney, 1977; Kereš et al., 2005). In the framework of hierarchical galaxy formation, new cold gas is added to the halo or deposited in the outer parts of galaxies where it forms a reservoir to fuel the inner parts of galaxies. However, the exact mechanism, how the gas cools (or remains cool), condenses and penetrates to the inner disk without getting shock heated is currently still under debate (e.g. Peek et al., 2008; Dekel & Birnboim, 2008; Kawata & Mulchaey, 2008; Brooks et al., 2009; Kereš & Hernquist, 2009).

Whether the accretion/merging of a few fairly massive satellites is the main disk building process or whether the continuous infall of many small gas clumps plays a dominant role for the continuing assembly of ETGs is not clear. Given the importance of cold gas for the evolution of ETGs, motivated by observations and theoretical work, it is essential to investigate the origin of cold gas in ETGs.

The question of how galaxies accrete gas is not only important for ETGs, but also for spiral galaxies and hence for galaxy evolution as a whole. Signs of gas accretion are found in a large number of galaxies (for instance: gas-rich minor mergers, lobsided disks, gas filaments, extra-planar H I; for a review, see Sancisi et al., 2008), showing the continuing assembly of galaxies. For spiral galaxies the continuous supply of cold gas is important because gas consumption times are usually short in the inner regions (typically $\leq 1-2$ Gyr; see, e.g., Bigiel et al., 2008). Hence, these galaxies can only maintain their observed star formation rates if they manage to keep on acquiring gas, either through merging or via the accretion of small gas clumps from the IGM. An interesting aspect in that respect is whether ETGs accrete gas in the same way, or if other mechanisms might suppress the accretion of cold gas onto the disk, which may then explain the absence of current star formation.

Neutral hydrogen studies of gas-rich, massive ETGs provide a powerful tool to investigate where the cold gas in these systems comes from. Because the cold gas column densities must be low (since large-scale star formation does not occur), the H I in H I-rich ETGs is often distributed in large structures (see, e.g., Morganti et al., 2006; Oosterloo et al., 2007b). At large radii, dynamical timescales are large, allowing to investigate the evolution of the galaxy over the past few Gyr. Since ETGs continue to form their structures down to the present day, the role of the H I in this formation process can be investigated over Gyr timescales.

A second reason to observe H I-rich ETGs is that it allows to study in detail the accretion of small gas clumps. In recent years, neutral hydrogen gas has been detected in the halo of spirals (for a review, see Sancisi et al., 2008) and the existence of H I in the halo could be partly explained by the accretion of small cold gas clumps. However, an alternative mechanism for bringing H I in the halo is star formation (supernova explosions and stellar winds blow gas into the halo) and it is not easy in spiral galaxies to determine which of the two mechanism is the most important one.

To study the accretion of small gas clouds, it is thus useful to observe galaxies with no or little star formation, such as early-type and low surface brightness galaxies that have no/few supernovae explosions. Only very few such galaxies have been studied so far. Matthews & Wood (2003) detected H I in the halo of the LSB galaxy UGC 7321 but concluded that even in this galaxy the energy provided by supernovae explosions might be sufficient to explain the gas in the halo.

In this chapter we investigate how the cold gas in the early-type (SA0) galaxy NGC 1167 (UGC 2487) is accreted in order to understand where the H I comes from. We present deep H I observations performed with the Westerbork Synthesis Radio Telescope (WSRT). NGC 1167 is a giant disk galaxy ($M_B = -21.7$ mag, $D_{25} = 56$ kpc), seen at low inclination, known to host a relatively powerful (10^{24} W Hz^{-1} at 1.4 GHz) radio source (B2 0258+35). What makes this galaxy interesting for the study of the origin of the cold gas is that previous H I observations had shown a regular rotating 160 kpc disk with a total H I mass $> 10^{10}$ $M_\odot$ (Noordermeer et al., 2005; Emonts et al., 2007). The H I surface density is low (≤ 2 $M_\odot$ pc^{-2}) and the H I disk extends beyond the optical disk out to ten R-band disk scale lengths. Deep optical observations show a faint, tightly wound spiral structure at $r < 30$ kpc (Emonts et al., 2010). No stellar bar structure is visible in the data. Hα emission-line imaging revealed no emission ($\log L < 37.6$), except for close to the AGN ($r < 5$ kpc), and hence no sign of

Table 6.1: *Optical and radio parameters for NGC 1167.*

Parameter	Value	Reference
Morphological type	SA0	1
Center α (J2000.0)	03 01 42.4	1
Center δ (J2000.0)	35 12 20.7	1
Distance (Mpc)	70	1
L_B ($L_\odot$)	7.4×10^{10}	2
Systemic velocity (km s^{-1})	4951 ± 3	3
D_{25} (kpc)	49	1
$D_{\rm HI}$ (kpc)	160	3
Total H I mass ($M_\odot$)	1.5×10^{10}	3
H I inclination (deg)	38	3
Mean P.A. (no warp) (deg)	75	3
Total mass ($M_\odot$)	$> 1.6 \times 10^{12}$	3

Note. – Units of right ascension are hours, minutes, and seconds and units of declination are degrees, arcminutes, and arcseconds. References. – (1) NED; (2) based on LEDA; (3) this work.

ongoing star formation (Pogge & Eskridge, 1993) – in agreement with Hα long-slit observations obtained by Emonts (2006). X-ray observations at 2 – 10 keV (Akylas & Georgantopoulos, 2009) show a X-ray halo which extends beyond D_{25} (J. Rasmussen, private communication). In addition to the investigation of the origin of the cold gas, the very extended H I disk allows to derive a rotation curve out to large radii and to investigate the mass distribution out to large distances from the centre. Some optical and radio parameters are given in Table 6.1.

The organisation of this chapter is as follows: in Sect. 6.2 we describe the observations, while Sect. 6.3 presents the observational results and in Sect. 6.4 we search for a possible H I halo component. In Sect. 6.5 we derive a rotation curve to investigate the disk dynamics. A discussion is given in Sect. 6.6 and a summary in Sect. 6.7. The redshift of NGC 1167 (z = 0.0165) translates to a distance of D = 70 Mpc assuming H_0 = 71 km s^{-1} and consequently 3″ correspond to about 1 kpc.

6.2 Observations and data reduction

A ten-hour WSRT service observation in 2006 was followed-up by eleven 12-h observing runs in 2008 (see Tab. 6.2). The net on-source integration time is about 107 h. The strong radio continuum source in the centre (1.8 Jy) required non-standard calibration. In order to guarantee a stable bandpass, calibration observations of 15 minutes were performed every two hours. 3C48 and 3C147 were used as calibrators. An almost uniformly filled uv-plane could be achieved for the combined data by interleaving the hour angle of the calibration observations between individual observations.

Table 6.2: *Summary of observations.*

Total observing time	138 h
Total on-source integration time	~ 107 h
Observing period	Oct. 2006 to Nov. 2008
Bandwidth	20 MHz
Number of spectral channels	1024
Channel separation	8.5 km s^{-1}
Velocity resolution (after Hanning)	17.0 km s^{-1}
Bandpass/flux calibrator	3C48 and 3C147
Weighting scheme	robust 0.4
Resolution	28.″9 x 16.″8
Beam position angle	1.°5
rms noise (mJy beam^{-1}) in the cubes	0.125
rms noise per channel (10^{18}atoms cm^{-2})	4.8
rms noise per channel ($M_\odot$ pc $^{-2}$)	0.039
Detection limit (3σ over 3 channels) ($10^6 M_\odot$)	5.6

The observing band was centred on the redshift of NGC 1167. The total bandwidth was 20 MHz, corresponding to a velocity range of ~3700 km s^{-1} , and was covered with 1024 channels (dual polarisation). In order to increase the signal-to-noise ratio, two channels were binned and subsequently Hanning smoothed resulting in a spectral resolution of 17 km s^{-1} in the output data cube. The data reduction was performed using the MIRIAD package (Sault et al., 1995).

After flagging, bandpass and phase calibration were performed. In addition, on every individual data set self-calibration of the continuum emission was done and the results of this also applied to the line data. The continuum model was subtracted from the line data and the residual continuum emission was removed by making a fit to the line-free channels of each visibility record. The data cube was cleaned using the Clark algorithm. For the extended emission a cube with robust weighting of 0.4 gives the best compromise between spatial resolution and sensitivity, which is used for the analysis of the H I data.

6.3 Results

6.3.1 NGC 1167

The high sensitivity of our observations has allowed to detect new faint H I structures compared to earlier observations. Figure 6.1 shows the total H I image of NGC 1167 and its neighbours. This image was obtained by smoothing the data cube to 35″ resolution and using this smoothed cube to create a mask (blanking all signal below $+3\sigma_{\rm rms}$ in the smoothed cube) which was applied to the original cube. The H I extends over 160 kpc in diameter ($\approx 3 \times D_{25}$), with a total H I mass detected in

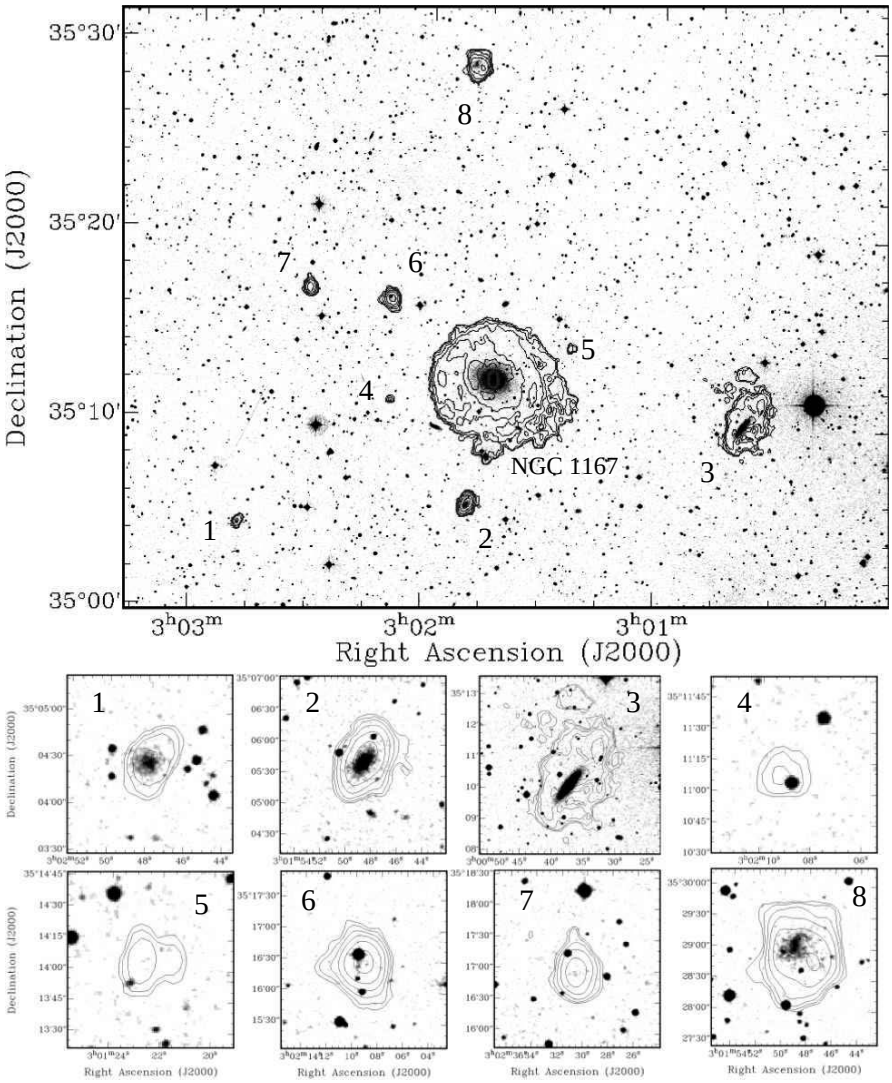

Figure 6.1: *DSS2 image showing the* H I *group environment of NGC 1167. Numbers correspond to numbers in Table 6.3.* H I *contour levels are: 1, 2, 4, 8, 16 and* 32×10^{19} *atoms cm*$^{-2}$.

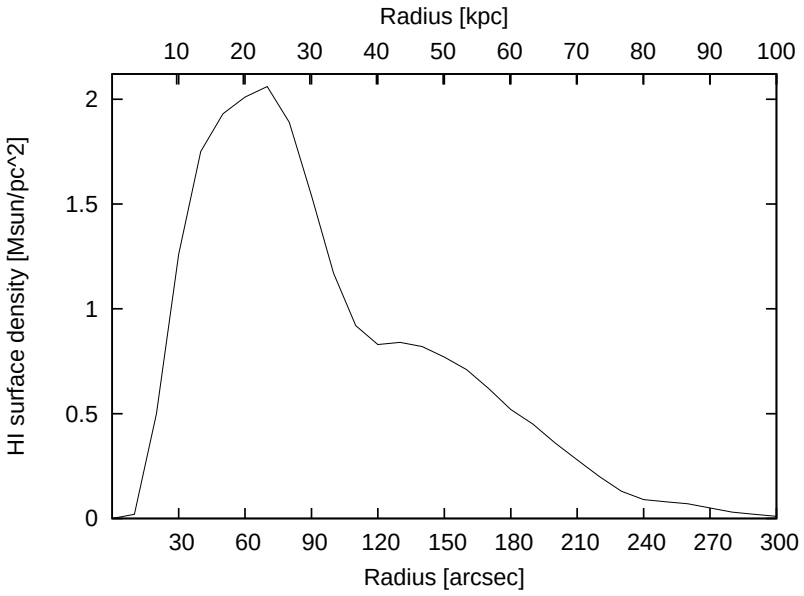

Figure 6.2: *Radial* H I *surface density profile.*

emission of $1.5{\times}10^{10}\,M_{\odot}$ (which is roughly three times the H I mass of the Milky Way; Henderson et al., 1982). Channel maps are shown in Fig. 6.11 and the radial H I density profile in Figure 6.2. The highest H I surface density is found at the radius of the faint, tightly wound spiral structure found in optical images (Fig. 6.3; see also Emonts et al. 2010). Absorption is detected against the strong central continuum, which is unresolved at our resolution. Higher resolution observations show that the absorption is detected against a kpc scale structure. This is discussed in more detail in Chapter 7. The apparent central drop in surface density (Fig. 6.2) is affected by the absorption. Despite the large H I mass, the surface density is too low for star formation to occur globally.

To the southwest of NGC 1167, the H I extends to larger radii as compared to the rest of the galaxy (see Fig. 6.4, left panel). The gas in this region does not follow exactly the rotation of the regularly rotating ~65 kpc disk (see also Fig. 6.11).

The derivation of a velocity field is not straightforward. Some of the velocity profiles are broad (see Fig. 6.5 and 6.7 for a few examples) and close to the centre ($r < 100''$) beamsmearing becomes severe due to the large beam size (9.6 x 5.6 kpc) and the steep velocity gradients. To minimise beamsmearing effects, we use the velocity of the peak of the profile instead of the intensity weighted mean. The resulting velocity field (Fig. 6.4, right panel) shows that the gas kinematics for $r < 65$ kpc is dominated by regular large-scale rotation.

The radial velocities along the major axis and the main rotational properties are shown in Fig. 6.5. The rotation curve (derived in Sect. 6.5 and over-plotted on the major-axis slice in Fig. 6.5) is rising within the central beam and is essentially flat out to the largest radii measured. However, on both the approaching and receding side,

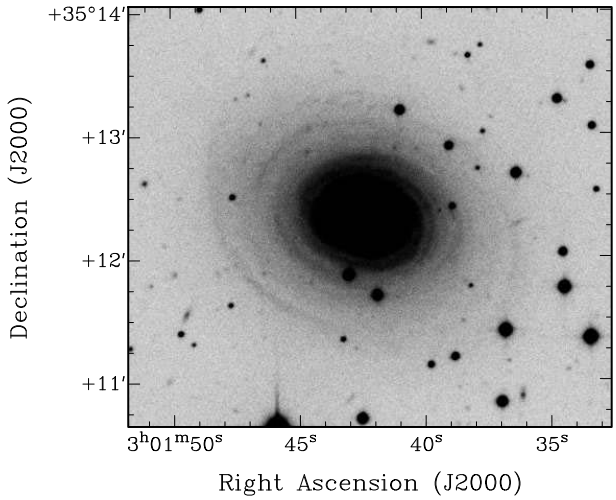

Figure 6.3: *B-band image from Emonts et al. (2010) showing the faint spiral structure of the stellar disk.*

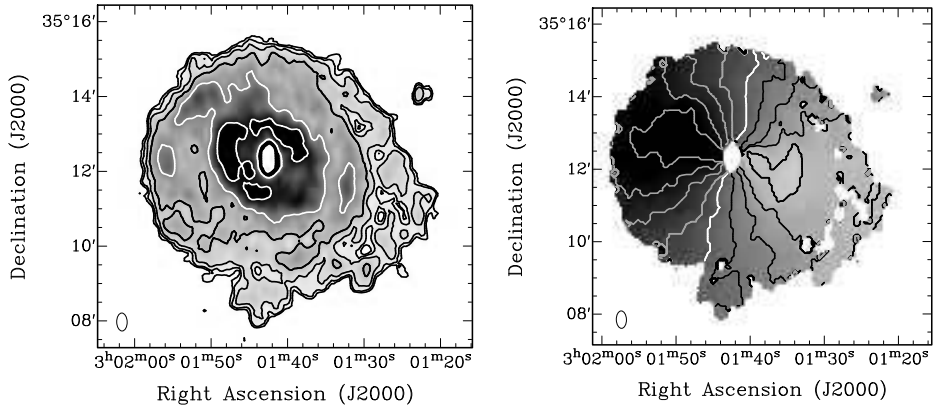

Figure 6.4: *Left panel: Total* H I *intensity map of NGC 1167. Contour levels are: 1, 2, 4, 8, 16 and* 32×10^{19} *atoms cm*$^{-2}$*. Right panel: Velocity field based on the peak of the profile (see text). The white contour indicates the systemic velocity, 4951* km s^{-1} *, the black and grey contours give the velocity in increments of 50* km s^{-1} *. The approaching side is to the East. The beam is indicated in the lower left corners.*

Table 6.3: *Properties of* H I *detections.*

No.	Identification	RA	Dec	v_{sys}	Δv	Δv_{off}	D	D_{off}	D_{off}	F_o	F_c	M_{HI}
(1)	(2)	(3)	(4)	(5)	(6)	(7)	(8)	(9)	(10)	(11)	(12)	(13)
0	NGC 1167	03 01 42.4	35 12 20.7	4951	520	-	69.7	-	-	457.65	461.33	15.324
1	J0302478+3504284[1]	03 02 47.8	35 04 28.4	4864	103	-87	68.5	15.5	310.4	1.62	2.54	0.081
2	2MASX[2]	03 01 48.6	35 05 42.4	4903	213	-48	69.1	6.7	134.8	16.29	17.70	0.578
3	UGC 2465	03 00 37.4	35 10 08.7	5065	529	114	71.3	13.4	267.6	57.23	80.90	2.812
4	J0302091+3511120[3]	03 02 09.1	35 11 12.0	4907	34	-44	69.1	5.6	111.6	0.39	0.41	0.013
5	J0301222+3514055[4]	03 01 22.2	35 14 05.5	5057	42	106	71.2	4.5	89.4	0.78	0.81	0.028
6	J0302095+3516308[3]	03 02 09.5	35 16 30.8	4903	77	-48	69.1	6.9	138.0	13.20	14.39	0.470
7	J0302307+3516581[4]	03 02 30.7	35 16 58.1	5245	128	194	73.9	10.9	217.9	6.07	7.56	0.282
8	J0301491+3529012[1]	03 01 49.1	35 29 01.2	4954	94	3	69.8	16.7	334.0	25.59	43.10	1.436

Note – (1) Number in Fig. 6.1. (2) Name (NED)/Identification. (3) Centre: Right ascension. (4) Centre: Declination. (5) Systemic velocity [km s^{-1}]. (6) Line width above 3σ. (7) Velocity off-set from NGC 1167. (8) Distance from Earth assuming Hubble flow (H_0 = 71) [Mpc]. (9) Off-set from NGC 1167 [arcmin]. (10) Off-set from NGC 1167 [kpc]. (11) Integrated flux [Jy km s^{-1}]. (12) Primary beam corrected Flux [Jy km s^{-1}]. (13) H I mass [$10^9 M_\odot$]. [1] counterpart on DSS image; [2] full name is: 2MASX J03014864+3505423; [3] star in front; [4] no counterpart on DSS image.

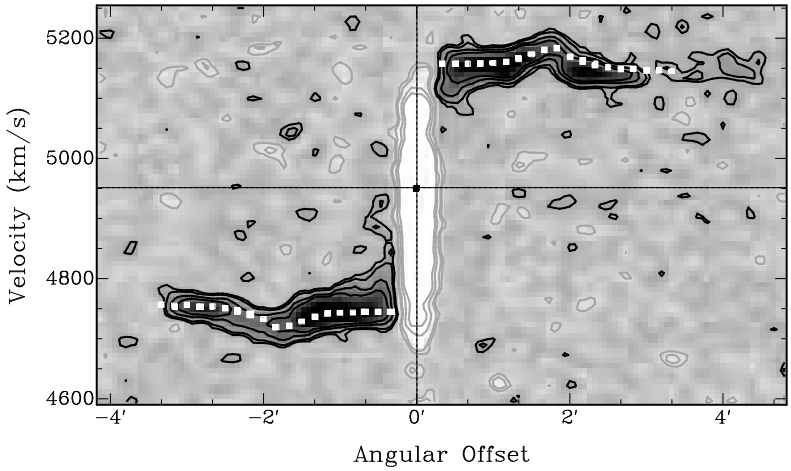

Figure 6.5: *Position-velocity slice along the major axis. The white squares give the rotation curve as derived from modelling (see Sect. 6.5). The bump in the rotation curve is clearly visible. Contour levels: –9, –6, –3, –2 (thin black), 2, 3, 6 and 9σ (thick black). The horizontal dashed line indicates the systemic velocity.*

at radii between ~26 and ~45 kpc, the rotation curve makes a 25 km s^{-1} jump up and goes down again by about 37 km s^{-1} (uncorrected for inclination). The radius of the peak of the jump ($r \approx 36$ kpc) and the radial extent of this jump are similar, but not completely identical for the approaching and receding side. This "bump" in velocity occurs just outside the bright optical disk at $r \approx 1.3 \times R_{25}$, exactly at the radius where the H I surface brightness rapidly drops (Fig. 6.2). This is further discussed in Sect. 6.6.3.

6.3.2 The (H I) environment of NGC 1167

We detect eight sources (Fig. 6.1) in the vicinity of NGC 1167 with H I masses between $\sim 1 \times 10^7\ M_\odot$ and $3 \times 10^9\ M_\odot$ within a projected radius of 350 kpc. The total amount of H I in the environment is $5.7 \times 10^9\ M_\odot$. Two of the detections are identified with catalogued galaxies. Table 6.3 summarizes the basic properties of all H I detections.

The most massive galaxy besides NGC 1167, UGC 2465, is located 268 kpc (projected) west and shows a distorted H I morphology and kinematics. In addition, deep optical observations (for details, see Emonts et al., 2010) show a disrupted satellite at the northern edge of the H I disk with a possible tail towards the region of the southwestern H I extension (Fig. 6.6, see also Sect. 6.6.1). Besides these two cases, none of the other H I detections show hints of an interaction with NGC 1167 in terms of bridges or tails.

Five detected galaxies (No. 1, 2, 6, 7 and 8 in Tab. 6.3) show indications of regular rotation, despite the low spatial resolution. Objects No. 2, 6 and 7 are fairly gas-rich

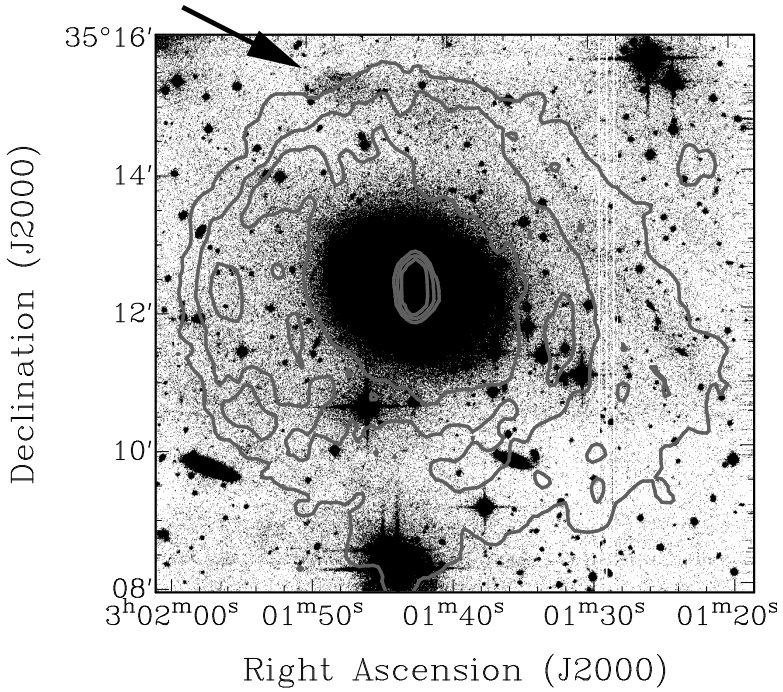

Figure 6.6: *B-band image from Emonts et al. (2010) overlaid with* H I *density contours. Contour levels: 1, 8 and* 16×10^{19} *atoms cm*$^{-2}$*. The arrow indicates the location of the disrupted satellite.*

with H I masses above 10^8 $M_\odot$. DSS2 images do not show an optical counterpart for No. 6 and 7 (see Fig. 6.1). However, the DSS2 images are shallow and optical counterparts with luminosities several times 10^7 $L_\odot$ could still be present. Close to NGC 1167, at distances of 90 to 110 kpc from the centre, we detect two unresolved H I clouds (No. 4 and 5) with masses just above our detection limit which do not have an optical counterpart in DSS2 either. No additional low-mass H I clouds were found in a systematic search using the source finder Duchamp (Whiting, 2008).

6.4 The search for an H I halo

One of the main reasons to observe NGC 1167 is to investigate the origin of the large amount of H I in this early-type galaxy. One possibility is the long-term accretion of a large number of small cold gas clumps. Signs for the accretion of such gas clouds have been found in the halos of a few spiral galaxies (for a review, see Sancisi et al., 2008). Over a Hubble time, galaxies could accrete a significant fraction ($> 10^9$ $M_\odot$) of their cold gas in this way. In order to investigate the possibility that NGC 1167 also accretes such gas condensations, we search for an extended halo of H I clouds. In

Sect. 6.4.1 we explain how to identify gas that is located in the halo and in Sect. 6.4.2 we show that no H I clouds are detected in the halo of NGC 1167 and place upper limits to the accretion of small gas clumps.

6.4.1 Identifying halo gas

In low-inclination galaxies, such as NGC 1167, the separation of gas located in the disk and the halo is not straightforward. This is because gas located in the halo lies along the same line-of-sight as disk gas, unlike in edge-on systems. However, the kinematics of the halo gas differs from the disk kinematics such that the velocities of the gas can be used to separate the halo component from disk gas. For instance, it has been found that gaseous halos observed in spirals are lagging with respect to disk rotation (Fraternali et al., 2002; Heald et al., 2007; Oosterloo et al., 2007a). This lagging gas is most clearly seen in a *pv*-diagram along the major axis in the form of wings on the side of the lower rotation velocities, toward systemic. These systematic asymmetries in the H I velocity profiles have been refered to as *beards* (Sancisi et al., 2001). Low-inclination galaxies that show prominent beards are e.g. NGC 2403 (Fraternali et al., 2002) and NGC 6946 (Boomsma et al., 2008).

Position-velocity slices along the major axis of NGC 1167 (Fig. 6.5) or near the major axis (Fig. 6.7, right panel) show H I line profiles that are strongly asymmetric with respect to the peak of the line, in particular in the inner part of the disk (similar to NGC 2403 and NGC 6946). Note that the white squares, which mark the rotation curve (which we derive in Sect. 6.5), follow closely the peaks of the profiles. In some locations the profiles extend (as a beard) 200 km s^{-1} toward the systemic velocity (Fig. 6.7, right panel).

However, there is a major difference between NGC 1167 and previously studied low-inclination galaxies: NGC 1167 is located relatively far away such that the linear resolution of our observations is coarse (beam is 9.6×5.6 kpc). As a consequence the velocity gradients within a beam are large. Hence, broad velocity profiles are observed, in particular close to the centre where the velocity gradients are largest. Because of the large rotation amplitude, the velocity gradients would even be larger if NGC 1167 would be observed at the same resolution as the previously studied objects. The convolution of the signal with the observed beam spreads the emission to neighbouring locations such that the broad profiles observed in Fig 6.5 and 6.7 could be the result of beamsmearing instead of indicating a halo. To identify a possible H I halo component, it is therefore important to compare the data to a model that takes beamsmearing into account. In addition to the velocity gradients near the centre, NGC 1167 shows evidence for large, local velocity gradients at other locations due to streaming motions in the disk (see Sect. 6.5). Also these require that beamsmearing is taken into account in modelling the H I disk of NGC 1167.

The thin disk of NGC 1167 is modeled by placing at every pixel in the cube a Gaussian profile centred at the velocity at that location as derived from the observed velocity field. This cube is then convolved with the beam. Thus, this approach ensures that the local velocity structure and beamsmearing effects are taken into account. The intensity of the profile is taken from the total H I map at the position. For the Gaussian profile, a velocity dispersion of 9 km s^{-1} is assumed.

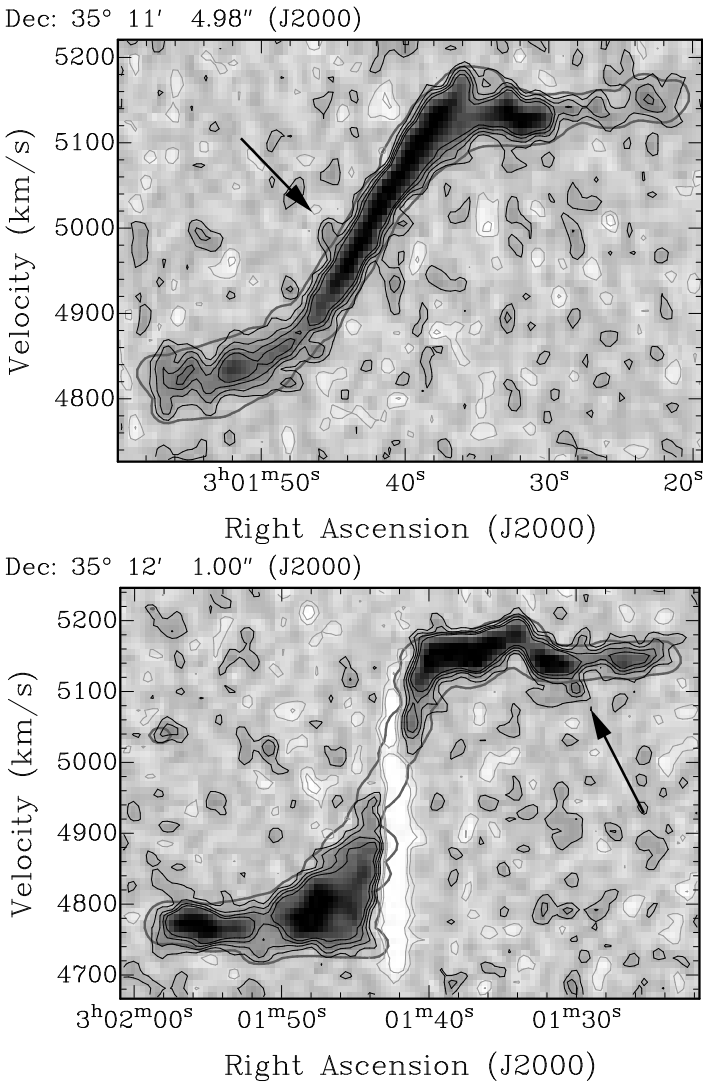

Figure 6.7: *Two east-west pv-slices of the data cube overplotted with the* 1σ *contour level (thick contour) of our model. Contour levels of the data: -3, -1.5 (thin grey), 1.5, 3, 4.5 and* 6σ *(thin black).* H I *emission not covered by the model is indicated by arrows.*

6.4.2 An upper limit to the H I halo

Comparing the model cube with the data shows that the model describes the overall kinematics of the H I in NGC 1167, including the broad profiles seen in many locations. This is illustrated in Fig. 6.7 where we show two representative *pv* slices. The fact that our beamsmeared model of the thin H I disk does explain the broad profiles indicates that these are due to beamsmearing and that we do *not* observe H I clouds in the halo of NGC 1167, in contrast to what is seen in many later-type spiral galaxies.

Figure 6.7 also illustrates that the only features not consistent with our model are at the noise level. However, many other such "blobs" are present in the data cube, also at locations and velocities quite remote from NGC 1167. Therefore, we take the masses and column densities of the clouds of the kind indicated in Fig. 6.7 as the upper limit for any halo population in NGC 1167.

The upper limit of the peak surface density of a possible H I halo component is hence 0.05 $M_\odot$ pc^{-2}, which corresponds to a column density of 6×10^{18} cm^{-2} and any cloud in the halo of NGC 1167 has an H I mass of less than 10^7 $M_\odot$. We note, for comparison, that in some spiral galaxies halos have been observed with average column densities well above 10^{19} cm^{-2} while the regions with highest H I surface density in the halo of, e.g., NGC 2403 and NGC 6946 have column densities above 10^{20} cm^{-2} (Fraternali et al., 2002; Boomsma et al., 2008), which is a factor ~20 above the upper limit for NGC 1167. We can, therefore, rule out that NGC 1167 has an H I halo with similar (column) densities as compared to those late-type, star-forming galaxies. The mean density contrast ratio between H I located in the disk and in the halo is > 20 for NGC 1167. This is significantly larger than for NGC 2403 and NGC 891 (ratio is 10 and 2.3 respectively), but is similar to the one of NGC 6946 (ratio is 22).

6.5 Rotation curve

In this section we further investigate the nature of the velocity bump seen in the kinematics of NGC 1167, as described in Sect. 6.3.1. In particular, we investigate whether this feature reflects the overall mass distribution of this galaxy, or whether it could be indicative of a recent disturbance suffered by NGC 1167. We derive a rotation curve and show that none of our applied mass models explains the feature in the kinematics satisfactorily. We conclude that large-scale streaming motions must be present in the disk.

The rotation curve is derived by fitting a set of tilted rings to the observed velocity field (Fig. 6.4, right panel) (following Begeman, 1987). The resulting rotation curve, plotted in Fig. 6.8 and given in Tab. 6.4. The rotation curve has two sources of uncertainty. Every data point has an individual error of ~13 km s^{-1} (estimated from the residuals in the velocity field, Fig. 6.9). In addition, a systematic uncertainty exists which depends on the inclination of the disk. Following Begeman (1987), the systematic uncertainty in inclination for NGC 1167 is 2°, which is constant with radius ($i = 38° \pm 2°$). This translates into a possible systematic offset of 15 km s^{-1} . The position angle is constant within the uncertainties ($PA = 75° \pm 3°$). The remarkable

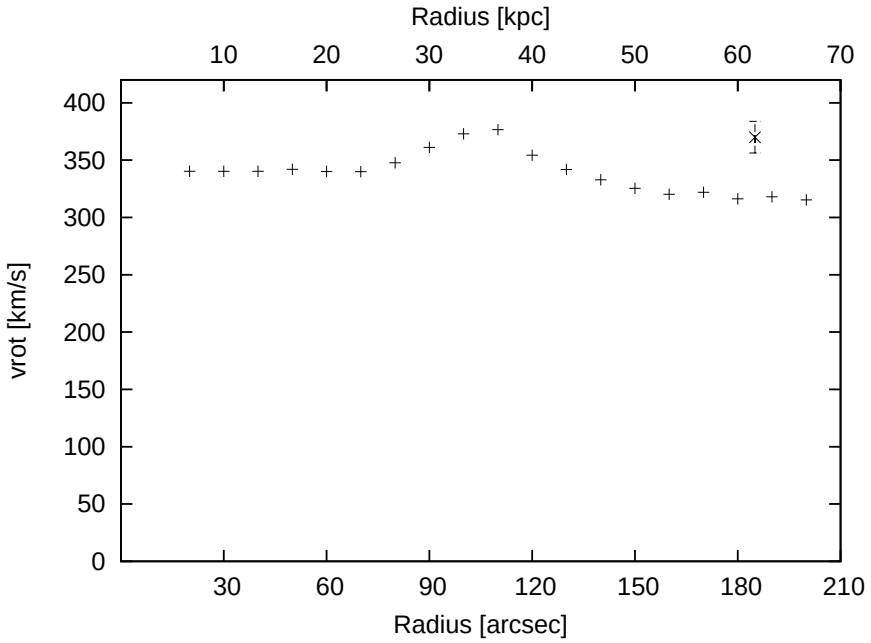

Figure 6.8: *Rotation curve. The error bar indicates the uncertainties.*

bump seen in Fig. 6.5 is also visible in the rotation curve as a distinct feature at radii between 80″ and 130″. In principle, the feature in the kinematics could also be explained as the result of a change in inclination instead of rotation velocity. However, a bending up and down in inclination of ∼6° would be required. Such a bending is not observed in other galaxies and therefore we think that it is unlikely that this feature reflects such a change in inclination.

6.5.1 Large-scale streaming motions

The presence of non-circular motions is also evident from the residual velocity field. In Figure 6.9 (top panel) the velocity field of an axisymmetric model, which is based on our derived rotation curve, has been subtracted from the observed velocity field. A large-scale residual structure is seen at the radius of the feature in the rotation curve. We note that the residuals are not completely axisymmetric, in agreement with the slightly asymmetric appearance of the feature in the rotation curve (Sect. 6.3.1). This residual structure is even more prominent assuming a purely flat model rotation curve (i.e. without a bump), as shown in the bottom panel of Fig. 6.9. Additional velocity deviations from the axisymmetric model at larger and smaller radii are also present.

The systematic residuals imply that streaming motions must be present in the disk. Simple radial motions are excluded because the feature in the rotation curve is seen strongest along the major axis (where radial motions should be zero) and not

Table 6.4: *Rotation curve.*

Radius [″]	Radius [kpc]	velocity [km s^{-1}]
20	6.7	334
30	10.0	335
40	13.3	335
50	16.7	337
60	20.0	340
70	23.3	340
80	26.7	348
90	30.0	361
100	33.3	373
110	36.7	377
120	40.0	354
130	43.3	342
140	46.7	333
150	50.0	325
160	53.3	320
170	56.7	322
180	60.0	316
190	63.3	318
200	66.7	315

Table 6.5: *Parameters for mass models with isothermal halos,* H I *scaling and MOND.*

model	Γ_b	Γ_d	η	r_c	ρ_0	A	χ^2
	$M_\odot/L_\odot$	$M_\odot/L_\odot$		kpc	$M_\odot$pc^{-3}		
(1)	(2)	(3)	(4)	(5)	(6)	(7)	(8)
minimal χ^2	4.1	3.6	1.4	10.6	14.5	-	12.2
max. allowed disk	4.3	4.7	1.4	25.6	3.0	-	16.3
min. allowed disk	3.8	1.0	1.4	2.7	249.0	-	18.7
constant M/L	4.2	4.2	1.4	21.0	4.4	-	16.6
H I scaling	4.5	4.9	46.4	-	-	-	11.2
MOND	3.8	4.9	1.4	-	-	3565	13.8

Note – (1) model; (2) bulge *R*-band mass-to-light ratio; (3) disk *R*-band mass-to-light ratio; (4) H I scaling factor; (5) halo core radius; (6) halo central density; (7) Mond factor; (8) χ^2 value from fit.

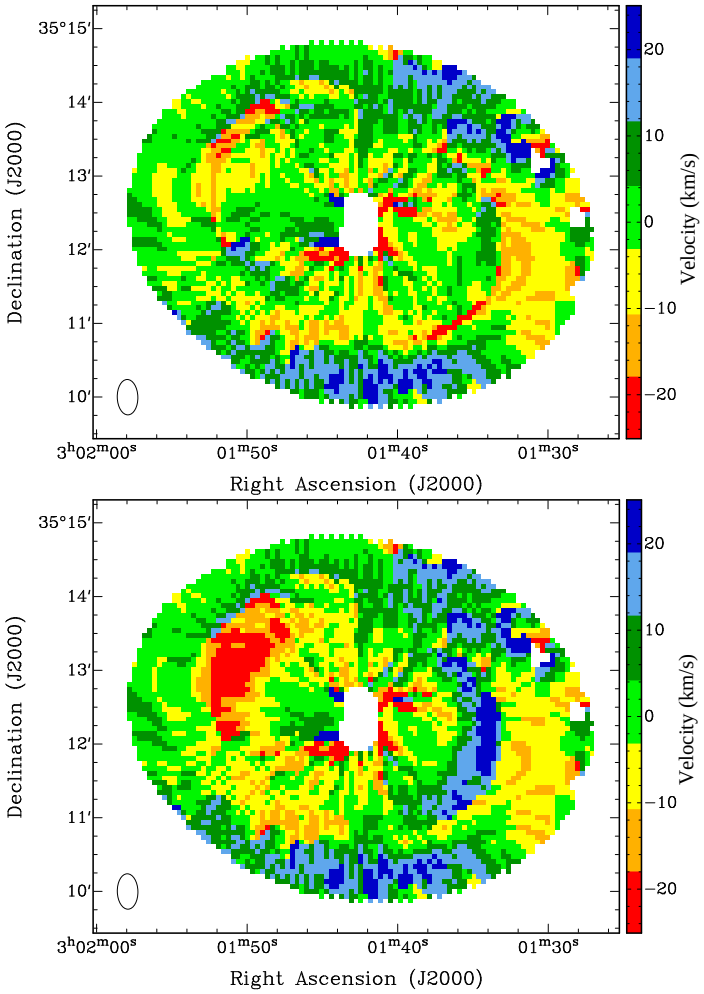

Figure 6.9: *Top panel: Residual velocity field based on the derived rotation curve (Fig. 6.8). Bottom panel: Residual velocity field assuming a flat rotation curve (see text). The beam is indicated in the lower left corners.*

along the minor axis (where they should be maximal). The measured peak velocity of the large-scale residuals is above 34 km s^{-1} corresponding to a deprojected amplitude (i.e. velocity in the plane of the disk) of 55 km s^{-1} . In Sect. 6.6.3 we argue that these large-scale streaming motions may be caused by an interaction/merging event.

6.5.2 Mass models

We model the mass distribution in order to investigate whether the feature in the rotation curve can be explained by one of the standard models. We assume that the gravitational potential of a disk galaxy can be written as the sum of the individual components: stellar bulge, stellar disk, gaseous disk (multiplied with the H I scaling factor η) and a dark matter halo. To model the stellar mass distribution we use published R-band photometry (Noordermeer, 2006) and adopt Noordermeer's disk/bulge separation. The uncertainty of the rotation curve affects the M/L estimate by ≤ 0.3.

None of the tested models reproduces the feature in the rotation curve satisfactorily (see Fig. 6.10 and Tab. 6.5). A truncated optical disk (see e.g. van der Kruit, 2007) is not observed and, therefore, neither explains the feature in the rotation curve. Moreover, even if a truncation in the optical disk would have been observed at the right radius, it would not have been able, given the faintness of the disk, to explain the amplitude of the bump.

The best model (smallest overall χ^2) is that of a scaled-up version of the H I mass distribution with no dark matter halo. The H I scaling factor of 33 (correcting for helium) is higher than the average value that Hoekstra et al. (2001) found for a sample of 24 spiral galaxies ($\eta = 6.5$), but is in agreement with the systematic trend that more luminous systems require higher scaling factors than low luminosity systems. High scaling factors have also been found for other luminous galaxies, e.g., $\eta = 37$ for UGC 6787 (Noordermeer, 2006). However, also in the H I scaling model the feature in the rotation curve is not perfectly reproduced. The predicted bump is approximately 5 kpc closer to the centre than the observed bump.

The fact that none of the tested models fits the observed rotation curve suggests that the feature in the rotation curve does not reflect an equilibrium mass distribution of NGC 1167. In Sect. 6.6.3 we will argue that the bump in velocity is consistent with the presence of large-scale streaming motions in the disk, as already suggested from the residual velocity field (Fig. 6.9 and Sect. 6.5.1).

6.6 Discussion

We start this section by discussing the formation of the H I disk and the role of different accretion mechanisms (Sect. 6.6.1). In Sect. 6.6.2 we give possible explanations for the absence of a population of cold gas clouds and Sect. 6.6.3 briefly comments on a possible connection between the H I density and the large-scale streaming motions in the disk.

6.6.1 Formation of the H I disk

Where does the H I in NGC 1167 come from? The various signs of merging and interaction activities suggest that currently the H I is brought in by fairly massive satellite galaxies. This means that most of the H I arrives in large quantities in a few events.

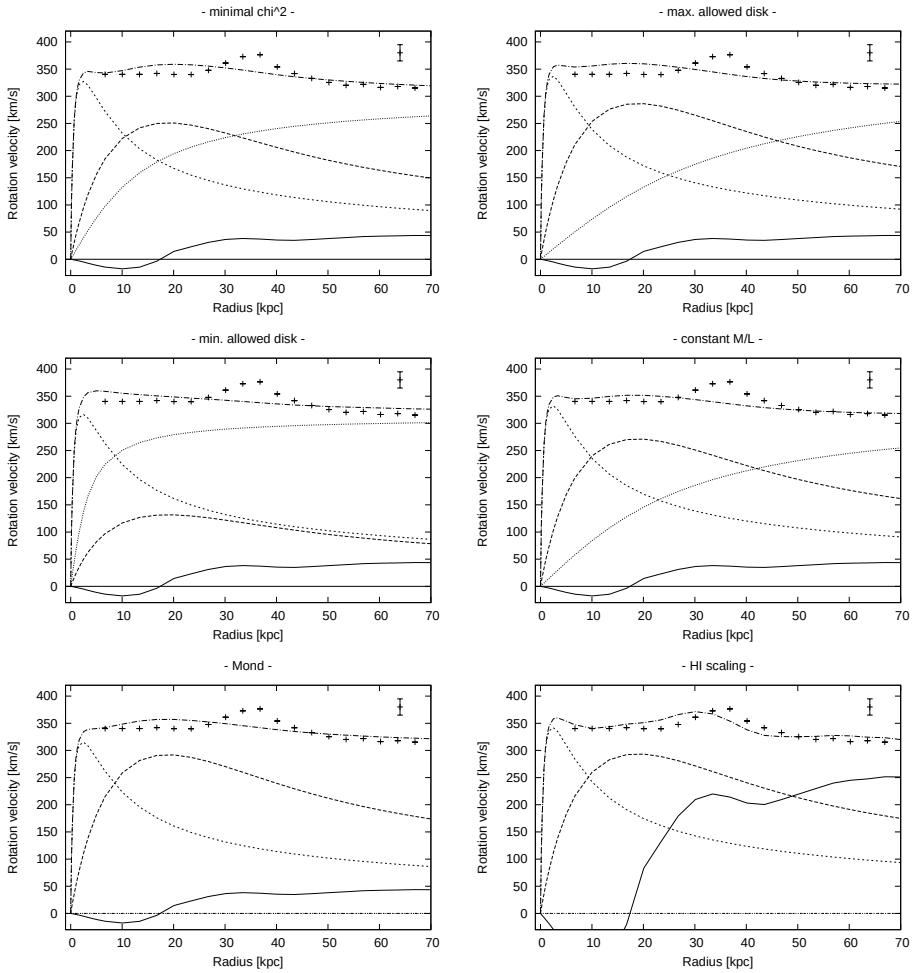

Figure 6.10: *Mass models. The fitted individual contributions to the rotation curve are stellar bulge (short dashed), stellar disk (long dashed), gas disk (continuous line) and dark halo (dotted). The dot-dashed line shows the resulting model rotation curve. The error bar indicates the uncertainty for an individual data point of the observed rotation curve.*

Signs of recent and/or ongoing interactions with the environment of NGC 1167 are, for instance, the southwestern extension of the H I disk, the feature in the rotation curve, the disturbed H I morphology and kinematics of UGC 2465 and the disrupted satellite at the northern edge of the H I disk (Sect. 6.3.2). All of these signs are pointing towards an ongoing assembly of the H I disk. About 30% of the detected H I in the data cube is located in companions. Hence, it might be possible that, over the course of several Gyr, NGC 1167 has built-up a large fraction of its H I disk via minor mergers and interactions with the environment.

The southwestern extension could be the result of such a minor merger. Figure 6.6 shows the disrupted satellite at the northern edge of the H I disk with a possible tail-like structure all the way to the H I extension (Sect. 6.3.2). Therefore, we might see also the disrupted H I in the aftermath of a minor merger. The H I mass of the southwestern extension is at least $9 \times 10^8\ M_\odot$, showing that the accretion of satellite galaxies can bring in large amounts of H I. This minor merger may have also induced the large-scale streaming motions in the disk that are seen as the feature in the rotation curve (Sect. 6.5.2, see also Sect. 6.6.3). The non-circular motions provide, therefore, another piece of evidence for the accretion of, fairly massive, companion galaxies.

Another possibility is that the H I extension could be caused by a recent interaction with UGC 2465. In this case, the past interaction time estimate is roughly 1 Gyr, given the projected distance between both galaxies and assuming a relative velocity offset of 200 $\mathrm{km\,s^{-1}}$. This time estimate equals one revolution of NGC 1167 (at r = 65 kpc), but is less than the 1.3 Gyr that one revolution of UGC 2465 takes. After an interaction it takes a few rotations before the gas settles in a rotating disk structure. Hence, it is not a surprise that the southwestern extension and part of the H I structure of UGC 2465 is not completely settled.

Other mechanisms that could contribute to the H I disk building process do not seem to play a major role. Below, we briefly discuss the relevance of small gas clouds, the possibility of a major merger and the role of stellar mass loss.

Accretion of small gas clumps:

We do not find a large number of small gas clumps. In fact, only two clouds just outside the H I disk (No. 4 and 5 in Tab. 6.3) are detected. The very few tentative H I structures (with masses of $\sim 10^7\ M_\odot$), which are not explained by the model (Sect. 6.4), are features at the noise level and form an upper limit for a possible halo cloud population. The two detected clouds have masses at the high mass end of the high velocity clouds (HVCs) observed around the Milky Way and other nearby galaxies ($10^4 \leq M_{\mathrm{HI}} \leq 10^7\ M_\odot$; e.g. Thilker et al., 2004; Westmeier et al., 2005; Wakker et al., 2007, 2008). Clouds with H I masses $\sim 10^7\ M_\odot$ were also detected around NGC 2403 (Fraternali et al., 2002), NGC 891 (Oosterloo et al., 2007a), NGC 6946 (Boomsma et al., 2008) and NGC 2997 (Hess et al., 2009). What makes these HVCs interesting is that they could be, at least in some cases, gas condensations from the IGM. The presence of two such clouds around NGC 1167 might, therefore, indicate that the accretion of small gas clouds, at a low level, occurs.

Nevertheless, the absence of a large number of such clouds shows that the "dif-

fuse" accretion of small cold gas clumps from the IGM is not the dominant disk building process. The number of required clumps ($> 10^3$) would be unphysically large, given that we detect only very few such gas clouds. Possible explanations for the absence of gas clouds located in the halo are discussed in Sect. 6.6.2.

Major merger:
While gas-rich major mergers can form giant low column density H I disks (Sect. 6.1), we have no evidence in our H I data that this is actually the case for NGC 1167. Neither do the deep optical images show any indication of a major merger. Such a dramatic event would certainly need to be older than a few Gyr, given that the H I disk shows regular rotation for $r < 65$ kpc. After a major merger, it takes at least a few revolutions (corresponding to a few Gyr at $r = 65$ kpc) before the gas settles in a regular disk structure. A stellar population analysis of Emonts (2006) also suggests that the last interaction (that caused a burst of star formation) occured at least one to several Gyr ago, but this starburst may be the result of a smaller accretion event and is no evidence for a major merger.

Stellar mass loss:
The H I can not originate from stellar mass loss. All stars shed mass over their lifetimes. According to models of Ciotti et al. (1991) and Brighenti & Mathews (2000), the expected cold gas mass from stellar mass loss processes for massive galaxies could be $> 10^{10}\ M_\odot$ over a Hubble time. In the case of NGC 1167 it is *unlikely* that the H I results from stellar mass loss because the H I disk extends well beyond the optical disk ($D_{\rm HI} = 3 \times R_{25}$) and carries therefore more angular momentum than the stars. Also in other galaxies there is little evidence that cold gas comes from mass loss processes. In the cases where gas could be associated with stellar mass loss, it is ionised (see, e.g., Sarzi et al., 2006).

As a final remark, we would like to note that all eight detected companions of NGC 1167 have systemic velocities close to that of NGC 1167 (none is deviating by more than 200 km s^{-1} , see Tab. 6.3). Furthermore, all but No. 7 (in Tab. 6.3) have systemic velocities which follow the sense of rotation of NGC 1167. We cannot rule out that this is the result of projection effects. However, Erickson et al. (1999) found the trend that companions seem to be close in velocity to the host galaxy in a number of (late-type) spiral galaxies. They argue that their sample is not affected by projection effects and they find evidence for varying sizes of dark matter halos. However, for galaxy sizes above 200 kpc their constraints become weak. Larger statistical samples are needed to shed more light on this issue.

6.6.2 The absence of an H I halo

Different theoretical explanations have been proposed that could explain the absence of an extended halo of cold gas clouds. In principal, small cold gas clouds from the IGM can be accreted onto the disks of galaxies (Binney, 1977, see also Sect. 6.1). However, the surrounding x-ray halo of massive galaxies ionises the cold gas before it can reach the disk (e.g. Nipoti & Binney, 2007). According to simulations of e.g. Dekel & Birnboim (2008), accretion of cold gas is not expected at galaxy masses above

$\sim 10^{12}\ M_\odot$. The dynamical mass of NGC 1167 is at least $M_{\rm dyn} > 1.6 \times 10^{12}\ M_\odot$ (for $r_{\rm max} = 65$ kpc and $v_{\rm rot} = 330\ {\rm km\,s^{-1}}$). Hence, NGC 1167 may simply be too massive for the accretion of small gas clumps.

Another possible explanation for the absence of an extended halo of cold gas clouds in NGC 1167 is the hypothesis that cold halos are caused, directly and indirectly, by star formation. Because NGC 1167 does not form stars, galactic fountains from supernovae explosions do not blow any gas into the halo. However, according to e.g. Marinacci et al. (2010), this galactic fountain gas would be needed to create Kelvin-Helmholtz instabilities in the hot corona such that (hot) gas can condense to clouds that are able to reach the disk. With the presence of supernovae, star-forming galaxies can accumulate enough cold gas to sustain their observed star formation rates (see also Hopkins et al., 2008a) while in early-type galaxies, like NGC 1167, the creation of instabilities in the halo is prevented (due to the absence of galactic fountains). Hence, no new cold gas complexes can reach the disk of NGC 1167.

6.6.3 Streaming motions, rotation curve and H I density distribution

Streaming motions in disks are a well known phenomenon and observed in many galaxies (see e.g. Knapen, 1997; Pisano et al., 1998; Fathi et al., 2006). However, it is remarkable that the streaming motions in NGC 1167 are (to first order) symmetric. The amplitude is relatively large ($\approx 50\ {\rm km\,s^{-1}}$, deprojected), at the high end of what is detected in a number of other early-type galaxies (Noordermeer, 2006). Interestingly, most of these galaxies, like NGC 1167, also show clear signs of interaction and/or tidal distortions with some of them having bumps and wiggles in the rotation curve as well (see also Noordermeer et al., 2007).

The feature in the rotation curve of NGC 1167 occurs at the radius where the H I surface density drops significantly (see Fig. 6.2 and 6.5). The drop in surface density results in the bump in the H I scaling model rotation curve (Fig. 6.10 and Sect. 6.5.1), suggesting that a connection between large-scale streaming motions and H I density distribution exists.

H I scaling has previously been tried in the analysis of rotation curves and has even led to suggestions of a possible coupling of dark matter with the gas component (see, e.g., Broeils, 1992; Swaters, 1999; Hoekstra et al., 2001; Noordermeer, 2006). Remarkably, in galaxies with bumps and wiggles, the rotation curves are fitted best by models with scaled H I disks (e.g. in UGC 2916, UGC 5253, UGC 6787 and UGC 11852; see Noordermeer, 2006). We therefore suspect that in many galaxies a connection between H I density distributions and streaming motions in the disks may exist – because both are the result of an interaction. This may be the reason for the apparent success of H I scaling in describing such rotation curves.

6.7 Summary

In this chapter we reported deep WSRT H I observations of the early-type galaxy NGC 1167. Our main conclusions are:

(i) NGC 1167 is a very massive early-type galaxy with a giant H I disk ($D_{\rm HI}$ = 160 kpc). The H I mass of $1.5 \times 10^{10}\ M_\odot$ contributes about 1% to the total mass, the H I surface density ($\leq 2\ M_\odot\ {\rm pc}^{-2}$) is too low for starformation to occur.

(ii) The H I disk shows regular rotation for $r < 65$ kpc with a flat rotation curve of ~340 km s^{-1} amplitude. At $r \approx 1.3 \times R_{25}$ the rotation curve shows a bump of ~50 km s^{-1} on the approaching and receding side which is due to large-scale streaming motions in the disk. We argue that both the streaming motions and density features are due to interactions and that this explains the success of H I scaling in fitting rotation curves.

(iii) NGC 1167 shows various signs of recent satellite accretion, interaction and merging activities as well as eight H I companions (with $r < 350$ kpc). No extended halo of cold gas clouds is detected with column densities above 6×10^{18} cm^{-2}. This suggests that the H I disk is currently primarily formed through the accretion of companion galaxies which bring in large amounts of H I to NGC 1167 and that the accretion of small cold gas clumps is not an important disk building mechanism in this massive galaxy.

Acknowledgements: We thank the referee Jacqueline van Gorkom for her helpful suggestions which improved the paper. CS was supported during this research by the EU Framework 6 Marie Curie Early Stage Training programme under contract number MEST-CT-2005-19669 ESTRELA. The WSRT is operated by the Netherlands Foundation for Research in Astronomy with support from the Netherlands Foundation for Scientific Research. This research has made use of the NASA/IPAC Extragalactic Database. The Digitized Sky Survey was produced at the Space Telescope Science Institute under US government grant NAG W-2166.

6.A Appendix: Channel maps

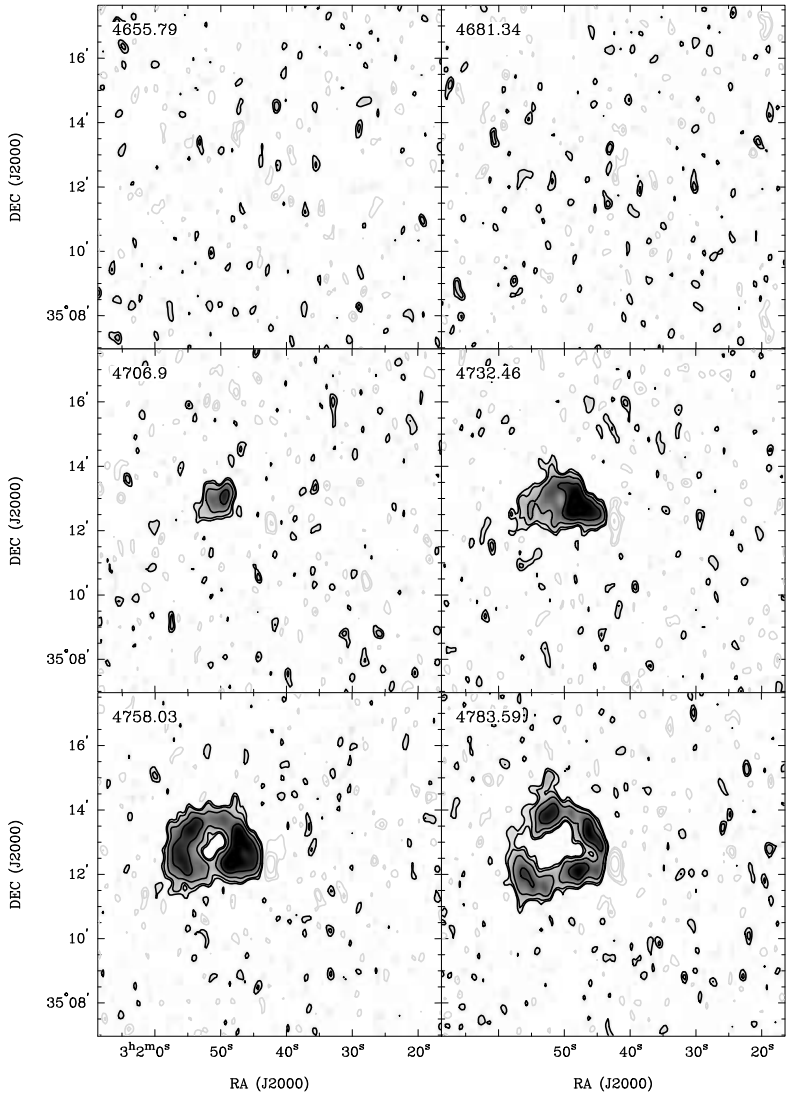

Figure 6.11: *Channel maps showing every third velocity channel of the data cube. Contour levels: -24, -12, -6, -3, -2 (grey), 2, 3, 6, 12 and 24σ (black).*

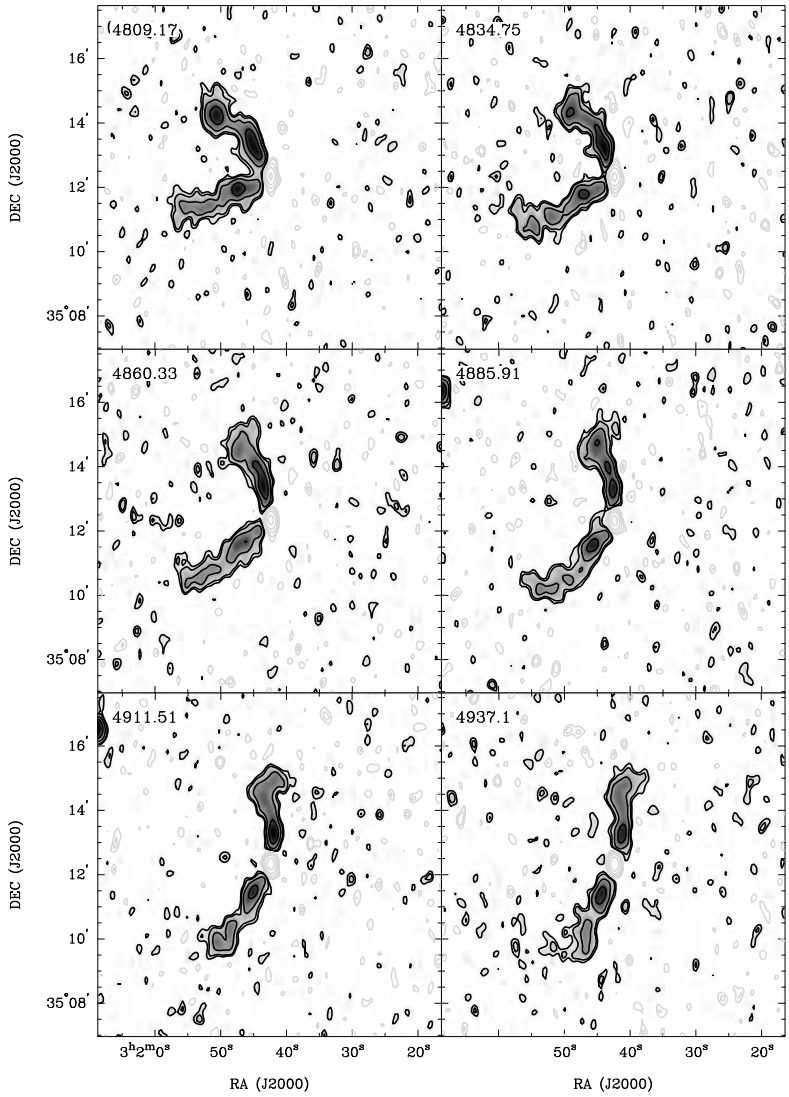
4809.17
4834.75
4860.33
4885.91
4911.51
4937.1
DEC (J2000)
RA (J2000)
16'
14'
12'
10'
35°08'
3h2m0s
50s
40s
30s
20s

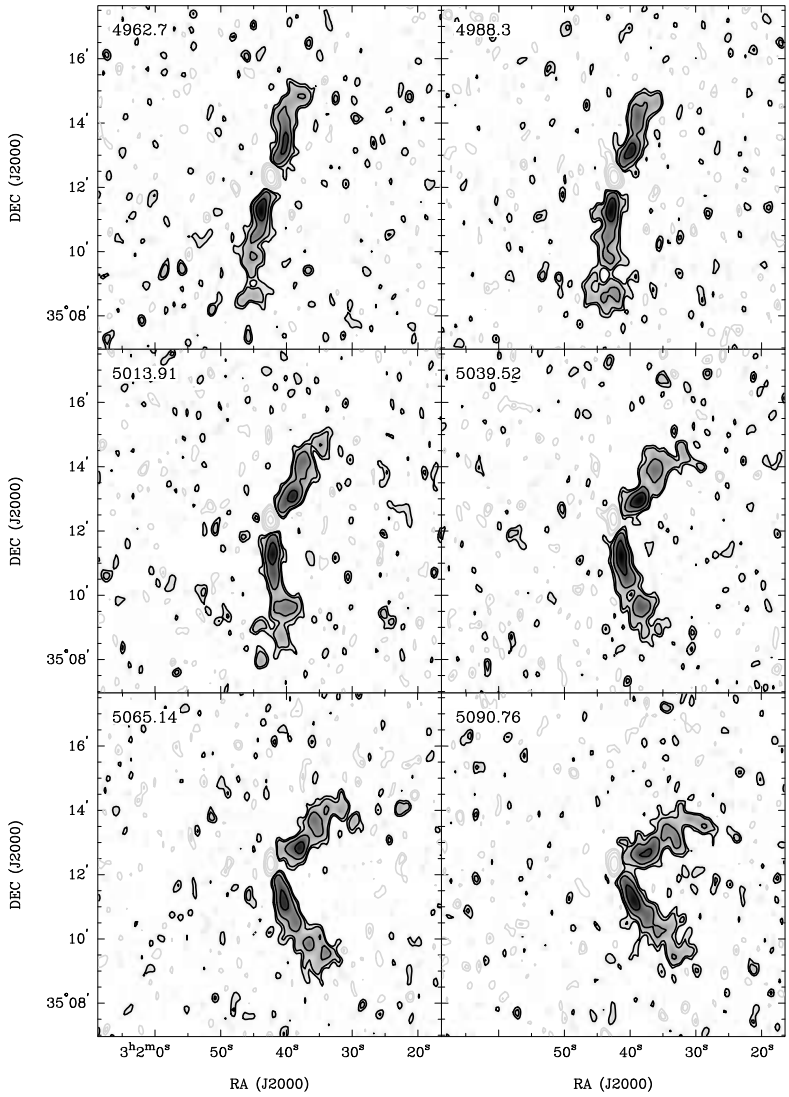
4962.7
4988.3
5013.91
5039.52
5065.14
5090.76
DEC (J2000)
RA (J2000)
16'
14'
12'
10'
35°08'
3h2m0s
50s
40s
30s
20s

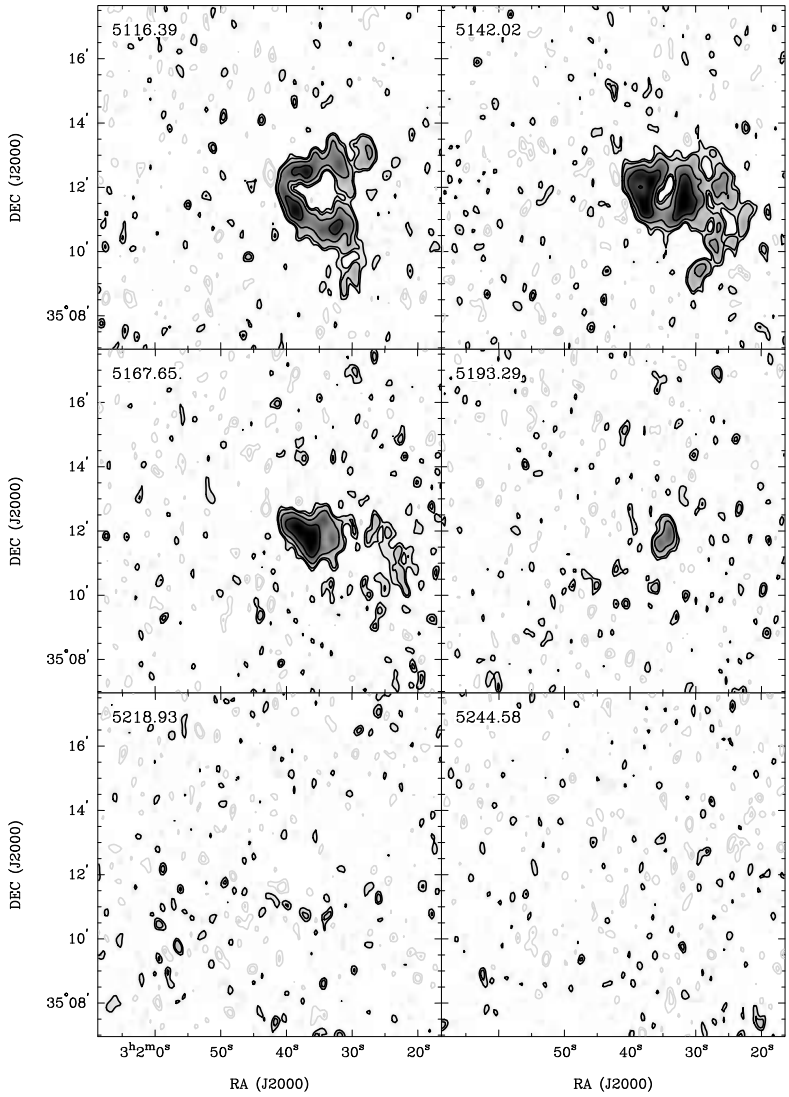
5116.39
5142.02
5167.65
5193.29
5218.93
5244.58
DEC (J2000)
16′
14′
12′
10′
35°08′
3h2m0s
50s
40s
30s
20s
RA (J2000)

7 The intriguing radio source B2 0258+35

— C. Struve, R. Morganti, B.H.C. Emonts & T.A. Oosterloo —

Abstract

We present H I observations of the radio galaxy NGC 1167 (B2 0258+35) performed with the VLA in A-array. Absorption is detected against the nucleus and the south-eastern jet but not against the north-western counter-jet. The spatially unresolved red- and blueshifted absorption (with respect to systemic) seen against the nucleus is most likely due to a circumnuclear disk (with $r_{\rm max} < 170$ pc), but an additional outflowing component must be present. The absorption against the jet is solely blueshifted. Further along the south-eastern jet direction, a tentative absorption structure is found at a location where no underlying continuum is detected at higher frequencies. New observations are necessary to confirm this absorption feature. A comparison with the flux detected at other wavelengths shows that a diffuse continuum component may be present.

The continuum image of NGC 1167, obtained from our WSRT 21-cm line observations presented in Chapter 6, reveals a 240-kpc radio relic in addition to the known, compact radio source B2 0258+35. This discovery is exciting since it shows that radio galaxies with large amounts of H I can also host extended radio sources, a result missing in previous studies. The existence of the relic shows that the presence of large amounts of H I does not necessarily confine or frustrate a young radio source – as previously suggested.

7.1 Introduction

An interesting result from the study of the complete sample of radio galaxies (Chapter 2), is that the extended radio sources do not contain large amounts of H I gas, in

In preparation for publication in A&A.

contrast to some of the compact sources (for details, see Emonts et al., 2007, 2010). In some cases, the sources may be confined or frustrated by the ISM in the central region of the galaxy, so that they cannot grow into extended sources. The presence of H I gas could significantly contribute to the confinement (see, e.g., Emonts et al., 2010).

This chapter investigates the radio source properties of the compact source B2 0258+35 (hosted by NGC 1167), for which confinement has been suggested (Giroletti et al., 2005). The large-scale H I properties of this radio galaxy have been presented in detail in Chapter 6. B2 0258+35 is a compact (D = 1.4 kpc), young ($< 10^6$ yr), relatively powerful (1.0×10^{24} W Hz^{-1} at 1.4 GHz) radio source that has been classified as having a Compact Steep Spectrum (CSS Sanghera et al., 1995). In contrast to most CSS sources (which usually have higher radio power), B2 0258+35 shows plume-like lobes without prominent hot-spots. Giroletti et al. (2005) speculate that this compact source will not grow into a large extended radio galaxy because the source structure appears to strongly interact with the ISM, as shown by the large bending of the arcsecond structure of the southern jet. Hence, B2 0258+35 may be one of the compact sources confined by the surrounding ISM. Alternatively, the AGN activity may have been temporary interrupted.

The outline of this chapter is as follows: Section 7.2 describes the discovery of a 240-kpc radio relic that shows that NGC 1167 has recently experienced a previous phase of radio activity. In Sect. 7.3 we present new VLA H I absorption observations that are aimed at resolving the H I gas in the nuclear region. This is followed by a discussion on the circumnuclear gas structure and the recurrent phases of AGN activity (Sect. 7.4). A short summary is given in Sect. 7.5.

7.2 A 240-kpc radio relic structure

The H I observations of NGC 1167, presented in detail in Chapter 6, allow to image (besides the large-scale H I structure) the radio continuum structure of the radio source B2 0258+35. To image the continuum, the line-free channels of the 20 MHz observing bandwidth (which were covered with 1024 channels) have been used. Although this setup is not ideal for continuum observations, it still allows the detection of emission at the few hundred μJy level. A careful self-calibration of the continuum in each WSRT data set revealed (besides the known, unresolved 1.85 Jy compact source) a faint extended (~240 kpc long and ~60 kpc wide) relic structure at the sub-mJy level.

Figure 7.1 shows the natural weighted (robust +2) continuum image. The beam size of the natural weighted image is 38.″0×25.″5 (PA = 2.0°) and the noise in a single data set is $\sigma_{\rm rms}$ = 240 μJy beam^{-1}. Some calibration artifacts are clearly present in the data on the few hundred μJy level. The extended continuum structure is at the edge of what can be detected in a single line observation, but is clearly present in all data sets. The dynamic range in the continuum image is better than 1:8000. Hints of the relic are also found in more uniform weighted cubes, but the extended structure is seen best in the (lower resolution) natural weighted image.

The orientation of the relic structure is approximately directed in the same direc-

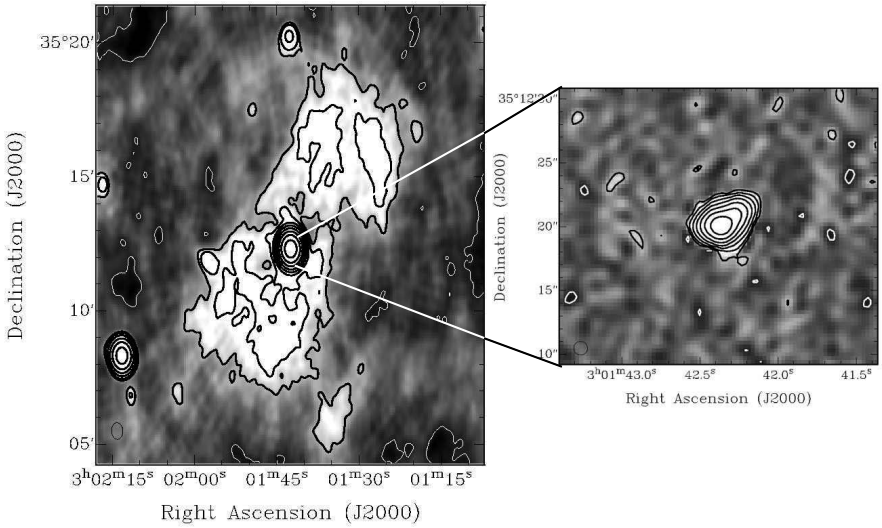

Figure 7.1: *Left panel: WSRT radio continuum image of NGC 1167 (B2 0258+35) showing the 240 kpc relic structure. Contour levels: –0.6 (white), 0.6 (= $2\sigma_{\rm rms}$), 1.2 mJy beam^{-1} (black) and increasing by a factor of 3. Right panel: VLA radio continuum image of the compact radio source. Contour levels: -0.6 (white), 0.6 mJy beam^{-1} (black) and increasing by a factor of 3. The peak flux is 1.04 Jy beam^{-1}. The beams of the WSRT and VLA observations are plotted in the bottom left corner of the images respectively.*

tion (PA = 132°±3°) as the inner, compact (D = 1.4 kpc) radio source (see Giroletti et al., 2005). The relic morphology is diffuse, intensity variations over the structure are small – less than a factor of ∼3.

7.3 The nuclear H I absorption

In Chapter 4 and 5 we showed that the red- and blueshifted absorption detected in the circumnuclear environment of Centaurus A and Cygnus A, are (likely) caused by circumnuclear H I absorbing disks. Sources in which both the nuclear absorption and the tens of kpc-scale H I emission can be studied in detail are rare (see Chapter 3). We have therefore performed higher-resolution observations of NGC 1167, with the aim of spatially resolving the red- and blueshifted nuclear absorption detected with the WSRT (Chapter 6).

7.3.1 VLA observations and data reduction

NGC 1167 has been observed with the VLA in A-array configuration in October 2008, see Tab. 7.1 for some basic properties of the observations. Two 6.25 MHz IFs overlapping in frequency have been used. At the moment of observation, the VLA was

Table 7.1: *Summary of observations.*

Total observing time	8.0 h
Total on-source integration time	6.5 h
Observation date	11 Oct. 2008
Bandwidth	6.25 MHz
No. of IFs (overlapping in frequency)	2
Number of channels in the cubes	64
Velocity resolution (no Hanning)	21.4 km s^{-1}
Bandpass/phase calibrator	0319+415
Flux calibrator	0542+498
Weighting scheme	uniform
Beam (HPBW)	1.″02 x 1.″02
rms noise (mJy beam^{-1}) in line cube	0.35
rms noise (mJy beam^{-1}) in continuum image	0.24

in the upgrading phase to the EVLA. As a consequence, 17 out of the 26 antennas used in the experiment had already been upgraded to EVLA antennas complicating, the calibration because of "aliasing". The hardware used to convert digital signals from the EVLA antennas into analog signals to be fed into the VLA correlator, caused power to be aliased in the bottom $\leq$ 2 MHz of the bandwidth, affecting all sources with continuum emission (including the calibrators). To minimize the effect of aliasing, phase and bandpass calibration were performed (after initial flagging of RFI) for each antenna by relying only on the VLA-EVLA and VLA-VLA baselines (i.e. discarding aliased EVLA-EVLA baselines). Because this is an antenna-based calibration strategy, all the baselines have still been calibrated. Nevertheless, some baselines (not used for calibration) still show strong aliasing in the bottom 2 MHz of the bandwidth. We have therefore excluded the first 20 channels of the band from the remaining data reduction. For the flux calibration, the uv-restriction in A-array, as specified on the VLA calibrator web site, has been used, in preference to a model.

The remaining data reduction has been performed using the MIRIAD package; self-calibration of the continuum emission has also been performed. The continuum model has been subtracted from the line data and the residual continuum emission has been removed, after making a second order fit to the line-free channels of each visibility record. The observing band was centred such that without the first 20 channels, enough line-free channels with velocities above and below the H I absorption can be used for the fit. The signal in the data has been cleaned (line cube and continuum image). The final line cube has 39 velocity channels, covering 810 km s^{-1} in velocity and a spatial resolution of 1″, corresponding to a linear scale of ~330 pc (see Tab. 7.1).

7.3.2 Results

Figure 7.1 (right panel) shows the compact radio source at 1.4 GHz. The continuum peak has brightness 1.04 Jy beam^{-1} and the total continuum flux recovered in the

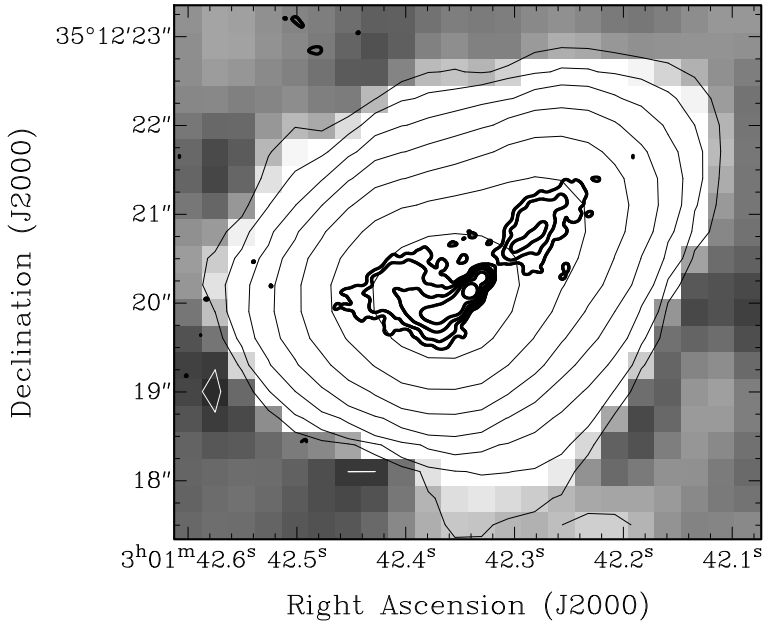

Figure 7.2: *Zoom-in of the right panel of Fig. 7.1 showing the continuum structure of the compact radio source over-plotted with the contours of the 22 GHz continuum map of Giroletti et al. (2005, thick contours). Contour levels of the 22 GHz map: 0.25 mJy beam^{-1} and increasing by a factor of 3.*

observation is 1.87 Jy, which is within ≈1% of the flux in the WSRT observations (Chapter 6). The radio source is resolved along the jet axis (PA = 132°), but also perpendicular to it. The radio-jet axis is *not* aligned with the minor axis of the large-scale H I emission disk ($PA_{\rm minor-axis}$ = 165°; see Chapter 6), as is often the case in other radio galaxies.

Figure 7.2 shows a zoom-in of the VLA continuum and includes an overlay of the (much higher resolution) 22 GHz continuum map (beam is 0.″12 × 0.″12; map kindly provided by Marcello Giroletti). The nucleus of B2 0258+35 is approximately 0.″18 north-east of the brightest peak in the 22 GHz map. This shift corresponds to ≤ 1 pixel in our VLA data (∼ 1/5 of the beam) and an overlay of both data sets shows that the nucleus is one pixel west of the peak in the 1.4 GHz map.

It is evident from Fig. 7.2 that the 1.4 GHz continuum map extends to larger radii from the nucleus in all directions, compared to what is detected in the 22 GHz observations. This is, at least to a large extent, an observational effect that is due to the much larger beam size. Whether a more diffuse component in addition to the structure seen at 22 GHz on the < 2 kpc scale exists around the compact source (i.e. on a scale much smaller than the 240 kpc relic size) is not clear. Figure 4 of Giroletti et al. (2005) shows that the spectral index changes with frequency, making it difficult to estimate whether any diffuse structure is resolved out in the 22 GHz map.

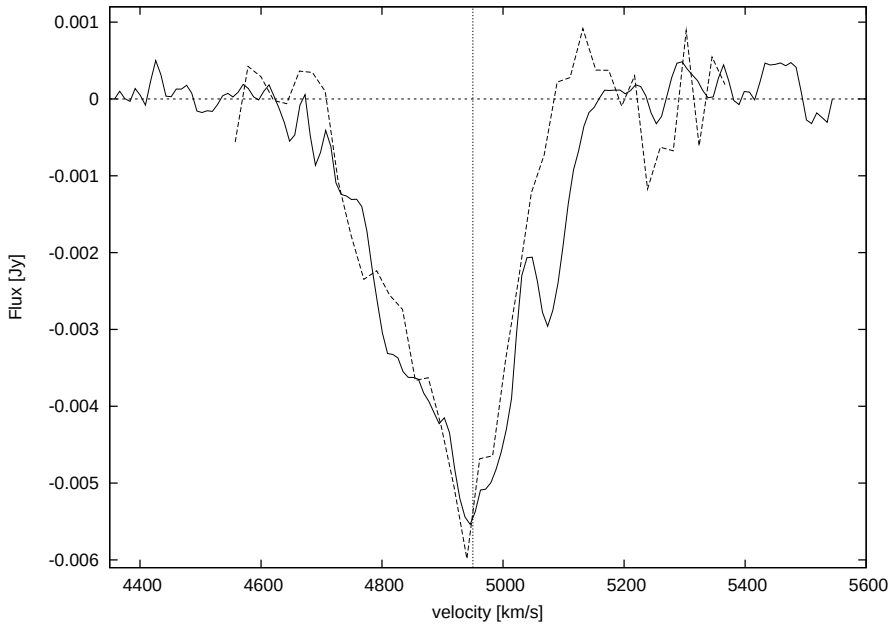

Figure 7.3: *Integrated absorption spectrum of the core region. The dashed line shows the VLA spectrum and the solid line the WSRT data. The systemic velocity is indicated by the vertical line.*

Sanghera et al. (1995) combined MERLIN and VLBI observations at 1.6 GHz. Their image resembles the 22 GHz map of Giroletti et al. (2005). Based on the flux in the 1.6 GHz observations (1.60 Jy), one would expect a flux of 1.70 Jy at 1.4 GHz, assuming a spectral index of 0.70. The exact spectral index is unknown, but it must certainly be shallower than the $\alpha_{8.4}^{22} = 0.88$ that Giroletti et al. (2005) found at higher frequencies (see their Fig. 4). Given that in our VLA observations we detect a total flux of 1.87 Jy, a diffuse (< 2 kpc) radio continuum component may be surrounding the 22 GHz structure with a flux of about 170 mJy (depending on the exact spectral index) – about 9% of the total flux. Observational evidence for (or against) the existence of such a diffuse component is desirable. Convolving the 22 GHz map to the resolution of the 1.4 GHz VLA data results in a continuum structure which is very similar to the observed structure at 1.4 GHz (Fig. 7.2). However, this does not necessarily imply that no diffuse component exists, as an additional component might be smoothly spread over the region where the continuum is detected. An alternative, to explain the difference between the measured and the expected flux at 1.4 GHz is that the source could be variable over the timescale of a few years. Whether this is indeed the case can only be investigated with additional observations at the previously observed frequencies. The WSRT observations of NGC 1167 (Chapter 6) cover a time span of approximately two years and do not indicate a significant change of the flux level.

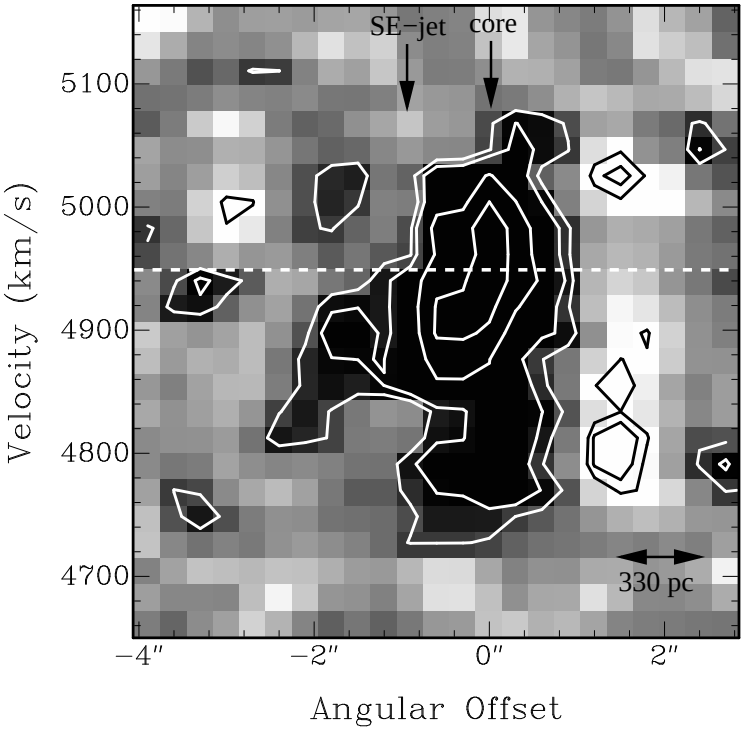

Figure 7.4: *Position-velocity slice along PA = 132°. The absorption shows two structures with one of them being spatially resolved. Contour levels: -9, -6, -3, -2 (white), 2 and 3$\sigma_{\rm rms}$ (black). The systemic velocity of the kpc-scale* H I *emission disk is indicated by the dashed line.*

An integrated H I absorption spectrum over our spectral-line cube is shown in Fig. 7.3, as well as the WSRT spectrum. While the redshifted absorption of the WSRT observations reaches velocities nicely consistent with the large-scale H I emission disk, the blueshifted absorption exceeds the emission velocities by about 34 km s^{-1} (see Fig. 6.5 in Chapter 6). In the VLA data we recover the entire blueshifted part and a large fraction of the redshifted absorption detected with the WSRT. However, the gas with the highest redshifted velocities (5078 km s^{-1} $< v <$ 5155 km s^{-1}) are not detected in the VLA data. For the remaining part of the spectrum, the match between both observations is excellent. This suggests that the mismatch for the highest velocities presents a real observational effect and is not due to, e.g., the higher noise or wavy baselines in the VLA data. It is unclear where the absorbing flux is located which is not recovered in the VLA observations. Since the continuum flux of the WSRT observations is recovered in the VLA data, we are confident that no faint continuum structure has been resolved out.

Inspection of the line cube shows that the absorption consists of two structures

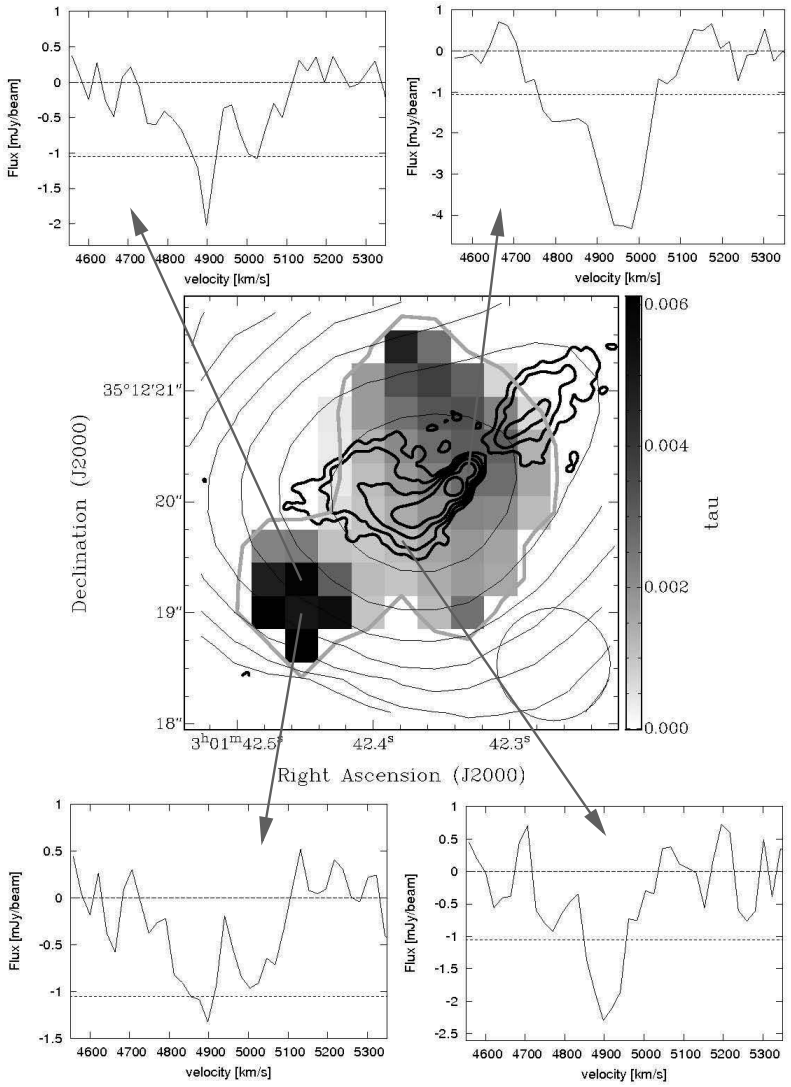

Figure 7.5: *Opacity map (greyscale; middle panel) showing the spatially resolved* H I *absorption. Over-plotted is the VLA continuum (thin black contours, 0.6 mJy beam*$^{-1}$ *and increasing by a factor of 3) and the 22 GHz continuum from Giroletti et al. (2005, Contour levels: 0.25 mJy beam*$^{-1}$ *and increasing by a factor of 3). The beam is indicated in the bottom right corner. The four surrounding plots show the absorption spectra at the locations indicated by the arrows. The dashed line indicates the* 3σ *noise level.*

(Fig. 7.4). Deep, unresolved absorption is detected against the nucleus over the full velocity range which is recovered in the VLA observations (see Fig. 7.3). The second component stretches from the core to the south-east, along the jet axis, though it is difficult to establish how far this absorption structure extends. The *pv* diagram (Fig. 7.4) suggests that the resolved absorption structure may stretch up to 2'' (= 660 pc) from the core – which is beyond the continuum structure imaged at higher frequencies. This is illustrated in Fig. 7.5 (middle panel), where an opacity map with radio continuum contours is over-plotted (from our 1.4 GHz and Giroletti et al.'s 22 GHz observations). If the outermost absorption structure in the south-east indeed exists, a diffuse continuum component must be present in this region for which *direct* evidence is yet missing. However, the flux comparison with the 1.6 GHz observations indicates that such a component may be present (see above). In Fig. 7.5 we show two H I absorption spectra from the outermost south-eastern location, as well as spectra from the core and the southern jet for comparison. As is evident from the spectra, the S/N is low in the south-eastern location, so that *more sensitive observations are required to confirm this part of the absorption structure as well as higher resolution observations to identify whether or not a diffuse continuum component is present*. Recent tests of other strong radio continuum sources revealed that data taken during the VLA upgrade can show weak absorption features that are not detected in new observations (which do not suffer from aliasing; B. Emonts, private communication). Re-observing NGC 1167 is therefore absolutely crucial to find out about the tentative absorption feature.

The integrated absorption spectrum does not help in disentangling whether the outermost absorption structure is real. In the spectrum shown in Fig. 7.3, the region has been included. Excluding it would present a very similar spectrum with somewhat lower absorbed fluxes between $4800 < v < 4900$ km s^{-1} , but this may be within the noise of the observations.

Absorption is detected only against the unresolved core and along the south-eastern jet direction, but not against the north-western (counter-) jet or at the eastern end of the southern jet. However, the underlying continuum in the south-eastern jet direction is at least a factor 3 to 4 stronger than in the other two locations (see Fig. 7.5). Given the sensitivity of the observations, H I structures in these locations (with the same opacity as the H I absorbing structure detected against the south-eastern jet) would therefore not be detectable. Thus, the possibility that with more sensitive observations H I absorption may be detected against the north-eastern jet and/or against the eastern end of the south-eastern jet cannot be excluded.

The resolved absorption structure (i.e. against the south-eastern jet and possibly beyond) has velocities that are solely blueshifted (with respect to the systemic velocity of the kpc-scale H I disk; see Fig. 7.4 and Chapter 6), even though they are not as blueshifted as the most blueshifted absorption, which has been detected against the core. Absorption with redshifted velocities is solely detected against the core. The opacity gradient in the core region is likely to be not real as the absorption is unresolved and hence, the exact location of the absorbing gas could originate in a region smaller than the beam.

7.4 Discussion

We start with discussing the structure of the gas in the core region (Sect. 7.4.1) and show that part of the absorbing gas is located in a disk, while another part of the absorption is most-likely caused by outflowing gas. Section 7.4.2 investigates the recurrent nuclear activity of B2 0258+35.

7.4.1 The circumnuclear gas structure

The south-eastern radio jet is much stronger than the north-eastern jet. Based on the jet brightness ratio, Giroletti et al. (2005) calculated a viewing angle of $40^\circ \leq \theta \leq 50^\circ$. However, Giroletti et al. (2005) cannot rule out the possibility that the jet/counter-jet ratio (and hence the viewing angle) is not meaningful, as the knot in the jet may have been produced in a peculiar event (e.g. the jet could have hit a dense gas/dust cloud). Assuming that the viewing angle *is* meaningful, the relative orientation of the jet with respect to the large-scale disk can be deduced. From the faint spiral arm structure detected in the optical (see Chapter 6), it is known that the southern side of the large-scale disk is the near and the northern part of the disk the far side. This implies that the angle between the disk ($i = 38^\circ$, Chapter 6) and the jet is relatively small, $\sim 16^\circ \pm 5^\circ$, and that the jet moves inside the disk for the inner few hundred parsec. At $r = 500$ pc (i.e. where the jet sharply bends), the jet is ≈ 140 pc above the plane of the disk. This is likely to be within one H I scaleheight of the H I disk.

There are not many constraints on the H I absorbing structure detected against the south-eastern jet. However, given the position angle of the jet (which is misaligned with the minor axis) and considering the fact that the jet may move inside the H I disk, the blueshifted velocities of the absorption are consistent with gas being located in the disk. Note, however, that we cannot exclude other explanations for the absorption detected against the jet. Since the counter-jet is weak, it is no surprise that absorption is only detected against the jet.

Further along the south-eastern jet direction, the tentative absorption feature is located (Sect. 7.3.2). We stress once again that this outermost absorbing H I structure needs to be confirmed with more sensitive observations. Assuming that this absorption structure is real, a rough estimate of the column density can be derived. The continuum flux comparison shows that ~170 mJy of diffuse flux may be spread around the source, compared to what is detected at higher frequencies (Sect. 7.3.2). Under the assumption that at the location of this outermost absorption structure the continuum is 10 mJy, we get a peak opacity of $\tau = 0.16 \pm 0.05$, which translates into a column density of $N_{\rm HI} \approx 1 \times 10^{19} T_{\rm spin}$ cm^{-2}. For $T_{\rm spin} = 100$ K the H I gas column density is therefore $N_{\rm HI} \approx 1 \times 10^{21} T_{\rm spin}$ cm^{-2}, but $N_{\rm HI}$ could be larger as close to an AGN the spin temperature is likely to be increased (see Chapter 4 and 5 and Bahcall & Ekers, 1969). Column densities of H I clouds in the range of 10^{21} cm^{-2} to a few $\times 10^{22}$ cm^{-2}, are large, but not impossible.

The situation for this outermost absorption is somewhat similar to the absorption detected against the south-eastern jet. We cannot really constrain the location/kinematics of the absorbing H I, but the velocities are consistent with gas being located in the disk (see also Fig. 7.4). Giroletti et al. (2005) have suggested that the

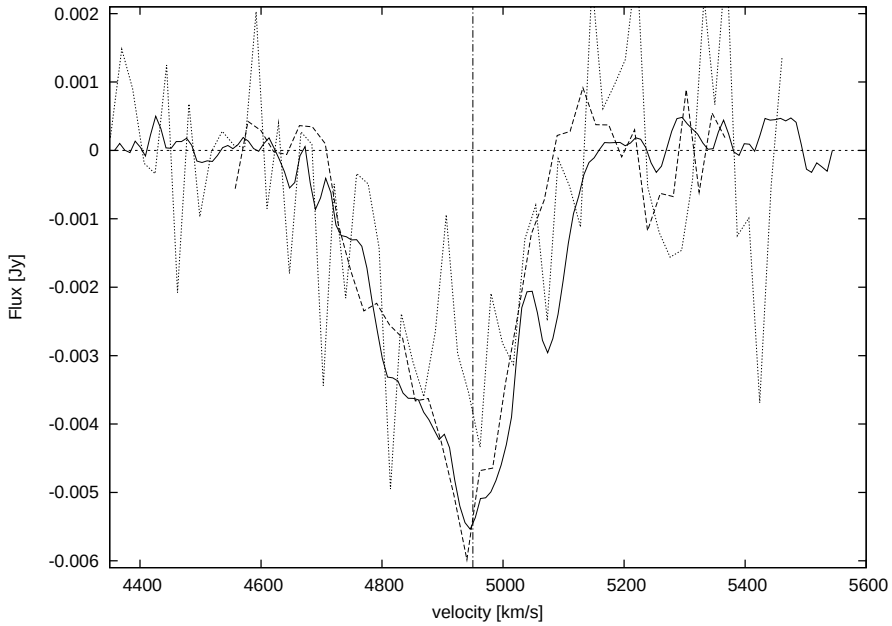

Figure 7.6: *Same integrated absorption spectrum of the core region as shown in Fig. 7.3 but with the CO emission spectrum of Prandoni et al. (2007) overlaid (dotted line, multiplied with -1 to allow for an easy comparison with the* H I *absorption).*

compact source is confined or frustrated by the surrounding medium. While there appear to be no strong constraints on the resolved absorption structures, it is conceivable that the jet interacts with the ISM (which the H I is part of). Simulations by e.g. (Bicknell & Sutherland, 2006) suggest that jets can heavily interact with the surrounding ISM, such that the jet gets slowed down by the ISM. Whether this is indeed the case for B2 0258+35 cannot be concluded from the available observations, but higher resolution observations of e.g. molecular gas (detected in emission) may help to shed more light on this issue.

For the unresolved absorption component detected against the core we have better constraints on the gas structure. The absorption is red- and blueshifted, similar – to first order – to the nuclear absorption in Cen A (Chapter 4). However, there is an important difference: the blueshifted absorption exceeds the velocities of the large-scale rotating disk by about 34 km s^{-1} , whereas the highest redshifted velocities (detected in the WSRT observations) match the velocities of the large-scale disk emission (see Fig. 6.5 in Chapter 6).

What causes the asymmetry in the red- and blueshifted circumnuclear absorption? Is it possible that part of the redshifted H I is located behind the radio source and hence can not be detected in absorption? Figure 7.6 shows a comparison of the integrated H I absorption spectrum with the CO observations from Prandoni et al.

(2007). The CO is detected in emission (but has been multiplied with −1 in Fig. 7.6 to allow for an easy comparison with the H I) and therefore does not depend on any underlying continuum structure. The CO spectrum is more noisy but covers the same velocity width as the H I, including the most blueshifted part. The match between the H I and the CO suggests that this study does not miss any H I at redshifted velocities which would result in an H I integrated spectrum that is symmetric with respect to systemic. That is, the asymmetry of the absorption profile is not due to insufficient underlying continuum (as is the case in several other radio sources including Centaurus A and Cygnus A, Chapter 4 and 5), but is rather an intrinsic feature.

The most natural explanation for the observed nuclear absorption spectrum is therefore that a circumnuclear disk with $r_{\rm max} < 170$ pc plus an outflow exists. A circumnuclear disk explains the redshifted absorption and a large fraction of the blueshifted wing. However, it cannot explain the most blueshifted velocities observed against the core, which therefore suggests that an additional outflow component must be present. In other sources with a detected outflow, the location of the outflow is off-nucleus. In 3C 305 and IC 5063, for instance, the H I outflows are located 1.6 kpc and 0.5 kpc from the core (Morganti et al., 2005a, 2007). Whether the outflow in NGC 1167 also occurs off-nucleus can only be investigated with higher resolution (VLBI) observations. A candidate location may be the bright continuum knot 0.″18 along the jet from the core (see Fig. 7.5 and Giroletti et al., 2005).

7.4.2 Recurrent phases of radio activity

It has been known for a long time that radio activity can be recurrent (for a recent review, see for instance Saikia & Jamrozy, 2009). Nevertheless, the discovery of the 240 kpc-size relic structure is exciting. The existence of the relic structure shows that early-type galaxies with large amounts of H I gas can host extended radio sources; a result not found in the study of the complete sample of radio galaxies (see Chapter 2 and Emonts et al., 2010).

While the age of the B2 0258+35 relic is difficult to estimate from our observations, numerous studies suggest that the maximum lifetime of relics is generally of the order of $\leq 10^8$ yr (see, e.g., Slee et al., 2001; Lara et al., 2004; Parma et al., 2007; Dwarakanath & Kale, 2009; Orrù et al., 2010). This means that the relic is much younger than the H I disk, which must be at least a few Gyr old (Chapter 6). Hence, the H I disk has already been in place during the previous phase of activity. Several signs of recent interactions with the environment have been observed in NGC 1167 (Chapter 6); thus, interactions may still have stimulated the previous (and/or current) phase of activity. However, other mechanisms cannot be generally excluded.

Independent of the mechanism that causes the current phase of nuclear activity, it is clear that something must have changed between the previous and the current phase of activity, as the compact source seems to evolve differently from the relic structure. One possibility is that the compact source is indeed confined or frustrated, as suggested by the sharp bending of the jet (see Giroletti et al., 2005). In this case, the ISM properties in the central ~1 kpc must have changed significantly over the last 10^8 yr. An alternative hypothesis proposes that the jet orientation (with respect to the disk) has changed such that in the previous phase the jet did not have to fight

his way through the disk/ISM. Moreover, there is no information available on the power of the previous AGN phase. Perhaps the jet was stronger and could therefore more easily expand into a 240 kpc size structure.

The presence of the relic certainly shows that a radio source is not necessarily confined by the presence of a large cold gas reservoir. This has previously been suggested to account for the fact that large amounts of H I have only been found around compact low-power radio sources (see Emonts et al., 2007, 2010). If cold gas can hinder or even confine a source to grow into a large FR-I type structure, it rather depends critically on the specific jet/ISM properties in the vicinity of the black hole.

7.5 Summary

We have presented VLA H I absorption observations of the central region of the radio galaxy NGC 1167 (B2 0258+35). Two components have been detected. Unresolved red- and blueshifted absorption (with respect to systemic) has been detected against the nucleus; blueshifted absorption is seen against the south-eastern jet 300 pc from the core, possibly extending further out to 660 pc from the nucleus. This outermost absorption component, together with the presence of a diffuse continuum component at this location, needs to be confirmed with deeper observations as aliasing may have erroneously introduced this absorption feature. We do not have many constraints on the structure of the resolved absorption components. However, these are consistent with the assumption of gas being located in the disk.

The unresolved absorption detected against the core is most-likely caused by a circumnuclear disk with $r_{\rm max} < 170$ pc. However, the blueshifted wing of the nuclear absorption exceeds the redshifted velocities, which suggests – together with CO observations – that an additional outflowing velocity component must be present close to the black hole.

Our WSRT 21-cm line observations of NGC 1167 (presented in Chapter 6) reveal a faint 240-kpc size radio relic structure, showing that the radio source B2 0258+35 has experienced a previous phase of activity. The relic structure is at the edge of what can be detected in a single 12-h line observation. It is therefore possible that future surveys will more often find such relic sources. This discovery of the relic in NGC 1167 is exciting, since it proves that H I-rich galaxies can also host radio sources that grow into extended sources; a result that has thus far been missing in previous studies. The presence of large amounts of cold gas therefore does not necessarily mean that the radio source is confined.

Acknowledgements: We wish to thank Marcello Giroletti for kindly providing us with the fits file of his 22 GHz map and Isabella Prandoni for her CO spectrum. The VLA is operated by the National Radio Astronomy Observatory which is a facility of the National Science Foundation operated under cooperative agreement by Associated Universities, Inc. This research was supported by the EU Framework 6 Marie Curie Early Stage Training programme under contract number MEST-CT-2005-19669 "ESTRELA".

8 Summary and future perspectives

In this thesis we studied the neutral hydrogen properties of radio galaxies (mainly with power $< 10^{25}$ W Hz^{-1}) on various scales: from the 300 kpc environment to tens of kpc disk structures to the ~100 pc circumnuclear scale, with the overall aim of understanding the role cold gas plays in the evolution of radio sources and their host galaxies. This final chapter summarizes the main results (Sect. 8.1). The main conclusions of this thesis, as well as still unanswered questions are discussed in Sect. 8.2. Section 8.3 presents a brief outlook.

8.1 H I properties of radio galaxies – results of this thesis

Following is a brief summary of the results, ordered according to topic.

8.1.1 300 kpc scale: environment

Statistical study (Chapter 2):

- We do not find a statistically significant difference in the environment of radio-loud galaxies compared to radio-quiet galaxies. Thus, gas-rich interactions are likely not the main mechanism, which causes radio activity. However, this does not mean that interactions cannot stimulate nuclear activity.
- At a high significance level, no difference is found in the average number of H I companions within the radio-loud and radio-quiet sample for $r < 150$ kpc. For radii $150 < r < 300$ kpc, only a small increase in the number of companions around the radio-loud targets could be detected, though this difference is not statistically significant.
- The average amount of H I located in the environment of the targets in both samples is comparable. No difference is found for the typical H I mass of the companions (few $\times 10^8$ $M_\odot$).
- Several companions in both samples show signs of disturbance. Hence, such signs are neither a distinguishing characteristic for the environment of radio-loud from radio-quiet galaxies.

8.1.2 Tens of kpc scale: disk structures

Statistical study (Chapter 2):

- In the sample of radio galaxies, we detect H I in emission associated with the host galaxy in 29% of the sources (detection limit $\sim 10^8\ M_\odot$). No evidence is found for ongoing gas-rich galaxy mergers or violent interactions – in agreement with the results of our environment study.
- The H I properties (e.g. detection rate) of radio-loud and radio-quiet galaxies are comparable, taking into account the different detection limits.

Centaurus A (Chapter 3):

- $4.9 \times 10^8\ M_\odot$ of H I is detected in emission in Cen A. The kinematics of the H I is dominated by rotation down to the nuclear regions. Our tilted-ring model describes the warped disk morphology and kinematics. No evidence for non-circular motions is found for $r < 6$ kpc.
- Our model parameters also describe the dust morphology, as seen by Spitzer (Quillen et al., 2006) and are consistent with the values found in the study on the central stellar ring (Kainulainen et al., 2009).
- At $r > 6$ kpc, asymmetries and arm structures are observed, including radial motions. We conclude that the accretion of a small gas-rich companion has taken place about $1.6 - 3.2 \times 10^8$ yr ago, in agreement with previous estimates.
- The merging event is too old to directly trigger the current phase of activity, but may have interrupted the previous AGN cycle. This finding is in line with the results from the environment study, which show that interactions are not likely to be the main mechanism causing nuclear activity.
- A large fraction of the newly discovered broad ($\Delta v = 400\ \mathrm{km\,s^{-1}}$) nuclear absorption component is not part of the large-scale disk, but instead must be located close to the black hole.

8.1.3 100 pc scale: circumnuclear structures

Centaurus A (Chapter 4):

- For the first time, blueshifted absorption (with respect to the systemic velocity) has been detected against the radio core of Centaurus A; the redshifted absorption is broader than previously reported.
- Various arguments, in particular a comparison to the molecular gas, suggest that the absorbing H I is located in a circumnuclear disk with $r < 120$ pc.
- No direct evidence of gas infall into the AGN has been found.

Cygnus A (Chapter 5):

- Broad ($FWHM = 231 \pm 21$ km s^{-1}) velocity width absorption components have been detected against the VLBI counter-jet and the core of Cygnus A. No absorption has been detected on the jet side.
- The absorption can be explained by a circumnuclear absorbing H I disk, with a radius of 80 pc which is orientated roughly perpendicular to the jet direction. The minimum gas density is $n > 10^4$ cm^{-3} and the total gas column density must be in the range of 10^{23} cm$^{-2} < N < 10^{24}$ cm^{-2}.
- The circumnuclear torus ($r \approx 3$ pc) in Cygnus A contains too little mass to power the AGN over $> 10^7$ yr, while the material in the outer H I absorbing gas disk can provide a reservoir to fuel the AGN and replenish torus clouds.

NGC 1167 (Chapter 7):

- Red- and blueshifted absorption (with respect to the systemic velocity) is detected against the core. We argue that a large fraction of the absorption is most likely due to a circumnuclear disk with $r < 170$ pc. However, an additional outflowing component must be present.
- Absorption is detected against the jet and possibly beyond to where no jet structure has been observed at higher frequencies. A diffuse continuum component, however, may possibly be present. We do not have many constraints on these two absorption structures, but they are consistent with gas being located in the disk. The counter-jet is too weak to detect absorption.
- We found a 240 kpc relic structure (in addition to the known compact source), showing that the radio source B2 0258+35 has experienced a previous phase of activity. This discovery is exciting as it shows that radio galaxies with large amounts of H I can also host extended sources; a result that has been missing thus far in previous studies.

8.1.4 The origin of cold gas in massive early-type galaxies

NGC 1167 (Chapter 6):

- We detect 1.5×10^{10} $M_\odot$ of H I in emission in NGC 1167, distributed in a 160 kpc disk.
- The disk shows regular rotation for $r < 65$ kpc with a prominent bump in velocity at $r \approx 1.3 \times R_{25}$, which is due to large-scale streaming motions in the disk.
- Various signs of recent satellite accretion, interaction and merging activities, as well as the presence of eight companions detected in H I, suggest that the disk is primarily formed through the accretion of fairly massive companion galaxies. The accretion of many small gas clumps is not an important disk building mechanism.

- We suspect that a connection between large-scale streaming motions and H I density distribution in this and other galaxies exists.

8.2 Main conclusions and open questions

In Sect. 8.1 we have summarized many single results that are important for understanding origin and evolution of radio sources and their hosts. The results are briefly put in a broader context by revisiting four main topics addressed in the introduction (Chapter 1) and we point out a few questions that remain.

Which are the dominant mechanisms that cause nuclear activity and what distinguishes a radio-loud from a radio-quiet galaxy?

Various mechanisms have been proposed that can cause radio activity in early-type galaxies. This includes galaxy mergers and interactions, satellite accretions, the accretion of cold gas from the IGM, or the accretion of circum-galactic hot gas (for a summary, see Chapter 1). Undoubtedly, different mechanisms do occur. In this thesis we have investigated the H I environment of radio galaxies (Chapter 2) and found no statistically significant difference in the environment ($r < 300$ kpc), compared to radio-quiet galaxies. This suggests that gas-rich interactions are not the main mechanism causing a radio-loud phase in low-power radio galaxies. Certainly, not every interaction causes a radio-loud phase, as many interactions are also observed in radio-quiet galaxies. However, this does not imply that gas-rich interactions cannot stimulate nuclear activity in single cases. Moreover, a merging event/interaction may even interrupt a phase of nuclear activity – as we have pointed out for Centaurus A (Chapter 3). Thus, the relationship "interaction – AGN activity" is certainly not one-to-one. To first order, the H I properties of the radio-loud and radio-quiet host galaxies are similar (see Chapter 2 and Emonts et al., 2010) in such a way that – from the point of view of the neutral hydrogen – no intrinsic difference is found, suggesting that many (or even all) early-type galaxies may experience a radio-loud phase during a Hubble time.

Which are the timescales involved in the triggering of radio sources and can the ISM properties change significantly between recurrent phases of AGN activity?

The current episode of nuclear activity in Cen A started late after the merger (between 1.5 and 3.2×10^8 yr, which is in line with several other studies that observe similar time delays (see Chapter 3). This suggests that after a merger or interaction, the gas needs time to settle in a stable cold accretion flow. Alternatively, if the black hole is fuelled by circum-galactic hot gas, the time delay may be related to the time required by the X-ray halo to build up again after the interaction.

Many radio galaxies experience recurrent phases of radio activity, including Cen A (Chapter 3). Even though an AGN cycle is only a short episode (typically $\leq 10^8$ yr; Parma et al., 2002) in the evolution of an early-type galaxy, the ISM properties in the central regions may change significantly between two cycles. In the current AGN

phase, for instance, the radio source of NGC 1167 seems to interact with the ISM and may struggle to grow into a large, FR-I type, radio structure, while at the same time a 240 kpc relic structure is detected, indicating that the ISM did not hinder the growth of the radio source during the previous episode (Chapter 7). However, the orientation of the jet (with respect to the disk and/or the jet power) may have been different in the previous phase, so that they may also have an effect on the evolution of the radio source.

Is cold gas fuelling the AGN?

Originally, only redshifted H I absorption was detected in radio galaxies (e.g. van Gorkom et al., 1989). This was interpreted as evidence for cold gas fuelling the AGN. More recent observations show that blueshifted absorption occurs at least as often as redshifted absorption (e.g. Vermeulen et al., 2003; Morganti et al., 2005b). In several radio sources, red- and blueshifted absorption has been detected, including Centaurus A, Cygnus A and NGC 1167 (Chapter 4, 5 and 7). Our analysis shows that in Cen A and Cygnus A (and likely in NGC 1167 as well), H I absorbing circumnuclear disks on scales below ~100 pc do exist. Direct evidence that cold gas fuels the AGN in any of the three sources has not been found. However, at least in the case of Cygnus A, we could show that the circumnuclear H I disk can provide the gas reservoir necessary to fuel the AGN and replenish torus clouds. Thus, cold gas could still be the material that is needed to trigger radio activity.

How do massive early-type galaxies build up their giant H I *disks?*

Early-type galaxies continue to form their structures over cosmic times down to the present day, with some of them having giant, regular rotating H I disks. At least in the case of NGC 1167 it seems that the main disk building mechanism is the accretion of a few fairly massive companion galaxies, rather than the accretion of a large number of small clumps of material (Chapter 6).

Open questions

Besides the contribution of this thesis to the understanding of the role cold gas plays in the evolution of radio galaxies, several questions remain, requiring further investigation:

- *Are different triggering mechanisms related to different types of radio sources?* Radio sources appear in a great variety of forms, for instance Seyfert I, Seyfert II, LINER, BL-Lac, FR-I, FR-II, compact low luminosity sources, quasars etc. While part of the radio source "zoo" is attributed to orientation differences (Antonucci, 1993; Urry & Padovani, 1995), it is clear that intrinsic differences between different classes of AGN exist. Are these different classes due to differences in the triggering mechanism? There is growing evidence that at least some FR-I type of galaxies accrete gas in a hot mode, while the more powerful FR-II sources

seem to be (most often) the result of gas-rich mergers (see Chapter 1). But are there exceptions in the sense that FR-Is can be triggered by cold gas due to an interaction, i.e. do interactions play a role at all in triggering low-power radio galaxies? Are all FR-IIs triggered by gas-rich interactions? Large statistical samples are needed to investigate intrinsic differences between the different types of radio galaxies.

- *What is the exact fuelling mechanism of black holes?*
  We still lack direct evidence for gas infall onto the black hole. How does the (cold) gas get channeled to the nucleus? Are the detected circumnuclear H I absorbing disks the gas reservoirs that replenish the torus, which ultimately fuels the black hole? Depending on the physical conditions, the gas may also be molecular close to the AGN (see, e.g., Maloney et al., 1996). Thus, to understand the exact accretion mechanisms, observations of CO and other molecular tracers may be necessary.

- *What determines the life cycle of an AGN?*
  When and why does a black hole become active? If mergers and interactions play a role, at what stage does the triggering start and what determines the length of the nuclear phase? Why is there a time delay between the starburst and the onset of nuclear activity? If black holes accrete in a hot mode, what are the conditions that cause a burst of activity and do mergers and accretion events influence this process? Studying the AGN outburst history will be an effective way to better understand the duty cycle of active galactic nuclei.

- *Feedback: what is the impact of an AGN on its surrounding gas/host galaxy?*
  For a long time AGN were treated as exotic objects in the universe, without an impact on the evolution of their host galaxies. However, cosmological simulations show that mechanical feedback from AGN strongly regulates the growth of galaxies (Croton et al., 2006). In that respect, it is important to understand the impact of the AGN on its surrounding gas. For instance, how do the outflows that are detected in some radio galaxies (including NGC 1167), affect the growths of the galaxy? Several studies (see, e.g., Holt et al., 2008) have already investigated this issue, but it seems that the detected outflows do not contain as much mass as predicted by the simulations. Further studies are needed to better understand the interplay between AGN and host galaxy.

8.3 Outlook

Given that radio sources may be dominant players in the formation and evolution of galaxies, and hence are important in the evolution of the universe as a whole, it is absolutely crucial to understand in detail the mechanisms at work.

A number of next-generation instruments are being built at the moment and more facilities are expected to come on-line later this decade. This will greatly enhance the possibilities to study AGN and their hosts in detail, not only in the nearby universe, but also at cosmological redshifts. Below, we give a brief overview of the planned telescopes and their potential use for studying radio galaxies.

LOFAR
The LOw Frequency ARray (LOFAR) was opened in June 2010 and operates at frequencies between 10 and 250 MHz. The antennas are organized in aperture array stations that are distributed over an area of about 100 km in diameter in the northwestern part of the Netherlands. Several international stations are added, providing baselines of up to 1500 km. LOFAR allows to investigate radio sources in detail, for instance it can be used to study the AGN duty cycle of a radio galaxy. Since radio relics usually have a steep spectrum, they are often not detected at higher radio frequencies.

ALMA
The Atacama Large Millimeter Array (ALMA) will, once completed in 2013, consist of 66 movable antennas with baselines up to 12 km, operating at frequencies between 84 and 950 GHz. ALMA will allow to observe dust and cold gas out to the redshifts, when the first stars and galaxies formed. The superb sub-arcsecond resolution offers the possibility of studying the circumnuclear morphology and kinematics of nearby AGN at the parsec scale, allowing to investigate the fuelling mechanism and the chemistry of the surrounding gas.

WSRT-Apertif and ASKAP
Twelve Westerbork Synthesis Radio Telescope (WSRT) antennas will be equipped with a focal plane array system called APERTIF (APERture Tile In Focus), which increases the current FOV by a factor of 25. A second focal plane array is being built in Australia, called ASKAP (Australian SKA Pathfinder), which will consists of 36 12-m antennas. Both telescopes will allow, once operational in 2012/2013, L-band surveys of the entire sky at relatively high angular resolution (tens of arcseconds). Mapping the entire sky in neutral hydrogen out to a redshift of $z \approx 0.25$ offers the possibility to study in H I well-selected, large statistical samples and sub-samples of different AGN hosts and their environments.

EVLA and MeerKAT
The upgraded Very Large Array (EVLA) and the South African Karoo Array Telescope (MeerKAT, commissioning expected in 2013) are optimized for deep and high fidelity imaging at frequencies in the range of 1 to 50 GHz. Both telescopes will allow studies of single objects, for instance radio galaxies, in great detail with very good sensitivity.

SKA
The Square Kilometre Array (SKA) will be the ultimate next-generation radio telescope, with a collecting area of 1 km^2; it is expected to be operational by the end of this decade. 50% of the antennas will be placed in the 5 km core (in diameter), with the longest baselines exceeding 3000 km. The expected frequency coverage ranges from 100 MHz up to 25 GHz. The SKA will offer an unprecedented view (both in spatial resolution and sensitivity) of nearby and more distant galaxies, most likely revolutionising our understanding of the universe. Circumnuclear H I structures in

nearby (radio) galaxies will be detectable in emission and absorption at resolutions better than 0.″1. H I on the kpc-scale will be detectable to a redshift of 1.5, making it possible to investigate the cosmic evolution of AGN and their host galaxies over the past ~9 billion years.

Bibliography

Abraham, Z., Barres de Almeida, U., Dominici, T. P., & Caproni, A. 2007, MNRAS, 375, 171

Akylas, A. & Georgantopoulos, I. 2009, A&A, 500, 999

Allen, S. W., Dunn, R. J. H., Fabian, A. C., Taylor, G. B., & Reynolds, C. S. 2006, MNRAS, 372, 21

Alvarez, H., Aparici, J., May, J., & Reich, P. 2000, A&A, 355, 863

Antonucci, R. 1993, ARAA, 31, 473

Baade, W. & Minkowski, R. 1954, ApJ, 119, 215

Baganoff, F. K., Maeda, Y., Morris, M., et al. 2003, ApJ, 591, 891

Bahcall, J. N. & Ekers, R. D. 1969, ApJ, 157, 1055

Balmaverde, B., Baldi, R. D., & Capetti, A. 2008, A&A, 486, 119

Barnes, D. G., Staveley-Smith, L., de Blok, W. J. G., et al. 2001, MNRAS, 322, 486

Barnes, J. E. 2002, MNRAS, 333, 481

Barvainis, R. & Antonucci, R. 1994, AJ, 107, 1291

Baum, S. A., Heckman, T. M., & van Breugel, W. 1992, ApJ, 389, 208

Begeman, K. 1987, Ph.D. Thesis, Univ. Groningen

Bell, E. F., Naab, T., McIntosh, D. H., et al. 2006, ApJ, 640, 241

Bellamy, M. J. & Tadhunter, C. N. 2004, MNRAS, 353, 105

Bennert, N., Canalizo, G., Jungwiert, B., et al. 2008, ApJ, 677, 846

Best, P. N., Kaiser, C. R., Heckman, T. M., & Kauffmann, G. 2006, MNRAS, 368, L67

Best, P. N., Kauffmann, G., Heckman, T. M., et al. 2005, MNRAS, 362, 25

Bicknell, G. V. & Sutherland, R. S. 2006, Astronomische Nachrichten, 327, 235

Bigiel, F., Leroy, A., Walter, F., et al. 2008, AJ, 136, 2846

Binney, J. 1977, ApJ, 215, 483

Bland, J., Taylor, K., & Atherton, P. D. 1987, MNRAS, 228, 595

Bolton, J. G. 1948, Nature, 162, 141

Bolton, J. G. & Stanley, G. J. 1948a, Australian Journal of Scientific Research A Physical Sciences, 1, 58

Bolton, J. G. & Stanley, G. J. 1948b, Nature, 161, 312

Boomsma, R., Oosterloo, T. A., Fraternali, F., van der Hulst, J. M., & Sancisi, R. 2008, A&A, 490, 555

Bournaud, F., Jog, C. J., & Combes, F. 2005, A&A, 437, 69

Bridle, A. H., Davis, M. M., Fomalont, E. B., Willis, A. G., & Strom, R. G. 1979, ApJL, 228, L9

Briggs, F. H. 1990, ApJ, 352, 15

Briggs, D., S. 1995, PhD thesis, New Mexico Institute of Mining and Technology

Brighenti, F. & Mathews, W. G. 2000, ApJ, 535, 650
Broeils, A. H. 1992, A&A, 256, 19
Broeils, A. H. & van Woerden, H. 1994, A&AS, 107, 129
Brooks, A. M., Governato, F., Quinn, T., Brook, C. B., & Wadsley, J. 2009, ApJ, 694, 396
Burbidge, G. & Crowne, A. H. 1979, ApJS, 40, 583
Burns, J. O., Feigelson, E. D., & Schreier, E. J. 1983, ApJ, 273, 128
Canalizo, G., Bennert, N., Jungwiert, B., et al. 2007, ApJ, 669, 801
Canalizo, G., Max, C., Whysong, D., Antonucci, R., & Dahm, S. E. 2003, ApJ, 597, 823
Canalizo, G. & Stockton, A. 2001, ApJ, 555, 719
Cappellari, M., Neumayer, N., Reunanen, J., et al. 2009, MNRAS, 394, 660
Carilli, C. L. & Barthel, P. D. 1996, A&AR, 7, 1
Carilli, C. L., Perley, R. A., Dreher, J. W., & Leahy, J. P. 1991, ApJ, 383, 554
Carilli, C. L., Wrobel, J. M., & Ulvestad, J. S. 1998, AJ, 115, 928
Cattaneo, A., Faber, S. M., Binney, J., et al. 2009, Nature, 460, 213
Charmandaris, V., Combes, F., & van der Hulst, J. M. 2000, A&A, 356, L1
Ciotti, L., D'Ercole, A., Pellegrini, S., & Renzini, A. 1991, ApJ, 376, 380
Clarke, D. A., Burns, J. O., & Norman, M. L. 1992, ApJ, 395, 444
Colina, L. & de Juan, L. 1995, ApJ, 448, 548
Colla, G., Fanti, C., Ficarra, A., et al. 1970, A&AS, 1, 281
Combes, F., Young, L. M., & Bureau, M. 2007, MNRAS, 377, 1795
Conway, J. E. 1999, in Astronomical Society of the Pacific Conference Series, Vol. 156, Highly Redshifted Radio Lines, ed. C. L. Carilli, S. J. E. Radford, K. M. Menten, & G. I. Langston, 259–+
Conway, J. E. & Blanco, P. R. 1995, ApJL, 449, L131+
Cooper, B. F. C., Price, R. M., & Cole, D. J. 1965, Australian Journal of Physics, 18, 589
Coziol, R., Iovino, A., & de Carvalho, R. R. 2000, AJ, 120, 47
Croston, J. H., Kraft, R. P., Hardcastle, M. J., et al. 2009, MNRAS, 395, 1999
Croton, D. J., Springel, V., White, S. D. M., et al. 2006, MNRAS, 365, 11
Davies, R. I., Sánchez, F. M., Genzel, R., et al. 2007, ApJ, 671, 1388
de Ruiter, H. R., Parma, P., Fanti, C., & Fanti, R. 1986, A&AS, 65, 111
Dekel, A. & Birnboim, Y. 2008, MNRAS, 383, 119
Di Matteo, P., Combes, F., Melchior, A., & Semelin, B. 2007, A&A, 468, 61
Di Matteo, T., Springel, V., & Hernquist, L. 2005, Nature, 433, 604
Donovan, J. L., Serra, P., van Gorkom, J. H., et al. 2009, AJ, 137, 5037
Dufour, R. J. & van den Bergh, S. 1978, ApJL, 226, L73
Dultzin-Hacyan, D., Krongold, Y., Fuentes-Guridi, I., & Marziani, P. 1999, ApJL, 513, L111
Dwarakanath, K. S. & Kale, R. 2009, ApJL, 698, L163
Eckart, A., Cameron, M., Rothermel, H., et al. 1990, ApJ, 363, 451
Ekers, R. D., Fanti, R., Lari, C., & Parma, P. 1981, A&A, 101, 194
Elitzur, M. 2008, New Astronomy Review, 52, 274
Elitzur, M. & Shlosman, I. 2006, ApJL, 648, L101
Emonts, B. H. C. 2006, Ph.D. Thesis, Univ. Groningen
Emonts, B. H. C., Morganti, R., Oosterloo, T. A., et al. 2007, A&A, 464, L1
Emonts, B. H. C., Morganti, R., Struve, C., et al. 2010, MNRAS, 406, 987

Emonts, B. H. C., Morganti, R., Tadhunter, C. N., et al. 2006, A&A, 454, 125
Emonts, B. H. C., Morganti, R., Tadhunter, C. N., et al. 2005, MNRAS, 362, 931
Emonts, B. H. C., Tadhunter, C. N., Morganti, R., et al. 2009, MNRAS, 396, 1522
Emsellem, E., Cappellari, M., Krajnović, D., et al. 2007, MNRAS, 379, 401
Erickson, L. K., Gottesman, S. T., & Hunter, Jr., J. H. 1999, ApJ, 515, 153
Espada, D., Matsushita, S., Peck, A., et al. 2009, ApJ, 695, 116
Evans, D. A., Kraft, R. P., Worrall, D. M., et al. 2004, ApJ, 612, 786
Faber, S. M., Tremaine, S., Ajhar, E. A., et al. 1997, AJ, 114, 1771
Fanaroff, B. L. & Riley, J. M. 1974, MNRAS, 167, 31P
Fanti, C., Fanti, R., de Ruiter, H. R., & Parma, P. 1986, A&AS, 65, 145
Fanti, C., Fanti, R., de Ruiter, H. R., & Parma, P. 1987, A&AS, 69, 57
Fathi, K., Storchi-Bergmann, T., Riffel, R. A., et al. 2006, ApJL, 641, L25
Feain, I. J., Ekers, R. D., Murphy, T., et al. 2009, ApJ, 707, 114
Ferrarese, L. & Merritt, D. 2000, ApJL, 539, L9
Franx, M., van Gorkom, J. H., & de Zeeuw, T. 1994, ApJ, 436, 642
Fraternali, F., van Moorsel, G., Sancisi, R., & Oosterloo, T. 2002, AJ, 123, 3124
Fuente, A., Black, J. H., Martín-Pintado, J., et al. 2000, ApJL, 545, L113
García-Burillo, S., Combes, F., Neri, R., et al. 2007, A&A, 468, L71
García-Ruiz, I., Sancisi, R., & Kuijken, K. 2002, A&A, 394, 769
Gebhardt, K., Bender, R., Bower, G., et al. 2000, ApJL, 539, L13
Giroletti, M., Giovannini, G., & Taylor, G. B. 2005, A&A, 441, 89
González Delgado, R. M., Tadhunter, C. N., Pérez, E., et al. 2006, Astronomische Nachrichten, 327, 159
Graham, A. W. & Driver, S. P. 2007, ApJ, 655, 77
Greene, J., Lim, J., & Ho, P. T. P. 2004, ApJS, 153, 93
Grossi, M., di Serego Alighieri, S., Giovanardi, C., et al. 2009, A&A, 498, 407
Grueff, G. & Vigotti, M. 1972, A&AS, 6, 1
Gültekin, K., Richstone, D. O., Gebhardt, K., et al. 2009, ApJ, 698, 198
Gupta, N., Salter, C. J., Saikia, D. J., Ghosh, T., & Jeyakumar, S. 2006, MNRAS, 373, 972
Haan, S., Schinnerer, E., Mundell, C. G., García-Burillo, S., & Combes, F. 2008, AJ, 135, 232
Hardcastle, M. J., Cheung, C. C., Feain, I. J., & Stawarz, Ł. 2009a, MNRAS, 393, 1041
Hardcastle, M. J., Evans, D. A., & Croston, J. H. 2007, MNRAS, 376, 1849
Hardcastle, M. J., Evans, D. A., & Croston, J. H. 2009b, MNRAS, 396, 1929
Hardcastle, M. J., Worrall, D. M., Kraft, R. P., et al. 2003, ApJ, 593, 169
Häring, N. & Rix, H. 2004, ApJL, 604, L89
Harris, G. L. H., Rejkuba, M., & Harris, W. E. 2009, ArXiv e-prints
Haynes, R. F., Cannon, R. D., & Ekers, R. D. 1983, Proceedings of the Astronomical Society of Australia, 5, 241
Heald, G. H., Rand, R. J., Benjamin, R. A., & Bershady, M. A. 2007, ApJ, 663, 933
Heckman, T. M., Miley, G. K., van Breugel, W. J. M., & Butcher, H. R. 1981, ApJ, 247, 403
Heckman, T. M., Smith, E. P., Baum, S. A., et al. 1986, ApJ, 311, 526
Henderson, A. P., Jackson, P. D., & Kerr, F. J. 1982, ApJ, 263, 116
Hess, K. M., Pisano, D. J., Wilcots, E. M., & Chengalur, J. N. 2009, ApJ, 699, 76

Hibbard, J. E. & van Gorkom, J. H. 1996, AJ, 111, 655
Hicks, E. K. S., Davies, R. I., Malkan, M. A., et al. 2009, ApJ, 696, 448
Hill, G. J. & Lilly, S. J. 1991, ApJ, 367, 1
Ho, L. C., Darling, J., & Greene, J. E. 2008a, ApJS, 177, 103
Ho, L. C., Darling, J., & Greene, J. E. 2008b, ApJ, 681, 128
Hoekstra, H., van Albada, T. S., & Sancisi, R. 2001, MNRAS, 323, 453
Holt, J., Tadhunter, C. N., & Morganti, R. 2003, MNRAS, 342, 227
Holt, J., Tadhunter, C. N., & Morganti, R. 2008, MNRAS, 387, 639
Hopkins, A. M., McClure-Griffiths, N. M., & Gaensler, B. M. 2008a, ApJL, 682, L13
Hopkins, P. F., Cox, T. J., Dutta, S. N., et al. 2009, ApJS, 181, 135
Hopkins, P. F., Cox, T. J., & Hernquist, L. 2008b, ApJ, 689, 17
Hopkins, P. F., Hernquist, L., Cox, T. J., et al. 2005, ApJ, 630, 705
Hopkins, P. F., Hernquist, L., Cox, T. J., Robertson, B., & Krause, E. 2007, ApJ, 669, 67
Horiuchi, S., Meier, D. L., Preston, R. A., & Tingay, S. J. 2006, PASJ, 58, 211
Impellizzeri, V., Roy, A. L., & Henkel, C. 2006, in Proceedings of the 8th European VLBI Network Symposium
Israel, F. P. 1998, A&AR, 8, 237
Jackson, N., Tadhunter, C., & Sparks, W. B. 1998, MNRAS, 301, 131
Jaffe, W., Meisenheimer, K., Röttgering, H. J. A., et al. 2004, Nature, 429, 47
Jesseit, R., Naab, T., Peletier, R. F., & Burkert, A. 2007, MNRAS, 376, 997
Jones, D. L., Tingay, S. J., Murphy, D. W., et al. 1996, ApJL, 466, L63+
Jones, D. L., Wehrle, A. E., Piner, B. G., & Meier, D. L. 2001, ApJ, 553, 968
Józsa, G. I. G., Oosterloo, T. A., Morganti, R., Klein, U., & Erben, T. 2009, A&A, 494, 489
Kainulainen, J. T., Alves, J. F., Beletsky, Y., et al. 2009, A&A, 502, L5
Kaufmann, T., Mayer, L., Wadsley, J., Stadel, J., & Moore, B. 2006, MNRAS, 370, 1612
Kawata, D. & Mulchaey, J. S. 2008, ApJL, 672, L103
Keene, J., Stern, D., Lawrence, C., et al. 2004, in Bulletin of the American Astronomical Society, Vol. 36, Bulletin of the American Astronomical Society, 725–+
Kellermann, K. I., Sramek, R., Schmidt, M., Shaffer, D. B., & Green, R. 1989, AJ, 98, 1195
Kereš, D. & Hernquist, L. 2009, ApJL, 700, L1
Kereš, D., Katz, N., Weinberg, D. H., & Davé, R. 2005, MNRAS, 363, 2
Knapen, J. H. 1997, MNRAS, 286, 403
Knapp, G. R., Turner, E. L., & Cunniffe, P. E. 1985, AJ, 90, 454
Kormendy, J., Fisher, D. B., Cornell, M. E., & Bender, R. 2009, ApJS, 182, 216
Kormendy, J. & Gebhardt, K. 2001, in American Institute of Physics Conference Series, Vol. 586, 20th Texas Symposium on relativistic astrophysics, ed. J. C. Wheeler & H. Martel, 363–381
Kormendy, J. & Richstone, D. 1995, ARAA, 33, 581
Koulouridis, E., Plionis, M., Chavushyan, V., et al. 2006, ApJ, 639, 37
Krajnović, D., Sharp, R., & Thatte, N. 2007, MNRAS, 374, 385
Krichbaum, T. P., Alef, W., Witzel, A., et al. 1998, A&A, 329, 873
Krolik, J. H. & Begelman, M. C. 1988, ApJ, 329, 702
Krolik, J. H. & Lepp, S. 1989, ApJ, 347, 179
Kuo, C., Lim, J., Tang, Y., & Ho, P. T. P. 2008, ApJ, 679, 1047

Labiano, A., O'Dea, C. P., Barthel, P. D., de Vries, W. H., & Baum, S. A. 2008, A&A, 477, 491
Laing, R. A. & Peacock, J. A. 1980, MNRAS, 190, 903
Lara, L., Giovannini, G., Cotton, W. D., et al. 2004, A&A, 421, 899
Leahy, J. P., Muxlow, T. W. B., & Stephens, P. W. 1989, MNRAS, 239, 401
Ledlow, M. J., Owen, F. N., & Eilek, J. A. 2002, New Astronomy Review, 46, 343
Lin, D. N. C., Pringle, J. E., & Rees, M. J. 1988, ApJ, 328, 103
Liszt, H. 2001, A&A, 371, 865
Lo, K. Y. 2005, ARAA, 43, 625
Longair, M. S. & Seldner, M. 1979, MNRAS, 189, 433
Macciò, A. V., Moore, B., & Stadel, J. 2006, ApJL, 636, L25
Magorrian, J., Tremaine, S., Richstone, D., et al. 1998, AJ, 115, 2285
Malin, D. F. & Carter, D. 1983, ApJ, 274, 534
Maloney, P. R., Begelman, M. C., & Rees, M. J. 1994, ApJ, 432, 606
Maloney, P. R., Hollenbach, D. J., & Tielens, A. G. G. M. 1996, ApJ, 466, 561
Marconi, A., Capetti, A., Axon, D. J., et al. 2001, ApJ, 549, 915
Marconi, A. & Hunt, L. K. 2003, ApJL, 589, L21
Marconi, A., Risaliti, G., Gilli, R., et al. 2004, MNRAS, 351, 169
Marinacci, F., Binney, J., Fraternali, F., et al. 2010, MNRAS, 347
Marzke, R. O., Geller, M. J., da Costa, L. N., & Huchra, J. P. 1995, AJ, 110, 477
Matthews, L. D. & Wood, K. 2003, ApJ, 593, 721
Meier, D. L., Koide, S., & Uchida, Y. 2001, Science, 291, 84
Merloni, A. & Heinz, S. 2008, MNRAS, 388, 1011
Meyer, M. J., Zwaan, M. A., Webster, R. L., et al. 2004, MNRAS, 350, 1195
Miley, G. & De Breuck, C. 2008, A&AR, 15, 67
Mirabel, I. F., Laurent, O., Sanders, D. B., et al. 1999, A&A, 341, 667
Mo, H., van den Bosch, F., & White, S. 2010, Galaxy Formation and Evolution
Momjian, E., Romney, J. D., Carilli, C. L., Troland, T. H., & Taylor, G. B. 2003, ApJ, 587, 160
Momjian, E., Romney, J. D., & Troland, T. H. 2002, ApJ, 566, 195
Monaco, P., Giuricin, G., Mardirossian, F., & Mezzetti, M. 1994, ApJ, 436, 576
Morganti, R. 2010, ArXiv e-prints
Morganti, R., de Zeeuw, P. T., Oosterloo, T. A., et al. 2006, MNRAS, 371, 157
Morganti, R., Holt, J., Saripalli, L., Oosterloo, T. A., & Tadhunter, C. N. 2007, A&A, 476, 735
Morganti, R., Killeen, N. E. B., Ekers, R. D., & Oosterloo, T. A. 1999, MNRAS, 307, 750
Morganti, R., Oosterloo, T., Struve, C., & Saripalli, L. 2008, A&A, 485, L5
Morganti, R., Oosterloo, T. A., Capetti, A., et al. 2003, A&A, 399, 511
Morganti, R., Oosterloo, T. A., Tadhunter, C. N., van Moorsel, G., & Emonts, B. 2005a, A&A, 439, 521
Morganti, R., Oosterloo, T. A., Tadhunter, C. N., et al. 2004, A&A, 424, 119
Morganti, R., Oosterloo, T. A., van Moorsel, G., Tadhunter, C. N., & Killeen, N. 2000, ArXiv Astrophysics e-prints
Morganti, R., Peck, A. B., Oosterloo, T. A., et al. 2009, A&A, 505, 559
Morganti, R., Robinson, A., Fosbury, R. A. E., et al. 1991, MNRAS, 249, 91

Morganti, R., Tadhunter, C. N., & Oosterloo, T. A. 2005b, A&A, 444, L9
Naab, T., Jesseit, R., & Burkert, A. 2006, MNRAS, 372, 839
Nenkova, M., Sirocky, M. M., Ivezić, Ž., & Elitzur, M. 2008a, ApJ, 685, 147
Nenkova, M., Sirocky, M. M., Nikutta, R., Ivezić, Ž., & Elitzur, M. 2008b, ApJ, 685, 160
Neumayer, N., Cappellari, M., Reunanen, J., et al. 2007, ApJ, 671, 1329
Nicholson, R. A., Bland-Hawthorn, J., & Taylor, K. 1992, ApJ, 387, 503
Nipoti, C. & Binney, J. 2007, MNRAS, 382, 1481
Nipoti, C., Treu, T., & Bolton, A. S. 2009, ApJ, 703, 1531
Noordermeer, E. 2006, Ph.D. Thesis, Univ. Groningen
Noordermeer, E., van der Hulst, J. M., Sancisi, R., Swaters, R. A., & van Albada, T. S. 2005, A&A, 442, 137
Noordermeer, E., van der Hulst, J. M., Sancisi, R., Swaters, R. S., & van Albada, T. S. 2007, MNRAS, 376, 1513
Ocaña Flaquer, B., Leon, S., Lim, J., Combes, F., & Dinh-v-Trung. 2008, in American Institute of Physics Conference Series, Vol. 1035, The Evolution of Galaxies Through the Neutral Hydrogen Window, ed. R. Minchin & E. Momjian, 132–134
O'Dea, C. P. 1998, PASP, 110, 493
O'Dea, C. P., Baum, S. A., & Stanghellini, C. 1991, ApJ, 380, 66
Ogle, P. M., Cohen, M. H., Miller, J. S., et al. 1997, ApJL, 482, L37+
Oosterloo, T., Fraternali, F., & Sancisi, R. 2007a, AJ, 134, 1019
Oosterloo, T., Morganti, R., Crocker, A., et al. 2010, ArXiv e-prints
Oosterloo, T. A. & Morganti, R. 2005, A&A, 429, 469
Oosterloo, T. A., Morganti, R., Sadler, E. M., van der Hulst, T., & Serra, P. 2007b, A&A, 465, 787
Oosterloo, T. A., Morganti, R., Sadler, E. M., Vergani, D., & Caldwell, N. 2002, AJ, 123, 729
Orrù, E., Murgia, M., Feretti, L., et al. 2010, A&A, 515, A50+
Owen, F. N. & White, R. A. 1991, MNRAS, 249, 164
Padovani, P. & Urry, C. M. 1992, ApJ, 387, 449
Parma, P., de Ruiter, H. R., Fanti, C., & Fanti, R. 1986, A&AS, 64, 135
Parma, P., Murgia, M., de Ruiter, H. R., & Fanti, R. 2002, New Astronomy Review, 46, 313
Parma, P., Murgia, M., de Ruiter, H. R., et al. 2007, A&A, 470, 875
Peck, A. B. & Taylor, G. B. 2001, ApJL, 554, L147
Peek, J. E. G., Putman, M. E., & Sommer-Larsen, J. 2008, ApJ, 674, 227
Peng, E. W., Ford, H. C., & Freeman, K. C. 2004, ApJ, 602, 705
Peng, E. W., Ford, H. C., Freeman, K. C., & White, R. L. 2002, AJ, 124, 3144
Peterson, B. M. 1997, An Introduction to Active Galactic Nuclei (Cambridge University Press)
Pihlström, Y. M., Conway, J. E., & Vermeulen, R. C. 2003, A&A, 404, 871
Pisano, D. J., Wilcots, E. M., & Elmegreen, B. G. 1998, AJ, 115, 975
Pogge, R. W. & Eskridge, P. B. 1993, AJ, 106, 1405
Prandoni, I., Laing, R. A., Parma, P., et al. 2007, New Astronomy Review, 51, 43
Prestage, R. M. & Peacock, J. A. 1988, MNRAS, 230, 131
Prieto, M. A., Maciejewski, W., & Reunanen, J. 2005, AJ, 130, 1472

Privon, G. C. 2009, ArXiv e-prints
Quillen, A. C., Brookes, M. H., Keene, J., et al. 2006, ApJ, 645, 1092
Quillen, A. C., de Zeeuw, P. T., Phinney, E. S., & Phillips, T. G. 1992, ApJ, 391, 121
Quillen, A. C., Graham, J. R., & Frogel, J. A. 1993, ApJ, 412, 550
Raimond, E., Faber, S. M., Gallagher, III, J. S., & Knapp, G. R. 1981, ApJ, 246, 708
Ramos Almeida, C., Tadhunter, C. N., Inskip, K. J., et al. 2010, ArXiv e-prints
Rees, M. J. 1984, ARAA, 22, 471
Roberts, M. S. 1970, ApJL, 161, L9+
Roberts, M. S. & Haynes, M. P. 1994, ARAA, 32, 115
Roche, N. & Eales, S. A. 2000, MNRAS, 317, 120
Rogstad, D. H. & Shostak, G. S. 1972, ApJ, 176, 315
Romero, G. E., Benaglia, P., & Combi, J. A. 1997, A&AS, 124, 307
Rydbeck, G., Wiklind, T., Cameron, M., et al. 1993, A&A, 270, L13
Sadler, E. M. 2001, in Astronomical Society of the Pacific Conference Series, Vol. 240, Gas and Galaxy Evolution, ed. J. E. Hibbard, M. Rupen, & J. H. van Gorkom, 445–+
Sadler, E. M. & Gerhard, O. E. 1985, MNRAS, 214, 177
Sadler, E. M., Jenkins, C. R., & Kotanyi, C. G. 1989, MNRAS, 240, 591
Saikia, D. J. & Jamrozy, M. 2009, Bulletin of the Astronomical Society of India, 37, 63
Salomé, P. & Combes, F. 2003, A&A, 412, 657
Sancisi, R., Fraternali, F., Oosterloo, T., & van der Hulst, T. 2008, A&AR, 15, 189
Sancisi, R., Fraternali, F., Oosterloo, T., & van Moorsel, G. 2001, in Astronomical Society of the Pacific Conference Series, Vol. 240, Gas and Galaxy Evolution, ed. J. E. Hibbard, M. Rupen, & J. H. van Gorkom, 241–+
Sanghera, H. S., Saikia, D. J., Luedke, E., et al. 1995, A&A, 295, 629
Sansom, A. E., Hibbard, J. E., & Schweizer, F. 2000, AJ, 120, 1946
Sarma, A. P., Troland, T. H., & Rupen, M. P. 2002, ApJ, 564, 696
Sarzi, M., Falcón-Barroso, J., Davies, R. L., et al. 2006, MNRAS, 366, 1151
Sault, R. J., Teuben, P. J., & Wright, M. C. H. 1995, in Astronomical Society of the Pacific Conference Series, Vol. 77, Astronomical Data Analysis Software and Systems IV, ed. R. A. Shaw, H. E. Payne, & J. J. E. Hayes, 433–+
Saxton, C. J., Sutherland, R. S., & Bicknell, G. V. 2001, ApJ, 563, 103
Schiminovich, D., van Gorkom, J. H., van der Hulst, J. M., & Kasow, S. 1994, ApJL, 423, L101+
Schinnerer, E., Böker, T., Emsellem, E., & Downes, D. 2007, A&A, 462, L27
Schinnerer, E., Eckart, A., Tacconi, L. J., Genzel, R., & Downes, D. 2000, ApJ, 533, 850
Schoenmakers, A. P., de Bruyn, A. G., Röttgering, H. J. A., van der Laan, H., & Kaiser, C. R. 2000, MNRAS, 315, 371
Schweizer, F. & Seitzer, P. 1992, AJ, 104, 1039
Schweizer, F., van Gorkom, J. H., & Seitzer, P. 1989, ApJ, 338, 770
Seldner, M. & Peebles, P. J. E. 1978, ApJ, 225, 7
Serra, P. & Oosterloo, T. A. 2010, MNRAS, 401, L29
Serra, P., Trager, S. C., van der Hulst, J. M., Oosterloo, T. A., & Morganti, R. 2006, A&A, 453, 493
Shankar, F., Salucci, P., Granato, G. L., De Zotti, G., & Danese, L. 2004, MNRAS, 354, 1020
Shlosman, I., Frank, J., & Begelman, M. C. 1989, Nature, 338, 45

Slee, O. B., Roy, A. L., Murgia, M., Andernach, H., & Ehle, M. 2001, AJ, 122, 1172
Smith, E. P. & Heckman, T. M. 1989, ApJ, 341, 658
Soltan, A. 1982, MNRAS, 200, 115
Somerville, R. S., Hopkins, P. F., Cox, T. J., Robertson, B. E., & Hernquist, L. 2008, MNRAS, 391, 481
Sparke, L. S. 1996, ApJ, 473, 810
Springel, V., Di Matteo, T., & Hernquist, L. 2005, MNRAS, 361, 776
Struve, C. & Conway, J. E. 2010, A&A, 513, A10+
Struve, C., Morganti, R., & Oosterloo, T. A. 2008a, in Astronomical Society of the Pacific Conference Series, Vol. 396, Astronomical Society of the Pacific Conference Series, ed. J. G. Funes & E. M. Corsini, 161–+
Struve, C., Morganti, R., & Oosterloo, T. A. 2008b, Memorie della Societa Astronomica Italiana, 79, 1096
Struve, C., Morganti, R., Oosterloo, T. A., & Emonts, B. H. C. 2009, ArXiv e-prints
Struve, C., Oosterloo, T. A., Morganti, R., & Saripalli, L. 2010, A&A, 515, A67+
Swaters, R. 1999, Ph.D. Thesis, Univ. Groningen
Tadhunter, C. 2008, New Astronomy Review, 52, 227
Tadhunter, C., Marconi, A., Axon, D., et al. 2003, MNRAS, 342, 861
Tadhunter, C., Robinson, T. G., González Delgado, R. M., Wills, K., & Morganti, R. 2005, MNRAS, 356, 480
Tadhunter, C. N., Dickson, R. C., & Shaw, M. A. 1996, MNRAS, 281, 591
Tadhunter, C. N., Morganti, R., di Serego-Alighieri, S., Fosbury, R. A. E., & Danziger, I. J. 1993, MNRAS, 263, 999
Tadhunter, C. N., Packham, C., Axon, D. J., et al. 1999, ApJL, 512, L91
Tang, Y., Kuo, C., Lim, J., & Ho, P. T. P. 2008, ApJ, 679, 1094
Tasse, C., Best, P. N., Röttgering, H., & Le Borgne, D. 2008, A&A, 490, 893
Taylor, G. B. 1996, ApJ, 470, 394
Taylor, G. B., Wrobel, J. M., & Vermeulen, R. C. 1998, ApJ, 498, 619
Thilker, D. A., Braun, R., Walterbos, R. A. M., et al. 2004, ApJL, 601, L39
Tingay, S. J., Jauncey, D. L., Reynolds, J. E., et al. 1998, AJ, 115, 960
Tingay, S. J. & Murphy, D. W. 2001, ApJ, 546, 210
Tonry, J. L., Dressler, A., Blakeslee, J. P., et al. 2001, ApJ, 546, 681
Trager, S. C., Faber, S. M., Worthey, G., & González, J. J. 2000, AJ, 119, 1645
Tristram, K. R. W., Raban, D., Meisenheimer, K., et al. 2009, A&A, 502, 67
Tubbs, A. D. 1980, ApJ, 241, 969
Urry, C. M. & Padovani, P. 1995, PASP, 107, 803
van Breugel, W., Nan, R., Schilizzi, R. T., Fanti, C., & Fanti, R. 1988, in IAU Symposium, Vol. 129, The Impact of VLBI on Astrophysics and Geophysics, ed. M. J. Reid & J. M. Moran, 115–+
van der Hulst, J. M., Golisch, W. F., & Haschick, A. D. 1983, ApJL, 264, L37
van der Kruit, P. C. 2007, A&A, 466, 883
van der Wolk, G., Barthel, P. D., Peletier, R. F., & Pel, J. W. 2010, A&A, 511, A64+
van Gorkom, J. H., Knapp, G. R., Ekers, R. D., et al. 1989, AJ, 97, 708
van Gorkom, J. H., Knapp, G. R., Raimond, E., Faber, S. M., & Gallagher, J. S. 1986, AJ, 91, 791
van Gorkom, J. H., van der Hulst, J. M., Haschick, A. D., & Tubbs, A. D. 1990, AJ, 99,

1781
van Langevelde, H. J., Pihlström, Y. M., Conway, J. E., Jaffe, W., & Schilizzi, R. T. 2000, A&A, 354, L45
Vermeulen, R. C., Pihlström, Y. M., Tschager, W., et al. 2003, A&A, 404, 861
Vermeulen, R. C., Readhead, A. C. S., & Backer, D. C. 1994, ApJL, 430, L41
Veron-Cetty, M., Woltjer, L., Ekers, R. D., & Staveley-Smith, L. 1995, A&A, 297, L79+
Wakker, B. P., York, D. G., Howk, J. C., et al. 2007, ApJL, 670, L113
Wakker, B. P., York, D. G., Wilhelm, R., et al. 2008, ApJ, 672, 298
Westmeier, T., Braun, R., & Thilker, D. 2005, A&A, 436, 101
White, R. L. & Becker, R. H. 1992, ApJS, 79, 331
Whiting, M. 2008, http://www.atnf.csiro.au/people/Matthew.Whiting/Duchamp
Whysong, D. & Antonucci, R. 2004, ApJ, 602, 116
Wilcots, E. M., Turnbull, M. C., & Brinks, E. 2001, ApJ, 560, 110
Wild, V., Heckman, T., & Charlot, S. 2010, MNRAS, 405, 933
Wilkinson, P. N., Browne, I. W. A., Patnaik, A. R., Wrobel, J. M., & Sorathia, B. 1998, MNRAS, 300, 790
Woodley, K. A., Harris, W. E., Puzia, T. H., et al. 2010, ApJ, 708, 1335
Wrobel, J. M. & Heeschen, D. S. 1991, AJ, 101, 148
Wu, H., Zou, Z. L., Xia, X. Y., & Deng, Z. G. 1998, A&AS, 132, 181
Yates, M. G., Miller, L., & Peacock, J. A. 1989, MNRAS, 240, 129
Young, A. J., Wilson, A. S., Terashima, Y., Arnaud, K. A., & Smith, D. A. 2002, ApJ, 564, 176
Yun, M. S., Ho, P. T. P., & Lo, K. Y. 1994, Nature, 372, 530
Zirbel, E. L. 1997, ApJ, 476, 489

Nederlandse samenvatting

Sinds het ontstaan van de mensheid hebben mensen zich afgevraagd waar de Aarde, de Zon en alle andere objecten die we aan de (nachtelijke) hemel kunnen observeren, vandaan komen. Een natuurlijke benadering van deze vraag is het observeren van objecten aan de hemel met als doel het bepalen van fundamentele eigenschappen[1]. Zulke eigenschappen kunnen vervolgens gebruikt worden om fysische "wetten" te onthullen[2], die helpen te begrijpen hoe het Universum is gevormd en geëvolueerd.

In het Universum bestaat een verscheidenheid aan objecten, zoals bijvoorbeeld "planeten", die cirkelen rond "sterren", welke zelf samenclusteren in grote groepen genaamd "sterrenstelsels". Afhankelijk van een aantal parameters, zoals de verdeling van de sterren over het stelsel, worden sterrenstelsels verdeeld in verschillende sub-groepen. Een belangrijke eigenschappen die gebruikt wordt om een tweedeling tussen verschillende types sterrenstelsels te maken is het al dan niet aanwezig zijn van recente stervorming. Sterrenstelsels die nog steeds sterren vormen worden "laat-type (spiraal) stelsels" genoemd, terwijl stelsels waar stervorming ontbreekt worden geclassificeerd als "vroeg-type (elliptische en lensvormige) stelsels". Koud gas (voornamelijk atomair en moleculair waterstof) is het hoofd ingrediënt voor de vorming van sterren. In vroeg-type stelsels bevinden zich veelal wel detecteerbare hoeveelheden koud gas, maar is de dichtheid van te laag om stervorming toe te staan. Koud gas in vroeg-type stelsels speelt mogelijk ook een belangrijke rol bij een van de meest energetische processen in de evolutie van sterrenstelsels: "Actieve Galactische Kernen". Het begrijpen van deze extreme objecten is van groot belang voor het begrijpen van de vorming en evolutie van het Universum als geheel.

Van Zwarte Gaten tot Actieve Galactische Kernen tot Radiostelsels

Een zwart gat is een massa condensatie die een singulariteit in de ruimte vormt; geen enkele materie – zelfs geen licht – kan ontsnappen aan deze singulariteit wanneer het binnen de kritische grens van het zwarte gat komt. Materie en licht op grotere afstand worden afgebogen, zodat zwarte gaten indirect "gezien" kunnen worden door observaties van het omringende materiaal. Het merendeel, zo niet alle, sterrenstelsels bevatten een superzwaar zwart gat (SMBH) in hun centrum, met een massa oplopend tot enkele miljarden maal de massa van de Zon.

[1] Deze benadering is zeker niet de enige mogelijke, zoals verschillende filosofische en religieuze stellingen laten zien.

[2] Een beroemd voorbeeld van zo'n wet is de zwaartekrachtwet van Newton, die zegt dat alle deeltjes (met een massa) een aantrekkingskracht uitoefenen op elk ander deeltje met een massa in het Universum.

Een aantal relaties tussen de massa van de SMBH en de eigenschappen van het sterrenstelsels waarin het zich bevindt (het "host" sterrenstelsel) zijn gevonden, wat duidt op een gemeenschappelijk evolutieproces tussen SMBH en host sterrenstelsel. De groei van een SMBH kan grofweg op twee manieren gebeuren, ofwel door het samensmelten met een andere SMBH gedurende een botsing tussen twee sterrenstelsels, ofwel door de accretie van gas en stof in het zwarte gat. De groei van SMBH wordt gedomineerd door de accretie van gas en stof naar de directe nabijheid van het zwarte gat (< 1 pc)[3], waarna het opgeslokt wordt door de singulariteit zelf.

Superzware zwarte gaten die actief massa accreteren worden "Actieve Galactische Kernen" (AGN) genoemd. Gedurende een lange tijd werden deze actieve kernen gezien als exotische objecten die geen significante invloed hadden op de evolutie van het Universum. Echter, recente computer simulaties laten zien dat "terugkoppeling" een sterk regulerende invloed heeft op de groei van sterrenstelsels: AGNs verhitten het omringende gas en verstoten het uit de nucleaire omgeving. Zulke uitstromen van gas zijn geobserveerd in enkele sterrenstelsels die een AGN bevatten. Dit suggereert dat het proces van de groei van zwarte gaten een zelfregulerende component bevat en daarmee, tenminste gedeeltelijk, de geobserveerde relaties (zie boven) verklaard. Sterker nog, het bestaan van deze relaties suggereert dat het merendeel van alle sterrenstelsels gedurende hun levensduur AGN fases ondergaan. Het begrijpen van deze actieve fases is dus van het allergrootste belang als we willen begrijpen hoe sterrenstelsels evolueren.

Hoe accreteren superzware zwarte gaten gas en stof? Volgens de wetten van de natuurkunde ("behoud van impulsmoment"), vormt het invallende materiaal een platte structuur rond het zwarte gat, een zogenaamde "accretieschijf". De verwachtte grootte van zo'n accretieschijf is heel klein (typisch 0.001 pc); het materiaal in de schijf roteert met een hoge snelheid, terwijl grote hoeveelheden straling worden uitgezonden met verschillende golflengtes in het elektromagnetische spectrum (bv. in het optisch, ultra-violet en röntgen). In ongeveer 15 – 20% van de AGNs, kan een gedeelte van het invallende materiaal ontsnappen van de schijf door aan beide kanten jets te vormen loodrecht op de accretie-schijf. Deze jets kunnen uitgroeien tot structuren ter grootte van een Mpc[4] (veel groter dan het sterrenstelsel waarin ze ontstaan) en bestaan uit een plasma die straling uitzendt in radio golflengtes. Met behulp van gespecialiseerde telescopen ("radio-telescopen") kan de straling van deze jet structuren geobserveerd worden. Zwarte gaten met sterke radio emissie worden "radio-luide" AGNs genoemd, terwijl zwarte gaten met zwakke of geen radio emissie "radio-zwak" worden genoemd.

Waar komt het materiaal dat dient als voeding voor het zwarte gat vandaan? Volgens het standaardmodel voor AGNs, worden het zwarte gat en de accretie-schijf omringd door een schijf-achtige structuur (genaamd "torus") bestaande uit stof en gas ter grootte van 1 – 10 pc. Op grotere schalen (tientallen pc) bestaan ook soortgelijke schijven van atomair en moleculair gas. Zulke "circumnucleaire schijven" kunnen de benodigde gasmassa verzorgen die nodig is om de AGN te activeren. De

[3] 1 pc is de afstand die licht aflegt in ongeveer 3 jaar tijd. De typische grootte van een sterrenstelsel bedraagt tientallen kpc (1 kpc = 1 000 pc).

[4] 1 Mpc = 1 000 kpc

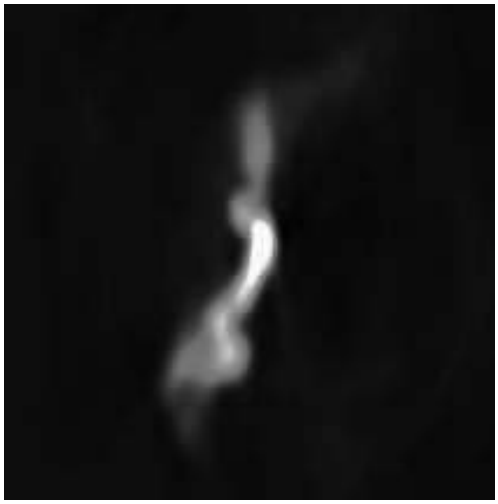

Figuur 1: *FR-I radiobron B2 0104+32. Dit is één van de bronnen die bestudeerd worden in Hoofdstuk 2.*

exacte circumnucleaire structuren en accretie-mechanismen worden echter nog niet volledig begrepen.

Er bestaat een grote verscheidenheid aan verschillende soorten AGNs. Radio-luide AGNs bevinden zich voornamelijk in vroeg-type sterrenstelsels, genaamd radiostelsels. De morfologie van de radio structuur hangt vooral af van de hoeveelheid straling uitgezonden in radio golflengtes. Fanaroff en Riley (1974) classificeerden radiostelsels in twee groepen; Sterke radio bronnen (Fanaroff-Riley type II, FR-II) hebben supersonische jets waarvan de uiteinden oplichten door botsingen met het intergalactische medium in een zogenaamde "hot-spot" (Fig. 2). De zwakkere radio bronnen (Fanaroff-Riley type I, FR-I) hebben jets waarvan de uiteinden (radio lobben) niet oplichten, en dus een donkere rand hebben (Fig. 1). In beide gevallen worden de jets grofweg uitgezonden in het hemelvlak. Radiobronnen waar de jets loodrecht op het hemelvlak (in de richting van de waarnemer) worden uitgezonden zijn BL Lacs (FR-I type) en quasars (FR-II type) genoemd.

Sommige radiobronnen zijn compact (typisch $\leq$ 10 kpc) en worden gedacht jonge bronnen te zijn, die later uitgroeien tot grote, klassieke FR-I of FR-II type bronnen. Echter, sommige compacte bronnen worden misschien nooit grote, uitgebreide radiobronnen. De dichtheid van het gas en stof in sommige host sterrenstelsel is zo hoog dat de jets van de AGN er nooit in slagen om hun weg naar buiten te vechten en uit te groeien tot klassieke FR-I en FR-II structuren.

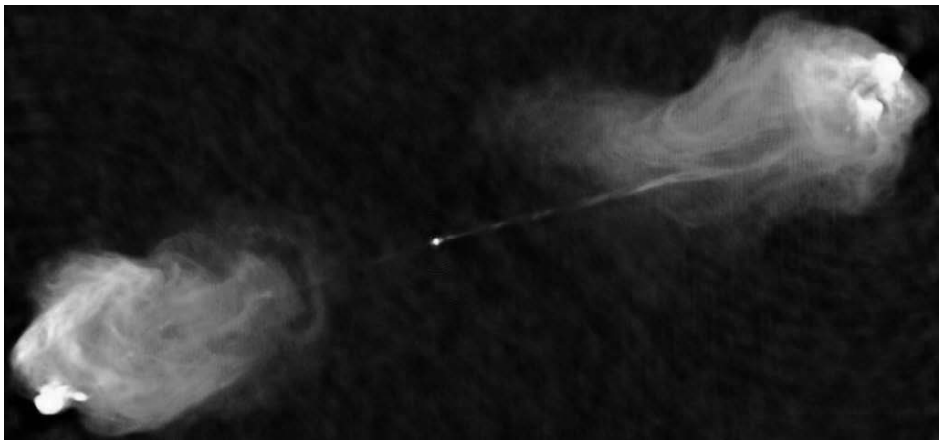

Figuur 2: *FR-II radiobron Cygnus A (Credit: C. Carilli). De binnenste regionen van deze bron worden bestudeerd in Hoofdstuk 5.*

Activeringsmechanismen

Er zijn verschillende mechanismen voorgesteld voor het bevoorraden en transporteren van gas naar de nucleaire regionen van een sterrenstelsel, waar het een actieve fase kan activeren.

Major mergers, satelliet accretie en getijde interacties:

Een mogelijke manier om gas naar de binnenste delen van een sterrenstelsel te geleiden – dit is nodig om een radio-luide fase te activeren – is om het sterrenstelsel te verstoren. Botsingen tussen sterrenstelsels (zogenaamde "mergers") en accretie van satellietstelsels kunnen resulteren in verstoringen van het gas (dat mogelijk al een lange tijd op grote afstand rond het zwarte gat roteerde) dat op die manier naar de binnenste delen van het sterrenstelsel wordt geleidt waar het eventueel het zwarte gat kan voeden.

Verscheidene onderzoeken hebben gezocht naar aanwijzingen van verstoringen in radiostelsels. Dit heeft geleid tot bewijzen voor mergers en/of getijde interacties in een grote fractie van de radiostelsels (tot > 85%), inclusief de drie radiostelsels die in detail bestudeerd zijn in deze scriptie (Centaurus A, Cygnus A and NGC 1167). Botsingen tussen sterrenstelsels en accretie van satellieten spelen dus mogelijk een belangrijke rol voor radiostelsels. Hoewel interacties van objecten die veel gas bevatten AGN activiteit kan veroorzaken, is enkel de aanwezigheid van een grote hoeveelheid gas niet genoeg om een AGN te activeren. Meerdere recente observaties hebben grote hoeveelheden atomair waterstofgas (H I) gedetecteerd in vroeg-type stelsels, waarvan de meerderheid niet over een AGN beschikt.

Koude en hete accretie:

Sterrenstelsels hebben de mogelijkheid om koud gas te accreteren dat afkomstig is uit de intergalactische ruimte (gas dat zich oorspronkelijk tussen de sterrenstelsels bevond). Sinds er slechts kleine hoeveelheden gas nodig zijn om zwarte gaten te activeren is dit mogelijk een relevant mechanisme dat een fase van nucleaire activiteit kan veroorzaken. Een alternatief voor de activering van het zwarte gat is de accretie van heet gas, dat gevonden kan worden rond de vroeg-type sterrenstelsels. Het hete gas kan direct geaccreteerd worden naar de nabijheid van het centrale zwarte gat, waar het de centrale AGN kan voorzien van brandstof. Echter, hoe de accretie van koud en heet gas precies in zijn werk gaat is niet duidelijk.

Eerdere neutraal waterstof observaties en open vragen:

Gezien het mogelijke belang van koud gas in de activering van radiobronnen zijn er in het verleden meerdere studies gedaan om de eigenschappen van neutraal waterstof in radiostelsels te onderzoeken. Neutraal waterstof in de jets en radio lobben zendt straling uit in radio golflengtes, zodat al deze structuren tegelijkertijd bestudeerd kunnen worden. H I kan zowel gedetecteerd worden in emissie als in absorptie tegen een radio continuüm structuur (zoals het radio plasma van de jets/lobben). Observaties van de H I emissie laten onderzoekers vaak de eigenschappen van het gas bestuderen op schalen van tientallen kpc (om bijvoorbeeld te zoeken naar sporen van galactische interacties of verstoringen). Studies van H Iabsorptie laten onderzoekers echter vaak het circumnucleaire gebied van radiostelsels bestuderen, waardoor de eigenschappen van het gas rondom het zwarte gat kunnen worden onderzocht.

Al gedurende tientallen jaren is H I gedetecteerd in absorptie in meerdere radiostelsels, waaronder Centaurus A. Gedurende vele jaren werd het H I dat gevonden werd in absorptie tegen de nucleus (het gebied rond het zwarte gat) gezien met een roodverschuiving van de snelheid ten opzichte van de snelheid van het host stelsel (het gas beweegt zich in de richting van het zwarte gat – in projectie). Het feit dat overwegend gas met een roodverschuiving werd gevonden is geïnterpreteerd als bewijs voor de accretie van koud gas naar het binnenste van het sterrenstelsel. Echter, het verhaal is een stuk complexer geworden met de vondst van gas met een blauwverschuiving (gas dat van de nucleus af beweegt – in projectie) in meerdere radiostelsels. Dit betekent dat de vondst van roodverschoven absorptie van gas in de nucleaire regionen op zich niet voldoende bewijs is voor de claim dat accretie van koud gas de AGN van brandstof voorziet. Naast H I in absorptie is in enkele stelsels ook H I in emissie gevonden, in structuren die variëren van kleine klompjes tot grote, 190 kpc schijven. Het meeste H I gas in deze structuren vertoont een beweging van regelmatige rotatie. Er zijn echter ook tekenen van verstoring gevonden in alle objecten, wat er op duidt dat galactische interacties en mergers een rol kunnen spelen bij het activeren van radiostelsels.

Ondanks de vooruitgang geboekt in het begrijpen van radiostelsels sinds hun ontdekking ongeveer 60 jaar geleden zijn er nog meerdere open vragen, waaronder deze:

- Wat is het precieze mechanisme dat nucleaire activiteit kan veroorzaken? Zijn mergers en getijde interacties verantwoordelijk voor de activering van AGNs, of speelt de accretie van koud en heet gas ook een rol. Meerdere interacties en mergers zijn gezien die niet hebben geleid tot een actieve AGN fase; de connectie tussen galactische interacties en AGN activiteit moet dus grondiger onderzocht worden.

- Wat is de brandstof voor AGN? Direct observationeel bewijs voor de inval van gas naar het zwarte gat is nog niet gevonden. Het is daarom noodzakelijk om de circumnucleaire regionen beter te onderzoeken om te zien of de inval van gas direct naar het zwarte gat bestaat of dat de circumnucleaire schijven het zwarte gat voeden.

- Welke tijdschalen zijn van belang voor de activering van radiostelsels? Een fase van radio activiteit (die meestal minder dan 100 miljoen jaar duurt) is slechts een korte episode in de levensduur van een vroeg-type sterrenstelsel. Het is echter niet duidelijk hoe vaak een actieve fase herhaald wordt, en hoe lang dat duurt (de zogenaamde "duty cycle"). Een andere belangrijke vraag is wat de oorzaak is voor de herstart van een AGN. Herhaalde AGN activiteit is geobserveerd in meerdere stelsels, maar het is niet duidelijk wat het proces is dat zorgt voor de re-activatie.

- Hoe beïnvloedt het ISM de AGN? Wat is de invloed van het ISM (interstellaire materie) op radiostelsels? De radio structuren die ontstaan als het gevolg van AGN activiteit worden vaak groter dan het host stelsel (tot schalen van enkele Mpc), terwijl andere structuren compact blijven. Zijn deze compacte structuren jong, of verhinderd het omringende gas en stof de groei van grotere structuren.

Dit proefschrift:

Dit proefschrift bestudeerd de evolutie van nabije radiobronnen en de stelsels waarin ze gevonden worden. De belangrijkste punten die in dit proefschrift behandeld worden zijn gerelateerd aan de vier vragen die boven gesteld worden. Sinds koud gas mogelijk een belangrijke rol kan spelen in het activeren van radiostelsels is het essentieel om de rol van neutraal waterstof te bestuderen in de evolutie van radiostelsels. H I structuren kunnen geobserveerd worden op heel verschillende schalen met behulp van radio telescopen. De H I morfologie en kinematica kunnen bestudeerd worden op schalen van enkele honderden kpc tot enkele tientallen pc; dat wil zeggen, over vier ordes van grootte – van de omgeving van het sterrenstelsel tot en met het circumnucleaire gebied, waar gas direct geaccreteerd wordt door het zwarte gat.

Het bestuderen van de omgeving geeft de mogelijkheid om te zoeken naar sporen van galactische getijde interacties en om te onderzoeken of de omgeving van radio-luide stelsels anders is dan de omgeving van radio-zwakke stelsels. Dit laatste zou een indicatie kunnen geven waarom sommige stelsels wel een actieve fase ondergaan en andere niet.

Het bestuderen van grote H I structuren (op schalen van tientallen kpc) biedt de mogelijkheid om de evolutie van een sterrenstelsel te onderzoeken. Op grote afstand van het centrum worden de dynamische tijdschalen groot (tot ~1 Gyr[5]), zodat tekenen van interacties zichtbaar worden, evenals klompen gas die van buiten het stelsel geaccreteerd worden. Tegelijkertijd kan onderzocht worden of niet-cirkelvormige bewegingen ervoor kunnen zorgen dat gas naar de binnenste 100 pc grote nucleaire regionen gedreven worden. Met observaties van nucleaire absorptie kunnen structuren dichtbij het zwarte gat onderzocht worden, die nieuwe inzichten kunnen geven over de voeding van het zwarte gat met gas. Wat nu volgt is een korte samenvatting van de resulataten van dit proefschrift, gerangschikt volgens overwerp.

300 kpc schaal: omgeving
We hebben een aantal radiostelsels onderzocht (met behulp van de Westerbork Synthesis Radio Telescope, WSRT), met de bedoeling om de H I omgeving te bestuderen. Het specifieke doel was om te zoeken naar tekenen van verstoringen in nabijgelegen met elkaar geassocieerde stelsels en om het belang van koud gas te onderzoeken in radiostelsels. Onze data worden vergeleken met een aantal radio-zwakke vroeg-type stelsels.

We vinden geen statistisch significante verschillen tussen de omgeving van radioluide en radio-zwakke stelsels in termen van het aantal nabijgelegen H I stelsels binnen 300 kpc van het bestudeerde stelsel. Daarnaast is de gemiddelde hoeveelheid H I gas dat zich bevindt in de omgeving van radio-luide en radio-zwakke stelsels vergelijkbaar. Meerdere nabijgelegen stelsels vertonen tekenen van verstoring, wat erop duidt dat het aanwezig zijn van verstoringen geen goede manier is om radioluide van radio-zwakke stelsels te onderscheiden.

Tientallen kpc schaal: schijf structuren
We hebben H I observaties uitgevoerd (met behulp van de Australian Telescope Compact Array, ATCA) van het meest nabij gelegen radio-luide stelsel, Centaurus A. De H I schijf (te zien in Fig. 3) wordt gedomineerd door rotatie tot en met de nucleaire regionen. Er is geen bewijs gevonden voor niet-cirkelvormige beweging binnen een straal kleiner dan 6 kpc. Op grotere schalen worden asymmetrische en arm structuren gevonden, inclusief niet-cirkelvormige bewegingen. We concluderen dat de accretie van een klein gas-rijk stelsel heeft plaatsgevonden ongeveer een paar honderd miljoen jaar geleden, wat in overeenkomst is met eerdere conclusies. Echter, het opslokken van het buurstelsel gebeurde te lang geleden om de huidige actieve fase te activeren, al kan deze merger wel de eerdere AGN cyclus verstoord hebben.

Een tweede object dat in detail is bestudeerd is NGC 1167, welke is geobserveerd met behulp van de WSRT. Het H I gas in emissie is verdeeld over een schijf met een grootte van 160 kpc en vertoont regelmatige rotatie. Verschillende tekenen van recente interactie of accretie van een satelliet stelsels zijn gevonden in dit stelsel, evenals tekenen van recente merger activiteit. Accretie van koud gas in dit stelsel is niet gevonden.

[5] 1 Gyr = 1 000 000 000 yr

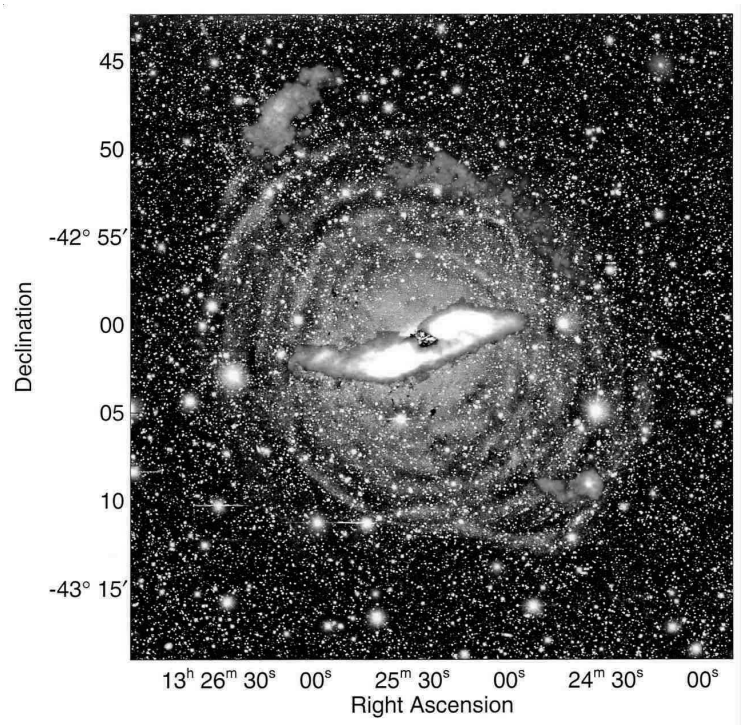

Figuur 3: H I *emissie behaald uit de ATCA observaties overlappend op een "optische foto" die het licht van de sterren in Centaurus A laat zien. De optische foto is genomen uit Peng et al. (2002).*

100 pc schaal: circumnucleaire structuren
De circumnucleaire H I structuren van drie radiostelsels zijn onderzocht: Centaurus A, Cygnus A and NGC 1167. In alle drie objecten is zowel roodverschoven gas als blauwverschoven gas gevonden. In het geval van Centaurus A en Cygnus A konden we laten zien dat de absorptie waarschijnlijk veroorzaakt wordt door een circumnucleaire schijf, wat mogelijk ook het geval is in NGC 1167. In NGC 1167 is het ook noodzakelijk dat er een naar buiten bewegende gas component aanwezig is. In geen van de drie bestudeerde stelsels is bewijs gevonden van gas dat direct naar de AGN invalt. Desalniettemin kan in het geval van Cygnus A de H I schijf dienen als het gas reservoir dat nodig is om de AGN te voeden.

NGC 1167 staat bekend als een compacte radio bron, die waarschijnlijk bezig is om uit te groeien tot een uitgebreide klassieke FR-I type radio structuur. Daarnaast onthult onze data een 240 kpc grote oude structuur die laat zien dat het zwarte gat een eerdere actieve fase heeft ondergaan. Dit is een spannende ontdekking, sinds het laat zien dat stelsels met een grote hoeveelheid H I gas ook tevens een grote uitgebreide structuur kunnen bezitten; een resultaat dat tot nu toe onderbrak.

Belangrijkste conclusies:

De bovenstaande paragraaf geeft een korte samenvatting van de resultaten behaald in dit proefschrift. Wat volgt is een kort overzicht van de belangrijkste conclusies die getrokken kunnen worden uit de afzonderlijke resultaten.

Wat zijn de belangrijkste mechanismen die nucleaire activiteit veroorzaken, en wat onderscheidt een radio-luid van een radio-zwak sterrenstelsel?
Er zijn verschillende mechanismen voorgesteld die nucleaire activiteit kunnen veroorzaken in vroeg-type sterrenstelsels. Onze resultaten laten zien dat er geen statistisch significant verschil bestaat tussen de omgeving van radio-luide en radio-zwakke stelsels. Dit betekent dus dat gas-rijke interacties waarschijnlijk niet het belangrijkste mechanisme is dat zorgt voor nucleaire activiteit. Zeker is dat niet elke interactie een radio-luide fase veroorzaakt, sinds vele interacties geobserveerd zijn in radio-zwakke stelsels. Dit is in overeenstemming met onze Centaurus A analyse, die laat zien dat de recente merger niet verantwoordelijk is voor de huidige fase van verhoogde activiteit. Er bestaat dus zeker geen één-tot-één relatie tussen interactie en AGN activiteit.

Wat zijn de tijdschalen die geassocieerd worden met het activeren van radiostelsels en kunnen de eigenschappen van het ISM significant veranderen in de periode tussen herhaalde fases van AGN activiteit?
De huidige episode van nucleaire activiteit in Centaurus A is begonnen een relatief lange tijd na de merger. Dit suggereert dat na een merger het gas enige tijd nodig heeft om een stabiele accretie stroom te vormen (onafhankelijk van de staat van het gas dat de AGN voedt).

Veel radiostelsels ervaren herhaaldelijke fases van radio activiteit, inclusief Centaurus A. Ondanks dat een AGN episode slechts een korte periode (minder dan 100 miljoen jaar) is in de evolutie van een vroeg-type stelsel kunnen de eigenschappen van het gas en stof in de centrale delen van het sterrenstelsel radicaal veranderen in de periode tussen twee AGN episodes. Een goed voorbeeld is NGC 1167, waar tijdens de huidige AGN fase de radio bron een interactie aangaat met het omringende gas en probeert uit te groeien tot een grote FR-I type radio structuur. Op dezelfde tijd wordt een 240 kpc grote oude structuur ontdekt, wat er op duidt dat het omringende gas tijdens de vorige AGN fase geen belemmering vormde voor de groei van de radio structuur.

Worden AGNs gevoed door koud gas?
Oorspronkelijk werd de overvloed van roodverschoven H I absorptie detecties in radiostelsels gezien als bewijs dat de inval van koud gas verantwoordelijk was voor de voeding van AGNs. De aanwezigheid van blauwverschoven absorptie in veel radiostelsels maakt deze theorie een stuk complexer. Onze analyse laat zien dat H I absorberende circumnucleaire schijven bestaan (bv. in Centaurus A en Cygnus A en waarschijnlijk ook in NGC 1167). Echter, direct bewijs dat koud gas inderdaad de centrale AGN van brandstof voorziet ontbreekt nog. De H I circumnucleaire schijf zou echter alsnog kunnen zorgen voor de brandstof die de AGN actief houdt. Koud gas kan dus nog steeds het materiaal zijn dat nodig is om radio activiteit te activeren.

Open vragen en de toekomst:

Ondanks de bijdrage van dit proefschrift aan het begrip van de rol van koud gas in de evolutie van radiostelsels blijven er nog open vragen over, waarvoor meer onderzoek nodig is, zoals:

Zijn verschillende activeringsmechanismen gerelateerd aan verschillende types radiostelsels?
Er bestaat een grote variatie aan radiostelsels (niet enkel de FR-I en FR-II types die in dit proefschrift bestudeerd worden). Sommige verschillen tussen de types worden toegeschreven aan verschillen in oriëntatie, maar het is ook bekend dat er intrinsieke verschillen bestaan tussen verschillende types AGN. Zijn deze verschillen het resultaat van verschillende AGN activeringsmechanismen?

Wat is het exacte mechanisme dat zwarte gaten van brandstof voorziet?
Het ontbreekt nog steeds aan direct bewijs voor de inval van gas naar het centrale zwarte gat. Hoe wordt het (koude) gas naar de nucleus geleid? Zijn de gevonden H I circumnucleaire schijven de reservoirs die gas voeden aan de torus die uiteindelijk het zwarte gat van brandstof voorziet?

Wat bepaalt de levenscyclus van een AGN?
Hoe en wanneer wordt een zwart gat actief? Als mergers en interacties een rol spelen, wanneer wordt dan het zwarte gat geactiveerd en wat bepaalt de duur van de actieve fase? Als zwarte gaten heet gas accreteren, wat zijn dan de voorwaarden die een AGN activeren en kunnen mergers en satelliet accretie dit proces beïnvloeden?

Feedback: wat is de invloed van een AGN op het omringende gas/host sterrenstelsel?
Computer simulaties laten zien dat "feedback" van AGNs een sterk regulerend effect heeft op de groei van het host sterrenstelsel. Vanuit dat oogpunt is het belangrijk om de invloed van AGNs op het omringende gas te begrijpen. Bijvoorbeeld, wat is de invloed van uitstromingen van gas die gedetecteerd zijn in sommige radiostelsels (inclusief NGC 1167) op de groei van het sterrenstelsel?

Gegeven het feit dat radiobronnen mogelijk een dominante rol spelen in de formatie en evolutie van sterrenstelsels, en dus belangrijk zijn voor de evolutie van het Universum als geheel, is het absoluut noodzakelijk om de mechanismen die hier aan het werk zijn te begrijpen.

Over de hele wereld worden momenteel een aantal nieuwe-generatie instrumenten gebouwd (en meer faciliteiten worden geacht later dit decennium werkzaam te worden) die observaties zullen verrichten in radio golflengtes. Met deze instrumenten zullen de mogelijkheden om AGNs en hun host sterrenstelsels in detail te bestuderen (hun radio jets/lobben and hun hoeveelheden atomair en moleculair waterstof) enorm toenemen, niet alleen in het nabije Universum, maar ook op kosmologische roodverschuivingen (afstanden).

Acknowledgements

"How is it over there in the Netherlands?" This was one of the questions I heard in Germany from time to time. The appropriate answer to this question given Dutch style is: "not bad"[1] or "okay"[2]. Well, I could have also tried to give a more detailed answer, but my main conclusion is very short: Dutch and Germans have more things/habits in common than both sides are usually willing to admit (including myself!!!). To decide whether or not this is a good thing, is up to the reader.

It is impossible to do a PhD on your own. There is a large number of people that contribute to the thesis in very different ways. However, one person is of great importance, the supervisor. **Raffaella**, without you, your enthusiasm, your encouragement, your help and your guidance, this piece of work would have not been possible. I do not know how you have always managed to write, read and reply to e-mails, but I received a few 10^3 emails from you over the last four years. Often, you even replied within less than 15 minutes to my emails! How much more can a supervisor spoil a student? I am deeply indebted to you for all the time and effort you invested in me and this project. Grazie mille!!!

Tom, you are the hardest person to convince and, therefore, it is always a big challenge to argue against you. I could not have benefited from it more! If you agree with something, it must be true/real. Bedankt dat je mijn co-supervisor wilde zijn.

John, I haven't met any other astronomer who is so enthusiastic about his research. It is a great pleasure and very motivating to work with you. I am looking forward to my time in Sweden!

Renzo, your ideas and pieces of advice have been a big benefit for me. Thank you for teaching me all the things one can learn about a galaxy by simply looking at the data cube over and over again. I would like to thank you, **Thijs**, for being my promoter. It was not necessary to interact a lot, but whenever I approached you, you made time for me – great! A big thank you also to the reading committee members for being part of the committee and approving the thesis. **Bjorn**, you are a great collaborator, always interested and always very helpful. I very much enjoy working with you on our projects!

During my PhD, I have benefited enormously from the European PhD network ESTRELA. **Neal**, you have been a great organiser. A thank you to all "estrelians" (**Maciej, John, Elena, Lyshia, Kalle, Rossa, Evan, Hayden, Nikta, Sarah, Chin-Shin,**

[1] meaning: "I have nothing to complain about."
[2] meaning: "Actually, quite good."

Francesco and **Rashmi**). The ESTRELA workshops are memorable.

I was lucky to be part of two institutes, ASTRON and Kapteyn. **Yang-Shyang, Alvaro, Eva, Ayçin, Oscar** and **John**, thanks for being such easy-going office mates. Yang-Shyang and Alvaro, thanks for your help in the beginning. Ayçin, your very presence helped a lot! I will miss our conversations and you distracting me from work (e.g. by playing "in-office football"), just joking. I would also like to thank the group of "radio" fellows that kept on dropping by my office with "stupid" or "simple" "radio" questions (**Seungyoup, Alicia, Roberto** and **Boris**). Often, the questions were neither "stupid" nor "simple", and sometimes not even "radio". To be fair, I also bothered you guys with questions. Seungyoup, the institute has not been the same since you left. Hopefully you can come back soon. All the best! **Kyle**, thanks for your help with my "optical" questions. A big thank you also to the Postdoc crowd in Dwingeloo (**George, Paolo, Josh, Jean-Mathias**, Eva and John) for scientific discussion, carpooling and much more. Thank you **Thomas** for translating my dutch summary and many thanks to all the staff members and PhD students that I did not mention in detail, but should have (e.g. **Facundo, JP, Erwin, Peter, Edo, Antonela, Burçu, Else, Bertrand, Vibor, Chris, the Kapteyn football crowd, ...**). A big 'thank you' goes to the **secretaries** and **computer groups** at ASTRON and Kapteyn and a special 'thank you' to **Fabien** and **Francesco**. We basically swapped our lifes for a few weeks last year in January (Fabien) and May (Francesco). I stayed in your apartments in Gothenburg while you took care of my flat here in Groningen. Fabien, imagine if your flight would have been delayed. How would we have exchanged keys at Schiphol?

During my four years in Groningen, I tried to get integrated into Dutch society – at least a little bit – by joining GTTC. This was a great decision for three reasons: to distract myself from work every now and then, to learn a little bit of dutch, and – most important – to enjoy "gezellige avonden". Er gaat niets boven GTTC.

The last few lines are dedicated to my family. I would like to thank **my parents** and **sisters** for the continuous support and encouragement during my whole studies. The jewel in the end: **Alice**, you hold the record by sending me almost 10^4 e-mails. I cannot thank you enough for your presence, patience, encouragement, phone chats and all the things we experienced together. You contributed to large parts of this thesis.

Many thanks to all of you who directly or indirectly contributed to this work. Bedankt! Danke schön!

Christian Struve

Groningen, September 2010